

A Different Peat Perspective: Quantifying Tropical Peatland Ecosystem Variables from the
Ground and from Space

By

Nikaan Koupaei Abyazani

A dissertation submitted in partial fulfillment of

the requirements for the degree of

Doctor of Philosophy

(Atmospheric and Oceanic Sciences)

at the

UNIVERSITY OF WISCONSIN-MADISON

2025

Date of final oral examination: 11/20/2025

The dissertation is approved by the following members of the Final Oral Committee:

Ankur Desai, Professor, Atmospheric and Oceanic Sciences

Paul Stoy, Associate Professor, Biological Systems Engineering

Min Chen, Assistant Professor, Forest and Wildlife Ecology

Ángel Adames Corraliza, Associate Professor, Atmospheric and Oceanic Sciences

Jingyi Huang, Associate Professor, Soil and Environmental Sciences

Abstract

Peatlands are ecosystems that store immense amounts of carbon in their soil and therefore play a critical role in the global carbon cycle. However, due to climate change and anthropogenic disturbance, these ecosystems are transitioning from net carbon sinks to net carbon sources. This is especially true for tropical peatlands due to the extensive conversion of these systems to agricultural land. Despite their important ecosystem services and high vulnerability to becoming net carbon sources, tropical peatlands are not well represented in the literature relative to their temperate and boreal counterparts. This may perhaps be due to harsh environmental conditions and/or due to site remoteness. In this dissertation, I explore the possibility of tropical peatland study through an unconventional methodology, while also conducting field measurements to contribute to the expanding literature of in situ observations in tropical peatlands. The first project focuses on testing whether the Optical Trapezoid Model (OPTRAM), a remote sensing-based model, is capable of reproducing the temporal water table fluctuations in tropical peatlands. I found that OPTRAM performs optimally in minimally forested and non-forested areas ($0.7 < R < 1$). On the other hand, in heavily forested areas, OPTRAM performance was substantially weaker (average R of -0.04 to 0.24). The second project aims to expand on the first project by testing OPTRAM's ability for predicting the probability of burned area occurrence multiple days ahead of time. I acquired burned area data from the Global Fire Emissions Database (version 4.1s). It was found that the OPTRAM value ten days prior was a relatively good indicator of burned area. Low OPTRAM values ten days prior generally had non-zero probability values, while high OPTRAM values ten days prior typically had a value of zero. The third project aims to compare the peat soil greenhouse gas fluxes between an undrained peat swamp forest, a young oil palm plantation, and a mature oil palm plantation (during second

rotation of planting). Additionally, environmental variables such as air temperature, vapor pressure deficit, water table level, and precipitation were compared and their relationship with soil carbon dioxide, methane, and nitrous oxide fluxes was assessed. I found that soil methane fluxes were diminished and soil nitrous oxide and carbon dioxide fluxes were generally elevated at the plantation sites relative to the undrained site. Additionally, air temperature and water table level were found to be the largest contributors to soil greenhouse gas flux variability, while the effects of vapor pressure deficit and precipitation were minimal. Overall, this dissertation shows the successful application of remote sensing in tropical peatlands and has implications for better understanding the role these systems play in the global carbon cycle and in contributing to ongoing climate change. Furthermore, it contributes to the much-needed on-the-ground measurements in these ecosystems which may inform future conservation and sustainability policies in the region.

Acknowledgements

I am grateful for my PhD advisor, Dr. Ankur R. Desai, who has helped me immensely throughout my PhD career. Not only has he provided invaluable mentoring on my research, but he has also helped me in other matters such as providing guidance on the timeline for the PhD and providing me with strong letters of recommendation for numerous applications. I am very lucky to have called him my PhD advisor. I would also like to thank the other members of my PhD committee, Dr. Paul Stoy, Dr. Min Chen, Dr. Ángel Adames-Corraliza, and Dr. Jingyi Huang for taking the time to read this dissertation and provide helpful comments. I would like to express my gratitude to Dr. Paul Stoy for supporting many of my applications by providing strong letters of recommendation. I would also like to thank Susan Nossal, who has also supported me many times with a strong letter of recommendation for my applications during my PhD. I am also very thankful to all collaborators who supported these research projects. This includes Dr. Iuliia Burdun, Dr. Kristell Hergoualc'h, Dr. Takashi Hirano, Dr. Lulie Melling, Dr. Erin Swails, Dr. Angela Che Ing Tang, Dr. Guan Xhuan Wong, Dr. Hafsah binti Nahrawi, Dr. Faustina Elfrida Anak Sangok, Dr. Auldry Chaddy Anak Petrus Rudut, and Yazid Imran bin Muhammad Faizul. I would like to extend my gratitude to the staff at the Sarawak Tropical Peat Research Institute in Malaysia for assisting me with fieldwork at the research sites and also with analyses in the lab. I would also like to thank the Fulbright U.S. Student Program, The Malaysian-American Commission on Educational Exchange, especially Leena Rajagopal, and The Institute of International Education for making fieldwork in Malaysia possible. Additionally, I would like to acknowledge support from the University of Wisconsin-Madison (UW) Center for Climatic Research, Climate, People, and Environment Program and the UW Atmospheric and

Oceanic Sciences Department. Lastly, I would like to give special thanks to my family for their patience and support throughout this whole process. I will always be grateful for everything you've done for me.

Contents

Abstract	i
Acknowledgements	iii
Contents	v
1. Chapter 1: Introduction and Background	1
1.1 The Global Carbon Cycle	1
1.2 Peatlands in the Global Carbon Cycle	4
1.3 The Significance and Vulnerability of Tropical Peatlands	5
1.4 Dissertation Objectives and Questions	13
1.5 References	16
2. Chapter 2: Tropical Peatland Water Table Estimations From Space	24
2.1 Introduction	24
2.2 Methods	27
2.2.1 The Optical Trapezoid Model (OPTRAM)	27
2.2.2 Satellite Images	31
2.2.3 Site Descriptions	33
2.2.4 Data Computation and Statistical Testing	37
2.2.5 OPTRAM and Vegetation Density	38
2.2.6 Testing Relationship Differences Between El Niño and Non-El Niño Years	39
2.2.7 Uncertainty Analysis	39
2.3 Results	40

2.3.1 OPTRAM Parameterization	40
2.3.2 In Situ Water Table Variability	42
2.3.3 Estimating Tropical Peatland Water Table Variability via OPTRAM	44
2.3.4 NDVI's Influence on OPTRAM Performance	49
2.3.5 The Number of Data Points and OPTRAM Performance	51
2.3.6 Impact of El Niño and Non-El Niño Years	52
2.3.7 Uncertainty in OPTRAM Index-Water Table Relationship	53
2.4 Discussion	54
2.4.1 Comparison with Past Studies	55
2.4.2 Study Limitations and Application Approaches to Other Tropical Peatlands	57
2.4.3 Implications for OPTRAM's Ability to Detect Changes in Tropical Peatland Water Table	60
2.5 Conclusion	62
2.6 Global Research Collaboration	63
2.7 Open Research	64
2.8 Acknowledgements	64
2.9 Supporting Information	66
2.10 References	68
 3. Chapter 3: Forecasting Tropical Peatland Burned Area Potential 10-30 Days in Advance	 78
3.1 Introduction	78

3.2 Methods	80
3.2.1 The Optical Trapezoid Model (OPTRAM)	80
3.2.2 The Global Fire Emissions Database (Version 4.1s)	83
3.2.3 Testing OPTRAM's Capability of Predicting Burned Area	84
3.2.4 Study Sites	85
3.3 Results	89
3.3.1 Indonesia Sites	89
3.3.1.1 10, 20, and 30-day forward shifted OPTRAM values	89
3.3.1.2 Peat Burned Area Dependence on Continuously Low OPTRAM Indices in Indonesia	95
3.3.2 Malaysia Sites	97
3.3.2.1 10, 20, and 30-day forward shifted OPTRAM values	97
3.3.2.2 Peat Burned Area Dependence on Continuously Low OPTRAM Indices in Malaysia	99
3.3.3 Peru Sites	99
3.3.3.1 10, 20, and 30-day forward shifted OPTRAM values	99
3.3.3.2 Peat Burned Area Dependence on Continuously Low OPTRAM Indices in Peru	101
3.3.4 Congo Basin Sites	102
3.3.4.1 10, 20, and 30-day forward shifted OPTRAM values	102
3.3.4.2 Peat Burned Area Dependence on Continuously Low OPTRAM Indices in the Congo Basin	104
3.4 Discussion	104

3.4.1 OPTRAM's Capability for Predicting Tropical	
Peatland Burned Area	105
3.4.2 Comparison with Other Studies	107
3.4.3 Study Limitations	108
3.4.4 Implications of Using OPTRAM for Burned Area Prediction	109
3.5 Conclusion	110
3.6 Supplemental Figures	112
3.7 References	126
4. Chapter 4: Impacts of Anthropogenic Disturbance on Soil Greenhouse Gas Fluxes	
 in Malaysian Peatlands	133
4.1 Introduction	133
4.2 Methods	136
4.2.1 Site Description	136
4.2.2 Soil and Soil Gas Samples	140
4.2.3 Other Measured Variables	141
4.2.4 Data Analysis	141
4.3 Results	142
4.3.1 Impact of Peatland Conversion to Oil Palm on Soil Greenhouse Gas	
Fluxes	142
4.3.2 Carbon Dioxide Flux	142
4.3.3 Methane Flux	146
4.3.4 Nitrous Oxide Flux	148

4.3.5 Role of Environmental Drivers on Soil Greenhouse	
Gas Fluxes in Undrained and Drained Tropical Peatlands	151
4.3.5.1 Water Table Level	151
4.3.5.2 Average Air Temperature	153
4.3.5.3 Soil Temperature at 5 cm and 10 cm Depth	155
4.3.5.4 Precipitation	159
4.3.5.5 Vapor Pressure Deficit	161
4.4 Discussion	163
4.4.1 Drainage and Oil Palm Cultivation on Tropical Peat Decreases Methane Emissions and Promotes Carbon Dioxide and Nitrous Oxide Emissions	165
4.4.2 Drivers of Soil Greenhouse Gas Fluxes	168
4.4.3 Recommendations for Tropical Peatland Restoration and Sustainability	171
4.5 Conclusion	172
4.6 References	173
5. Chapter 5: Conclusion	182
5.1 Dissertation Overview	182
5.2 Study Limitations	184
5.3 Implications	185
5.4 Future Directions	187
5.5 Concluding Remarks	189

5.6 References

191

Chapter 1: Introduction and Background

1.1 The Global Carbon Cycle

The global carbon (C) cycle is a crucial process that can have effects on Earth's climate and its inhabitants. While some C is immobile and may have been stored underground and “untouched” for millions to billions of years, a great amount of it is also being transferred between different reservoirs ([Bruhwiler et al., 2018](#)). Mobile C may be exchanged from and to many different reservoirs, including between the atmosphere, ocean, land, and living organisms ([Bruhwiler et al., 2018](#)) (Figure 1.1). During its movement through the cycle, the C may take on many forms, including carbon-dioxide (CO₂) and methane (CH₄) which are considered “greenhouse gases” or “GHGs” for their capacity to trap heat from the Sun. A portion of the incoming shortwave radiation from the Sun is absorbed by the Earth, which is then re-emitted back to space in the form of infrared radiation. The infrared radiation is then absorbed by GHGs in the atmosphere and is eventually re-radiated in all directions, thereby warming the Earth. For decades, scientists have warned that an increased concentration of atmospheric CO₂ and CH₄ would lead to a gradual warming of the Earth, and therefore affect its climate in a multitude of ways. The Intergovernmental Panel on Climate Change (IPCC), a United Nations body for assessing climate change-related science, has reported over the years that not only has the planet already warmed significantly, but it is also on track to warm even more if no mitigation efforts are performed ([IPCC, 2023](#)).

The global carbon cycle

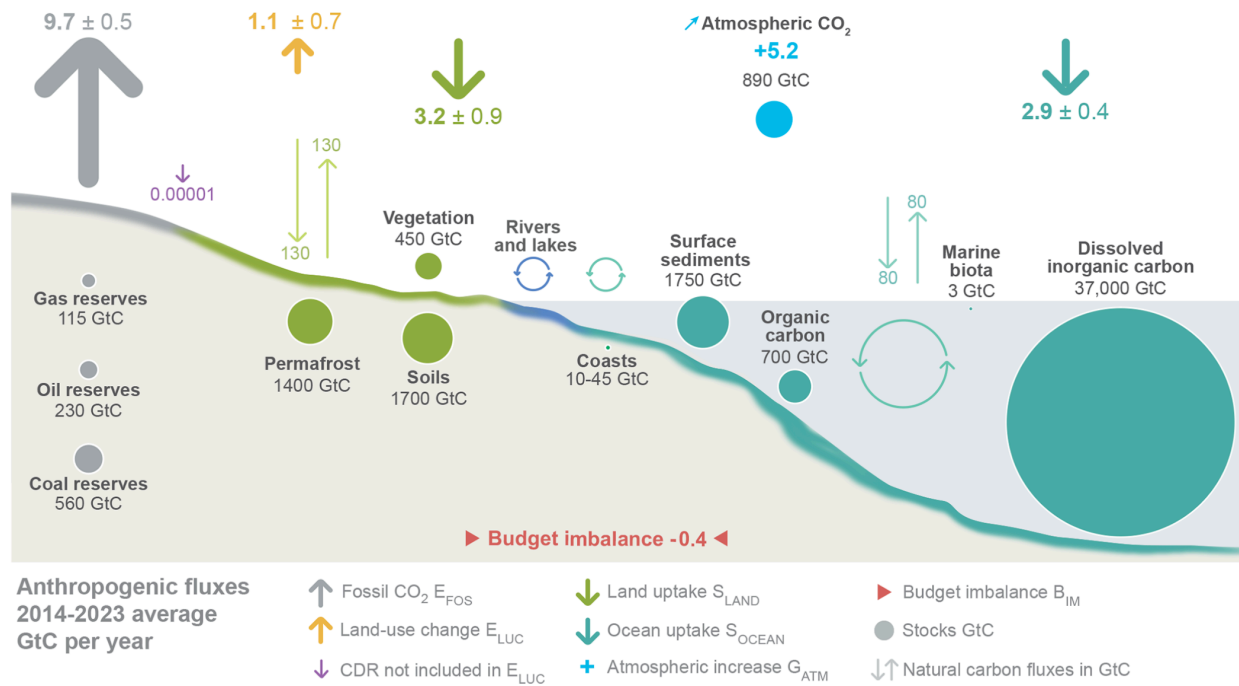


Figure 1.1: An illustration of the global carbon cycle with carbon pools and fluxes. Figure reproduced from [Friedlingstein et al., 2025](#).

While much commentary has focused on the industrial contributions to climate change, there are also critical GHG emissions from land ([Friedlingstein et al., 2025](#)). The terrestrial C cycle is one of the most important and unique components of the global C cycle since humans may have a direct influence on it. It is also one of the largest sources of uncertainty among the many C sources and sinks and has substantial year-to-year variation ([Friedlingstein et al., 2020](#); [Zeng et](#)

al., 2005). This has been attributed to both natural climatic variability such as the El Niño-Southern Oscillation (ENSO) (Cox, 2019; Cox et al., 2013; Liu et al., 2017; Wang et al., 2013; Zeng et al., 2005) and also anthropogenic factors (Friedlingstein et al., 2025). For thousands of years, agricultural practices have altered land cover for the benefits of food production, but the environmental consequences of these practices have just been relatively recently revealed. These consequences mainly originate from the soil, which are one of the largest belowground C stores on land. When preparing the land for food production, certain practices disturb the soil, resulting in large gas emissions which include GHGs. Additionally, aboveground C stores, such as trees, may be cut down and removed as part of land preparation, resulting in a direct removal of C from the system, which also has an impact on tree-to-soil carbon fluxes such as in the form of root exudates (Tresder et al., 2005). Moreover, it is important to note that humans do not necessarily need to be present for the land to be disturbed. Terrestrial systems are also subject to natural disturbances. These may include lightning-induced fires or impacts on the frequency and intensity of precipitation due to the El Niño-Southern Oscillation (ENSO). Like anthropogenic disturbances, these also in gas emissions which include GHGs. Interestingly, since anthropogenic disturbances are believed to be driving a change in climate, it may very well be that the natural disturbances are somewhat linked to anthropogenic activity as well in the long term. Since terrestrial systems are subject to direct impact by humans, there are considered to be a vulnerable store of C. Poor land management may potentially result in high C emissions from the land to atmosphere in the form of CO₂, therefore exacerbating ongoing climate change. As a result, it is vital that practices are implemented to retain as much C in the system as possible.

1.2 Peatlands in the Global Carbon Cycle

When considering systems that are most likely to contribute the most to global warming, one must consider the magnitude of C that is currently stored. A higher amount of C storage means that, if disturbed, the system has the potential to release more C (in the form of GHGs) to the atmosphere and therefore would have a greater impact on the climate. One system that has some of the largest stores of soil C are peatlands (Page et al., 2011; Ribeiro et al., 2021; Yu, 2012), making them an important area of study among scientists. Peatlands are primarily composed of peat, a type of soil that is mostly made of organic rather than mineral content. This organic content is typically composed of plant materials such as leaves and branches. When the accumulation rate of these organic materials exceeds the microbial decomposition rate, peat is formed and then piled up layer by layer (Vitt, 2013). After thousands of years, this process can result in the accumulation of a thick peat layer above the mineral substrate or bedrock. Due to its organic contents, this layer is rich in C and can have a thickness of less than a meter to more than five meters (Hooijer et al., 2012; Page et al., 2011). The key to peat accumulation is in the system's environmental conditions. Typically, waterlogged systems facilitate peat accumulation due to causing anaerobic conditions (Vitt, 2013). The absence of oxygen slows microbial decomposition rates and thereby promotes the accumulation of peat (Vitt, 2013). The condition of high water table (WT) means that peatlands may form in a myriad of areas across the globe. This includes its formation in boreal, temperate, tropical regions (Immirzi et al., 1992; Page et al., 2011). Even though these systems are estimated to only cover ~3% of the global land surface, they store approximately ~33% of the global soil C (Yu et al., 2010; Huang et al., 2021), which renders them as being a significant contributor to not only the terrestrial C cycle, but also the global C cycle (Figure 1.2). In addition to C sequestration, peatlands provide a variety of other

ecosystem services. This includes serving as a habitat for numerous plants and animals while also acting as a hydrological regulator (Ribeiro et al., 2021; Harenda et al., 2018).

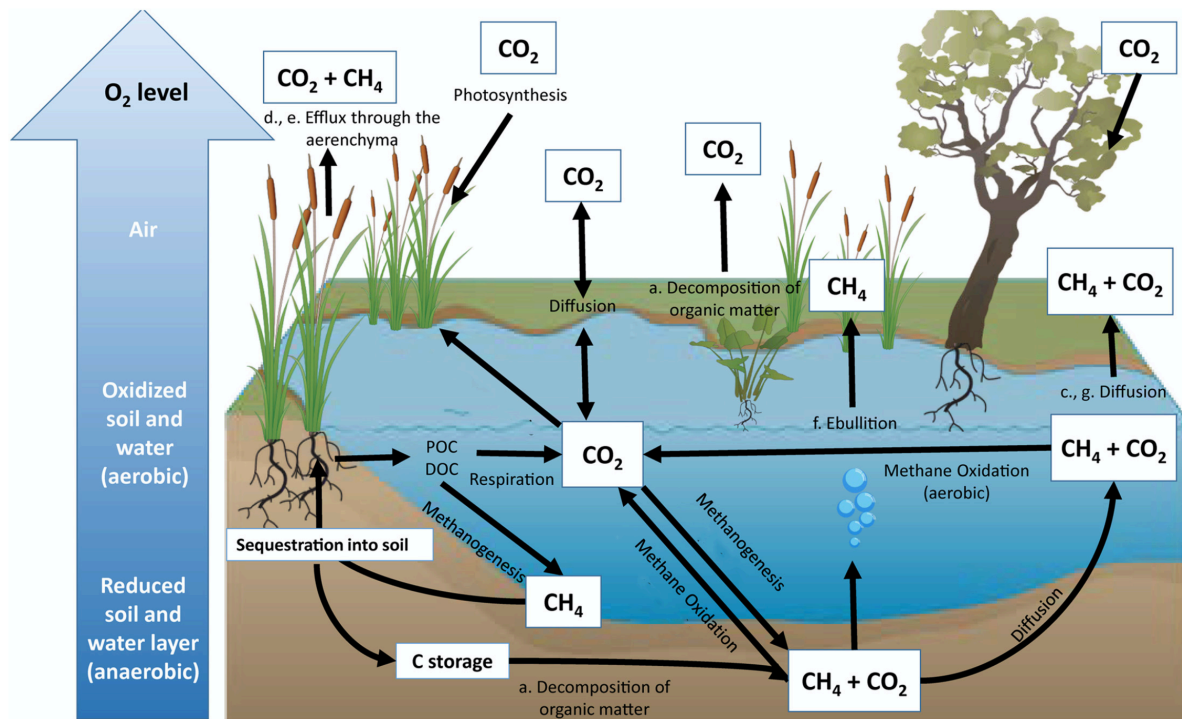


Figure 1.2: An illustration showcasing the wetland carbon cycle which is similar to the peatland carbon cycle. Figure reproduced from Limpert et al., 2020.

1.3 The Significance and Vulnerability of Tropical Peatlands

Of the regions where peatlands may be found around the globe (Figure 1.3), peatlands in the tropics are relatively understudied. This may be due to the characteristically harsh and humid

conditions of tropical systems, making it challenging to establish and maintain research sites.

The tropical environmental conditions have even led many researchers to believe that C turnover in these systems is large, and therefore the peat C pool is relatively small. However, recent reported estimates have demonstrated otherwise ([Ribeiro et al., 2021](#); [Leifeld & Menichetti, 2018](#); [Dargie et al., 2017](#); [Moore et al., 2013](#); [Page et al., 2011](#)). Many of these systems are also located in remote areas which makes them difficult to access. Furthermore, the lack of tropical peatland studies reflects the historical bias of researchers of the global north. Years of colonization, exploitation, and exclusion of researchers in the tropics has contributed to so-called “parachute science”, where northern scientists (typically from wealthy countries) conduct fieldwork in the region without properly engaging and/or acknowledging the local scientists and community.

This tropical peatland knowledge gap is unfortunate since estimations suggest that these systems disproportionately contribute to the global peatland C stock relative to their areal coverage (~12% of global peatland area but contributing ~20% of the global peatland C stock) ([Joosten, 2010](#); [Dohong et al., 2017](#); [Page et al., 2011](#)). It is also an area of great disturbance due to the development of plantations within the last few decades ([Dohong et al., 2017](#); [Koh et al., 2011](#)).

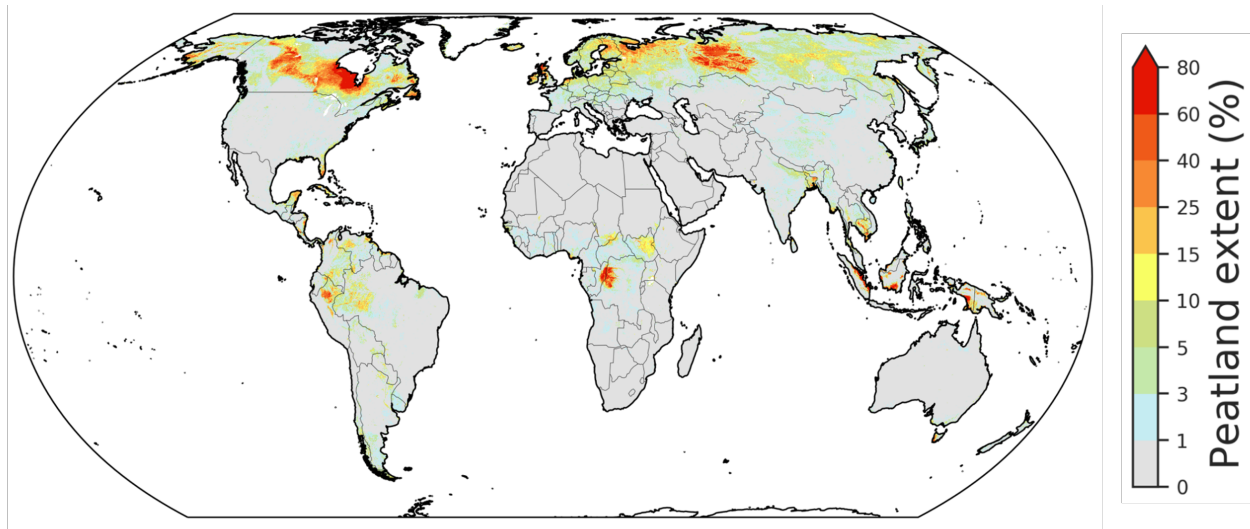


Figure 1.3: A global map of peatland extent. Figure reproduced from [Melton et al., 2022](#).

Peatlands in the tropics are different from those located in temperate and boreal regions due to their more predominant occurrence in lush forests. More frequent rainfall also lowers decomposition rates due to high WT and facilitates peat accumulation. Conversely, temperate and boreal peatlands are typically composed of mosses and generally receive less rainfall relative to tropical peatlands. Even though less attention has been given to tropical peatland research, it is not to say that high quality in-situ studies of these systems do not exist. There have been many projects that set out to quantify tropical peatland gas fluxes, and these have been carried out using two popular methods: soil flux chambers ([Melling et al., 2005](#); [Murdiyarso et al., 2010](#); [Hadi et al., 2005](#); [Inubushi et al., 2003](#); [Couwenberg et al., 2009](#); [Rieley et al., 2008](#); [Furukawa et al., 2005](#); [Jauhiainen et al., 2012](#)) and eddy covariance ([Hirano et al., 2007](#); [Deshmukh et al., 2020](#); [Deshmukh et al., 2021](#); [Tang et al., 2018](#); [Deshmukh et al., 2023](#)). These studies have indicated tropical peatland gas fluxes to be highly reliant on environmental variables. It is shown

that a high WT generally leads to less CO₂ emissions but higher CH₄ emissions, while a low WT promotes the opposite, less CH₄ emissions but higher CO₂ emissions (Huang et al., 2021). Some researchers have also attempted to quantify tropical peatland C stocks. This has been done through the estimation of peatland coverage (Gumbricht et al., 2017; Xu et al., 2018), of which then peat depth and volume may be deduced to obtain a value for C stocks. For all tropical peatlands, this number has been calculated to be ~152-288 Gt C (Ribeiro et al., 2021). C stock estimates for individual peatland regions have also been made, with Indonesia, Malaysia, Peru (Pastaza-Marañón), and Africa (Cuvette Centrale, Congo) having ~30 Gt C, ~9.1 Gt C, ~3.14 Gt C, ~30.6 Gt C, respectively (Rudiyanto et al., 2015; Page et al., 2011; Draper et al., 2014; Dargie et al., 2017). Southeast Asian peatlands, in particular, are at a high risk of losing their C stocks due to the immense amount of land cover change that has occurred in recent decades. The largest peat C stock in Asia is also located within the southeastern region (mostly in Indonesia and Malaysia) (Dommain et al., 2011; Dommain et al., 2015; Rudiyanto et al., 2015; Page et al., 2011; Sjögersten et al., 2014), meaning that the magnitude of C release may also be greater if these systems are disturbed. Due to this reason, studies on Southeast Asian peatlands may be some of the most abundant within the realms of tropical peatland research. On the other hand, although limited, there is also published literature on tropical peatlands located outside of the Southeast Asian region, such as those in Africa (i.e. the Rugezi Marsh in Rwanda, Okavango Delta in Botswana, Sudd catchment in Sudan and the Cuvette Centrale within the Congo Basin (Grundlings and Grootjans, 2018; Bwangoy et al., 2010; Dargie et al., 2017) and South America (i.e. Rio Basin in Brazil, Pastaza-Marañón Foreland Basin in Peru, and the northern Peruvian Amazon (Draper et al., 2014; Lähteenoja et al., 2013; Lähteenoja et al., 2009a; Lähteenoja et al.,

2009b; Hergoualc'h et al., 2020; Hergoualc'h et al., 2023). The fact that these peatland areas are understudied makes them all the more appealing for further research.

Relatively recently, in 2017, [Dargie et al.](#) published a paper showing that the Cuvette Centrale is the largest peatland complex in the tropics. The fact that the mere existence of this peat layer was just recently found indicates that there may be more tropical peatland areas yet to be discovered. Even with these unknowns, there have been multiple efforts to map the global peatland spatial distribution ([Lappalainen, 1996](#); [Parish et al., 2008](#); [Joosten, 2010](#)). One recent study introduced PEATMAP, which used high spatial resolution inventories of wetland distributions on regional, national, and global scales to create a new global peatland map. Another map, Peat-ML, used a machine learning approach and utilized soil and geomorphological data as inputs to create a spatially continuous estimate of global peatland extent ([Melton et al., 2022](#)). Yet another study aimed to estimate the peatland areas, depths, and volumes in the subtropics and tropics using an expert system model that relied on biophysical indices ([Gumbricht et al., 2017](#)). The [Gumbricht et al \(2017\)](#) study, PEATMAP ([Xu et al., 2018](#)), and Peat-ML ([Melton et al., 2022](#)) estimated tropical (23.5°S - 23.5°N) peatland extent to be $1.70 \times 10^6 \text{ km}^2$, $0.94 \times 10^6 \text{ km}^2$, $0.96 \times 10^6 \text{ km}^2$, respectively.

These areas are currently at risk of becoming C sources. In fact, many tropical peatlands have been reported as being sources of C in recent decades due to heavy disturbance ([Khakim et al., 2020](#); [Leng et al., 2019](#); [Lee et al., 2012](#); [Saharjo, 2006](#); [Simorangkir, 2006](#)). This disturbance can rise from both natural and anthropogenic sources. Natural disturbances in tropical peatlands typically occur due to drastic changes in the intensity and frequency of rainfall. The most intense

disturbances have occurred as a result of the strong effects caused by the El Niño-Southern Oscillation ([Page et al., 2002](#); [Khakim et al., 2020](#)). During periods of El Niño, the magnitude of the trade winds are weakened, resulting in an increase in sea surface temperatures (SST) in the central and eastern tropical Pacific Ocean. The above-average SST causes a change in atmospheric circulation, which thereby decreases rainfall in Southeast Asia and increases rainfall on the west coast of South America (i.e. in areas such as Peru). The relatively recent extreme instances of El Niño occurred in 1997 and 2015. In these instances, many Southeast Asian countries experienced heavy droughts which had a large impact on peatlands in the region ([Page et al., 2002](#); [Khakim et al., 2020](#)). If peat does not receive rainfall for an extended period of time, the surface layer will typically become abnormally dry. This dry surface peat layer will then be at a high risk of catching fire.

Tropical peatland fires are known to release a substantial amount of C to the atmosphere, and many of the fires persist due to smoldering combustion ([Turetsky et al., 2015](#)). In 1997 and 2015, the El Niño event played a significant role in the drying of the peat in Southeast Asia which resulted in devastating fires ([Page et al., 2002](#); [Khakim et al., 2020](#)). In addition to C emission, these tropical peatland fires emit immense amounts of particulate matter (PM). The combination of C and PM emissions can cause extreme reductions in air quality and may even lead to transboundary haze events ([Varkkey, 2013](#)). For instance, Kuching, a city in Malaysia on the island of Borneo, experienced drastically elevated PM, sulfur dioxide, carbon monoxide, and methane concentrations as a result of forest fires in Indonesia ([Davies et al., 1999](#)). Haze events can also decrease visibility, impact vegetation productivity ([Fan et al., 1990](#)), and result in severe economic losses ([Barber and Schweithelm, 2000](#)). One of the more major concerns, however, is

regarding its health effects. Lower fetal/infant survival rates ([Jayachandran, 2009](#)), increases in mortality rates ([Sahani et al., 2014](#); [Kopplitz et al., 2016](#)) and increases of respiratory problems ([Kunii et al., 2002](#)) have all been reported due to the hazardous air quality associated with haze events.

While natural disturbances can have large impacts on tropical peatlands, it is important to note that these are exacerbated by anthropogenic activity. Since anthropogenic disturbances are more prominent than natural disturbances in these systems, their impact is most often the greatest. Land conversion to agriculture has some of the largest impacts which, for tropical peatlands, mainly takes the form of creating land that is suitable for palm plantation establishment. First, the land is deforested, which directly removes the aboveground C store from the system. One of the more prominent methods for clearing land is called the “slash and burn” technique. This involves cutting down existing vegetation and then burning it to clear the land ([Lee et al., 2012](#); [Saharjo, 2006](#); [Simorangkir, 2006](#)). If not managed properly, these burning practices may turn into mega-fires, especially during times of extreme drought (i.e. during strong El Niño periods in Southeast Asia).

Overtime, the removal of biomass decreases the net peat C accumulation ([Könönen et al., 2016](#)). The diminished canopy cover also increases the amount of direct solar radiation received by the soil. This increases the surface soil temperature and eventually causes the soil to dry due to increased evaporation ([Dargie et al., 2019](#); [Jauhiainen et al., 2012](#)). After deforestation, the land is typically drained by constructing drainage canals. One study showed that these canals are highly widespread, occurring in 65% of Southeast Asian peatlands ([Dadap et al., 2021](#)). Generally, drainage facilitates crop growth and ensures that they provide maximum yield ([Dargie](#)

et al., 2019). However, this also causes a lowering of the WT which exposes the top peat layers to the atmosphere. The increase in oxygen availability allows certain microbes to undergo aerobic decomposition and enhances the release of CO₂ to the atmosphere. In addition, the drying of the top layer causes the peat to shrink, resulting in subsidence and an increase in peat bulk density (Hooijer et al., 2012). The presence of heavy machinery on peat also contributes to an increase in peat bulk density (Hooijer et al., 2012), which lowers the overall water holding capacity of the peat and makes the land more susceptible to flooding (Holden, 2005; Wösten et al., 2008; Posa et al., 2011; Evers et al., 2017).

To combat the ongoing degradation of tropical peatlands, some nations have implemented policies that encourage or even legally require the proper management of peat. For example, the Indonesian government has implemented policies such as the *Protection and Management of Peatland Ecosystem* and *Guideline on Oil Palm Plantation on Peatland* that give details on mandatory management practices (Evers et al., 2017). These include policies such as maintaining the WT between 60 cm and 80 cm during palm oil cultivation and prohibiting cultivation on areas where the peat depth is greater than 3 meters (Evers et al., 2017). Malaysia has also implemented policies, but unlike Indonesia, most are merely guidelines and not legally binding. For instance, the *Malaysian National Action Plan for Peatlands* gives recommendations for fire prevention and zero-burn strategies (Evers et al., 2017). Furthermore, through various research publications, the Malaysia Palm Oil Board has provided guidance to planters for best practices when cultivating on peatland (Evers et al., 2017). As for tropical South America and Africa, peatland-specific policies pushing for sustainability and conservation are generally lacking. Other initiatives have also been introduced that cover the regional scale. These include the

Association of Southeast Asian Nations (ASEAN) Peatland Management Initiative, the *ASEAN Peatland Management Strategy*, and the *Action Plan for Sustainable Management of Peatlands in ASEAN Member Countries* (Evers et al., 2017). This dissertation will contribute to the ongoing research of tropical peatlands by not only providing further knowledge on these systems, but to also ultimately aid in forming new, actionable policies that promote sustainable practices and effective conservation.

1.4 Dissertation Objectives and Questions

Given these research gaps, here I aim to study the contribution of tropical peatlands to the C cycle using remote sensing and in-situ observations. To do so, this dissertation focuses on three aspects:

1. The detection of water table level from space
2. Utilizing the water table level information to forecast fire probability
3. Quantifying soil GHG fluxes and its sensitivity to various environmental variables in three peatlands with varying disturbance regimes

The second chapter of this dissertation will attempt to study tropical peatlands from a different angle, namely through remote sensing. This approach will allow many of the previously inaccessible tropical peatlands to be studied, and therefore will provide a crucial foundation of knowledge to stakeholders and practitioners. As previously discussed, one of the most important aspects of tropical peatlands is their high potential for emitting C to the atmosphere and exacerbating ongoing climate change. Therefore, given the strong relationship between C emissions and WT, I explore the efficacy of a remote sensing-based model in reproducing

temporal WT fluctuations in tropical peatlands. The research questions for the second chapter are the following:

- Is OPTRAM capable of capturing temporal variations in tropical peatland WT?
- Does OPTRAM performance depend on the area where applied and/or extent of disturbance?
- Does OPTRAM performance depend on surface vegetation density?

Inputs of this model require surface reflectance values which I obtained from the Landsat 7 Enhanced Thematic Mapper Plus and Landsat 8 Operational Land Imager data products. The model was then validated at six different peatland sites spanning the countries of Indonesia, Malaysia, and Peru. It was found that OPTRAM performed optimally over regions with sparse vegetation and performed poorly in regions with high vegetation cover. More detailed information regarding the findings of this study are discussed in chapter 2.

The third chapter will expand on the model application by testing whether it is effective in predicting the probability of tropical peatland burned area occurrence. Using both the model output and burned area data from the Global Fire Emissions Database, I will test how well the model predicts the probability of burned area occurrence in tropical peatlands. This study will cover tropical peatlands in Indonesia, Malaysia, Peru, and Africa. Our research question is:

- Can OPTRAM be used to reliably predict burned area occurrence in tropical peatlands multiple days ahead of time?

The fourth chapter aims to contribute to the traditional in situ study of tropical peatlands through fieldwork in Malaysia. This work will involve comparing peat GHG emissions and its relationship with environmental variables within three peatland ecosystems with varying disturbance in Sarawak, Malaysia. The three peat ecosystems will be the following: an undrained peat swamp forest, a young oil palm plantation, a mature oil palm plantation. The research questions are the following:

- Do the relationships between soil GHG fluxes and water table level hold across tropical peatlands with differing disturbance regimes?
- Does soil GHG flux sensitivity to environmental controls such as air temperature, soil temperature, vapor pressure deficit, and precipitation hold across differing tropical peatland disturbance regimes?

1.5 References

- Barber, Charles Victor, and James Schweithelm. "Trial by fire." World Resources Institute, Washington, DC (2000).
- Bruhwiller, L., A. M. Michalak, R. Birdsey, D. N. Huntzinger, J. B. Fisher, J. Miller, R. A. Houghton, et al. "Chapter 1: Overview of the Global Carbon Cycle. Second State of the Carbon Cycle Report." U.S. Global Change Research Program, 2018. <https://doi.org/10.7930/SOCCR2.2018.Ch1>.
- Bwangoy, Jean-Robert B., Matthew C. Hansen, David P. Roy, Gianfranco De Grandi, and Christopher O. Justice. "Wetland Mapping in the Congo Basin Using Optical and Radar Remotely Sensed Data and Derived Topographical Indices." *Remote Sensing of Environment* 114, no. 1 (January 2010): 73–86. <https://doi.org/10.1016/j.rse.2009.08.004>.
- Calvin, Katherine, Dipak Dasgupta, Gerhard Krinner, Aditi Mukherji, Peter W. Thorne, Christopher Trisos, José Romero, et al. "IPCC, 2023: Climate Change 2023: Synthesis Report. Contribution of Working Groups I, II and III to the Sixth Assessment Report of the Intergovernmental Panel on Climate Change [Core Writing Team, H. Lee and J. Romero (Eds.)]. IPCC, Geneva, Switzerland." First. Intergovernmental Panel on Climate Change (IPCC), July 25, 2023. <https://doi.org/10.59327/IPCC/AR6-9789291691647>.
- Couwenberg, John, René Dommain, and Hans Joosten. "Greenhouse Gas Fluxes from Tropical Peatlands in South-East Asia: GREENHOUSE GAS FLUXES FROM TROPICAL PEATLANDS." *Global Change Biology* 16, no. 6 (July 1, 2009): 1715–32. <https://doi.org/10.1111/j.1365-2486.2009.02016.x>.
- Cox, P. M., Pearson, D., Booth, B. B., Friedlingstein, P., Huntingford, C., Jones, C. D., & Luke, C. M. (2013). Sensitivity of tropical carbon to climate change constrained by carbon dioxide variability. *Nature*, 494(7437), 341–344. <https://doi.org/10.1038/nature11882>
- Cox, P. M. (2019). Emergent Constraints on Climate-Carbon Cycle Feedbacks. *Current Climate Change Reports*, 5(4), 275–281. <https://doi.org/10.1007/s40641-019-00141-y>
- Dadap, Nathan C., Alison M. Hoyt, Alexander R. Cobb, Doruk Oner, Mateusz Kozinski, Pascal V. Fua, Krishna Rao, Charles F. Harvey, and Alexandra G. Konings. "Drainage Canals in Southeast Asian Peatlands Increase Carbon Emissions." *AGU Advances* 2, no. 1 (March 2021). <https://doi.org/10.1029/2020AV000321>.
- Dargie, Greta C., Ian T. Lawson, Tim J. Rayden, Lera Miles, Edward T. A. Mitchard, Susan E. Page, Yannick E. Bocko, Suspense A. Ifo, and Simon L. Lewis. "Congo Basin Peatlands: Threats and Conservation Priorities." *Mitigation and Adaptation Strategies for Global Change* 24, no. 4 (April 2019): 669–86. <https://doi.org/10.1007/s11027-017-9774-8>.

- Dargie, Greta C., Simon L. Lewis, Ian T. Lawson, Edward T. A. Mitchard, Susan E. Page, Yannick E. Bocko, and Suspense A. Ifo. "Age, Extent and Carbon Storage of the Central Congo Basin Peatland Complex." *Nature* 542, no. 7639 (February 2017): 86–90. <https://doi.org/10.1038/nature21048>.
- Davies, Stuart J. "Smoke-Haze from the 1997 Indonesian Forest Fires: Effects on Pollution Levels, Local Climate, Atmospheric CO₂ Concentrations, and Tree Photosynthesis." *Forest Ecology and Management*, 1999, 8.
- Deshmukh, Chandra S., Dony Julius, Ankur R. Desai, Adibtya Asyhari, Susan E. Page, Nardi Nardi, Ari P. Susanto, et al. "Conservation Slows down Emission Increase from a Tropical Peatland in Indonesia." *Nature Geoscience* 14, no. 7 (July 2021): 484–90. <https://doi.org/10.1038/s41561-021-00785-2>.
- Deshmukh, Chandra S., Dony Julius, Chris D. Evans, Nardi, Ari P. Susanto, Susan E. Page, Vincent Gauci, et al. "Impact of Forest Plantation on Methane Emissions from Tropical Peatland." *Global Change Biology* 26, no. 4 (April 2020): 2477–95. <https://doi.org/10.1111/gcb.15019>.
- Deshmukh, C. S., Susanto, A. P., Nardi, N., Nurholis, N., Kurnianto, S., Suardiwerianto, Y., Hendrizal, M., Rhinaldy, A., Mahfiz, R. E., Desai, A. R., Page, S. E., Cobb, A. R., Hirano, T., Guérin, F., Serça, D., Prairie, Y. T., Agus, F., Astiani, D., Sabiham, S., & Evans, C. D. (2023). Net greenhouse gas balance of fibre wood plantation on peat in Indonesia. *Nature*, 616(7958), 740–746. <https://doi.org/10.1038/s41586-023-05860-9>
- Dohong, Alue, Ammar Abdul Aziz, and Paul Dargusch. "A Review of the Drivers of Tropical Peatland Degradation in South-East Asia." *Land Use Policy* 69 (December 2017): 349–60. <https://doi.org/10.1016/j.landusepol.2017.09.035>.
- Dommain, René, Alexander R. Cobb, Hans Joosten, Paul H. Glaser, Amy F. L. Chua, Laure Gandois, Fuu-Ming Kai, et al. "Forest Dynamics and Tip-up Pools Drive Pulses of High Carbon Accumulation Rates in a Tropical Peat Dome in Borneo (Southeast Asia): Carbon Accumulation in Tip-up Pools." *Journal of Geophysical Research: Biogeosciences* 120, no. 4 (April 2015): 617–40. <https://doi.org/10.1002/2014JG002796>.
- Dommain, René, John Couwenberg, and Hans Joosten. "Development and Carbon Sequestration of Tropical Peat Domes in South-East Asia: Links to Post-Glacial Sea-Level Changes and Holocene Climate Variability." *Quaternary Science Reviews* 30, no. 7–8 (April 2011): 999–1010. <https://doi.org/10.1016/j.quascirev.2011.01.018>.
- Draper, Frederick C, Katherine H Roucoux, Ian T Lawson, Edward T A Mitchard, Euridice N Honorio Coronado, Outi Lähteenoja, Luis Torres Montenegro, Elvis Valderrama Sandoval, Ricardo Zaráte, and Timothy R Baker. "The Distribution and Amount of Carbon in the Largest Peatland Complex in Amazonia." *Environmental Research Letters* 9, no. 12 (December 1, 2014): 124017. <https://doi.org/10.1088/1748-9326/9/12/124017>.

- Evers, Stephanie, Catherine M. Yule, Rory Padfield, Patrick O'Reilly, and Helena Varkkey. "Keep Wetlands Wet: The Myth of Sustainable Development of Tropical Peatlands - Implications for Policies and Management." *Global Change Biology* 23, no. 2 (February 2017): 534–49. <https://doi.org/10.1111/gcb.13422>.
- Fan, Song-Miao, Steven C. Wofsy, Peter S. Bakwin, Daniel J. Jacob, and David R. Fitzjarrald. "Atmosphere-Biosphere Exchange of CO₂ and O₃ in the Central Amazon Forest." *Journal of Geophysical Research* 95, no. D10 (1990): 16851. <https://doi.org/10.1029/JD095iD10p16851>.
- Friedlingstein, P., O'Sullivan, M., Jones, M. W., Andrew, R. M., Hauck, J., Olsen, A., Peters, G. P., Peters, W., Pongratz, J., Sitch, S., Le Quéré, C., Canadell, J. G., Ciais, P., Jackson, R. B., Alin, S., Aragão, L. E. O. C., Arneeth, A., Arora, V., Bates, N. R., ... Zaehle, S. (2020). Global Carbon Budget 2020. *Earth System Science Data*, 12(4), 3269–3340. <https://doi.org/10.5194/essd-12-3269-2020>
- Friedlingstein, P., O'Sullivan, M., Jones, M. W., Andrew, R. M., Hauck, J., Landschützer, P., Le Quéré, C., Li, H., Luijkx, I. T., Olsen, A., Peters, G. P., Peters, W., Pongratz, J., Schwingshackl, C., Sitch, S., Canadell, J. G., Ciais, P., Jackson, R. B., Alin, S. R., ... Zeng, J. (2025). Global Carbon Budget 2024. *Earth System Science Data*, 17(3), 965–1039. <https://doi.org/10.5194/essd-17-965-2025>
- Furukawa, Yuichiro, Kazuyuki Inubushi, Mochamad Ali, A. M. Itang, and Haruo Tsuruta. "Effect of Changing Groundwater Levels Caused by Land-Use Changes on Greenhouse Gas Fluxes from Tropical Peat Lands." *Nutrient Cycling in Agroecosystems* 71, no. 1 (January 2005): 81–91. <https://doi.org/10.1007/s10705-004-5286-5>.
- Grundling, PL., Grootjans, A.P. (2018). Peatlands of Africa. In: Finlayson, C., Milton, G., Prentice, R., Davidson, N. (eds) *The Wetland Book*. Springer, Dordrecht. https://doi.org/10.1007/978-94-007-4001-3_112
- Gumbrecht, Thomas, Rosa Maria Roman-Cuesta, Louis Verchot, Martin Herold, Florian Wittmann, Ethan Householder, Nadine Herold, and Daniel Murdiyarso. "An Expert System Model for Mapping Tropical Wetlands and Peatlands Reveals South America as the Largest Contributor." *Global Change Biology* 23, no. 9 (September 2017): 3581–99. <https://doi.org/10.1111/gcb.13689>.
- Hadi, Abdul, Kazuyuki Inubushi, Yuichiro Furukawa, Erry Purnomo, Muhammad Rasmadi, and Haruo Tsuruta. "Greenhouse Gas Emissions from Tropical Peatlands of Kalimantan, Indonesia." *Nutrient Cycling in Agroecosystems* 71, no. 1 (January 2005): 73–80. <https://doi.org/10.1007/s10705-004-0380-2>.
- Harenda, Kamila M., Mariusz Lamentowicz, Mateusz Samson, and Bogdan H. Chojnicki. "The Role of Peatlands and Their Carbon Storage Function in the Context of Climate Change." In *Interdisciplinary Approaches for Sustainable Development Goals*, edited by Tymon Zielinski, Iwona Sagan, and Waldemar Surosz, 169–87. GeoPlanet: Earth and Planetary

- Sciences. Cham: Springer International Publishing, 2018. https://doi.org/10.1007/978-3-319-71788-3_12.
- Hergoualc'h, Kristell, Nelda Dezzee, Louis V. Verchot, Christopher Martius, Jeffrey Van Lent, Jhon Del Aguila-Pasquel, and Mariela López Gonzales. "Spatial and Temporal Variability of Soil N₂O and CH₄ Fluxes along a Degradation Gradient in a Palm Swamp Peat Forest in the Peruvian Amazon." *Global Change Biology* 26, no. 12 (December 2020): 7198–7216. <https://doi.org/10.1111/gcb.15354>.
- Hergoualc'h, Kristell, Jeffrey Van Lent, Nelda Dezzee, Louis V. Verchot, Jan Willem Van Groenigen, Mariela López Gonzales, and Julio Grandez-Rios. "Major Carbon Losses from Degradation of *Mauritia Flexuosa* Peat Swamp Forests in Western Amazonia." *Biogeochemistry*, June 22, 2023. <https://doi.org/10.1007/s10533-023-01057-4>.
- Hirano, Takashi, Hendrik Segah, Tsuyoshi Harada, Suwido Limin, Tania June, Ryuichi Hirata, and Mitsuru Osaki. "Carbon Dioxide Balance of a Tropical Peat Swamp Forest in Kalimantan, Indonesia." *Global Change Biology* 13, no. 2 (February 2007): 412–25. <https://doi.org/10.1111/j.1365-2486.2006.01301.x>.
- Holden, Joseph. "Peatland Hydrology and Carbon Release: Why Small-Scale Process Matters." *Philosophical Transactions of the Royal Society A: Mathematical, Physical and Engineering Sciences* 363, no. 1837 (December 15, 2005): 2891–2913. <https://doi.org/10.1098/rsta.2005.1671>.
- Hooijer, A., S. Page, J. Jauhiainen, W. A. Lee, X. X. Lu, A. Idris, and G. Anshari. "Subsidence and Carbon Loss in Drained Tropical Peatlands." *Biogeosciences* 9, no. 3 (March 20, 2012): 1053–71. <https://doi.org/10.5194/bg-9-1053-2012>.
- Huang, Yuanyuan, Phillipe Ciais, Yiqi Luo, Dan Zhu, Yingping Wang, Chunjing Qiu, Daniel S. Goll, et al. "Tradeoff of CO₂ and CH₄ Emissions from Global Peatlands under Water-Table Drawdown." *Nature Climate Change* 11, no. 7 (July 2021): 618–22. <https://doi.org/10.1038/s41558-021-01059-w>.
- Immirzi, C. P., Edward Maltby, and Richard S. Clymo. "The global status of peatlands and their role in carbon cycling." (1992).
- Inubushi, K., Y. Furukawa, A. Hadi, E. Purnomo, and H. Tsuruta. "Seasonal Changes of CO₂, CH₄ and N₂O Fluxes in Relation to Land-Use Change in Tropical Peatlands Located in Coastal Area of South Kalimantan." *Chemosphere* 52, no. 3 (July 2003): 603–8. [https://doi.org/10.1016/S0045-6535\(03\)00242-X](https://doi.org/10.1016/S0045-6535(03)00242-X).
- Jauhiainen, J., A. Hooijer, and S. E. Page. "Carbon Dioxide Emissions from an Acacia Plantation on Peatland in Sumatra, Indonesia." *Biogeosciences* 9, no. 2 (February 1, 2012): 617–30. <https://doi.org/10.5194/bg-9-617-2012>.

- Jayachandran, Seema. "Air Quality And Early-Life Mortality: Evidence From Indonesia's Wildfires". *Journal Of Human Resources*, vol 44, no. 4, 2009, pp. 916-954. University Of Wisconsin Press, <https://doi.org/10.1353/jhr.2009.0001>.
- Joosten, Hans. "The Global Peatland CO2 Picture: peatland status and drainage related emissions in all countries of the world." *The Global Peatland CO2 Picture: peatland status and drainage related emissions in all countries of the world*. (2010).
- Khakim, Mokhammad Yusup Nur, Akhmad Aminuddin Bama, Indra Yustian, Pradanto Poerwono, Takeshi Tsuji, and Toshifumi Matsuoka. "Peatland Subsidence and Vegetation Cover Degradation as Impacts of the 2015 El Niño Event Revealed by Sentinel-1A SAR Data." *International Journal of Applied Earth Observation and Geoinformation* 84 (February 2020): 101953. <https://doi.org/10.1016/j.jag.2019.101953>.
- Koh, Lian Pin, Jukka Miettinen, Soo Chin Liew, and Jaboury Ghazoul. "Remotely Sensed Evidence of Tropical Peatland Conversion to Oil Palm." *Proceedings of the National Academy of Sciences* 108, no. 12 (March 22, 2011): 5127–32. <https://doi.org/10.1073/pnas.1018776108>.
- Könönen, M., J. Jauhiainen, R. Laiho, P. Spetz, K. Kusin, S. Limin, and H. Vasander. "Land Use Increases the Recalcitrance of Tropical Peat." *Wetlands Ecology and Management* 24, no. 6 (December 2016): 717–31. <https://doi.org/10.1007/s11273-016-9498-7>.
- Kopplitz, Shannon N, Loretta J Mickley, Miriam E Marlier, Jonathan J Buonocore, Patrick S Kim, Tianjia Liu, Melissa P Sulprizio, et al. "Public Health Impacts of the Severe Haze in Equatorial Asia in September–October 2015: Demonstration of a New Framework for Informing Fire Management Strategies to Reduce Downwind Smoke Exposure." *Environmental Research Letters* 11, no. 9 (September 1, 2016): 094023. <https://doi.org/10.1088/1748-9326/11/9/094023>.
- Kunii, Osamu, Shuzo Kanagawa, Iwao Yajima, Yoshiharu Hisamatsu, Sombo Yamamura, Takashi Amagai, and Ir T. Sachrul Ismail. "The 1997 Haze Disaster in Indonesia: Its Air Quality and Health Effects." *Archives of Environmental Health: An International Journal* 57, no. 1 (January 2002): 16–22. <https://doi.org/10.1080/00039890209602912>.
- Lähteenoja, Outi, Bernardo Flores, and Bruce Nelson. "Tropical Peat Accumulation in Central Amazonia." *Wetlands* 33, no. 3 (June 2013): 495–503. <https://doi.org/10.1007/s13157-013-0406-0>.
- Lähteenoja, Outi, Kalle Ruokolainen, Leif Schulman, and José Alvarez. "Amazonian Floodplains Harbour Minerotrophic and Ombrotrophic Peatlands." *CATENA* 79, no. 2 (November 2009) (2009a): 140–45. <https://doi.org/10.1016/j.catena.2009.06.006>.
- Lähteenoja, Outi, Kalle Ruokolainen, Leif Schulman, and Markku Oinonen. "Amazonian Peatlands: An Ignored C Sink and Potential Source." *Global Change Biology* 15, no. 9 (September 2009) (2009b): 2311–20. <https://doi.org/10.1111/j.1365-2486.2009.01920.x>.

- Lappalainen, Eino. "Global Peat Resources (International Peat Society, Jyskä)." (1996).
- Lee, J., John Garcia-Ulloa, and L. Koh. "Biofuel expansion in Southeast Asia: biodiversity impacts and policy guidelines." (2012).
<http://dx.doi.org/10.1017/CBO9780511920899.014>
- Leifeld, J., & Menichetti, L. (2018). The underappreciated potential of peatlands in global climate change mitigation strategies. *Nature Communications*, 9(1), 1071.
<https://doi.org/10.1038/s41467-018-03406-6>
- Leng, Lee Yit, Osumanu Haruna Ahmed, and Mohamadu Boyie Jalloh. "Brief Review on Climate Change and Tropical Peatlands." *Geoscience Frontiers* 10, no. 2 (March 2019): 373–80. <https://doi.org/10.1016/j.gsf.2017.12.018>.
- Limpert, K. E., Carnell, P. E., Trevathan-Tackett, S. M., & Macreadie, P. I. (2020). Reducing Emissions From Degraded Floodplain Wetlands. *Frontiers in Environmental Science*, 8, 8. <https://doi.org/10.3389/fenvs.2020.00008>
- Liu, J., Bowman, K. W., Schimel, D. S., Parazoo, N. C., Jiang, Z., Lee, M., Bloom, A. A., Wunch, D., Frankenberg, C., Sun, Y., O'Dell, C. W., Gurney, K. R., Menemenlis, D., Gierach, M., Crisp, D., & Eldering, A. (2017). Contrasting carbon cycle responses of the tropical continents to the 2015–2016 El Niño. *Science*, 358(6360), eaam5690.
<https://doi.org/10.1126/science.aam5690>
- Melling, Lulie, Ryusuke Hatano, and Kah Joo Goh. "Soil CO₂ Flux from Three Ecosystems in Tropical Peatland of Sarawak, Malaysia." *Tellus B: Chemical and Physical Meteorology* 57, no. 1 (January 2005): 1–11. <https://doi.org/10.3402/tellusb.v57i1.16772>.
- Melton, Joe R., Ed Chan, Koreen Millard, Matthew Fortier, R. Scott Winton, Javier M. Martín-López, Hinsby Cadillo-Quiroz, Darren Kidd, and Louis V. Verchot. "A Map of Global Peatland Extent Created Using Machine Learning (Peat-ML)." Preprint. Biogeosciences, February 14, 2022. <https://doi.org/10.5194/gmd-2021-426>.
- Moore, S., Evans, C. D., Page, S. E., Garnett, M. H., Jones, T. G., Freeman, C., Hooijer, A., Wiltshire, A. J., Limin, S. H., & Gauci, V. (2013). Deep instability of deforested tropical peatlands revealed by fluvial organic carbon fluxes. *Nature*, 493(7434), 660–663.
<https://doi.org/10.1038/nature11818>
- Murdiyarso, D., K. Hergoualc'h, and L. V. Verchot. "Opportunities for Reducing Greenhouse Gas Emissions in Tropical Peatlands." *Proceedings of the National Academy of Sciences* 107, no. 46 (November 16, 2010): 19655–60. <https://doi.org/10.1073/pnas.0911966107>.
- Page, Susan E., John O. Rieley, and Christopher J. Banks. "Global and Regional Importance of the Tropical Peatland Carbon Pool: TROPICAL PEATLAND CARBON POOL." *Global Change Biology* 17, no. 2 (February 2011): 798–818. <https://doi.org/10.1111/j.1365-2486.2010.02279.x>.

- Page, Susan E., Florian Siegert, John O. Rieley, Hans-Dieter V. Boehm, Adi Jaya, and Suwido Limin. "The Amount of Carbon Released from Peat and Forest Fires in Indonesia during 1997." *Nature* 420, no. 6911 (November 2002): 61–65.
<https://doi.org/10.1038/nature01131>.
- Parish, Faizal, et al. "Assessment on peatlands, biodiversity and climate change." (2008).
- Posa, Mary Rose C., Lahiru S. Wijedasa, and Richard T. Corlett. "Biodiversity and Conservation of Tropical Peat Swamp Forests." *BioScience* 61, no. 1 (January 2011): 49–57.
<https://doi.org/10.1525/bio.2011.61.1.10>.
- Ribeiro, Kelly, Felipe S. Pacheco, José W. Ferreira, Eráclito R. Sousa-Neto, Adam Hastie, Guenther C. Krieger Filho, Plínio C. Alvalá, Maria C. Forti, and Jean P. Ometto. "Tropical Peatlands and Their Contribution to the Global Carbon Cycle and Climate Change." *Global Change Biology* 27, no. 3 (February 2021): 489–505.
<https://doi.org/10.1111/gcb.15408>.
- Rieley, J. O., et al. "Tropical peatlands: carbon stores, carbon gas emissions and contribution to climate change processes." Peatlands and climate change. International Peat Society, 2008. 148–181. <https://library.wur.nl/WebQuery/wurpubs/fulltext/41970>
- Rudiyanto, Budi I. Setiawan, Chusnul Arief, Satyanto K. Saptomo, Adrianto Gunawan, Kuswarman, Sungkono, and Hendri Indriyanto. "Estimating Distribution of Carbon Stock in Tropical Peatland Using a Combination of an Empirical Peat Depth Model and GIS." *Procedia Environmental Sciences* 24 (2015): 152–57.
<https://doi.org/10.1016/j.proenv.2015.03.020>.
- Sahani, Mazrura, Nurul Ashikin Zainon, Wan Rozita Wan Mahiyuddin, Mohd Talib Latif, Rozita Hod, Md Firoz Khan, Norhayati Mohd Tahir, and Chang-Chuan Chan. "A Case-Crossover Analysis of Forest Fire Haze Events and Mortality in Malaysia." *Atmospheric Environment* 96 (October 2014): 257–65.
<https://doi.org/10.1016/j.atmosenv.2014.07.043>.
- Saharjo, B. H. (2006). Shifting cultivation in peatlands. *Mitigation and Adaptation Strategies for Global Change*, 12(1), 135–146. <https://doi.org/10.1007/s11027-006-9048-3>
- Simorangkir, D. (2006). Fire use: Is it really the cheaper land preparation method for large-scale plantations? *Mitigation and Adaptation Strategies for Global Change*, 12(1), 147–164.
<https://doi.org/10.1007/s11027-006-9049-2>
- Sjögersten, Sofie, Colin R. Black, Stephanie Evers, Jorge Hoyos-Santillan, Emma L. Wright, and Benjamin L. Turner. "Tropical Wetlands: A Missing Link in the Global Carbon Cycle?: Carbon Cycling in Tropical Wetlands." *Global Biogeochemical Cycles* 28, no. 12 (December 2014): 1371–86. <https://doi.org/10.1002/2014GB004844>.
- Tang, Angela C. I., Paul C. Stoy, Ryuichi Hirata, Kevin K. Musin, Edward B. Aeries, Joseph Wenceslaus, and Lulie Melling. "Eddy Covariance Measurements of Methane Flux at a

- Tropical Peat Forest in Sarawak, Malaysian Borneo.” *Geophysical Research Letters* 45, no. 9 (May 16, 2018): 4390–99. <https://doi.org/10.1029/2017GL076457>.
- Tresder, Kathleen K., Sherri J. Morris, and Michael F. Allen. “The Contribution of Root Exudates, Symbionts, and Detritus to Carbon Sequestration in the Soil.” In *Agronomy Monographs*, edited by Richard W. Zobel and Sara F. Wright, 145–62. Madison, WI, USA: American Society of Agronomy, Crop Science Society of America, Soil Science Society of America, 2005. <https://doi.org/10.2134/agronmonogr48.c8>.
- Turetsky, Merritt R., Brian Benscoter, Susan Page, Guillermo Rein, Guido R. van der Werf, and Adam Watts. “Global Vulnerability of Peatlands to Fire and Carbon Loss.” *Nature Geoscience* 8, no. 1 (January 2015): 11–14. <https://doi.org/10.1038/ngeo2325>.
- Varkkey, Helena. “Patronage Politics, Plantation Fires and Transboundary Haze.” *Environmental Hazards* 12, no. 3–4 (December 2013): 200–217. <https://doi.org/10.1080/17477891.2012.759524>.
- Vitt, D. H. (2013). Peatlands. In *Encyclopedia of ecology* (Vol. 2, 2nd ed., pp. 557–566). <https://doi.org/10.1016/B978-0-12-409548-9.00741-7>
- Wang, W., Ciais, P., Nemani, R. R., Canadell, J. G., Piao, S., Sitch, S., White, M. A., Hashimoto, H., Milesi, C., & Myneni, R. B. (2013). Variations in atmospheric CO₂ growth rates coupled with tropical temperature. *Proceedings of the National Academy of Sciences*, 110(32), 13061–13066. <https://doi.org/10.1073/pnas.1219683110>
- Wösten, J.H.M., E. Clymans, S.E. Page, J.O. Rieley, and S.H. Limin. “Peat–Water Interrelationships in a Tropical Peatland Ecosystem in Southeast Asia.” *CATENA* 73, no. 2 (April 2008): 212–24. <https://doi.org/10.1016/j.catena.2007.07.010>.
- Xu, Jiren, Paul J. Morris, Junguo Liu, and Joseph Holden. “PEATMAP: Refining Estimates of Global Peatland Distribution Based on a Meta-Analysis.” *CATENA* 160 (January 2018): 134–40. <https://doi.org/10.1016/j.catena.2017.09.010>.
- Yu, Z. C. “Northern Peatland Carbon Stocks and Dynamics: A Review.” *Biogeosciences* 9, no. 10 (October 22, 2012): 4071–85. <https://doi.org/10.5194/bg-9-4071-2012>.
- Yu, Zicheng, Julie Loisel, Daniel P. Brosseau, David W. Beilman, and Stephanie J. Hunt. “Global Peatland Dynamics since the Last Glacial Maximum: GLOBAL PEATLANDS SINCE THE LGM.” *Geophysical Research Letters* 37, no. 13 (July 2010): n/a-n/a. <https://doi.org/10.1029/2010GL043584>.
- Zeng, N., Mariotti, A., & Wetzel, P. (2005). Terrestrial mechanisms of interannual CO₂ variability. *Global Biogeochemical Cycles*, 19(1), 2004GB002273. <https://doi.org/10.1029/2004GB002273>

Chapter 2: Tropical Peatland Water Table Estimations from Space

Koupaei-Abyazani, N., Burdun, I., Desai, A. R., Hergoualc'h, K., Hirano, T., Melling, L., Swails, E., Ing Tang, A. C., & Wong, G. X.¹

2.1 Introduction

Tropical peatlands contain ~20% of the global peatland carbon (C) stock (Leifeld & Menichetti, 2018; Page et al., 2011) despite covering ~12% of the global peatland area (Dohong et al., 2017; Joosten, 2009; Melton et al., 2022; Xu et al., 2018). These biomes act as large reservoirs for C and play a critical role in the global C cycle (Page et al., 2011; Ribeiro et al., 2021). Changes in peatland WT are documented to govern GHG flux variability, especially in tropical regions where there is ample precipitation (Adeolu et al., 2015; Hergoualc'h et al., 2023; Hirano et al., 2014, 2015; Holden et al., 2004; Kwon et al., 2013; Rosenberry et al., 2006; Strack et al., 2005; Taufik et al., 2022, 2023). Carbon dioxide (CO₂) fluxes are recorded to be greater when WT is lowered, while methane (CH₄) fluxes increase at persistently high WT (Hoyos-Santillan et al., 2019; Wong et al., 2020). Nitrous oxide (N₂O) is emitted in both drained and undrained peatlands as it is produced through nitrification in aerobic conditions and denitrification in anaerobic conditions (Parn et al., 2018; Swails et al., 2021). The high dependency of GHG fluxes on WT suggests that rewetting drained tropical peatlands may aid in reducing CO₂ emissions or enhancing sequestration (Lestari et al., 2022).

¹Reprinted from Koupaei-Abyazani, N., Burdun, I., Desai, A. R., Hergoualc'h, K., Hirano, T., Melling, L., Swails, E., Ing Tang, A. C., & Wong, G. X. (2024). Tropical Peatland Water Table Estimations From Space. *Journal of Geophysical Research: Biogeosciences*, 129(6), e2024JG008116. <https://doi.org/10.1029/2024JG008116>

The associated risk of increased CH₄ emissions is low and, therefore, unlikely to negate CO₂ emission reductions ([Hergoualc'h & Verchot, 2012](#); [Jauhiainen et al., 2008](#)).

Most peatland soils are characterized by their high porosity, allowing for high water storage capacity and high hydraulic conductivity ([Evers et al., 2017](#); [Huat et al., 2011](#); [Melling, 2016](#); [Taufik et al., 2022](#)). Drastic change in WT has been documented to have effects on peat bulk density ([Hooijer et al., 2012](#)), hydraulic conductivity ([Price, 2003](#)), subsidence ([Wösten et al., 1997](#)), and surface-layer oxidation ([Hooijer et al., 2012](#)). This is especially the case for tropical peatlands during El Niño events ([Khakim et al., 2020](#)).

In addition, low WT leads to decreases in soil moisture and puts the aerated layer of peat at risk of fire ([Dadap et al., 2019](#); [Wösten et al., 2008](#)), especially during the dry season and associated El Niño events in Southeast Asia. This can lead to extended smoldering periods ([Turetsky et al., 2015](#)) and extreme C emissions ([Christian, 2003](#); [Kuwata et al., 2017](#); [Parker et al., 2016](#); [Stockwell et al., 2014](#)) which poses a serious health risk due to transboundary haze episodes ([Cheong et al., 2019](#); [Davies, 1999](#); [Gaveau et al., 2014](#); [Promsiri et al., 2023](#); [Varkkey, 2013](#)). Furthermore, fires can have large effects on hydrologic stability through the burning of low-density surface-layer peat ([Thompson & Waddington, 2013](#)). There is evidence, though, that peatland restoration by rewetting an area may reduce fire hazard ([Taufik et al., 2023](#)).

Despite its environmental impact, the quantification of tropical peatland WT variability has not been well-documented relative to peatlands in temperate and boreal regions. To date, continuous ground-based WT observations are scarce, and those that do exist are spatially and temporally

limited (Busman et al., 2023; Dargie et al., 2017; Hergoualc'h et al., 2020; Hirano et al., 2012; Swails et al., 2021; Tang et al., 2018; Wright et al., 2013). Therefore, the spatiotemporal variability of tropical peatland WT is largely unknown, increasing uncertainties in all WT-dependent variables. As a result, it is crucial to resolve WT dynamics at high spatial resolution across a broad area to better understand its regional and local effects on GHG emissions and fire.

Some studies have purely used synthetic aperture radar (SAR) to monitor peatland WT (Bechtold et al., 2018; Kim et al., 2017), while several more have focused on only using optical approaches (Harris & Bryant, 2009; Kalacska et al., 2018; Meingast et al., 2014; Šimanauskienė et al., 2019). One study has used machine learning to predict spatiotemporal variability in tropical peatland WT (Hikouei et al., 2023), while another monitored this parameter via variabilities in Earth's gravitational field (Swails et al., 2019).

Tropical peatland hydrology has been simulated in a scalar-based hydrologic model (Cobb & Harvey, 2019), process-based land models (Apers et al., 2022; Mezbahuddin et al., 2015) and also utilized for reproducing effects on GHG fluxes (Mezbahuddin et al., 2014). While these efforts have proven somewhat successful, restrictions persist due to limited spatial estimations of tropical peatland hydrological parameters. The Optical Trapezoid Model (OPTRAM) (Sadeghi et al., 2017) may aid in closing this gap by providing reliable estimates of WT in these systems, and therefore reducing model uncertainty and improving our understanding of peatland hydrology in the tropics.

Here, we test the effectiveness of OPTRAM ([Sadeghi et al., 2017](#)) in capturing temporal, spatial, and spatiotemporal WT variability for the first time in tropical peatlands. OPTRAM, originally developed for estimating soil moisture, has previously been shown to reliably retrieve water tables in boreal and temperate peatlands ([Burdun, Bechtold, Sagris, Komisarenko, et al., 2020](#); [Burdun, Bechtold, Sagris, Lohila, et al., 2020](#); [Burdun et al., 2023](#); [Räsänen et al., 2022](#)).

However, it is assumed that WT retrieval in forested tropical peatlands is weaker due to more dense vegetation cover, though this has not been evaluated. We use satellite images from the Landsat 8 Operational Land Imager Collection 2 Level 2 and Landsat 7 Enhanced Thematic Mapper Plus Collection 2 Level 2 Surface Reflectance Products as inputs and validate the model using in situ WT measurements from six tropical peatland sites in Southeast Asia (Sarawak, Malaysia and Central Kalimantan, Indonesia) and South America (Loreto, Peru) with various disturbance (i.e., drained, undrained, degraded, and converted). We set out to answer the following questions:

- Is OPTRAM capable of capturing temporal variations in tropical peatland WT?
- Does OPTRAM performance depend on the area where applied and/or extent of disturbance?
- Does OPTRAM performance depend on surface vegetation density?

2.2 Methods

2.2.1 The Optical Trapezoid Model (OPTRAM)

OPTRAM was first proposed by [Sadeghi et al. \(2017\)](#) in response to the Thermal-Optical Trapezoid Model's shortcomings (Figure 2.1).

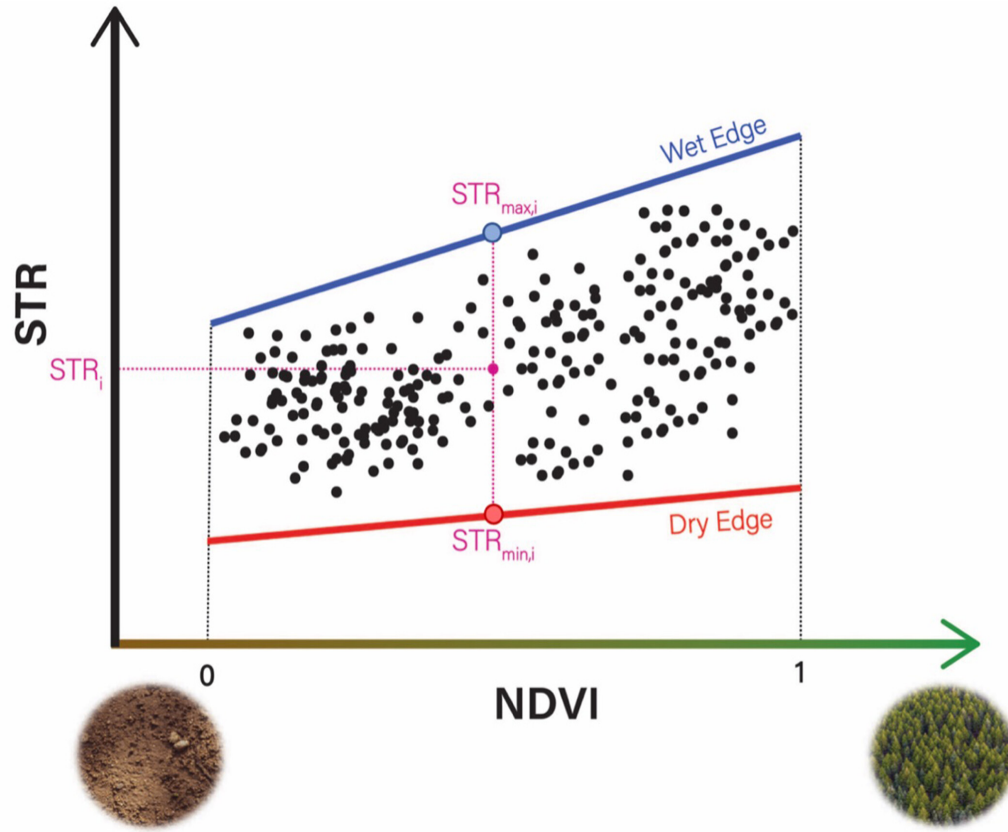


Figure 2.1: A diagram of the OPTRAM model. Individual pixels i (black dots) are plotted in the normalized difference vegetation index (NDVI) and shortwave infrared transformed reflectance (STR) space. Wet (blue line) and dry (red line) edges are determined through visual inspection. These edges are utilized in evaluating $STR_{max,i}$ and $STR_{min,i}$ for each pixel. STR_i represents the STR value for a given pixel. All three of these parameters are used in determining the OPTRAM index for each pixel via equation 2.5.

OPTRAM uses optical remote sensing data and relies on pixel distributions within the shortwave infrared transformed reflectance (STR) and normalized difference vegetation index (NDVI) space (Figure 2.2). NDVI acts as an indicator of vegetation density and health and is determined based on the interactions between light and chlorophyll ([Zeng et al., 2022](#)):

$$NDVI = \frac{S_{NIR} - S_{Red}}{S_{NIR} + S_{Red}} \quad (2.1)$$

where S_{NIR} and S_{Red} represent the near-infrared and red surface reflectance, respectively. STR is a manipulation of the shortwave infrared (SWIR) surface reflectance:

$$STR = \frac{(1 - S_{SWIR})^2}{(2)(S_{SWIR})} \quad (2.2)$$

where S_{SWIR} is the SWIR surface reflectance.

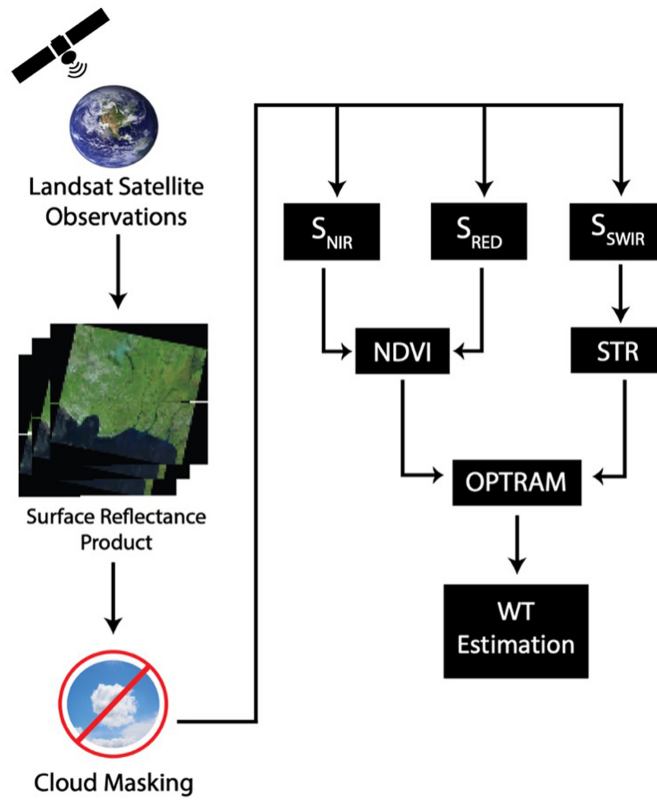


Figure 2.2: Flowchart illustrating steps followed for calculating OPTRAM and obtaining a WT estimation.

The STR-NDVI pixel distribution is used to define the dry and wet edges of the space (Figure 2.1), with each edge characterized by a linear equation:

$$STR_{min,i} = m_{min}NDVI + b_{min} \quad (2.3)$$

$$STR_{max,i} = m_{max}NDVI + b_{max} \quad (2.4)$$

$STR_{min,i}$, m_{min} , and b_{min} are the STR value, slope, and intercept for the dry edge, respectively. The same holds for $STR_{max,i}$, m_{max} , and b_{max} but for the wet edge. i indicates an arbitrary pixel in the STR-NDVI space within the dry and wet edges. These edges are typically drawn through visual inspection ([Chen et al., 2020](#); [Sadeghi et al., 2017](#)) and create a trapezoid around the pixel distribution (Figure 2.2).

After parameterization, $STR_{min,i}$ and $STR_{max,i}$ are used to calculate the OPTRAM index via the following equation:

$$OPTRAM\ INDEX = \frac{STR_i - STR_{min,i}}{STR_{max,i} - STR_{min,i}} \quad (2.5)$$

2.2.2 Satellite Images

For sites with in situ WT data during and after 2014 (Table 1), input variables for equations 2.1 and 2.2 were provided by the Landsat 8 Operational Land Imager Collection 2 Level 2 Surface Reflectance Product (L8 OLI). L8 OLI provides ground-level spectral reflectance across nine spectral bands at 30-m resolution every 16 days (Vermote et al., 2016). L8 OLI images were downloaded from the USGS Earth Explorer server (<https://earthexplorer.usgs.gov>) and the red, near-infrared (NIR), and SWIR surface reflectances were utilized for OPTRAM parameterization. This corresponds to bands 4 (0.64–0.67 μm), 5 (0.85–0.88 μm), and 7 (2.11–2.29 μm) in L8 OLI, respectively. Additionally, bands 4 and 5 were used to calculate NDVI, while band 7 was used to compute STR (Figure 2.2).

Country	Site ID	Coordinates	Years used	Publication	Nature of disturbance	Dominant vegetation cover
Indonesia	IN-undrained	2.32°S, 113.90°E	2015–2018	Hirano et al. (2012)	Selectively logged until late 1990s; Designated a National Park in 2006; Little drainage due to network of small canals	<i>Combretocarpus rotundatus</i> <i>Cratogeomys arborescens</i> <i>Buchanania sessifolia</i> <i>Tetramerista glabra</i>
	IN-drained	2.35°S, 114.04°E	2013–2017	Hirano et al. (2012)	Selectively logged until late 1990s; Drained	<i>Combretocarpus rotundatus</i> <i>Cratogeomys arborescens</i> <i>Buchanania sessifolia</i> <i>Tetramerista glabra</i>
Peru	PE-mDeg	3.8394°S, 73.3250°W	2015–2018	Hergoualc'h et al. (2020)	Moderately degraded (timber harvesting and palm cutting for fruit harvesting)	<i>Mauritia flexuosa</i>
	PE-hDeg	3.80898°S, 73.30713°W	2014–2018	Hergoualc'h et al. (2020)	Heavily degraded (timber harvesting and palm cutting for fruit harvesting)	<i>Mauritia flexuosa</i> <i>Cecropia membranacea</i>
Malaysia	MA-undrained	1.4536°N, 111.1494°E	2011–2014	Tang et al. (2020)	Logged before 2000; A totally protected area since 2000	<i>Shorea albida</i> <i>Lithocarpus</i> <i>Litsea</i> <i>Stemonurus</i>
	MA-converted	2.1860°N, 111.8459°E	2018–2019	Nishina et al. (2023)	Oil Palm Plantation converted from peat swamp forest in 2001	<i>Elaeis guineensis</i>

Table 2.1: Site Information Including Coordinates, Years of Data Used for Validation, Publication Source, Nature of Disturbance, and Dominant Vegetation Cover.

For sites with in situ data before 2014 (when L8 OLI was not yet online) (Table 1), we used the Landsat 7 Enhanced Thematic Mapper Plus Collection 2 Level 2 Surface Reflectance Product (L7 ETM+) (Masek et al., 2006). Like L8 OLI, L7 ETM+ provides ground-level spectral reflectance at 30-m resolution with a 16-day repeat cycle but has only eight spectral bands compared to L8 OLI's nine. These images were also downloaded from the USGS Earth Explorer server and were manipulated such that L7 ETM+ images overlapped with L8 OLI images to ensure similar regional coverage. The bands used from L7 ETM+ were bands 3 (red; 0.63–0.69 μm), 4 (NIR; 0.77–0.90 μm), and 7 (SWIR; 2.08–2.35 μm). L7 ETM+ and L8 OLI bands were not cross-harmonized. It is important to note that the Scan Line Corrector, which compensates for the forward motion of the Landsat 7 satellite, failed permanently in May 2003. As a result, the image area was duplicated. These duplicated areas have been removed, causing data gaps. Despite removing duplicated areas, about 78% of the pixels are still available (<https://www.usgs.gov/landsat-missions/landsat-7>). All calculations and analyses were conducted in Python (version 3.8.13 and 3.9.18).

Many L7 ETM+ and L8 OLI images contain cloudy pixels, especially in the tropics. This blocks specific wavelengths from reaching the instrument, and these pixels are therefore deemed unusable for OPTRAM. To account for this, we only used images with a cloud cover of 50% or less as determined by the “C function of mask” algorithm (Foga et al., 2017). To further omit cloudy L8 OLI pixels, we filtered pixels via the product's quality assurance flags outlined in the Landsat 8–9 Collection 2 Level 2 Science Product Guide version 5 (Masek et al., 2006). Only pixels labeled as “clear” were kept in our analysis. To further constrain the amount of cloudy L7 ETM+ pixels, we only kept pixels characterized as “low cloud confidence” according to the

Landsat 4–7 Collection 2 Level 2 Science Product Guide version 4 ([Cook, 2014](#); [Cook et al., 2014](#); [Vermote et al., 2016](#)). These measures allowed OPTRAM to be run with largely unobstructed surface reflectance values, resulting in more reliable OPTRAM indices and, consequently, a better representation of surface water content.

2.2.3 Site Descriptions

OPTRAM was validated using in situ WT from sites in Indonesia ([Hirano et al., 2012, 2015](#)), Malaysia ([Nishina et al., 2023](#); [Tang et al., 2020](#)), and Peru ([Hergoualc'h et al., 2020](#)). The Indonesian peat swamp forest sites are located near Palangkaraya in Central Kalimantan, Indonesia and vary in disturbance. One is relatively intact with little drainage (IN-undrained; 2.32°S, 113.90°E), while the other is drained (IN-drained; 2.35°S, 114.04°E) ([Ohkubo et al., 2021](#)) (Figures 2.3 and 2.4). Both were selectively logged until the late 1990s. IN-undrained resides in an area designated a National Park in 2006. The undrained site contains a network of small canals while the drained site contains a large canal (25 m wide and 3.5–4.5 m deep) which is ~400 m from the site ([Hirano et al., 2012](#)). At these two sites, WT was measured half-hourly via a water level logger (DL/N; Sensor Technik Sirnach AG, Sirnach, Switzerland or DCX-22 VG; Keller AG, Winterthur, Switzerland) ([Hirano et al., 2007](#); [Ohkubo et al., 2021](#)).

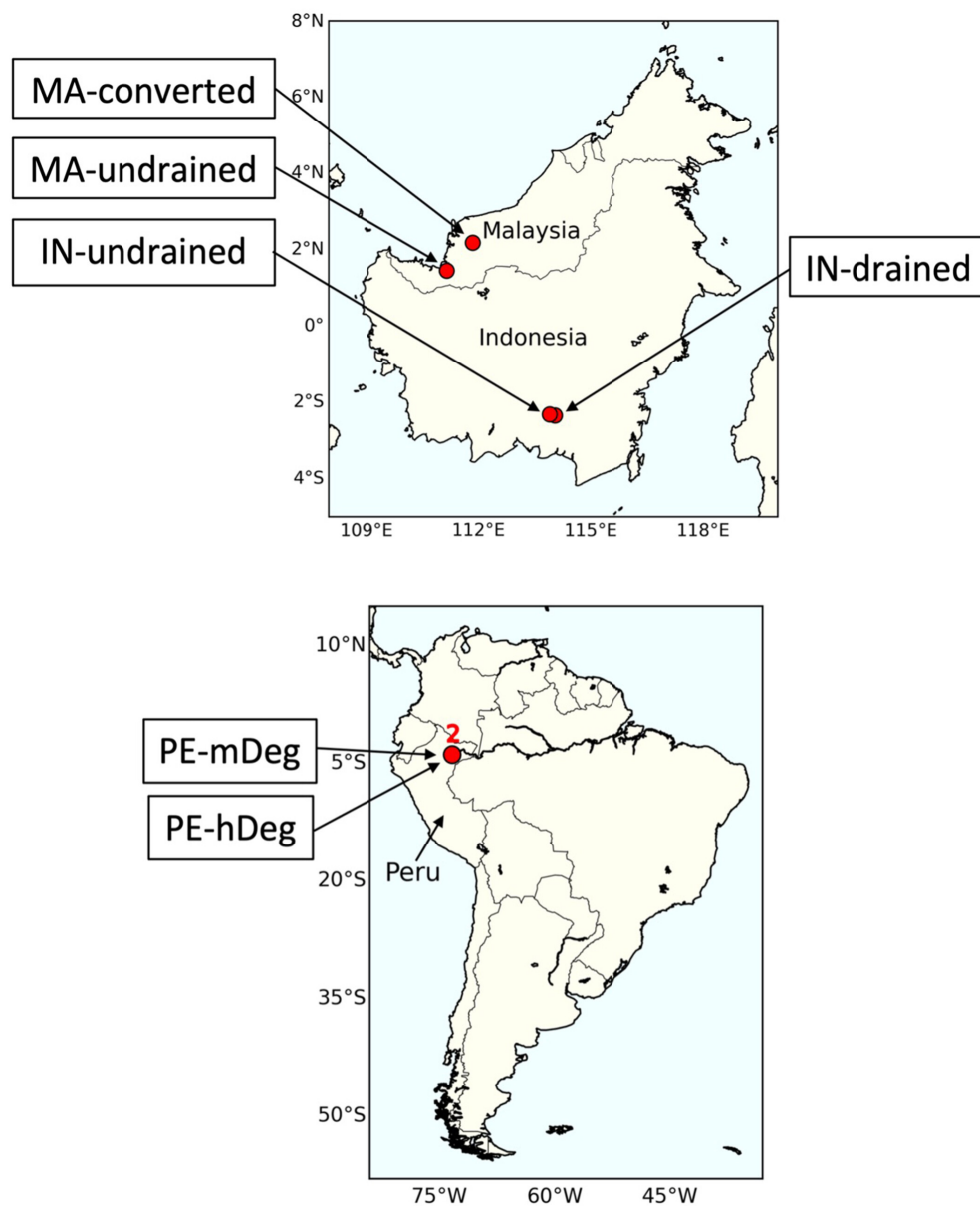


Figure 2.3: Locations of sites used for OPTRAM validation.

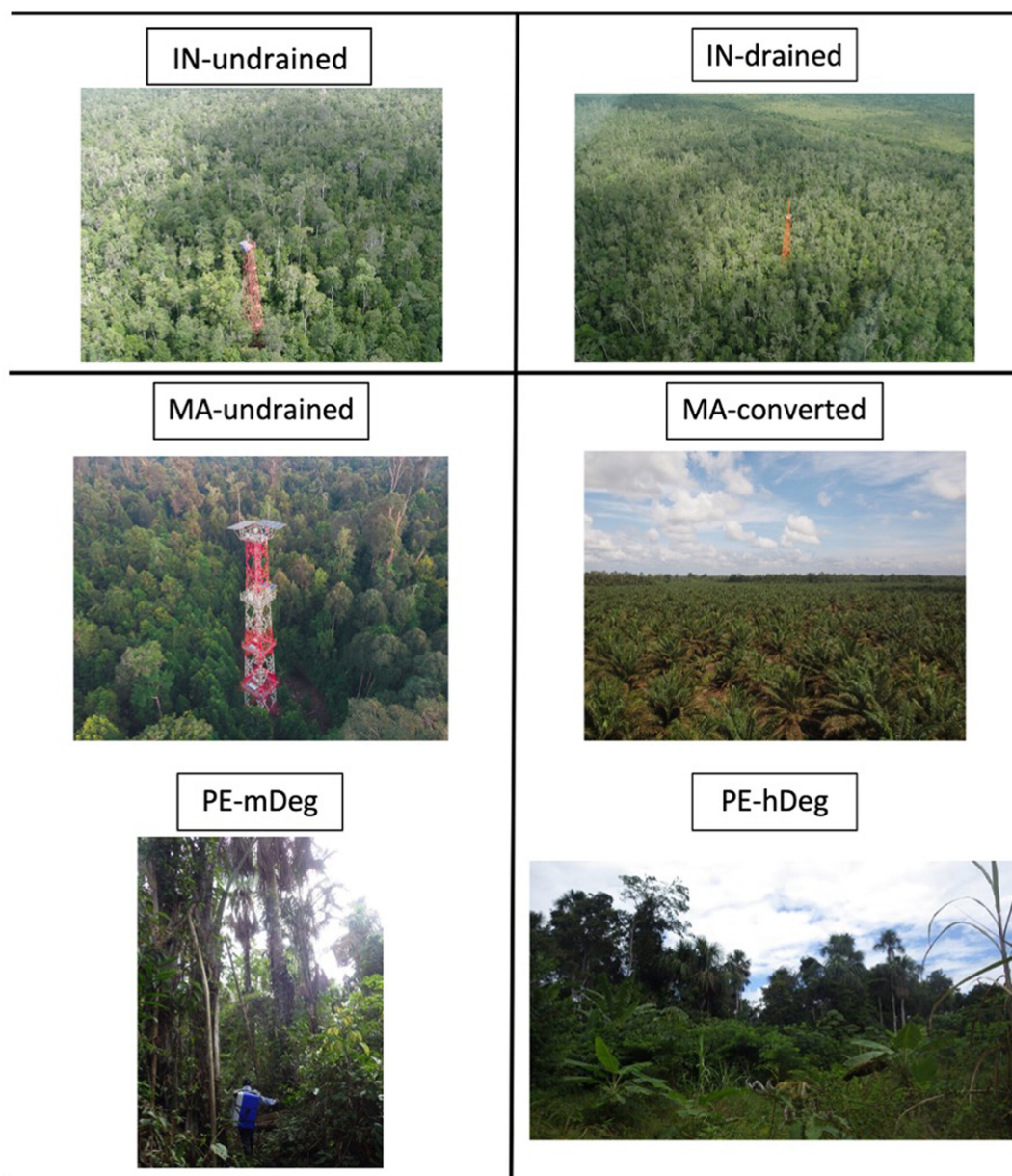


Figure 2.4: Pictures of sites used for OPTRAM validation.

Two other sites are located in Malaysia. One is an undrained peat swamp forest (PSF) in Maludam National Park in the Betong Division of Sarawak, Malaysia (MA-undrained; 1.4536°N, 111.1494°E) ([Tang et al., 2020](#)). This site has been subject to large-scale protection measures since 2000, and presents a WT near or above the peat surface ([Tang et al., 2020](#)). WT was measured on a half-hourly basis via a water level logger (DL/N 70 STS Sensor, Technik Sirnach AG) ([Tang et al., 2020](#)). The other site is an oil palm plantation converted from peat swamp forest in 2001 (MA-converted; 2.1860°N, 111.8459°E) ([Nishina et al., 2023](#)) (Figures 2.3 and 2.4). MA-converted contains numerous drainage ditches which were likely used to facilitate oil palm plantation establishment ([Nishina et al., 2023](#)). The water table at MA-converted was measured every half hour by a piezometer (HOBO, Onset, Bourne, MA, USA).

The Peruvian sites are located in the Northern Peruvian Amazon in Loreto province and comprise a moderately degraded (PE-mDeg; 3.8394°S, 73.32502°W) and heavily degraded (PE-hDeg; 3.80898°S, 73.30713°W) PSF ([Hergoualc'h et al., 2020](#)) (Figures 2.3 and 2.4). Both sites were subject to *M. flexuosa* palm cutting for fruit harvesting and logging. The WT relative to the soil surface was monitored in a perforated polyvinyl chloride tube (diameter: 5 cm; length: 1.5 m) installed permanently in the soil ([Hergoualc'h et al., 2020](#)). WT data at PE-mDeg and PE-hDeg were computed to site-scale using the relative proportion of area occupied by cut palms on a hummock and adjacent hollow, and live palms on a hummock and adjacent hollow ([Hergoualc'h et al., 2020](#); [Hergoualc'h, 2024](#)).

The site years used for OPTRAM validation were 2015–2018 for IN-undrained, 2013–2017 for IN-drained, 2011–2014 for MA-undrained, 2018–2019 for MA-converted, 2015–2018 for PE-

mDeg, and 2014–2018 for PE-hDeg (Table 1). Lack of continuous daily data for PE-mDeg and PE-hDeg forced us to use L8 OLI images that did not align exactly with dates of in situ WT data. Although WT did not substantially vary on small timescales (i.e., days to weeks) (Hergoualc'h et al., 2020), we caution that results at these sites may be affected by this misalignment to a certain degree.

2.2.4 Data Computation and Statistical Testing

To assess OPTRAM's capability for reproducing the variability in WT (and not exact values), we constructed a matrix of spatially identical in situ WT values covering a 5–9 km radius centered around the location of WT measurement. We also created a matrix of OPTRAM indices with values varying based on topographical characteristics (see summarized workflow in Figure 2.2). The Pearson correlation coefficient (R) was utilized to assess OPTRAM's effectiveness in capturing temporal variability in WT:

$$R = \frac{\sum_{i=1}^N (y_i - \bar{y})(p_i - \bar{p})}{\sqrt{\sum_{i=1}^N (y_i - \bar{y})^2 \sum_{i=1}^N (p_i - \bar{p})^2}} \quad (2.6)$$

where y_i and p_i represent the in situ WT observation and OPTRAM estimation at time index i , respectively. \bar{y} denotes the mean of the observations while \bar{p} indicates the mean of the estimates. N is the number of data points. The per-pixel correlation was then projected onto the map of the site to create a correlation map. Model performance was evaluated using the “best pixel” approach (Burdun, Bechtold, Sagris, Lohila, et al., 2020) which involves choosing the highest R -value to represent the correlation between OPTRAM index and in situ WT.

Due to cloud masking, the Pearson-R correlation value for each pixel was not calculated with the same number of data points. To test the impact of this issue on results, we constructed a spatial distribution of “number of data points” for each pixel and compared it with each site's Pearson-R correlation map. In addition, the scarcity of long-term data records further limited the number of data points that could be included. Therefore, we set a threshold for the number of data points to be included in certain sites when identifying the “best pixel.” This was done to omit erroneously high Pearson-R values due to a low number of data points. For MA-converted, PE-mDeg, and PE-hDeg, the “best pixel” was determined from a pool of pixels with a number of data points ≥ 13 . For IN-drained and MA-undrained, the threshold was set at 21 and 17, respectively. There was no threshold for other sites due to the relatively high number of data points at the “best pixel” location.

2.2.5 OPTRAM and Vegetation Density

In a previous study in northern peatlands ([Burdun, Bechtold, Sagris, Lohila, et al., 2020](#)), the performance of OPTRAM was optimal in areas with minimal shrubs or trees. To test this in tropical peatlands, we used NDVI as an indicator for vegetation density ([Zaitunah et al., 2018](#)). NDVI's assessment of vegetation “greenness” is correlated with vegetation crown density, allowing its use as a proxy for vegetation density ([Zaitunah et al., 2018](#)). Afterward, we assessed its relationship with the OPTRAM index-WT Pearson-R value on a per-pixel basis. High and low NDVI values represented high and low vegetation density, respectively. Since tropical PSF are characterized by evergreen vegetation, we calculated NDVI using only September surface reflectance values for each site. This month was chosen due to being at the end of the dry season

and consequently creating conditions where satellite images are less likely to be obscured by cloud cover.

2.2.6 Testing Relationship Differences Between El Niño and Non-El Niño Years

The years of data used for four of the sites fell within the 2015–2016 strong El Niño year (IN-undrained, IN-drained, PE-mDeg, and PE-hDeg). However, only the IN-undrained and IN-drained sites were used since PE-mDeg and PE-hDeg did not have sufficient data for analysis. The El Niño period was defined to occur from January 2015 through March 2016. A two-sided t-test was used to calculate the 95% confidence interval for the slopes of El Niño and non-El Niño regression lines. Slopes were considered significantly different if 95% confidence intervals did not overlap with one another. These were applied to pixels with the first, second, and third largest Pearson-R value.

2.2.7 Uncertainty Analysis

We utilized a cross-validation approach to incorporate uncertainty in OPTRAM's ability for detecting changes in WT. The best pixel for each site was chosen for this analysis. We fitted a regression line using the “linregress” function from the “stats” module within the “SciPy” library in Python. The regression line was fitted using all but one single data point. We then calculated the difference between the observed and predicted OPTRAM index values. This was repeated for all data points. The mean absolute error (MAE) was then calculated as:

$$MAE = \frac{\sum_{i=1}^n |x_i - y_i|}{n} \quad (2.7)$$

where x_i , y_i , and n represent the observed OPTRAM index value, predicted OPTRAM index value, and number of data points, respectively.

2.3 Results

2.3.1 OPTRAM Parameterization

We observed a positive relationship between the STR and NDVI across most sites, with varied type of relationship (i.e., linear, exponential, etc.) depending on the date (Figure 2.5). For example, Figure 2.5 shows a linear relationship between STR and NDVI at IN-undrained at the end of January and September 2018, while an exponential relationship was observed at the beginning of May and December 2018.

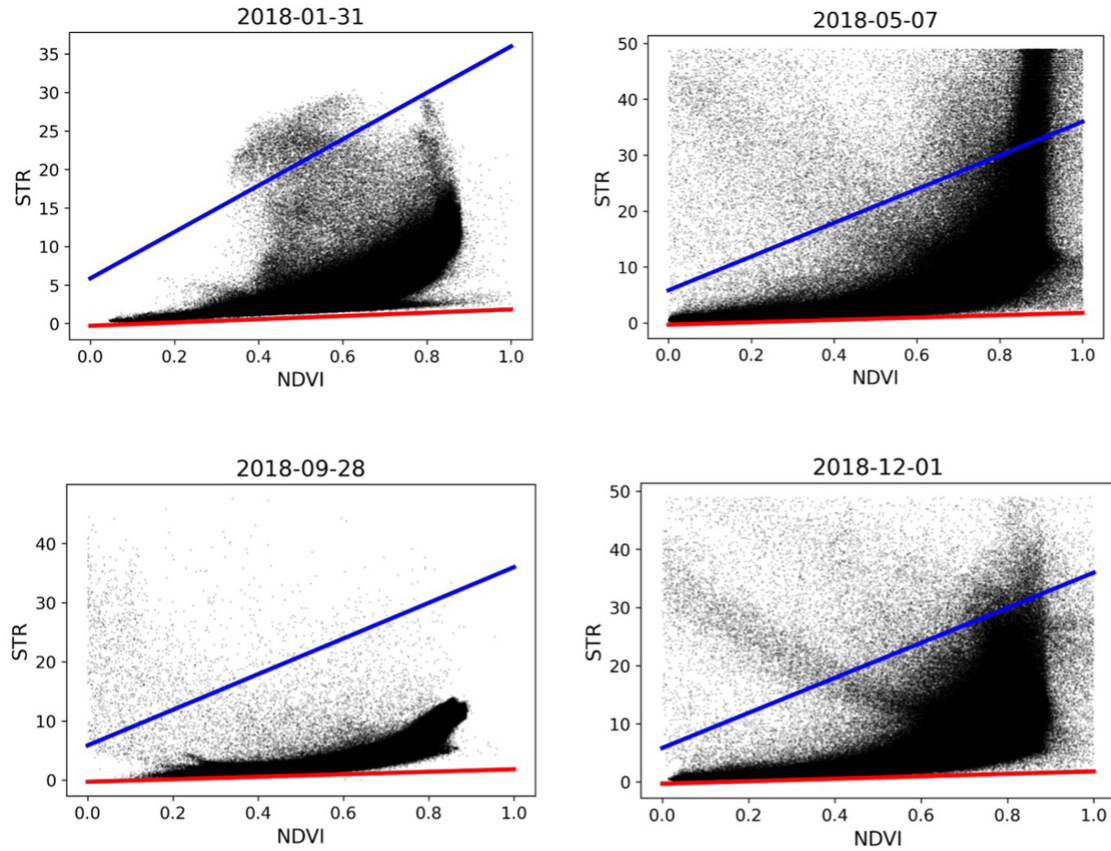


Figure 2.5: 30-m resolution Landsat 8 pixels plotted in the shortwave infrared transformed reflectance (STR) and normalized difference vegetation index (NDVI) space. Only four dates in 2018 are shown at IN-undrained to illustrate the diversity in pixel distributions. The wet edge is represented by the blue line and the dry edge is the red line. These were drawn through visual inspection such that most of the pixels resided between the two lines. Note that the slope and intercept of these lines remain constant for each date. m_{min} , b_{min} , m_{max} , and b_{max} were 2.121, -0.296 , 30.134, and 5.856, respectively.

The STR value peaked within the dense pixel area at an NDVI of ~ 0.85 – 0.9 on all four different dates (Figure 2.5). The wet and dry edges were determined via visual inspection by drawing two lines such that, between them, a majority of the pixels were contained (Figure 2.5). This resulted in the following parameterization:

$$STR_{min,i} = (2.121)(NDVI) - 0.296 \quad (2.8)$$

$$STR_{max,i} = (30.134)(NDVI) + 5.856 \quad (2.9)$$

These values for m_{min} , b_{min} , m_{max} , b_{max} were used for all sites and dates. While images with cloud cover of 50% or less were retained for analysis, we did not further filter pixels using quality assurance flags at this stage.

2.3.2 In Situ Water Table Variability

In situ WT varied considerably over time at all sites. At IN-undrained, WT exhibited a distinct seasonal cycle, fluctuating between an average depth of ~ -60 cm and the peat surface, with the exception of the 2015 dry season (very strong El Niño year) when WT reached a depth as low as ~ 140 cm below the peat surface (Hirano, 2023) (Figure 2.6). At IN-drained, similar temporal variability in WT was observed (Figure 2.6). At MA-undrained, WT had a seasonal cycle, with WT being mostly below the peat surface during the dry seasons and above during the wet seasons. From 2011 through 2014, WT varied between ~ -39 and ~ 24 cm (Figure 2.6) (Melling & Wong, 2024).

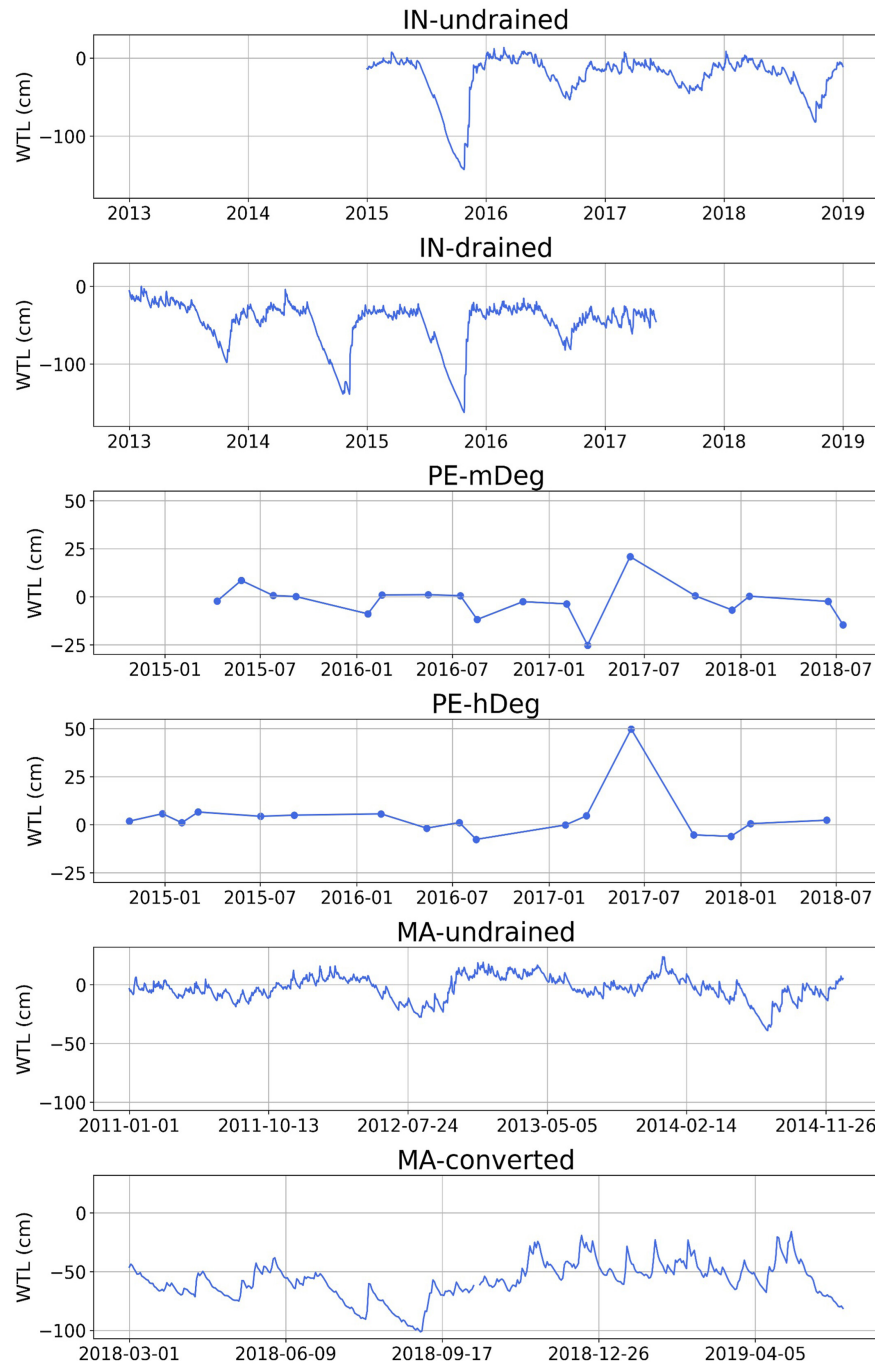


Figure 2.6: Time series of daily averaged in situ water table (WT) at the Indonesian and Malaysian sites. For Peruvian sites, time series shows the WT approximately every 2–5 months. A positive WT indicates a water table above the peat surface. Note that dates for IN-undrained and IN-drained and dates for PE-mDeg and PE-hDeg align. WT data used from [Hirano et al. \(2012\)](#), [Tang et al. \(2020\)](#), and [Hergoualc'h et al. \(2020\)](#).

The sampling frequency was lower at Peruvian sites, occurring monthly (we show every 2–5 months in Figure 2.6), compared to the daily sampling at IN-undrained and IN-drained (Hirano, 2023). At PE-mDeg, WT remained at or near the peat surface during the sampling period from 2015 to 2016 and increased to ~20 cm in mid-2017 (Figure 2.6) (Hergoualc'h, 2024). Similarly, WT was close to the peat surface throughout 2015 and 2016 at PE-hDeg. However, in mid-2017, WT at PE-hDeg increased to ~50 cm, concurrent with the increase observed at PE-mDeg (Figure 2.6) (Hergoualc'h, 2020; Hergoualc'h, 2024).

2.3.3 Estimating Tropical Peatland Water Table Variability via OPTRAM

Overall, the performance of OPTRAM in reproducing the temporal variability of tropical peatland WT varied spatially and was largely dependent on the density of vegetation. At IN-undrained, the relationship between OPTRAM index and in situ WT greatly varied ($\sim -0.7 < R < \sim 0.95$). In areas with little to no vegetation, OPTRAM performance was optimal, with Pearson-R values $> \sim 0.6$ (Figure 2.7). Moreover, Pearson-R correlations of up to 0.94 were found, with the “best pixel” ($R = 0.94$; $p < 0.001$) located in an area with minimal vegetation cover. Conversely, no significant correlation was found at the location of in situ WT measurement where there was abundant tree cover ($R = -0.17$; $p > 0.05$).

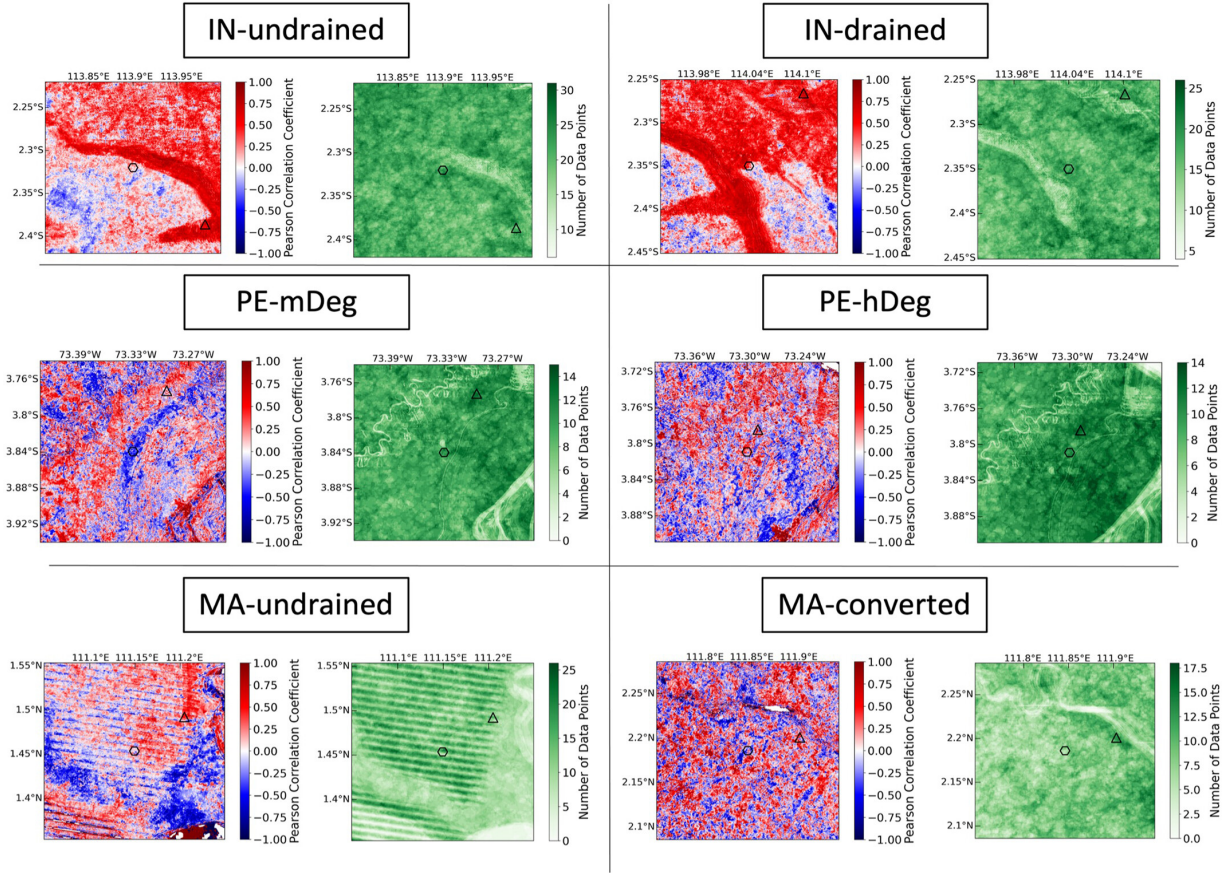


Figure 2.7: Pearson-R correlation values (30-m resolution) and number of data points (NDP) per pixel (30-m resolution) at all study sites. The middle hexagon is the location of in situ water table measurement and the triangle is the location of the “best pixel” (pixel with largest positive Pearson-R within the domain).

At IN-drained, a similar result was obtained. Areas with low vegetation cover were also areas where OPTRAM was best at detecting temporal WT variability (Figure 2.7). Areas with high vegetation showed spatially sporadic correlations ranging from $R = \sim -0.6$ to $R = \sim 0.5$ (Figure 2.7). At the location of in situ WT measurement, the R-value was 0.62 ($p < 0.05$; without outlier), with the “best pixel” yielding an R-value of 0.87 ($p < 0.001$; when only pixels with 21 or more data points were considered) (Figure 2.7).

For PE-mDeg, correlations were once again relatively high ($R > 0.5$) in areas with low vegetation cover (Figure 2.7). This was superimposed with areas that had zero correlation due to the presence of buildings and ponds. Areas with high vegetation cover were associated with sporadic correlations that ranged from $R = \sim -0.75$ to $R = \sim 0.5$) (Figure 2.7). OPTRAM did not capture WT variability at the location of WT measurement ($R = -0.32$; $p > 0.05$). The “best pixel” ($R = 0.82$; $p < 0.001$) was in an area with relatively minimal vegetation cover (Figure 2.7).

Correlation patterns at PE-hDeg varied drastically relative to that of PE-mDeg. Besides an area of high correlation values that was observed from the middle left section to the top middle section, there were no other notable patterns between vegetation density and correlation strength between OPTRAM index and in situ WT (Figure 2.7). A positive correlation was found at the location of WT measurement ($R = 0.57$; $p > 0.05$) (Figure 2.7). The “best pixel” ($R = 0.79$; $p < 0.05$; without outlier), in this case, should not be given credence due to the primarily disordered relationship between vegetation density and correlation strength.

Unlike other sites, MA-undrained showed higher correlations in the presence of moderate vegetation cover ($R = \sim 0.5$). The “best pixel” ($R = 0.49$; $p > 0.05$; without outlier) was in an area with relatively low vegetation cover. The location of WT measurement (Melling & Wong, 2024) was situated in an area with relatively high vegetation cover and yielded a correlation of $R = -0.17$; $p > 0.05$) (Figure 2.7).

Similar to PE-hDeg, the correlation distributions at MA-converted did not show a pattern between high and low vegetated areas (Figure 2.7). Therefore, the “best pixel” R-value ($R =$

0.88; $p < 0.001$) cannot be regarded as being an accurate representation of OPTRAM performance. At the location of WT measurement, the R-value was 0.007 with a corresponding p-value greater than 0.05 (Figure 2.7).

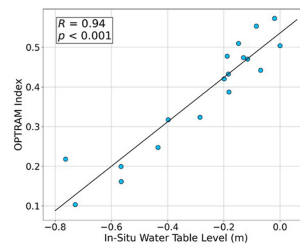
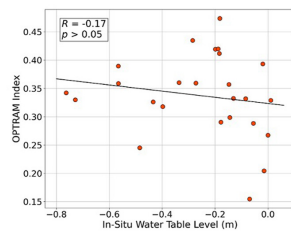
The “best pixel” scatterplots (Figure 2.8) show for all sites a fairly universal relationship between OPTRAM index and in situ WT, with an increase of OPTRAM index by ~ 0.1 for every ~ 20 cm increase in WT. This was true even for sites that had outliers.

Site

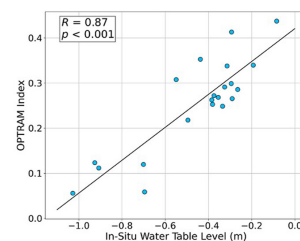
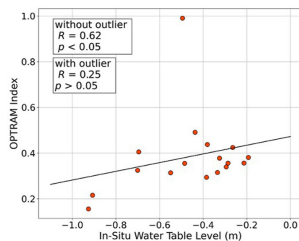
**WT
Monitoring
Location**

**“Best Pixel”
Location**

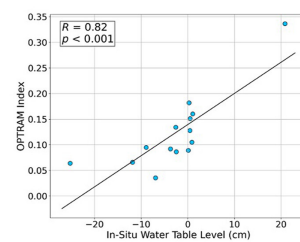
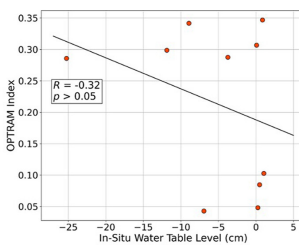
IN-undrained



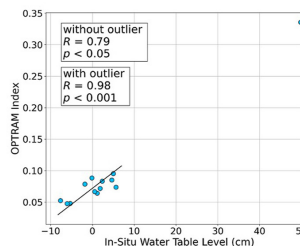
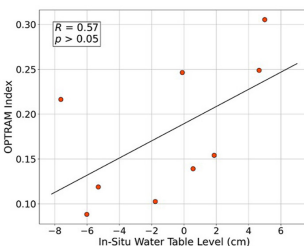
IN-drained



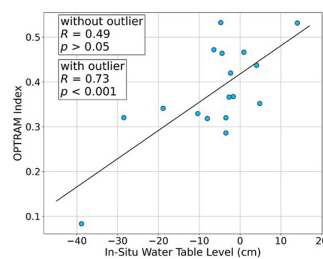
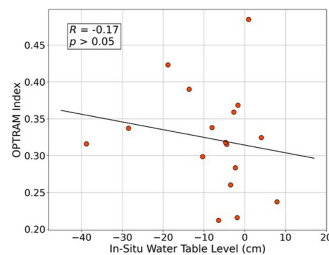
PE-mDeg



PE-hDeg



MA-undrained



MA-converted

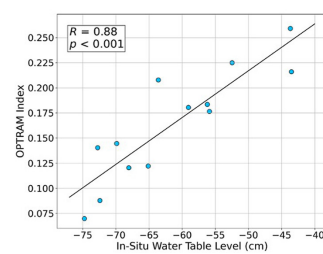
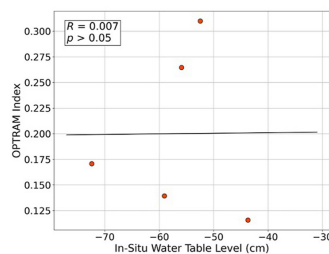


Figure 2.8: Scatterplots showcasing the correlation between OPTRAM index and in situ WT at each site. The red points are taken at the WT monitoring location and the blue are located at the “best pixel” location.

2.3.4 NDVI's Influence on OPTRAM Performance

For IN-undrained and IN-drained, as NDVI increased, Pearson-R tended to decrease (Figure 2.S1 in Supporting Information). The two Indonesian sites also experienced mostly positive Pearson-R values below an NDVI of ~ 0.6 (Figure 2.S1 in Supporting Information). For PE-mDeg and PE-hDeg, the pixels did not show a noticeable trend, and instead showed Pearson-R values that ranged from ~ -0.75 to 0.75 from an NDVI of ~ 0.15 – 0.85 (Figure 2.S1 in Supporting Information). However, at an NDVI of ~ 0.85 , most pixels were situated within a Pearson-R value of -0.5 to 0.5 (Figure 2.S1 in Supporting Information). MA-undrained showed little relationship between Pearson-R and NDVI. Most pixels were located at NDVI greater than ~ 0.6 and there was a wide spread of Pearson-R values above an NDVI of ~ 0.7 (Pearson-R value range of ~ -0.7 to 0.75) (Figure 2.S1 in Supporting Information). MA-converted, like PE-mDeg and PE-hDeg, did not show a noticeable trend, with Pearson-R values ranging from ~ -0.6 to ~ -0.85 across most NDVI values (mostly when NDVI $> \sim 0.6$) (Figure 2.S1 in Supporting Information).

At all sites, pixels with NDVI values 0 – 0.4 and 0.4 – 0.7 also had higher average correlation values relative to pixels with NDVI values between 0.7 and 1 (Figure 2.9). At IN-undrained, the average R values were approximately the same for NDVI values 0 – 0.4 and 0.4 – 0.7 (average R = ~ 0.35). However, for NDVI values between 0.7 and 1 , the average R value dropped to ~ 0.14 . IN-drained experienced a similar relationship, with an average R value of ~ 0.4 for NDVI of 0 –

0.4 and 0.4–0.7 and an average R value of ~ 0.24 for NDVI between 0.7 and 1. For PE-mDeg, the NDVI range 0.4–0.7, had the largest average R value (average R = ~ 0.14). This was followed by NDVI 0–0.4 (average R = ~ 0.1) and 0.7–1 (average R = ~ 0.01). While PE-hDeg showed positive average R values for NDVI thresholds 0–0.4 and 0.4–0.7 (average R values of ~ 0.01 and ~ 0.04 , respectively), the NDVI threshold of 0.7–1 yielded a negative average R value of ~ -0.035). Lastly, MA-undrained and MA-converted showed similar average R-values for each NDVI threshold. An average R value of ~ 0.12 for an NDVI range of 0–0.4 was found for both sites. For NDVI threshold 0.4–0.7, average R values of ~ 0.175 and ~ 0.16 were found at MA-undrained and MA-converted, respectively. For NDVI threshold 0.7–1, an average R value of ~ 0.075 was observed at MA-undrained, while an average R value of ~ 0.07 was found at MA-converted.

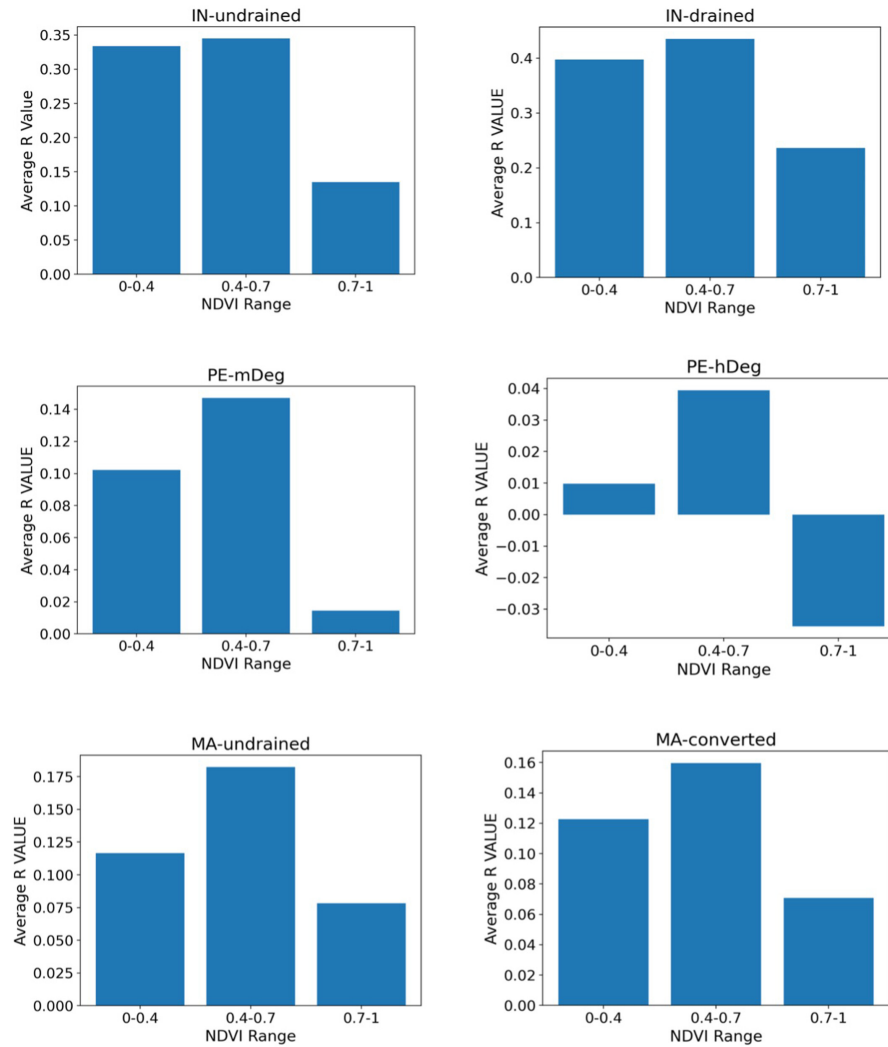


Figure 2.9: Histograms showing the average R-value for various NDVI classes (0–0.4, 0.4–0.7, 0.7–1) for each site. For these intervals, the lower bound is included but the upper bound is not.

2.3.5 The Number of Data Points and OPTRAM Performance

The number of data points per pixel (NDP) generally did not impact the correlation strength between OPTRAM index and in situ WT. The distribution was mainly a result of filtering cloudy pixels via the “C Function of Mask” algorithm to ensure pixel quality. Moreover, L7 ETM+ images were subject to data gaps due to permanent failure of the Scan Line Corrector.

At IN-undrained, there was a mixture of low and high NDP where high correlations were observed ($R > \sim 0.6$) (Figure 2.7). This did not, however, influence the strength of correlation (Figure 2.7). This was also the case for IN-drained. The remaining sites had lower NDP throughout the landscape relative to IN-undrained and IN-drained (with the exception of MA-undrained) (Figure 2.7). Therefore, we applied thresholds to use for NDP to obtain reliable results for the “best pixel” location. With that said, distributions of NDP on a site-by-site basis also did not greatly affect correlation strength (Figure 2.7).

2.3.6 Impact of El Niño and Non-El Niño Years

We could not show the significant difference between El Niño and non-El Niño years at all sites due to limited data. Here, we used the IN-undrained and IN-drained sites for this analysis. It is important to note that these sites had only 5 and 6 data points covering El Niño years, respectively. Despite Figure 2.10 showing different linear regression slopes for El Niño and non-El Niño years, 95% confidence intervals of these linear regression slopes are highly overlapped (Table 2.S1).

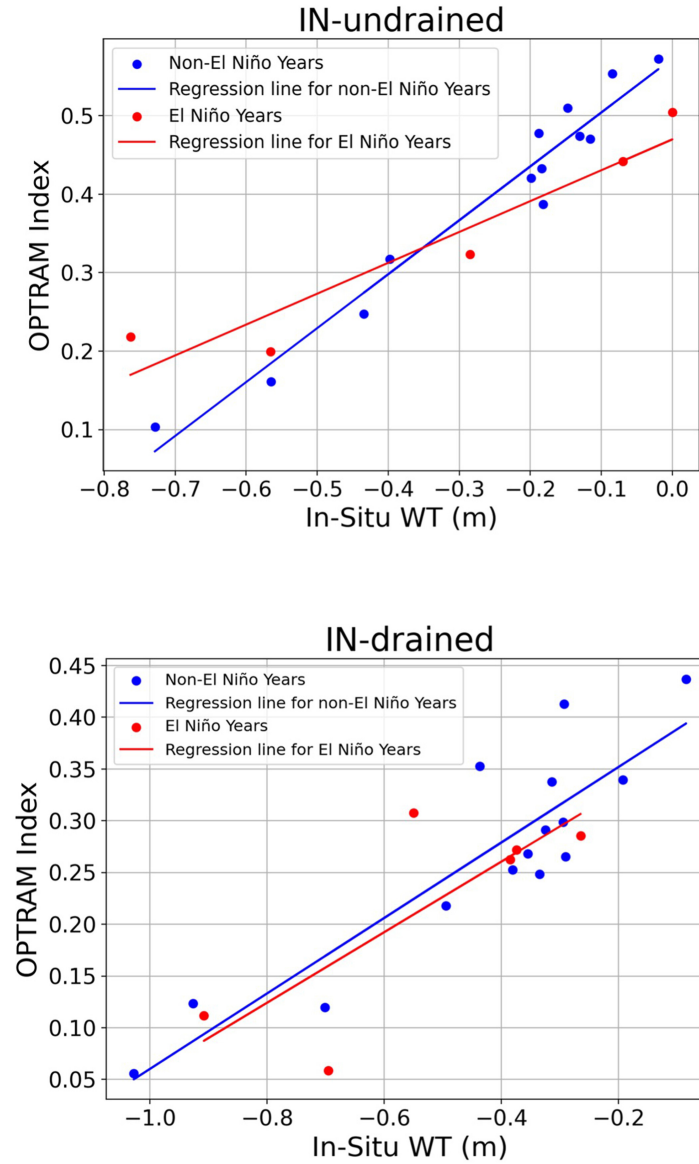


Figure 2.10: Scatterplot of OPTRAM versus in situ WT for IN-undrained and IN-drained. The data points and regression line are red for El Niño years and blue for non-El Niño years. These plots only show the pixel with the highest Pearson-R value.

2.3.7 Uncertainty in OPTRAM Index-Water Table Relationship

Using the cross-validation approach for each site's best pixel, we found the mean of the difference between the observed and predicted OPTRAM index values (observed OPTRAM

index value minus predicted OPTRAM index value) to be 0.001, 0.0007, 0.009, 0.009, -0.003 , -0.0008 for IN-undrained, IN-drained, PE-mDeg, PE-hDeg, MA-undrained, and MA-converted, respectively. The MAE was 0.044 for IN-undrained, 0.045 for IN-drained, 0.045 for PE-mDeg, 0.021 for PE-hDeg, 0.072 for MA-undrained, and 0.026 for MA-converted. The OPTRAM index is a unitless quantity and therefore MAE is also a unitless quantity. The values for the mean of the difference between observed and predicted OPTRAM index values and MAE are small relative to typical OPTRAM index values calculated in this study (~ 1 – 3 orders of magnitude smaller).

2.4 Discussion

This study shows OPTRAM to be capable of reproducing tropical peatland WT in areas with low vegetation density. In particular, it will allow stakeholders to estimate changes in WT using the OPTRAM index, where an increase of ~ 0.1 for the OPTRAM index is approximately equivalent to a 20 cm increase in WT over minimally vegetated areas. Stakeholders may then use this information to estimate WT-dependent variables such as the magnitude of carbon emissions and the probability of fire occurrence.

Temporal variability of in situ WT was similar among sites in close proximity such as IN-undrained and IN-drained (typically following rainfall patterns), and PE-mDeg and PE-hDeg. This supported our assumption that temporal fluctuations in WT within the same tropical peatland landscape are uniform ([Burdun, Bechtold, Sagris, Lohila, et al., 2020](#)), although specific magnitudes may differ. Our results indicate that OPTRAM may potentially be used for WT

estimation on different timescales, especially in areas where long-term in situ measurements are not available.

However, it is important to note that this study was carried out on a limited number of sites. Additionally, there were a limited number of observations which did not allow us to conclusively trace the effect of El Niño on OPTRAM performance.

2.4.1 Comparison with Past Studies

A direct comparison with past studies using OPTRAM is problematic since, to date, this is the first time this method has been used to replicate WT variability in tropical peatlands. The idea of utilizing OPTRAM for peatland WT retrieval is also in its infancy since its original intended use was for estimating soil moisture.

Our study shows that OPTRAM effectively monitors WT over areas with little to no vegetation cover. This is likely due to the vegetation moisture status of trees being less sensitive to WT fluctuations relative to that of grasses and shrubs ([Burdun et al., 2023](#)). Therefore, we posit that the model is successful even over non-tree species (i.e., shrubs, ferns, sedges, and pitcher plants).

One of the first applications of OPTRAM was in northern peatlands by Burdun, Bechtold, [Sagris, Lohila, et al. \(2020\)](#). This work also used the “best pixel” approach and found similar results to those found in this study—large correlations in areas with minimal vegetation cover and low correlations in areas with high vegetation cover. It was also concluded that the degree of spatial resolution affects OPTRAM performance, with higher resolutions (30-m) yielding higher

R-values relative to lower resolutions (500-m). A similar study compared two trapezoid models for WT retrieval at several northern bogs ([Burdun, Bechtold, Sagris, Komisarenko, et al., 2020](#))—namely, OPTRAM and the Thermal-Optical Trapezoid Model (TOTRAM). Results showed that temporal correlations with in situ WT were higher using OPTRAM versus TOTRAM indices.

That study concluded that neither model could recreate the spatial variability of WT, but instead, OPTRAM was observed to perform optimally over the treeless portions of the multiple bog landscapes ([Burdun, Bechtold, Sagris, Komisarenko, et al., 2020](#)). The same result was found when testing OPTRAM at 53 northern peatland sites ([Burdun et al., 2023](#)). Specifically, OPTRAM sensitivity to WT decreased when tree cover density was 50% or more ([Burdun et al., 2023](#)). Furthermore, the lack of spatial correlation may go beyond vegetation density and occur due to differences in the WT-soil moisture relationship in certain areas. A similar result was obtained in this study when applying OPTRAM to tropical peatlands, where spatial differences in OPTRAM performance were a function of vegetation density patterns.

Another study found a combination of optical and synthetic aperture radar (SAR) (multi-sensor approach) may better resolve in situ peatland WT measurements ([Räsänen et al., 2022](#)).

However, like methods solely using optical data, the same limitations were found, such as higher average regression performance over sparsely treed and open peatlands. Interestingly, it was also discovered that a multi-sensor approach performs best in undrained rather than restored peatlands ([Räsänen et al., 2022](#)), agreeing with our results when applying an optical method at tropical peatlands.

2.4.2 Study Limitations and Application Approaches to Other Tropical Peatlands

Due to the nature of the study area, this work is subject to limitations. First, the quality of surface reflectance data is restricted owing to the typically cloudy conditions of tropical regions. As a result, many pixels were discarded to maintain reliable calculations for OPTRAM index and NDVI. This filtering introduced many data gaps in the OPTRAM index time series. These were then exacerbated by limited temporal in situ WT at the sites. Therefore, regression analysis could not be conducted if in situ and OPTRAM index data were not available for the same timestamp, which further limited our data pool. Fortunately, this is compensated for by the high temporal representation of data points used, with a maximum of five site years of data.

Mean absolute errors (MAE) in the OPTRAM index-WT relationship were relatively small compared to OPTRAM index values, except for PE-hDeg. This potentially highlights the high uncertainty that comes with estimating WT via OPTRAM in degraded tropical peatland systems.

The lack of spatial pattern in correlations over an undrained heavily degraded forest (PE-hDeg) and a drained plantation (MA-converted) indicates OPTRAM to not be able to capture WT in areas with high disturbance and high drainage. One explanation may be that the relatively high bulk density of the upper peat layer limits horizontal water flow which affects vegetation moisture status ([Burdun et al., 2023](#)). Additionally, it may be that exceedingly low WT results in a loss of the WT and vegetation moisture status connection and therefore decreases OPTRAM performance (although this was not the case for Peruvian sites) ([Burdun et al., 2023](#)).

Many of the “best pixel” correlations at sites had notably high Pearson-R values. We caution readers not to attribute this to OPTRAM's overall effectiveness in monitoring WT. Rather, it is important to note that the main takeaway lies in the spatial distribution of the OPTRAM index-WT correlation strengths. To apply OPTRAM successfully at other tropical peatland sites, stakeholders must find either open or low-vegetated areas. We realize that some of these systems are densely vegetated, and that in most areas, OPTRAM would perform poorly. However, since the upper peat layer has high hydraulic conductivity due to saturation/inundation, temporal WT fluctuations are synchronized over several kilometers ([Hergoualc'h et al., 2020](#); [Hirano et al., 2012](#)). This, in turn, allows OPTRAM to reproduce WT fluctuations across the landscape using only a relatively small area within the peatland. However, WT synchronization may be lost due to drainage ditches (i.e., MA-converted), which may cause unreliable OPTRAM-based estimations of peatland WT.

Even in the case of densely vegetated tropical peatlands such as PSF, one can estimate WT variations using only non-forested areas or areas with low vegetation. Furthermore, some tropical peatlands are herbaceous swamps ([Hastie et al., 2022](#); [Urbina & Benavides, 2015](#); [Villa et al., 2019](#)), making these locations an ideal fit for OPTRAM application.

When comparing per-pixel NDVI and R-values, we assumed tropical NDVI to experience minimal variation at each site. Therefore, we used surface reflectance values from a date in September to represent NDVI at each site. We acknowledge that tropical vegetation surface reflectance values may differ temporally due to the wet and dry seasons, so we chose the

shoulder month of September to incorporate in our analyses. However, even with this approach, the reader should be cautioned when interpreting each pixel's R and NDVI relationship.

We can infer that pixels with high positive correlation values and high NDVI are not situated within the red clusters as shown in Figure 2.7. As established in the previous section, these clusters of red (high positive correlation between OPTRAM index and in situ WT) appeared in locations with low and intermediate NDVI (Figure 2.9). Therefore, pixels with both high Pearson-R and high NDVI are likely not included within the red pixel clusters and may instead be a speck of red within a sea of blue (negative correlation) or white (no correlation). This may be due to small data samples and spurious correlation, but future studies are encouraged to investigate further.

Future work should expand on tropical peatland WT retrieval via remote sensing through approaches that will not necessarily depend on vegetation cover and clouds. For example, the National Aeronautics and Space Administration's Soil Moisture Active Passive satellite measures soil water content in the L-band that may penetrate clouds and dense vegetation ([Dadap et al., 2019](#)), albeit with relatively coarse resolution (9 km). Leveraging these kinds of methods to also yield WT approximations must be a priority of future work, especially due to the overall limited representation in tropical peatland ecosystems.

Additionally, more on-the-ground data should be acquired in these systems to ensure the accuracy of these methods. In the context of this work, this would mean a higher temporal

representation of in situ WT at tropical peatland sites to enable a more robust calculation of the OPTRAM index-WT relationship.

2.4.3 Implications for OPTRAM's Ability to Detect Changes in Tropical Peatland Water Table

Tropical peatland hydrology remains understudied relative to temperate and boreal peatlands. Our findings can open many paths to further understanding these ecosystems—from determining GHG flux magnitudes to applying OPTRAM within global models to decrease uncertainties in model output. Additionally, we obtained promising results using identical OPTRAM parameterization for all studied sites, therefore suggesting that the same OPTRAM parameterization may be applicable in other tropical peatlands. In Figure 2.11, the points in the STR and NDVI space overlap, meaning that OPTRAM parameterization (and therefore calibration) is valid at each site. As a result, this may be the first step toward the applicability of universal OPTRAM parameterization over tropical peatlands. OPTRAM parameterization is a time-consuming process, so a universal parameterization may greatly facilitate OPTRAM application at a global scale. This can potentially increase the spatiotemporal coverage of WT variability estimates in tropical peatlands and will only be limited spatiotemporally by the surface reflectance product in use. Additionally, we showed that the OPTRAM-WT relationship does not differ significantly between El Niño and non-El Niño years. Therefore, OPTRAM may also be used during El Niño years to provide estimates of temporal variations in tropical peatland WT. However, it is important to note that cloudy conditions characteristic of El Niño years in certain regions may result in OPTRAM being less useful. Additionally, this analysis consisted of only 5–6 data points that were within El Niño years for two study sites. Future work should therefore utilize more data in order to reach a more robust conclusion.

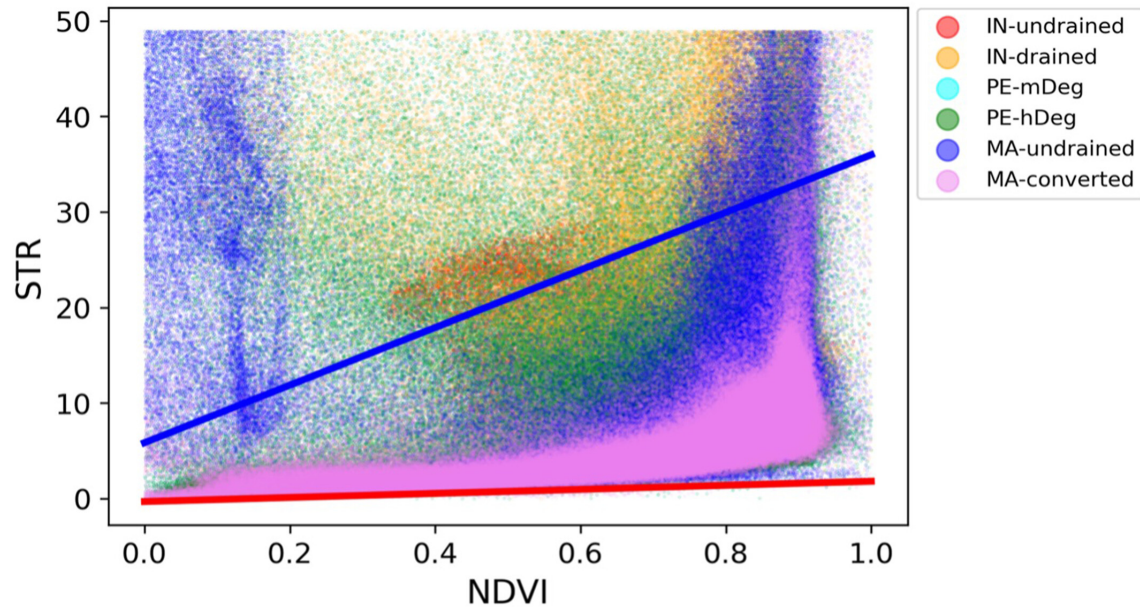


Figure 2.11: STR-NDVI space showing large overlap between all sites. This indicates that OPTRAM parameterization is valid for all sites. Only pixels labeled as “clear” are shown. NDVI and STR values were taken from three timesteps throughout the year (beginning, middle, and end of year) to take into account seasonality of the wet and dry seasons at each site. IN-undrained, IN-drained, PE-mDeg, PE-hDeg, MA-undrained, and MA-converted used values from 2018, 2017, 2018, 2018, 2014, and 2018, respectively. Blue line is the wet edge and red line is the dry edge.

OPTRAM's ability to estimate changes in WT may provide stakeholders with information on past and current hotspots where peat subsidence occurs. Therefore, it may also indicate areas prone to flooding (in the event of high precipitation) and fire (in the event of low precipitation) (Ballhorn et al., 2009; Hoscilo et al., 2011; Khakim et al., 2020; Page et al., 2002; Turetsky et al., 2015). Additionally, OPTRAM may be used as a line of evidence for tropical peatland areas in need of rewetting. Owing to its vast spatial representation via remote sensing, OPTRAM may

allow stakeholders to pinpoint locations of persisting low WT. This can prompt appropriate actions to prevent the risk of high CO₂ emissions ([Deshmukh et al., 2021](#)). However, it is important to note that this would be possible if WT synchronization is not lost due to anthropogenic drainage and/or rewetting.

Based on our results, it is likely possible to capture tropical peatland WT variability for a single landscape that may span many kilometers, regardless of vegetation cover. If one section of the peatland is covered with minimal vegetation, this will suffice as an area where OPTRAM may be applied to retrieve WT variability within the entire peatland landscape. Future studies should prioritize applying OPTRAM to other types of peatlands (i.e., mountain peatlands) to determine whether a non-lowland system would yield different results. Furthermore, studies may experiment with non-linear OPTRAM parametrizations ([Ambrosone et al., 2020](#)) and new variants of OPTRAM ([Sadeghi et al., 2023](#)) to determine whether correlations with WT improve.

2.5 Conclusion

This study used the 30-m resolution Landsat 7 ETM+ and Landsat 8 OLI surface reflectance products to test OPTRAM's capability for monitoring WT variations in tropical peatlands. We found a positive correlation ($0.7 < R < 1$) between OPTRAM index and in situ WT in areas that had low to intermediate vegetation cover (low to intermediate NDVI). The positive correlation strength decreased and, in some instances, became negative in areas with high vegetation cover (high NDVI). At each site, the pixel associated with the location of in situ WT measurement showed relatively smaller correlation between in situ WT (apart from IN-drained and PE-hDeg where $R = 0.62$ and $R = 0.57$, respectively). Site disturbance had an effect more on the pattern of

correlation distribution rather than strength, with low disturbance resulting in more structured patterns relative to sites with high disturbance. The main limitations of this study were cloud-induced data restrictions and the general lack of in situ WT data with high temporal resolution. Despite these shortcomings, our results indicate this method to be effective in monitoring tropical peatland WT variability over open and minimally vegetated areas. Furthermore, for tropical peatlands with high vegetation cover, one may apply OPTRAM to an open or minimally vegetated area to represent WT variability across the landscape.

The influence of WT on GHG emissions, surface-level peat subsidence, and fire vulnerability renders OPTRAM to be useful for understanding peatland features that are beyond hydrology. Moreover, since OPTRAM's methodology involves remotely sensed variables, one may apply this model to a broad range of tropical peatlands, including those currently not accessible by researchers. To improve on the OPTRAM method for application in tropical peatlands, future work may combine optical and SAR methods to investigate whether new approaches better reproduce in situ WT variability.

2.6 Global Research Collaboration

All principal investigators (PI) of the tropical peatland sites were included as co-authors on this study and made contributions to the manuscript. The in situ water table data in this work was used and shared online (via a public online repository) with permission from all site PIs. This includes Dr. Takashi Hirano for the Indonesian sites, Dr. Kristell Hergoualc'h for the Peruvian sites, and Dr. Guan Xhuan Wong and Dr. Lulie Melling for the Malaysian sites.

2.7 Open Research

Landsat surface reflectance data were downloaded from the USGS earth explorer. In situ water table data was used with permission from Takashi Hirano, Lulie Melling, Guan Xhuan Wong, and Kristell Hergoualc'h. Data for the Peruvian sites are available in [Hergoualc'h et al. \(2020\)](#) at <https://doi-org.ezproxy.library.wisc.edu/10.17528/CIFOR/DATA.00243>. Site-scale water table data for PE-mDeg and PE-hDeg used for analysis is available in [Hergoualc'h, 2024](#) at <https://doi-org.ezproxy.library.wisc.edu/10.6084/m9.figshare.25334854.v1>. Data for the Indonesian sites are available in [Hirano, 2023](#) at <https://doi-org.ezproxy.library.wisc.edu/10.6084/m9.figshare.22321129.v1>. Data for the Malaysian sites are available in [Melling & Wong, 2024](#) at <https://doi-org.ezproxy.library.wisc.edu/10.6084/m9.figshare.25299358.v1>. The code used for computing OPTRAM indices for each site may be accessed via https://github.com/koupsci/OPTRAM_code_updated.git.

2.8 Acknowledgements

We thank USGS for providing surface reflectance data and all members who took part in maintaining instruments at the tropical peatland sites. We acknowledge Iuliia Burdun for pioneering the implementation of OPTRAM for peatland water table retrieval. We also acknowledge support from the University of Wisconsin-Madison (UW) Center for Climatic Research, Climate, People, and Environment Program, the UW Atmospheric and Oceanic Sciences Department, the Fulbright Program, and The Malaysian-American Commission on Educational Exchange. Other financial supports include the Sustainable Wetlands Adaptation and Mitigation Program (SWAMP, Grant MTO-069018) by the United States of America and

the Global Comparative Study on REDD + (Grant agreement #QZA-12/0882) by the Government of Norway, and JSPS KAKENHI Grant (JP19H05666). IB acknowledged support from the Academy of Finland funding (PEATSPEC, decision no 341963). We would also like to thank the Sarawak Tropical Peat Research Institute and the team members, Edward Baran Aeries and Joseph Wenceslaus Waili, for maintaining all the water table loggers. Pictures in Figure 2.4 were provided by Kristell Hergoualc'h, Lulie Melling, Takashi Hirano, and Kazuya Nishina. N.K.-A. conceptualized and wrote the manuscript. A.R.D. supervised the research and all authors provided suggestions and feedback on the manuscript. In situ water table data was provided by Takashi Hirano, Lulie Melling, Guan Xhuan Wong, and Kristell Hergoualc'h.

2.9 Supporting Information

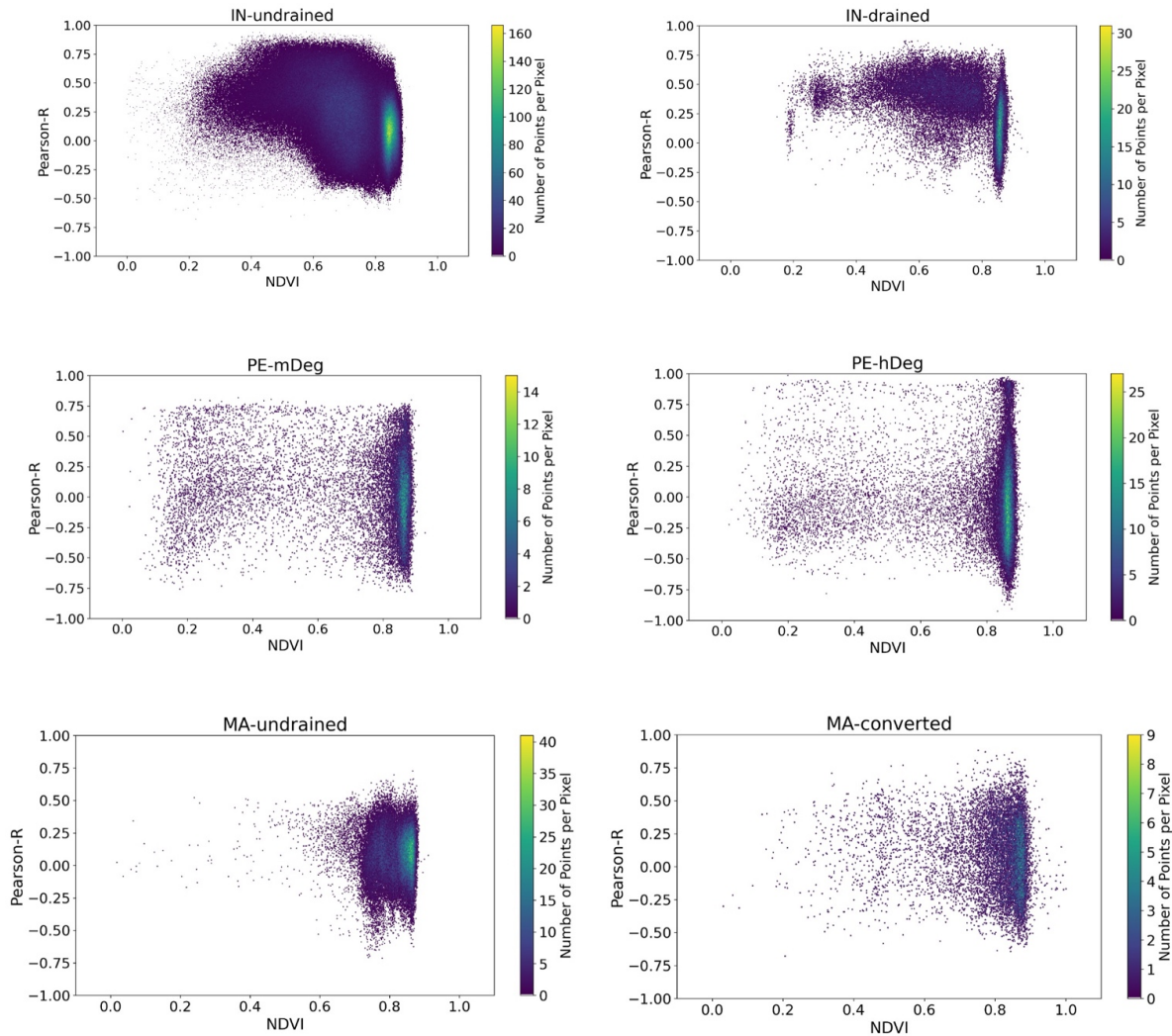


Figure 2.S1: Per-pixel Pearson correlation values plotted against per-pixel September NDVI values for each site. For IN-drained, PE-mDeg, PE-hDeg, MA-undrained, and MA-converted, a pool of data was used based on a threshold for the number of data points (number of data points was at least 21, 13, 13, 17, and 13, respectively). Each pixel's color represents the point density, with yellow representing the greatest and purple the least.

Site	Rank of Pearson-R	95% confidence interval for El Niño years	95% confidence interval for non-El Niño years	Slopes significantly different?
IN-undrained	1st largest	[0.157 , 0.629]	[0.588 , 0.786]	No
	2nd largest	[0.094 , 1.139]	[0.478 , 0.678]	No
	3rd largest	[0.026 , 1.996]	[0.587 , 1.425]	No
IN-drained	1st largest	[-0.034 , 0.716]	[0.255 , 0.475]	No
	2nd largest	[0.053 , 0.778]	[0.214 , 0.406]	No
	3rd largest	[-0.069 , 0.756]	[0.247 , 0.447]	No

Table 2.S1: 95% confidence intervals for regression line slopes for El Niño years and non-El Niño years. The regression line slopes were calculated with pixels containing the first, second, and third largest Pearson-R value.

Hergoualc'h, Kristell (2024). Site-scale Water Table Level at a Moderately Degraded and Heavily Degraded Site within a Peat Swamp Forest in the Northern Peruvian Amazon.. figshare. Dataset. <https://doi.org/10.6084/m9.figshare.25334854.v1>

Data Set 2.S1: This dataset contains site-scale water table level (WT) data at a moderately degraded (PE-mDeg) and heavily degraded (PE-hDeg) site within a peat swamp forest in the Northern Peruvian Amazon. Positive and negative values indicate WT above and below the surface, respectively.

The spatially stratified WT data from [Hergoualc'h et al. \(2020\)](#) was site-scaled using the following hummock to hollow relative proportions for the PE-mDeg and PE-hDeg sites:

- PE-mDeg
 - Live-hummock: 0.08
 - Live-hollow: 0.79
 - Cut-hummock: 0.01
 - Cut-hollow: 0.12
- PE-hDeg
 - Live-hummock: 0.02
 - Live-hollow: 0.59
 - Cut-hummock: 0.02
 - Cut-hollow: 0.38

This data was used to validate a WT-retrieval model based on Landsat 8 surface reflectance data. Therefore, in addition to the in-situ WT measurement dates, the acquisition dates of each Landsat 8 image are provided as well.

2.10 References

- Adeolu, A. R., Mohammad, T. A., Daud, N. N. N., Mustapha, S., Sayok, A. K., Rory, P., & Stephanie, E. (2015). Investigating the influence of rainfall on soil carbon quantity in a tropical peatland. *Procedia Environmental Sciences*, 30, 44–49.
<https://doi.org/10.1016/j.proenv.2015.10.008>
- Ambrosone, M., Matese, A., Di Gennaro, S. F., Gioli, B., Tudoroiu, M., Genesio, L., et al. (2020). Retrieving soil moisture in rainfed and irrigated fields using sentinel-2 observations and a modified OPTRAM approach. *International Journal of Applied Earth Observation and Geo- information*, 89, 102113.
<https://doi.org/10.1016/j.jag.2020.102113>
- Apers, S., De Lannoy, G. J. M., Baird, A. J., Cobb, A. R., Dargie, G. C., del Aguila Pasquel, J., et al. (2022). Tropical peatland hydrology simulated with a global land surface model. *Journal of Advances in Modeling Earth Systems*, 14(3), e2021MS002784.
<https://doi.org/10.1029/2021MS002784>
- Ballhorn, U., Siegert, F., Mason, M., & Limin, S. (2009). Derivation of burn scar depths and estimation of carbon emissions with LIDAR in Indonesian peatlands. *Proceedings of the National Academy of Sciences*, 106(50), 21213–21218.
<https://doi.org/10.1073/pnas.0906457106>
- Bechtold, M., Schlaffer, S., Tiemeyer, B., & De Lannoy, G. (2018). Inferring water table depth dynamics from ENVISAT-ASAR C-band backscatter over a range of peatlands from deeply-drained to natural conditions. *Remote Sensing*, 10(4), 536.
<https://doi.org/10.3390/rs10040536>
- Burdun, I., Bechtold, M., Aurela, M., De Lannoy, G., Desai, A. R., Humphreys, E., et al. (2023). Hidden becomes clear: Optical remote sensing of vegetation reveals water table dynamics in northern peatlands. *Remote Sensing of Environment*, 296, 113736.
<https://doi.org/10.1016/j.rse.2023.113736>
- Burdun, I., Bechtold, M., Sagris, V., Komisarenko, V., De Lannoy, G., & Mander, Ü. (2020). A comparison of three trapezoid models using optical and thermal satellite imagery for water table depth monitoring in Estonian bogs. *Remote Sensing*, 12(12), 1980.
<https://doi.org/10.3390/rs12121980>
- Burdun, I., Bechtold, M., Sagris, V., Lohila, A., Humphreys, E., Desai, A. R., et al. (2020). Satellite determination of peatland water table temporal dynamics by localizing representative pixels of A SWIR-based moisture index. *Remote Sensing*, 12(18), 2936.
<https://doi.org/10.3390/rs12182936>

- Busman, N. A., Melling, L., Goh, K. J., Imran, Y., Sangok, F. E., & Watanabe, A. (2023). Soil CO₂ and CH₄ fluxes from different forest types in tropical peat swamp forest. *Science of the Total Environment*, 858, 159973. <https://doi.org/10.1016/j.scitotenv.2022.159973>
- Chen, M., Zhang, Y., Yao, Y., Lu, J., Pu, X., Hu, T., & Wang, P. (2020). Evaluation of the OPTRAM model to retrieve soil moisture in the Sanjiang Plain of Northeast China. *Earth and Space Science*, 7(6). <https://doi.org/10.1029/2020EA001108>
- Cheong, N., Morgan, P., Tan, L., Koh, O., Ho, Lai, et al. (2019). Acute health impacts of the southeast asian transboundary haze problem—A review. *International Journal of Environmental Research and Public Health*, 16(18), 3286. <https://doi.org/10.3390/ijerph16183286>
- Christian, T. J., Kleiss, B., Yokelson, R. J., Holzinger, R., Crutzen, P. J., Hao, W. M., et al. (2003). Comprehensive laboratory measurements of biomass-burning emissions: 1. Emissions from Indonesian, African, and other fuels. *Journal of Geophysical Research*, 108(D23), 4719. <https://doi.org/10.1029/2003JD003704>
- Cobb, A. R., & Harvey, C. F. (2019). Scalar simulation and parameterization of water table dynamics in tropical peatlands. *Water Resources Research*, 55(11), 9351–9377. <https://doi.org/10.1029/2019WR025411>
- Cook, M., Schott, J. R., Mandel, J., & Raqueno, N. (2014). Development of an operational calibration methodology for the Landsat thermal data archive and initial testing of the atmospheric compensation component of a Land Surface Temperature (LST) Product from the archive. *Remote Sensing*, 6(11), 11244–11266. <https://doi.org/10.3390/rs6111244>
- Cook, M. J. (2014). Atmospheric compensation for a Landsat land surface temperature product [Thesis]. Rochester Institute of Technology. Retrieved from <http://scholarworks.rit.edu/theses/8513>
- Dadap, N. C., Cobb, A. R., Hoyt, A. M., Harvey, C. F., & Konings, A. G. (2019). Satellite soil moisture observations predict burned area in Southeast Asian peatlands. *Environmental Research Letters*, 14(9), 094014. <https://doi.org/10.1088/1748-9326/ab3891>
- Dargie, G. C., Lewis, S. L., Lawson, I. T., Mitchard, E. T. A., Page, S. E., Bocko, Y. E., & Ifo, S. A. (2017). Age, extent and carbon storage of the central Congo Basin peatland complex. *Nature*, 542(7639), 86–90. <https://doi.org/10.1038/nature21048>
- Davies, S. J. (1999). Smoke-haze from the 1997 Indonesian forest fires: Effects on pollution levels, local climate, atmospheric CO₂ concentrations, and tree photosynthesis. *Forest Ecology and Management*, 8.

- Deshmukh, C. S., Julius, D., Desai, A. R., Asyhari, A., Page, S. E., Nardi, N., et al. (2021). Conservation slows down emission increase from a tropical peatland in Indonesia. *Nature Geoscience*, 14(7), 484–490. <https://doi.org/10.1038/s41561-021-00785-2>
- Dohong, A., Aziz, A. A., & Dargusch, P. (2017). A review of the drivers of tropical peatland degradation in South-East Asia. *Land Use Policy*, 69, 349–360. <https://doi.org/10.1016/j.landusepol.2017.09.035>
- Evers, S., Yule, C. M., Padfield, R., O'Reilly, P., & Varkkey, H. (2017). Keep wetlands wet: The myth of sustainable development of tropical peatlands - Implications for policies and management. *Global Change Biology*, 23(2), 534–549. <https://doi.org/10.1111/gcb.13422>
- Foga, S., Scaramuzza, P. L., Guo, S., Zhu, Z., Dilley, R. D., Beckmann, T., et al. (2017). Cloud detection algorithm comparison and validation for operational Landsat data products. *Remote Sensing of Environment*, 194, 379–390. <https://doi.org/10.1016/j.rse.2017.03.026>
- Gaveau, D. L. A., Salim, M. A., Hergoualc'h, K., Locatelli, B., Sloan, S., Wooster, M., et al. (2014). Major atmospheric emissions from peat fires in Southeast Asia during non-drought years: Evidence from the 2013 Sumatran fires. *Scientific Reports*, 4(1), 6112. <https://doi.org/10.1038/srep06112>
- Harris, A., & Bryant, R. G. (2009). A multi-scale remote sensing approach for monitoring northern peatland hydrology: Present possibilities and future challenges. *Journal of Environmental Management*, 90(7), 2178–2188. <https://doi.org/10.1016/j.jenvman.2007.06.025>
- Hastie, A., Honorio Coronado, E. N., Reyna, J., Mitchard, E. T. A., Åkesson, C. M., Baker, T. R., et al. (2022). Risks to carbon storage from land- use change revealed by peat thickness maps of Peru. *Nature Geoscience*, 15(5), 369–374. <https://doi.org/10.1038/s41561-022-00923-4>
- Hergoualc'h, K. (2020). Replication Data for: Hergoualc'h et al. (2020) Spatial and temporal variability of soil N₂O and CH₄ fluxes along a degradation gradient in a palm swamp peat forest in the Peruvian Amazon [Dataset]. *Center for International Forestry Research (CIFOR)*. <https://doi.org/10.17528/CIFOR/DATA.00243>
- Hergoualc'h, K. (2024). Site-scale water table level at a moderately degraded and heavily degraded site within a peat swamp forest in the Northern Peruvian Amazon [Dataset]. *Figshare*. <https://doi.org/10.6084/m9.figshare.25334854.v1>
- Hergoualc'h, K., Dezzeo, N., Verchot, L. V., Martius, C., Lent, J., Aguila-Pasquel, J., & López Gonzales, M. (2020). Spatial and temporal variability of soil N₂O and CH₄ fluxes along a degradation gradient in a palm swamp peat forest in the Peruvian Amazon. *Global Change Biology*, 26(12), 7198–7216. <https://doi.org/10.1111/gcb.15354>

- Hergoualc'h, K., Van Lent, J., Dezzio, N., Verchot, L. V., Van Groenigen, J. W., López Gonzales, M., & Grandez-Rios, J. (2023). Major carbon losses from degradation of *Mauritia flexuosa* peat swamp forests in western Amazonia. *Biogeochemistry*, 167(4), 327–345. <https://doi.org/10.1007/s10533-023-01057-4>
- Hergoualc'h, K. A., & Verchot, L. V. (2012). Changes in soil CH₄ fluxes from the conversion of tropical peat swamp forests: A meta-analysis. *Journal of Integrative Environmental Sciences*, 9(1), 31–39. <https://doi.org/10.1080/1943815X.2012.747252>
- Hikouei, I. S., Eshleman, K. N., Saharjo, B. H., Graham, L. L. B., Applegate, G., & Cochrane, M. A. (2023). Using machine learning algorithms to predict groundwater levels in Indonesian tropical peatlands. *Science of the Total Environment*, 857, 159701. <https://doi.org/10.1016/j.scitotenv.2022.159701>
- Hirano, T. (2023). DailyGWL.xlsx [Dataset]. *Figshare*. <https://doi.org/10.6084/m9.figshare.22321129.v1>
- Hirano, T., Kusin, K., Limin, S., & Osaki, M. (2015). Evapotranspiration of tropical peat swamp forests. *Global Change Biology*, 21(5), 1914–1927. <https://doi.org/10.1111/gcb.12653>
- Hirano, T., Kusin, K., Limin, S., & Osaki, M. (2014). Carbon dioxide emissions through oxidative peat decomposition on a burnt tropical peatland. *Global Change Biology*, 20(2), 555–565. <https://doi.org/10.1111/gcb.12296>
- Hirano, T., Segah, H., Harada, T., Limin, S., June, T., Hirata, R., & Osaki, M. (2007). Carbon dioxide balance of a tropical peat swamp forest in Kalimantan, Indonesia. *Global Change Biology*, 13(2), 412–425. <https://doi.org/10.1111/j.1365-2486.2006.01301.x>
- Hirano, T., Segah, H., Kusin, K., Limin, S., Takahashi, H., & Osaki, M. (2012). Effects of disturbances on the carbon balance of tropical peat swamp forests. *Global Change Biology*, 18(11), 3410–3422. <https://doi.org/10.1111/j.1365-2486.2012.02793.x>
- Holden, J., Chapman, P. J., & Labadz, J. C. (2004). Artificial drainage of peatlands: Hydrological and hydrochemical process and wetland restoration. *Progress in Physical Geography: Earth and Environment*, 28(1), 95–123. <https://doi.org/10.1191/0309133304pp403ra>
- Hooijer, A., Page, S., Jauhiainen, J., Lee, W. A., Lu, X. X., Idris, A., & Anshari, G. (2012). Subsidence and carbon loss in drained tropical peatlands. *Biogeosciences*, 9(3), 1053–1071. <https://doi.org/10.5194/bg-9-1053-2012>

- Hoscilo, A., Page, S. E., Tansey, K. J., & Rieley, J. O. (2011). Effect of repeated fires on land-cover change on peatland in southern Central Kalimantan, Indonesia, from 1973 to 2005. *International Journal of Wildland Fire*, 20(4), 578. <https://doi.org/10.1071/WF10029>
- Hoyos-Santillan, J., Lomax, B. H., Large, D., Turner, B. L., Lopez, O. R., Boom, A., et al. (2019). Evaluation of vegetation communities, water table, and peat composition as drivers of greenhouse gas emissions in lowland tropical peatlands. *Science of the Total Environment*, 688, 1193–1204. <https://doi.org/10.1016/j.scitotenv.2019.06.366>
- Huat, B. B. K., Kazemian, S., Prasad, A., & Barghchi, M. (2011). State of an art review of peat: General perspective. *International Journal of the Physical Sciences*, 9.
- Jauhiainen, J., Limin, S., Silvennoinen, H., & Vasander, H. (2008). Carbon dioxide and methane fluxes in drained tropical peat before and after hydrological restoration. *Ecology*, 89(12), 3503–3514. <https://doi.org/10.1890/07-2038.1>
- Joosten, H. (2009). The global peatland CO₂ picture: Peatland status and drainage related emissions in all countries of the world.
- Kalacska, M., Arroyo-Mora, J., Soffer, R., Roulet, N., Moore, T., Humphreys, E., et al. (2018). Estimating peatland water table depth and net ecosystem exchange: A comparison between satellite and airborne imagery. *Remote Sensing*, 10(5), 687. <https://doi.org/10.3390/rs10050687>
- Khakim, M. Y. N., Bama, A. A., Yustian, I., Poerwono, P., Tsuji, T., & Matsuoka, T. (2020). Peatland subsidence and vegetation cover degradation as impacts of the 2015 El Niño event revealed by Sentinel-1A SAR data. *International Journal of Applied Earth Observation and Geoinformation*, 84, 101953. <https://doi.org/10.1016/j.jag.2019.101953>
- Kim, J.-W., Lu, Z., Gutenberg, L., & Zhu, Z. (2017). Characterizing hydrologic changes of the Great Dismal Swamp using SAR/InSAR. *Remote Sensing of Environment*, 198, 187–202. <https://doi.org/10.1016/j.rse.2017.06.009>
- Kuwata, M., Kai, F. M., Yang, L., Itoh, M., Gunawan, H., & Harvey, C. F. (2017). Temperature and burning history affect emissions of greenhouse gases and aerosol particles from tropical peatland fire: Emission from Peatland Fire. *Journal of Geophysical Research: Atmospheres*, 122(2), 1281–1292. <https://doi.org/10.1002/2016JD025897>
- Kwon, M. J., Haraguchi, A., & Kang, H. (2013). Long-term water regime differentiates changes in decomposition and microbial properties in tropical peat soils exposed to the short-term drought. *Soil Biology and Biochemistry*, 60, 33–44. <https://doi.org/10.1016/j.soilbio.2013.01.023>

- Leifeld, J., & Menichetti, L. (2018). The underappreciated potential of peatlands in global climate change mitigation strategies. *Nature Communications*, 9(1), 1071. <https://doi.org/10.1038/s41467-018-03406-6>
- Lestari, I., Murdiyarso, D., & Taufik, M. (2022). Rewetting tropical peatlands reduced net greenhouse gas emissions in Riau Province, Indonesia. *Forests*, 13(4), 505. <https://doi.org/10.3390/f13040505>
- Masek, J. G., Vermote, E. F., Saleous, N. E., Wolfe, R., Hall, F. G., Huemmrich, K. F., et al. (2006). A Landsat surface reflectance dataset for North America, 1990-2000 [Dataset]. *IEEE Geoscience and Remote Sensing Letters*, 3(1), 68–72. <https://doi.org/10.1109/lgrs.2005.857030>
- Meingast, K. M., Falkowski, M. J., Kane, E. S., Potvin, L. R., Benscoter, B. W., Smith, A. M. S., et al. (2014). Spectral detection of near-surface moisture content and water-table position in northern peatland ecosystems. *Remote Sensing of Environment*, 152, 536–546. <https://doi.org/10.1016/j.rse.2014.07.014>
- Melling, L. (2016). Peatland in Malaysia. *Tropical peatland ecosystems*, 59–73. https://doi.org/10.1007/978-4-431-55681-7_4
- Melling, L., & Wong, G. X. (2024). Groundwater levels in an undrained peat swamp forest and oil palm plantation on peat in Sarawak, Malaysia [Dataset]. *figshare*. <https://doi.org/10.6084/m9.figshare.25299358.v1>
- Melton, J. R., Chan, E., Millard, K., Fortier, M., Winton, R. S., Martín-López, J. M., et al. (2022). A map of global peatland extent created using machine learning (Peat-ML). *Geoscientific Model Development*, 15(12), 4709–4738. <https://doi.org/10.5194/gmd-15-4709-2022>
- Mezbahuddin, M., Grant, R. F., & Hirano, T. (2014). Modelling effects of seasonal variation in water table depth on net ecosystem CO₂ exchange of a tropical peatland. *Biogeosciences*, 11(3), 577–599. <https://doi.org/10.5194/bg-11-577-2014>
- Mezbahuddin, M., Grant, R. F., & Hirano, T. (2015). How hydrology determines seasonal and interannual variations in water table depth, surface energy exchange, and water stress in a tropical peatland: Modeling versus measurements: Modeling tropical peatland ecohydrology. *Journal of Geophysical Research: Biogeosciences*, 120(11), 2132–2157. <https://doi.org/10.1002/2015JG003005>
- Nishina, K., Melling, L., Toyoda, S., Itoh, M., Terajima, K., Waili, J. W. B., et al. (2023). Dissolved N₂O concentrations in oil palm plantation drainage in a peat swamp of Malaysia. *Science of the Total Environment*, 872, 162062. <https://doi.org/10.1016/j.scitotenv.2023.162062>

- Ohkubo, S., Hirano, T., & Kusin, K. (2021). Influence of disturbances and environmental changes on albedo in tropical peat ecosystems. *Agricultural and Forest Meteorology*, 301–302, 301–302. <https://doi.org/10.1016/j.agrformet.2021.108348>
- Page, S. E., Rieley, J. O., & Banks, C. J. (2011). Global and regional importance of the tropical peatland carbon pool: Tropical peatland carbon pool. *Global Change Biology*, 17(2), 798–818. <https://doi.org/10.1111/j.1365-2486.2010.02279.x>
- Page, S. E., Siegert, F., Rieley, J. O., Boehm, H.-D. V., Jaya, A., & Limin, S. (2002). The amount of carbon released from peat and forest fires in Indonesia during 1997. *Nature*, 420(6911), 61–65. <https://doi.org/10.1038/nature01131>
- Parker, R. J., Boesch, H., Wooster, M. J., Moore, D. P., Webb, A. J., Gaveau, D., & Murdiyarso, D. (2016). Atmospheric CH₄ and CO₂ enhancements and biomass burning emission ratios derived from satellite observations of the 2015 Indonesian fire plumes. *Atmospheric Chemistry and Physics*, 16(15), 10111–10131. <https://doi.org/10.5194/acp-16-10111-2016>
- Pärn, J., Verhoeven, J. T. A., Butterbach-Bahl, K., Dise, N. B., Ullah, S., Aasa, A., et al. (2018). Nitrogen-rich organic soils under warm well- drained conditions are global nitrous oxide emission hotspots. *Nature Communications*, 9(1), 1135. <https://doi.org/10.1038/s41467-018-03540-1>
- Price, J. S. (2003). Role and character of seasonal peat soil deformation on the hydrology of undisturbed and cutover peatlands: Peat volume- change hydrology. *Water Resources Research*, 39(9). <https://doi.org/10.1029/2002WR001302>
- Promsiri, P., Tekasakul, S., Thongyen, T., Suwattiga, P., Morris, J., Latif, M. T., et al. (2023). Transboundary haze from peatland fires and local source-derived PM_{2.5} in Southern Thailand. *Atmospheric Environment*, 294, 119512. <https://doi.org/10.1016/j.atmosenv.2022.119512>
- Räsänen, A., Tolvanen, A., & Kareksela, S. (2022). Monitoring peatland water table depth with optical and radar satellite imagery. *International Journal of Applied Earth Observation and Geoinformation*, 112, 102866. <https://doi.org/10.1016/j.jag.2022.102866>
- Ribeiro, K., Pacheco, F. S., Ferreira, J. W., Sousa-Neto, E. R., Hastie, A., Krieger Filho, G. C., et al. (2021). Tropical peatlands and their contribution to the global carbon cycle and climate change. *Global Change Biology*, 27(3), 489–505. <https://doi.org/10.1111/gcb.15408>
- Rosenberry, D. O., Glaser, P. H., & Siegel, D. I. (2006). The hydrology of northern peatlands as affected by biogenic gas: Current developments and research needs. *Hydrological Processes*, 20(17), 3601–3610. <https://doi.org/10.1002/hyp.6377>

- Sadeghi, M., Babaeian, E., Tuller, M., & Jones, S. B. (2017). The optical trapezoid model: A novel approach to remote sensing of soil moisture applied to Sentinel-2 and Landsat-8 observations. *Remote Sensing of Environment*, 198, 52–68. <https://doi.org/10.1016/j.rse.2017.05.041>
- Sadeghi, M., Mohamadzadeh, N., Liang, L., Bandara, U., Caldas, M. M., & Tyler, H. (2023). A new variant of the optical trapezoid model (OPTRAM) for remote sensing of soil moisture and water bodies. *Science of Remote Sensing*, 8, 100105. <https://doi.org/10.1016/j.srs.2023.100105>
- Šimanauskienė, R., Linkevičienė, R., Bartold, M., Dąbrowska-Zielińska, K., Slavinskienė, G., Veteikis, D., & Taminskas, J. (2019). Peatland degradation: The relationship between raised bog hydrology and normalized difference vegetation index. *Ecohydrology*, 12(8). <https://doi.org/10.1002/eco.2159>
- Stockwell, C. E., Yokelson, R. J., Kreidenweis, S. M., Robinson, A. L., DeMott, P. J., Sullivan, R. C., et al. (2014). Trace gas emissions from combustion of peat, crop residue, domestic biofuels, grasses, and other fuels: Configuration and Fourier transform infrared (FTIR) component of the fourth Fire Lab at Missoula Experiment (FLAME-4). *Atmospheric Chemistry and Physics*, 14(18), 9727–9754. <https://doi.org/10.5194/acp-14-9727-2014>
- Strack, M., Kellner, E., & Waddington, J. M. (2005). Dynamics of biogenic gas bubbles in peat and their effects on peatland biogeochemistry: Biogeochemical effects of gas bubbles in peat. *Global Biogeochemical Cycles*, 19(1). <https://doi.org/10.1029/2004GB002330>
- Swails, E., Hergoualc'h, K., Verchot, L., Novita, N., & Lawrence, D. (2021). Spatio-temporal variability of peat CH₄ and N₂O fluxes and their contribution to peat GHG budgets in Indonesian forests and oil palm plantations. *Frontiers in Environmental Science*, 9, 617828. <https://doi.org/10.3389/fenvs.2021.617828>
- Swails, E., Yang, X., Asefi, S., Hergoualc'h, K., Verchot, L., McRoberts, R. E., & Lawrence, D. (2019). Linking soil respiration and water table depth in tropical peatlands with remotely sensed changes in water storage from the gravity recovery and climate experiment. *Mitigation and Adaptation Strategies for Global Change*, 24(4), 575–590. <https://doi.org/10.1007/s11027-018-9822-z>
- Tang, A. C. I., Melling, L., Stoy, P. C., Musin, K. K., Aeries, E. B., Waili, J. W., et al. (2020). A Bornean peat swamp forest is a net source of carbon dioxide to the atmosphere. *Global Change Biology*, 26(12), 6931–6944. <https://doi.org/10.1111/gcb.15332>
- Tang, A. C. I., Stoy, P. C., Hirata, R., Musin, K. K., Aeries, E. B., Wenceslaus, J., & Melling, L. (2018). Eddy covariance measurements of methane flux at a tropical peat forest in Sarawak, Malaysian Borneo. *Geophysical Research Letters*, 45(9), 4390–4399. <https://doi.org/10.1029/2017GL076457>

- Taufik, M., Haikal, M., Widyastuti, M. T., Arif, C., & Santikayasa, I. P. (2023). The impact of rewetting peatland on fire hazard in riau, Indonesia. *Sustainability*, 15(3), 2169. <https://doi.org/10.3390/su15032169>
- Taufik, M., Widyastuti, M. T., Sulaiman, A., Murdiyarso, D., Santikayasa, I. P., & Minasny, B. (2022). An improved drought-fire assessment for managing fire risks in tropical peatlands. *Agricultural and Forest Meteorology*, 312, 108738. <https://doi.org/10.1016/j.agrformet.2021.108738>
- Thompson, D. K., & Waddington, J. M. (2013). Peat properties and water retention in boreal forested peatlands subject to wildfire: Peat properties in fire-affected peatlands. *Water Resources Research*, 49(6), 3651–3658. <https://doi.org/10.1002/wrcr.20278>
- Turetsky, M. R., Benscoter, B., Page, S., Rein, G., van der Werf, G. R., & Watts, A. (2015). Global vulnerability of peatlands to fire and carbon loss. *Nature Geoscience*, 8(1), 11–14. <https://doi.org/10.1038/ngeo2325>
- Urbina, J. C., & Benavides, J. C. (2015). Simulated small scale disturbances increase decomposition rates and facilitates invasive species encroachment in a high elevation tropical Andean peatland. *Biotropica*, 47(2), 143–151. <https://doi.org/10.1111/btp.12191>
- Varkkey, H. (2013). Patronage politics, plantation fires and transboundary haze. *Environmental Hazards*, 12(3–4), 200–217. <https://doi.org/10.1080/17477891.2012.759524>
- Vermote, E., Justice, C., Claverie, M., & Franch, B. (2016). Preliminary analysis of the performance of the Landsat 8/OLI land surface reflectance product [Dataset]. *Remote Sensing of Environment*, 185, 46–56. <https://doi.org/10.1016/j.rse.2016.04.008>
- Villa, J. A., Mejía, G. M., Velásquez, D., Botero, A., Acosta, S. A., Marulanda, J. M., et al. (2019). Carbon sequestration and methane emissions along a microtopographic gradient in a tropical Andean peatland. *Science of the Total Environment*, 654, 651–661. <https://doi.org/10.1016/j.scitotenv.2018.11.109>
- Wong, G. X., Hirata, R., Hirano, T., Kiew, F., Aeries, E. B., Musin, K. K., et al. (2020). How do land use practices affect methane emissions from tropical peat ecosystems? *Agricultural and Forest Meteorology*, 282–283, 107869. <https://doi.org/10.1016/j.agrformet.2019.107869>
- Wösten, J. H. M., Clymans, E., Page, S. E., Rieley, J. O., & Limin, S. H. (2008). Peat–water interrelationships in a tropical peatland ecosystem in Southeast Asia. *CATENA*, 73(2), 212–224. <https://doi.org/10.1016/j.catena.2007.07.010>
- Wösten, J. H. M., Ismail, A. B., & van Wijk, A. L. M. (1997). Peat subsidence and its practical implications: A case study in Malaysia. *Geoderma*, 78(1–2), 25–36. [https://doi.org/10.1016/S0016-7061\(97\)00013-X](https://doi.org/10.1016/S0016-7061(97)00013-X)

- Wright, E. L., Black, C. R., Turner, B. L., & Sjögersten, S. (2013). Environmental controls of temporal and spatial variability in CO₂ and CH₄ fluxes in a neotropical peatland. *Global Change Biology*, 19(12), 3775–3789. <https://doi.org/10.1111/gcb.12330>
- Xu, J., Morris, P. J., Liu, J., & Holden, J. (2018). Peatmap: Refining estimates of global peatland distribution based on a meta-analysis. *CATENA*, 160, 134–140. <https://doi.org/10.1016/j.catena.2017.09.010>
- Zaitunah, A. S., Ahmad, A. G., & Safitri, R. A. (2018). Normalized difference vegetation index (NDVI) analysis for land cover types using Landsat 8 OLI in Besitang watershed, Indonesia. *IOP Conference Series: Earth and Environmental Science*, 126, 012112. <https://doi.org/10.1088/1755-1315/126/1/012112>
- Zeng, Y., Hao, D., Huete, A., Dechant, B., Berry, J., Chen, J. M., et al. (2022). Optical vegetation indices for monitoring terrestrial ecosystems globally. *Nature Reviews Earth & Environment*, 3(7), 477–493. <https://doi.org/10.1038/s43017-022-00298-5>

Chapter 3: Forecasting Tropical Peatland Burned Area Potential 10-30 Days in Advance

3.1 Introduction

Peatlands are known for storing large amounts of carbon (C) in their soil ([Dohong et al., 2017](#); [Joosten, 2010](#); [Leifeld and Menichetti, 2018](#); [Melton et al., 2022](#); [Page et al., 2011](#); [Xu et al., 2018](#)). This is mainly due to litter deposition exceeding decomposition rates, resulting in a net accumulation of C. The high soil C stocks makes peatlands a major contributor to the global C cycle ([Page et al., 2011](#); [Ribeiro et al., 2021](#)). While undisturbed peatlands maintain their C within the soil, natural and anthropogenic disturbances cause immense amounts of C emissions ([Cooper et al., 2020](#); [Hooijer et al., 2010](#); [Turetsky et al., 2002](#); [Turetsky et al., 2015](#)). A vast number of peatlands have been drained for the purpose of creating favorable conditions for agriculture, and these activities are global, spanning boreal, temperate, and tropical peatlands ([Gerin et al., 2023](#); [Hapsari et al., 2017](#); [Knox et al., 2015](#)). In addition to anthropogenic disturbances, natural climatic phenomena such as El Niño have also contributed to peatland disturbance, particularly in tropical peatlands ([Khakim et al., 2020](#); [Parker et al., 2016](#)).

Whether it be anthropogenic drainage or El Niño-induced decreases in precipitation, these disturbances contribute to a decrease in water availability and, consequently, cause drying in the peat surface layer ([Page et al., 2009](#); [Turetsky et al., 2015](#); [Usup et al., 2004](#)). This may have many effects on the system including peat oxidation and subsidence. During peat oxidation, a great amount of carbon-dioxide is released ([Dohong et al., 2017](#); [Hooijer et al., 2012](#)), further exacerbating climate change. The compaction and shrinkage of the peat surface layer also causes

critical peatland ecosystem services (i.e. C sequestration and flood prevention) to be diminished (Evers et al., 2017).

Among these consequences is also an increase in fire risk due to the resulting drier conditions (Jaenicke et al., 2010; Dohong et al., 2017). Like many other disturbances, fires may naturally occur or be man-made. The most common form of natural fire ignition is known to be lightning (Kunii et al., 2002), while man-made fires are usually caused due to agricultural practices such as “slash and burn” (Dohong et al., 2017). Tropical peatlands are typically vulnerable to fire due to year-to-year climatic variability that may cause extreme droughts. For example, during the El Niño year of 2015 and 2016, the Southeast Asia region experienced drastic decreases in precipitation, resulting in large amounts of peat drying (Khakim et al., 2020; Parker et al., 2016). Some Indonesian peatlands, for example, emitted immense amounts of C, partly due to the expansive fires that occurred in the region during that time (mean emission rate of 11.3 Tg CO₂ per day during September-October 2015 over maritime Southeast Asia) (Huijnen et al., 2016; Khakim et al., 2020). Moreover, some fires cause transboundary haze events due to particulate matter (PM) emissions (Varkkey, 2013). The Malaysian city of Kuching, for instance, had elevated PM, sulfur dioxide, carbon monoxide, and methane concentration during the 1997 fires that occurred in Indonesia (Davies, 1999). These events can have a large impact on the regional economy, with an estimated 8.9 to 9.7 billion USD in economic losses after the 1997-1998 Southeast Asian haze episode (Barber & Schweithelm, 2000). Haze events also imply hazardous air quality, which can have serious negative health effects for the population. Health effects include a lowering of fetal/infant survival rates (Jayachandran, 2009), increases in mortality rates (Koplit et al., 2016; Sahani et al., 2014) and more cases of respiratory problems (Kunii et al.,

2002). In tropical peatlands, anthropogenic activity also increases peat fire susceptibility. A desire for more agricultural activity has led to more drainage (Fatoyinbo, 2017) and deforestation (Hirano et al., 2012) of these systems, ultimately leading to degradation, especially in Southeast Asia (Dohong et al., 2017; Ribeiro et al., 2021). Despite these drastic landscape changes and prominent fire occurrences, studies pertaining to tropical peatland fire risk are limited. In this study, we test the capability of the Optical Trapezoid Model (OPTRAM), as applied in the tropics (Koupaei-Abyazani et al., 2024), for predicting tropical peatland burned area.

3.2 Methods

3.2.1 The Optical Trapezoid Model (OPTRAM)

OPTRAM was utilized as a proxy for WTL (Burdun et al., 2020a; Burdun et al., 2020b; Burdun et al., 2023) in tropical peatlands. This model calculates the OPTRAM index, which has been found to be correlated to tropical peatland WTL variability over sparsely vegetated areas (Koupaei-Abyazani et al., 2024). OPTRAM uses the relationship between the normalized difference vegetation index (NDVI) and shortwave infrared transformed reflectance (STR) to determine the OPTRAM index (Figure 3.1). NDVI is dependent on surface reflectance in the red and near-infrared (NIR) (equation 3.1) while STR is a function of shortwave infrared reflectance (SWIR) (equation 3.2).

$$NDVI = \frac{NIR-RED}{NIR+RED} \quad (3.1)$$

$$STR = \frac{(1-SWIR)^2}{(2)(SWIR)} \quad (3.2)$$

Once the relationship between STR and NDVI is plotted, two lines are drawn that try to encompass most of the pixels. This is done through visual inspection (Chen et al., 2020; Sadeghi et al., 2017). The top and bottom lines are denoted as the wet and dry edges, respectively, and are represented by the following equations (equations 3.3 and 3.4):

$$STR_{min,i} = m_{min}NDVI + b_{min} \quad (3.3)$$

$$STR_{max,i} = m_{max}NDVI + b_{max} \quad (3.4)$$

$STR_{min,i}$, m_{min} , and b_{min} is the STR value, slope, and intercept of the dry edge, respectively, while the same is true for $STR_{max,i}$, m_{max} , and b_{max} but for the wet edge. The OPTRAM index is then calculated based on a ratio of the differences in certain STR values (equation 3.5).

$$OPTRAM\ INDEX = \frac{STR_i - STR_{min,i}}{STR_{max,i} - STR_{min,i}} \quad (3.5)$$

STR_i is the STR value of specific pixel within the wet and dry edges. $STR_{min,i}$ and $STR_{max,i}$ are the STR values at the dry and wet edge of that same pixel, respectively.

To obtain surface reflectance values, we used the Moderate Resolution Imaging Spectroradiometer (MODIS) MOD09GA product (version 6.1). MOD09GA provides daily surface reflectance values at 500-meter spatial resolution. We used band 1 (RED; 620-670 nm), 2 (NIR; 841-876 nm), and 7 (SWIR; 2105-2155 nm) for OPTRAM index calculation. It is also corrected for various atmospheric conditions such as Rayleigh scattering, gasses, and aerosols.

However, it is important to note that this product is not bidirectional reflectance distribution function (BRDF) corrected. Due to high cloud cover in the tropics, we omitted any pixels that were designated as “cloudy” and also those that had a cloud shadow. This was based on Table 13 of the “MODIS Collection 6.1 (C61) LSR

Product User Guide” (https://lpdaac.usgs.gov/documents/925/MOD09_User_Guide_V61.pdf).

We used the Google Earth Engine Code Editor (GEE) to obtain a daily time series of red, NIR, and SWIR surface reflectance and then proceeded to manipulate the values in Python (version 3.10.4).

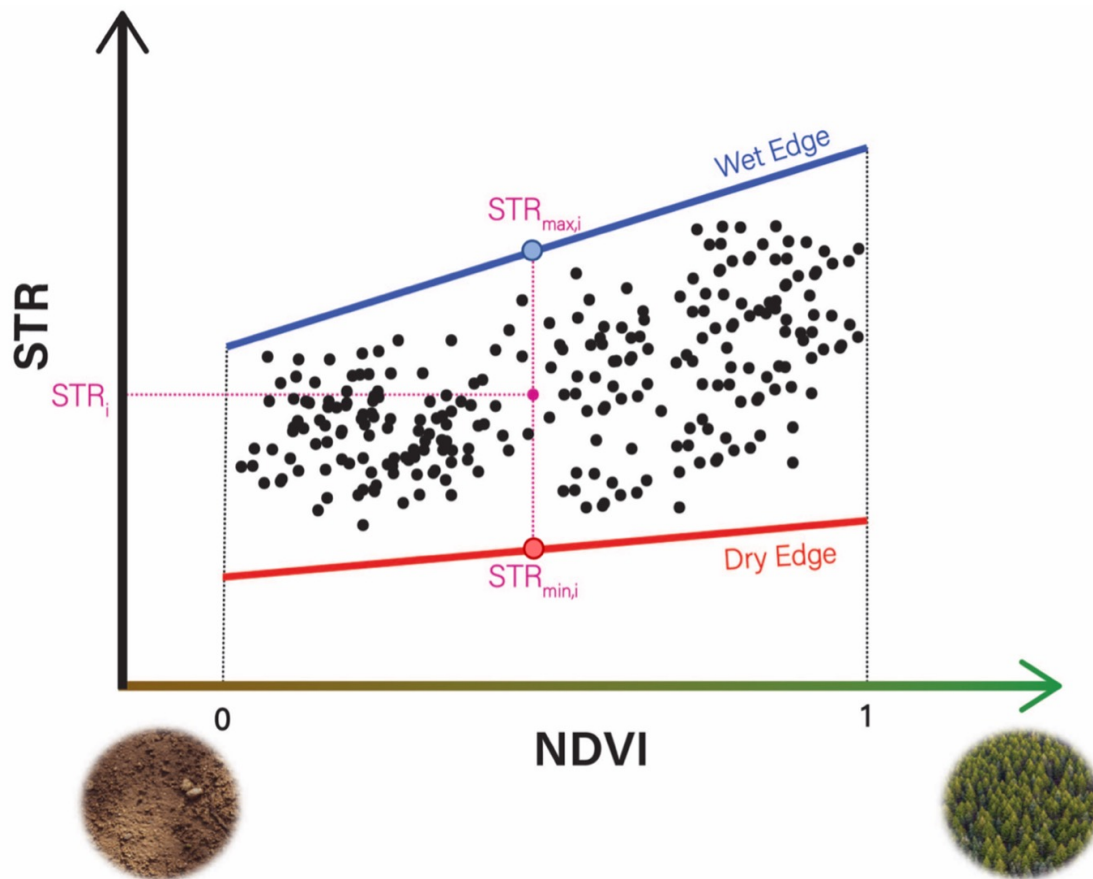


Figure 3.1: A diagram of the OPTRAM model. Individual pixels i (black dots) are plotted in the normalized difference vegetation index (NDVI) and shortwave infrared transformed reflectance (STR) space. Wet (blue line) and dry (red line) edges are determined through visual inspection.

These edges are utilized in evaluating $STR_{\max,i}$ and $STR_{\min,i}$ for each pixel. STR_i represents the STR value for a given pixel. All three of these parameters are used in determining the OPTRAM index for each pixel via equation 3.5.

3.2.2 The Global Fire Emissions Database (Version 4.1s)

The Global Fire Emissions Database (GFED) provides global monthly burned area from mid-1995 through 2016 at 0.25° spatial resolution (Giglio et al., 2013). This data product combines 500-meter MODIS burned area maps with active fire data from the Tropical Rainfall Measuring Mission (TRMM) and Visible and Infrared Scanner (VIRS) and the Along-Track Scanning Radiometer (ATSR) (Giglio et al., 2013). We used GFED version 4.1s which is boosted by small fire burned area (Randerson et al., 2012; Randerson et al., 2017). This specific dataset includes fires that are smaller than the 500-meter resolution of the MODIS burned area product used in other GFED versions (Dadap et al., 2019). We decided to include small fires since, on average, these represent ~39% of total burned area in insular Southeast Asian peatlands alone (Randerson et al., 2012).

GFED assumes a constant emission factor per unit burned area, making variations in daily emissions and burned area proportional (Dadap et al., 2019). Daily emissions data is provided in the form of a daily fraction, meaning that it indicates what fraction of total emissions was emitted in the different days of a given month. Daily fractions from each month were multiplied by the total burned area value for that month to obtain a proxy value for burned area at daily resolution. This allowed us to match the temporal scale of burned area with that of OPTRAM index. We used data from the year 2003 through 2016. Earlier years could not be used due to unavailability of daily emissions data. Furthermore, data for more recent years (2017 and

onwards) is still in “beta” and therefore incomplete, which is why data up to and including 2016 was used. We will be using only the dry season (defined here as June through October) of each respective region for analysis.

3.2.3 Testing OPTRAM’s Capability of Predicting Burned Area

We tested OPTRAM’s capability for predicting burned area by shifting the OPTRAM index time series 10, 20, and 30 days forward relative to the burned area time series. This allowed us to evaluate the relationship between current burned area and an OPTRAM index that was 10, 20, and 30 days in the past. These specific number of days were chosen based on a previous study involving tropical peatlands and burned area ([Dadap et al., 2019](#)). In this way, we may test whether OPTRAM indices are an indicator of burned area variability. We also explored how the number of consecutive low OPTRAM days (below a certain threshold) impacts the probability of burned area occurrence the next day. We used the top 100 longest streaks of consecutive days and each streak of consecutive days was unique (i.e. no double-counting).

The Python programming language (version 3.10.4) and “pandas” package was utilized to organize the time series and manipulate data. It is important to note that, due to cloud cover and cloud shadows, the OPTRAM index time series was subject to many data gaps. Additionally, we assumed that data gaps within the burned area time series indicated zero peatland burned area. As a result, we inserted the number “zero” within all gaps in the burned area time series.

3.2.4 Study Sites

We conducted our analyses in Indonesia, Malaysia, Peru, and Africa and chose points for OPTRAM evaluation that were within a GFED grid cell (Figure 3.2; Figure 3.S13; Figure 3.S14; Figure 3.S15). Peatland area was determined using two approaches. The first approach used GFED-identified peat area. The GFED dataset provides a “partitioning” component in its “emissions” group. Within this component, the type of fire contributing to the carbon emissions is identified, one of which is peat indicated as “C_PEAT” in GFED 4.1s. Using this methodology, we only included months within our defined dry season where “C_PEAT” is non-zero. If “C_PEAT” turned out to be zero for all months and years, we used the second approach. The second approach used Peat-ML ([Melton et al., 2022](#)) to determine peatland areas. Peat-ML is a product that provides a spatially continuous estimate of global peatland extent using machine learning ([Melton et al., 2022](#)). The product uses inputs such as soil and geomorphological data, vegetation indices via remote sensing, and drivers of peatland formation to create a map of global peatland extent ([Melton et al., 2022](#)). Areas with a peatland extent of greater than ~30% were used. These two approaches allowed us to have some confidence that OPTRAM was being applied on peatland.

Previous work has found OPTRAM performance to be dependent on vegetation density ([Koupaeei-Abyazani et al., 2024](#)). Therefore, we utilized NDVI time series at each site to determine whether it was a good fit for OPTRAM application. We omitted NDVI values designated as “cloudy” and also those that had a cloud shadow according to Table 13 of the “MODIS Collection 6.1 (C61) LSR Product User Guide”

(https://lpdaac.usgs.gov/documents/925/MOD09_User_Guide_V61.pdf). A previous study found that the average correlation between OPTRAM index and WTL was relatively high when NDVI was less 0.7 (Koupaei-Abyazani et al., 2024). Therefore, we only chose locations where the majority of daily NDVI values (greater than 50%) were less than 0.7 for Indonesia, Peru, and Africa during the defined dry seasons of 2003 through 2016 (Table 1). For Malaysia, we used a threshold of NDVI less than 0.75 since we could not find areas with NDVI less 0.7 (Table 1).

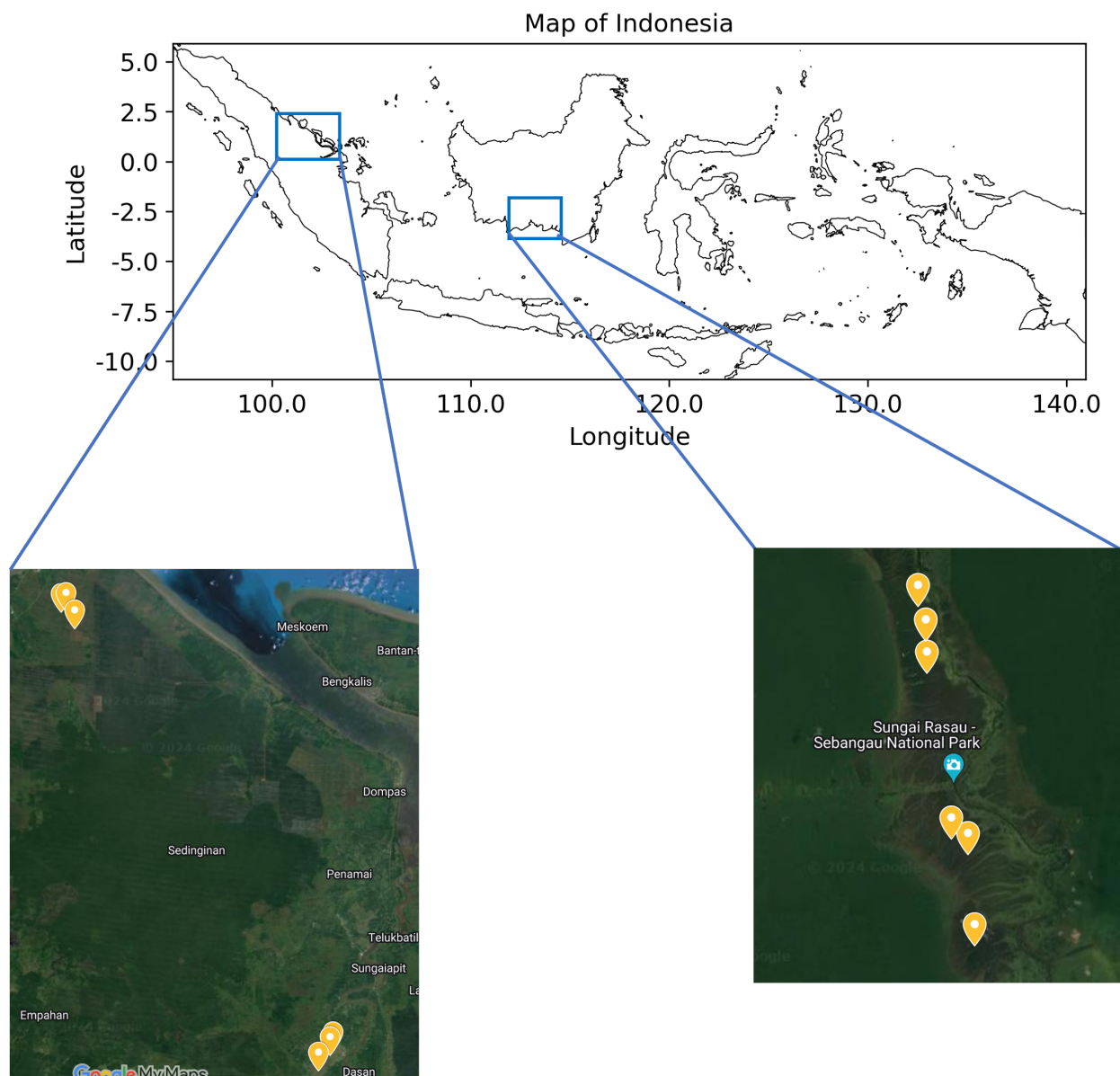


Figure 3.2: The twelve Indonesian site locations used in this study. Satellite images from Google Maps.

SITE	Location (Latitude, Longitude)	NDVI Threshold Used	Number of Data Points Below NDVI Threshold	Total Number of NDVI Data Points	Percentage of Data Points Below NDVI Threshold
Indonesia 1	-2.45218, 114.0321	<0.7	457	519	88.05
Indonesia 2	-2.44247, 114.03194	<0.7	427	524	81.49
Indonesia 3	-2.43158, 114.02958	<0.7	439	539	81.45
Indonesia 4	-2.50805, 114.04499	<0.7	464	483	96.07
Indonesia 5	-2.50399, 114.03973	<0.7	457	468	97.65
Indonesia 6	-2.53622, 114.047	<0.7	458	511	89.63
Indonesia 7	0.96675, 102.05946	<0.7	315	381	82.68
Indonesia 8	0.95964, 102.05467	<0.7	273	333	81.98
Indonesia 9	0.93827, 102.03848	<0.7	255	349	73.07
Indonesia 10	1.58873, 101.67299	<0.7	157	179	87.71
Indonesia 11	1.58882, 101.68041	<0.7	160	176	90.91
Indonesia 12	1.56454, 101.69234	<0.7	161	183	87.98
Peru 1	-4.82942, -75.57841	<0.7	303	550	55.09
Peru 2	-4.83549, -75.57602	<0.7	340	528	64.39
Peru 3	-4.83143, -75.57271	<0.7	328	531	61.77
Peru 4	-4.84181, -75.56847	<0.7	347	555	62.52
Peru 5	-4.83615, -75.56827	<0.7	387	543	71.27
Peru 6	-4.83918, -75.5617	<0.7	440	544	80.88
Peru 7	-4.5689, -75.82784	<0.7	264	499	52.91
Peru 8	-4.71029, -75.77343	<0.7	418	499	83.77
Peru 9	-4.71243, -75.77995	<0.7	345	498	69.28
Peru 10	-4.6928, -75.77117	<0.7	309	512	60.35
Peru 11	-4.68679, -75.77411	<0.7	256	503	50.89
Peru 12	-4.70136, -75.77821	<0.7	281	491	57.23
Malaysia 1	1.48541, 111.20297	<0.75	316	452	69.91
Malaysia 2	1.45348, 111.15488	<0.75	287	442	64.93
Malaysia 3	1.47893, 111.20095	<0.75	289	452	63.94
Malaysia 4	1.42418, 111.14592	<0.75	319	608	52.47
Malaysia 5	1.336, 111.15321	<0.75	312	592	52.7
Malaysia 6	1.41905, 111.22322	<0.75	339	568	59.68
Malaysia 7	1.52504, 111.18545	<0.75	238	411	57.91
Malaysia 8	1.52909, 111.17232	<0.75	249	431	57.77
Malaysia 9	1.53673, 111.18253	<0.75	249	424	58.73
Malaysia 10	1.51253, 111.18494	<0.75	256	442	57.92
Malaysia 11	1.50533, 111.17841	<0.75	257	440	58.41
Malaysia 12	1.51631, 111.17275	<0.75	253	438	57.76
CongoBasin 1	-0.11842, 17.06305	<0.7	439	468	93.8
CongoBasin 2	-0.11862, 17.07082	<0.7	436	460	94.78
CongoBasin 3	-0.12467, 17.06734	<0.7	439	460	95.43
CongoBasin 4	-0.13337, 17.06895	<0.7	411	450	91.33
CongoBasin 5	-0.14118, 17.06354	<0.7	432	462	93.3
CongoBasin 6	-0.14745, 17.07616	<0.7	392	472	83.05
CongoBasin 7	-0.1306, 17.15094	<0.7	364	540	67.41
CongoBasin 8	-0.12759, 17.14956	<0.7	338	509	66.4
CongoBasin 9	-0.12798, 17.15403	<0.7	385	539	71.43
CongoBasin 10	-0.14831, 17.15228	<0.7	361	522	69.16
CongoBasin 11	-0.14567, 17.15026	<0.7	350	522	67.05
CongoBasin 12	-0.1308, 17.14588	<0.7	329	509	64.64

Table 3.1: Table listing the site names, locations of sites, NDVI threshold used, number of total data points and number of data points below a specific NDVI, and percentage of data points below a specific NDVI threshold.

3.3 Results

3.3.1 Indonesia Sites

3.3.1.1 10, 20, and 30-day forward shifted OPTRAM values

When shifting OPTRAM values 10 days forward with respect to the burned area proxy, the Indonesian sites generally showed a higher value for burned area proxy when the OPTRAM value 10 days before was low (Figure 3.3). Note that high and low OPTRAM values indicate wet and dry surface conditions, respectively. Most burned area proxy values above 0.006 occurred when the OPTRAM value 10 days before was less than 0.4 (Figure 3.3). Conversely, when the OPTRAM value 10 days before was greater than 0.6, most of the burned area proxy values were zero (Figure 3.3).

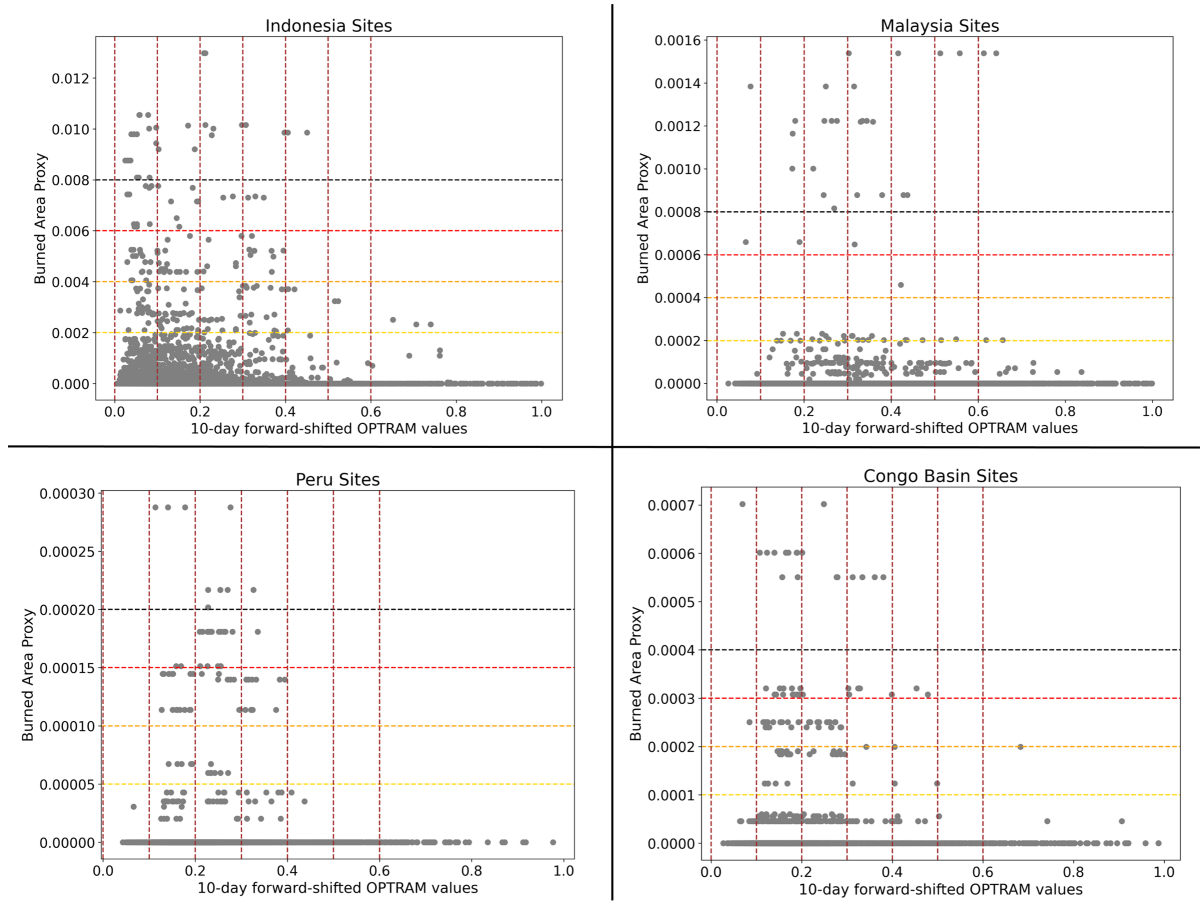


Figure 3.3: Scatterplot showing the relationship between burned area proxy (unitless) and 10-day forward-shifted OPTRAM values (unitless) at each site. Vertical brown dotted lines indicated constant OPTRAM values of 0, 0.1, 0.2, 0.3, 0.4, 0.5, and 0.6. The yellow, orange, red, and black horizontal dotted lines show constant burned area proxy values for each site. The dotted lines were added to facilitate data visualization.

When creating thresholds for 10-day forward shifted OPTRAM values and comparing to burned area proxy values, a clear decreasing trend becomes evident. For 10-day forward shifted OPTRAM values that are between zero and 0.05 (zero inclusive and 0.05 exclusive), the percentage of data points where the burned area proxy value was ≥ 0.0001 was $\sim 37\%$ (Figure 3.4). Therefore, the percentage of burned area proxy data points less than 0.0001 within the same

10-day forward shifted OPTRAM threshold was ~63% (Figure 3.4). The percentage of data points when the burned area proxy value was ≥ 0.0001 generally continued to decrease as the magnitude of 10-day forward shifted OPTRAM thresholds increased (Figure 3.4). Starting from ~37%, the percentage changed to ~35%, ~26%, ~24%, ~19%, ~18%, ~17%, ~18%, ~13%, ~10%, ~8%, ~2%, and ~4% as the magnitude of the 10-day forward shifted OPTRAM threshold increased (Figure 3.4).

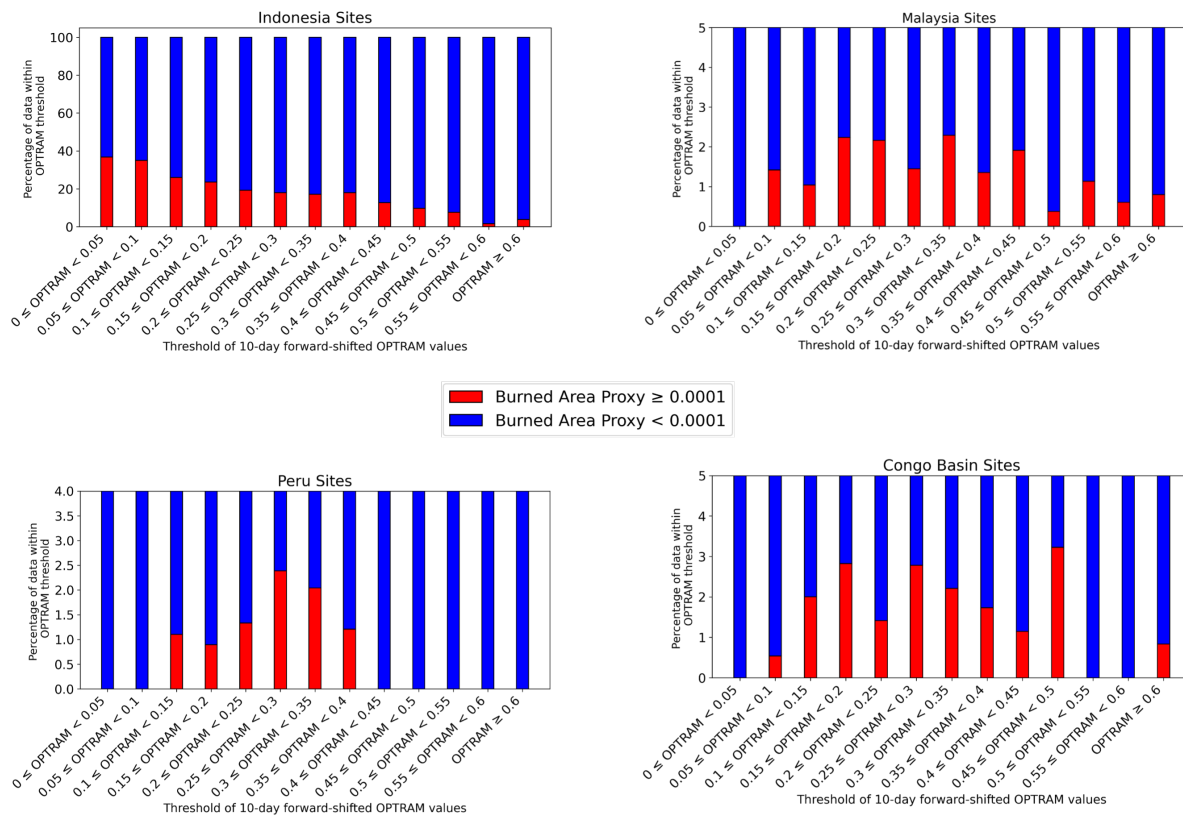


Figure 3.4: A histogram showcasing the relationship between the percentage of data with burned area proxy ≥ 0.0001 or < 0.0001 that are within each 10-day forward shifted OPTRAM threshold for each site. Red and blue indicate burned area proxy values ≥ 0.0001 and < 0.0001 , respectively. Note that the scale of the y-axis is different for each site.

Another analysis showed a similar trend but this time for burned area proxy values of strictly zero and non-zero. For 10-day forward shifted OPTRAM thresholds of zero to 0.05 (zero inclusive and 0.05 exclusive) and 0.05 to 0.1 (0.05 inclusive and 0.1 exclusive), the percentage of data points where the burned area proxy value was non-zero was ~41% and ~42%, respectively (Figure 3.5). This percentage generally decreased as the magnitude of the 10-day forward shifted OPTRAM threshold increased (Figure 3.5).

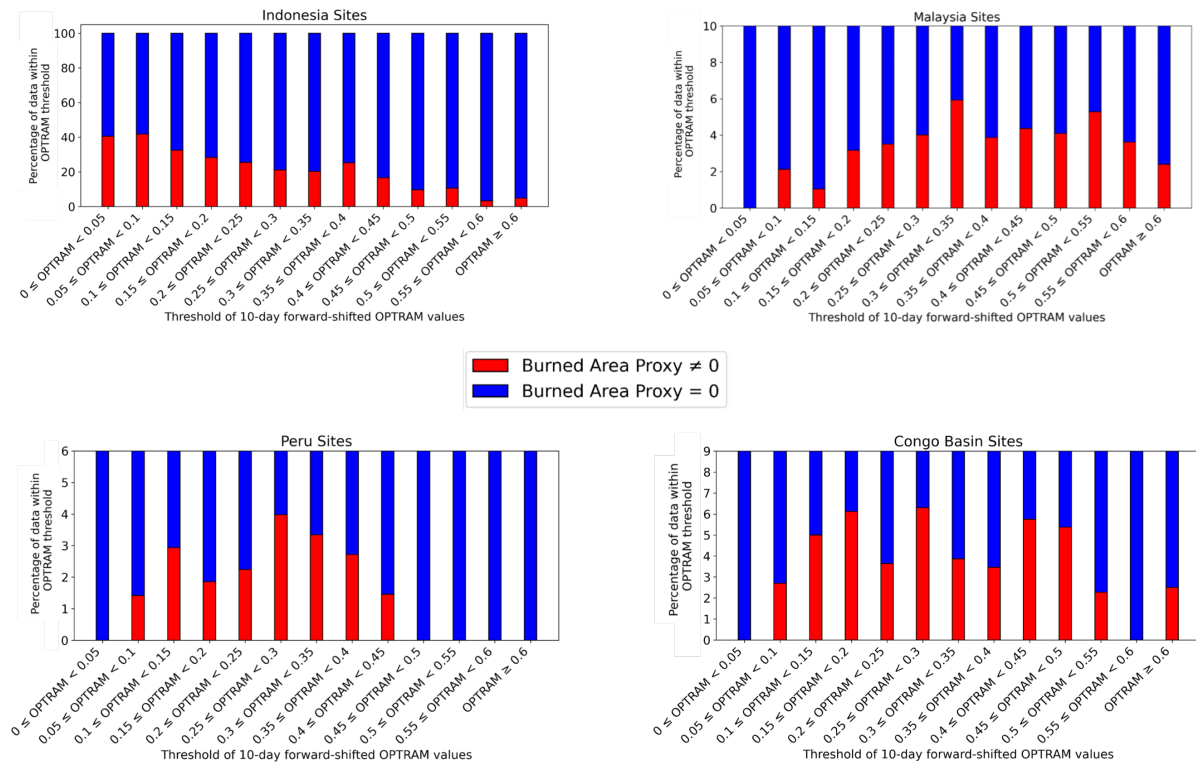


Figure 3.5: A histogram showcasing the relationship between the percentage of data with burned area proxy equal to zero or not equal to zero that are within each 10-day forward shifted OPTRAM threshold for each site. Red and blue indicate burned area proxy values not equal to zero and equal to zero, respectively. Note that the scale of the y-axis is different for each site.

In addition to only including 10-day forward shifted OPTRAM thresholds, we also performed analysis to include thresholds for both the 10-day forward shifted OPTRAM values *and* the burned area proxy values. We found that as the magnitude of 10-day forward shifted OPTRAM threshold increased, the percentage of data points with a burned area proxy equal to zero steadily increased (Figure 3.6). On the other hand, the percentage of data points with burned area proxy between zero and 0.002 (zero exclusive and 0.002 inclusive) steadily decreased (Figure 3.6). Other thresholds for the burned area proxy did not show a notable trend. Although, it is important to note that many instances where the percentage of non-zero burned area proxy data points was zero was when the 10-day forward shifted OPTRAM threshold was either 0.5 to 0.6 (0.5 inclusive and 0.6 exclusive) or ≥ 0.6 (Figure 3.6).

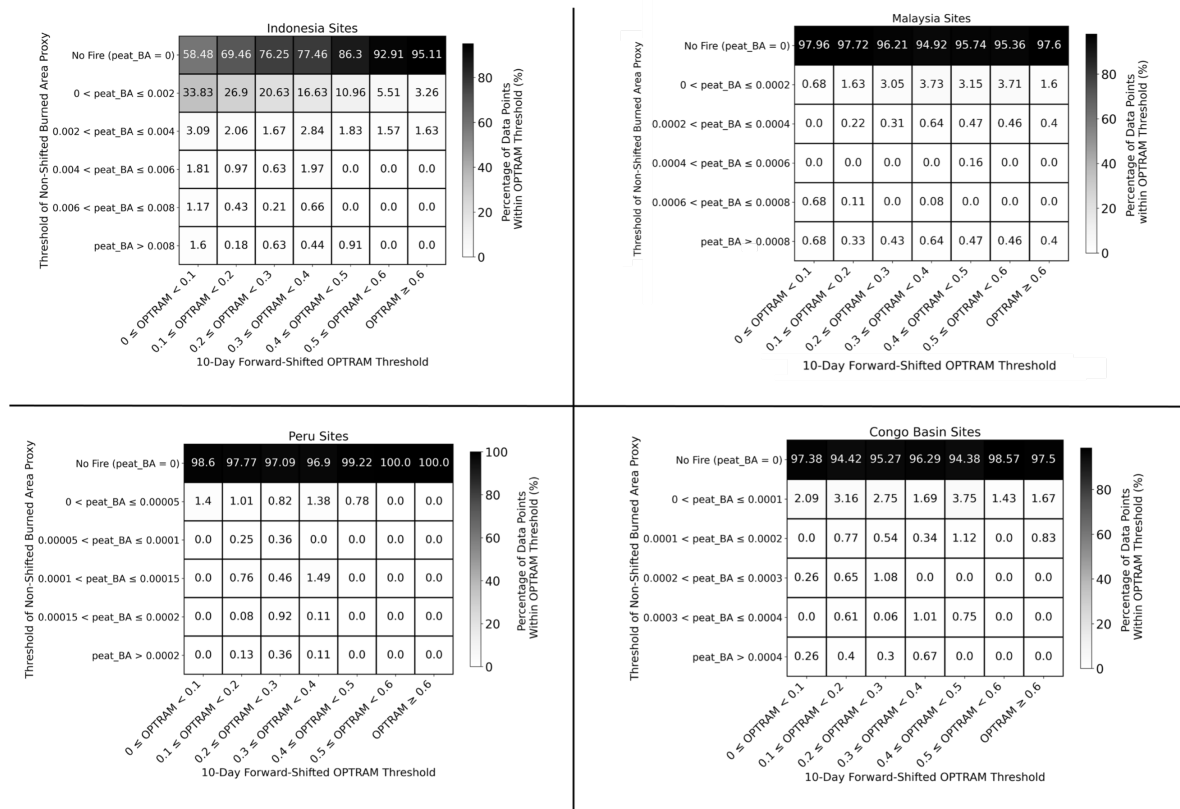


Figure 3.6: A two-dimensional histogram showing the percentage of data points that fall within a specific 10-day forward shifted OPTRAM threshold *and* peat_BA (burned area proxy) threshold at each site. Percentage values are indicated within each square with white, gray, and black colors representing low, intermediate, and high percentage values. Note that the burned area proxy thresholds vary for each site.

When shifting OPTRAM index values 20-days forward, a similar trend can be seen. Generally, higher burned area proxy values corresponded with lower 20-day forward-shifted OPTRAM index values (Figure 3.S1). The percentage of burned area values (whether ≥ 0.0001 or $\neq 0$) also followed a similar trend, with higher percentages occurring at lower OPTRAM index thresholds and then generally decreasing as the magnitude of the OPTRAM index thresholds increase (Figure 3.S2; Figure 3.S3). At the lowest OPTRAM index threshold ($0 \leq \text{OPTRAM index} < 0.05$), ~72% of the burned area proxy data points had values ≥ 0.0001 (when no burned area was defined as < 0.0001) (Figure 3.S2), while ~77% of the burned area proxy datapoints had values

that were non-zero (when no burned area was defined as strictly zero) (Figure 3.S3). The smallest percentage of burned area values occurred at relatively high OPTRAM index threshold values, with ~3.8% and ~5.8% at a threshold of $0.55 \leq \text{OPTRAM index} < 0.6$ for burned area defined as ≥ 0.0001 and $\neq 0$, respectively (Figure 3.S2; Figure 3.S3). A similar trend was observed when thresholds for the burned area proxy were added. Most of the burned area fell between the values of 0 (exclusive) and 0.002 (inclusive) and the percentage decreased with increasing OPTRAM index threshold (Figure 3.S7). Furthermore, when shifting OPTRAM values 30 days forward relative to the peat burned area, a similar relationship is seen to that of 10-day and 20-day forward shifted OPTRAM values. In other words, as the OPTRAM index value increased, the burned area proxy value (and the percentage of burned area proxy within a specific OPTRAM index threshold) decreased (Figure 3.S2; Figure 3.S5; Figure 3.S6; Figure 3.S8).

3.3.1.2 Peat Burned Area Dependence on Continuously Low OPTRAM Indices in Indonesia

The burned area proxy was also impacted by both the number of consecutive days OPTRAM indices were below a certain threshold and by the magnitude of that threshold. In general, as the number of consecutive days with OPTRAM below a certain threshold increased, the number of instances (presented as a percentage) of non-zero burned area proxy increased (Figure 3.7). This was not true when the OPTRAM threshold was increased (< 0.35 , < 0.4 , and < 0.45). In all those cases, the highest consecutive number of days was seven, and all had zero burned area the day after. Note, however, that the number of instances when this occurred was extremely limited ($n = 1$ or $n = 2$) (Figure 3.7).

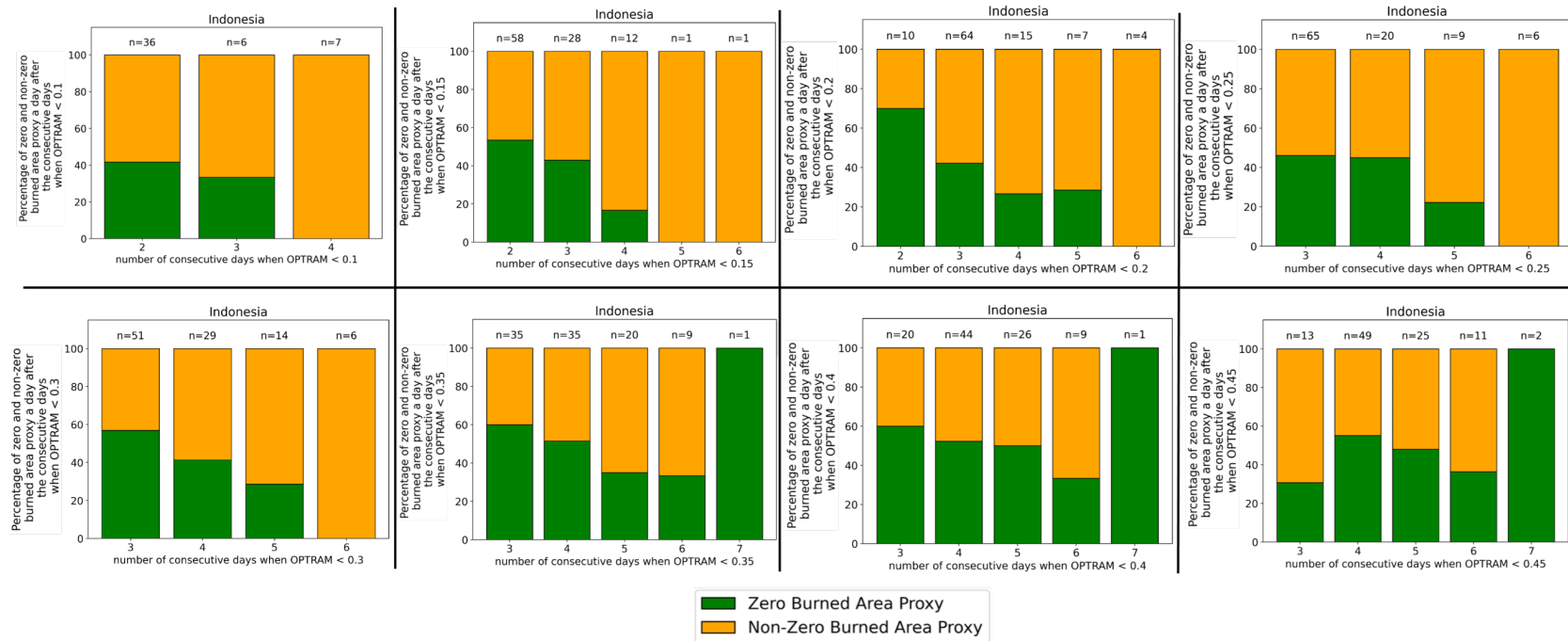


Figure 3.7: Percentage of zero and non-zero burned area proxy a day after consecutive days when OPTRAM was below a certain threshold at the Indonesian sites. X-axis shows the number of consecutive days that OPTRAM was below a certain threshold. The “n” value shows the number of instances of burned area proxy values for each number of consecutive days. Green and yellow represent zero and non-zero burned area proxy values respectively.

3.3.2 Malaysia Sites

3.3.2.1 10, 20, and 30-day forward shifted OPTRAM values

The relationship between the burned area proxy and 10-day forward shifted OPTRAM index for the Malaysian sites was quite different relative to that of the Indonesian sites. While most non-zero burned area data points resided at moderate to low OPTRAM values (< 0.5), there were still instances of high burned area (> 0.0014) for OPTRAM values greater than 0.6 (Figure 3.3).

The fraction of data points with a burned area proxy ≥ 0.0001 within each 10-day forward shifted OPTRAM threshold did not show any notable trend (Figure 3.4). Percentages varied between zero and $\sim 2.29\%$, with the largest number of points with ≥ 0.0001 proxy burned area residing within a 10-day forward shifted OPTRAM threshold of 0.3 to 0.35 (0.3 inclusive and 0.35 exclusive). The OPTRAM threshold of zero to 0.05 (zero inclusive and 0.05 exclusive) contained the smallest number of points with proxy burned area ≥ 0.0001 (Figure 3.4). There was also no notable trend when the burned area proxy was set to non-zero (Figure 3.5). Percentages varied between 0 and $\sim 5.93\%$ for non-zero burned area proxy within each 10-day forward shifted OPTRAM threshold. The largest number of instances occurred within the 10-day forward shifted OPTRAM threshold of 0.3 to 0.35 (0.3 inclusive and 0.35 exclusive), while the smallest occurred within 0 to 0.05 (0 inclusive and 0.05 exclusive) (Figure 3.5).

When including thresholds of burned area proxy in addition to the 10-day forward shifted OPTRAM thresholds, there were no notable trends when the burned area proxy was zero across

all OPTRAM thresholds (Figure 3.6). However, there was a larger percentage of data points with burned area proxy values of zero for OPTRAM thresholds between zero and 0.1 (zero inclusive and 0.1 exclusive) and 0.1 to 0.2 (0.1 inclusive and 0.2 exclusive). There were many instances where zero data points were found within relatively high OPTRAM thresholds. For example, for 10-day forward shifted OPTRAM thresholds of 0.5 and higher, there were no data points that had a burned area proxy between 0.0004 and 0.0006 (0.0004 exclusive and 0.0006 inclusive) and between 0.0006 and 0.0008 (0.0006 exclusive and 0.0008 inclusive). Although, it is important to note that, for the same OPTRAM thresholds, there were some data points that had an even greater burned area proxy value of greater than 0.0008 (Figure 3.6).

20-day forward shifts in the OPTRAM index relative to the burned area proxy did not drastically change results. The highest percentage of burned area proxy values occurred at OPTRAM indices between 0.35 (inclusive) and 0.4 (exclusive) for burned area defined as ≥ 0.0001 (Figure 3.S3) and between 0.55 (inclusive) and 0.6 (exclusive) for burned area defined as $\neq 0$ (Figure 3.S4). Like the 10-day forward shifted OPTRAM values, when introducing thresholds for the burned area proxy, no trend was observed. Although, there were many instances at high OPTRAM values (≥ 0.3) where large peat burned areas ($0.0004 < \text{burned area proxy} \leq 0.0008$) did not appear (Figure 3.S7). 30-day forward shifted OPTRAM values had high burned area proxy percentages occurring at moderate OPTRAM values ($0.3 \leq \text{OPTRAM} < 0.35$) (with the peak percentage occurring at $0.55 \leq \text{OPTRAM} < 0.6$ for when burned area occurrence was defined as being ≥ 0.0001) (Figure 3.S5; Figure 3.S6). In addition to the multiple instances of low/zero percentages when burned area proxy values were > 0.0004 and OPTRAM was ≥ 0.3 ,

there were also instances of zero percentages for burned area proxy values > 0.0004 when OPTRAM was low (< 0.3) (Figure 3.S8).

3.3.2.2 Peat Burned Area Dependence on Continuously Low OPTRAM Indices in Malaysia

Generally, the number of consecutive days that showed the largest percent of non-zero burned area proxy was between 2 and 4 days regardless of the OPTRAM index threshold (Figure 3.S9). For OPTRAM indices below 0.15, there were no instances of non-zero burned area proxy. In most instances, longer consecutive days below a certain OPTRAM threshold yielded higher non-zero burned area percentages (Figure 3.S9).

3.3.3 Peru Sites

3.3.3.1 10, 20, and 30-day forward shifted OPTRAM values

The sites in Peru showed a prominent relationship between 10-day forward shifted OPTRAM thresholds and burned area proxy values. Most instances of non-zero burned area proxy values occurred below a 10-day forward shifted OPTRAM value of 0.4 (Figure 3.3). The largest burned area proxy values occurred between OPTRAM values of 0.1 and 0.3 (Figure 3.3).

The only instances of burned area proxy ≥ 0.0001 were for 10-day forward shifted OPTRAM thresholds of 0.1 to 0.15 (0.1 inclusive and 0.15 exclusive), 0.15 to 0.2 (0.15 inclusive and 0.2 exclusive), 0.2 to 0.25 (0.2 inclusive and 0.25 exclusive), 0.25 to 0.3 (0.25 inclusive and 0.3 exclusive), 0.3 to 0.35 (0.3 inclusive and 0.35 exclusive), 0.35 to 0.4 (0.35 inclusive and 0.4 exclusive) (Figure 3.4). A decreasing trend was found when moving from an OPTRAM threshold of 0.25 to 0.3 (0.25 inclusive and 0.3 exclusive) to a threshold of 0.35 to 0.4 (0.35 inclusive and 0.4 exclusive). The highest number of data points that had a burned area value \geq

0.0001 was between 0.25 to 0.3 (0.25 inclusive and 0.3 exclusive) (~2.4% of data points within the specific OPTRAM threshold) (Figure 3.4).

Results were similar for when the burned area proxy was set to zero and non-zero values. In addition to the previously mentioned 10-day forward shifted OPTRAM thresholds, two additional thresholds also contained non-zero burned area proxy values, being 0.05 to 0.1 (0.05 inclusive and 0.1 exclusive) and 0.4 to 0.45 (0.4 inclusive and 0.45 exclusive) (Figure 3.5). No apparent trend was found other than a decreasing percentage of data points having non-zero burned area proxy values from an OPTRAM threshold of 0.25 to 0.3 (0.25 inclusive and 0.3 exclusive) to a threshold of 0.4 to 0.45 (0.4 inclusive and 0.45 exclusive). The highest percentage was between an OPTRAM threshold of 0.25 and 0.3 (0.25 inclusive and 0.3 exclusive) (~4%) (Figure 3.5).

When including thresholds for burned area proxy, there was an increasing trend from an OPTRAM threshold of 0.3 to 0.4 (0.3 inclusive and 0.4 exclusive) up to when OPTRAM was ≥ 0.6 when the burned area proxy value equaled zero (Figure 3.6). At the 10-day forward shifted OPTRAM thresholds of 0.5 to 0.6 (0.5 inclusive and 0.6 exclusive) and ≥ 0.6 , all data points had a burned area proxy value of zero. It is important to note that, within the OPTRAM threshold of zero to 0.1 (zero inclusive and 0.1 exclusive), all non-zero burned area proxy data points had a value between zero and 0.00005 (zero exclusive and 0.00005 inclusive) (Figure 3.6).

Interestingly, when shifting OPTRAM values 20 days forward, the trends become almost opposite relative to when OPTRAM is shifted 10 days forward. For the case when burned area is defined as ≥ 0.0001 , 20 day forward shifted OPTRAM values showed minimal burned area proxy percentages for an OPTRAM index of $\sim 0.25-0.45$. Instead, larger relative values occurred when OPTRAM was small ($0.05-0.2$) and large ($0.45 \leq \text{OPTRAM} < 0.5$ and $0.55 \leq \text{OPTRAM} < 0.6$) (Figure 3.S3). A similar change may be seen when peat burned area was defined as being $\neq 0$ (Figure 3.S4). When burned area proxy was given multiple thresholds, the percentage of burned area proxy data points with a value of zero increased as OPTRAM index increased (Figure 3.S7). Furthermore, it should be noted that 20-day forward shifted OPTRAM values had more instances of non-zero burned area proxy percentages at high OPTRAM values (≥ 0.4) relative to that of 10-day forward shifted OPTRAM values (Figure 3.S7; Figure 3.6).

The relationship between burned area proxy and 30-day forward shifted OPTRAM values did not have as strong of a trend when compared to 10-day and 20-day forward shifted OPTRAM values. Besides the dramatic 100% non-zero and ≥ 0.0001 peat burned area values between OPTRAM values of 0 (inclusive) and 0.05 (exclusive), the burned area proxy percentages stayed relatively consistent with one another as OPTRAM index increased. Although, it is important to note that there was a large increase at $0.45 \leq \text{OPTRAM} < 0.5$ and $0.55 \leq \text{OPTRAM} < 0.6$ for both the non-zero and ≥ 0.0001 peat burned area cases (Figure 3.S5; Figure 3.S6). When including multiple burned area proxy thresholds in the analysis, no apparent trend was found (Figure 3.S8).

3.3.3.2 Peat Burned Area Dependence on Continuously Low OPTRAM Indices in Peru

The number of consecutive days where burned area proxy was non-zero was between 2 and 5 days. As the OPTRAM index threshold increased, the number of consecutive days with non-zero peat burned area data points increased as well (Figure 3.S10). Non-zero burned area proxy values occurred a day after when the OPTRAM index threshold was below 0.15 for two consecutive days. Alternatively, non-zero burned area proxy values occurred a day after when the OPTRAM index threshold was below 0.45 for five consecutive days (Figure 3.S10).

3.3.4 Congo Basin Sites

3.3.4.1 10, 20, and 30-day forward shifted OPTRAM values

For sites in the Congo Basin, all burned area proxy values above 0.0004 occurred at 10-day forward shifted OPTRAM values that were below 0.4 (Figure 3.3). Additionally, there were only three data points with non-zero burned area proxy values that also had OPTRAM values greater than 0.68 (Figure 3.3).

When the burned area proxy was set to ≥ 0.0001 , there were no data points within the 10-day forward shifted OPTRAM thresholds of 0 to 0.05 (0 inclusive and 0.05 exclusive), 0.5 to 0.55 (0.5 inclusive and 0.55 exclusive), 0.55 to 0.6 (0.55 inclusive and 0.6 exclusive) (Figure 3.4). All other OPTRAM thresholds contained a non-zero percentage of data points with burned area proxy ≥ 0.0001 . There was a decreasing trend of percentage of data points from OPTRAM thresholds of 0.25 to 0.3 (0.25 inclusive and 0.3 exclusive) to a threshold of 0.4 to 0.45 (0.4 inclusive and 0.45 exclusive) ($\sim 2.79\%$ to $\sim 1.15\%$). There was also a large rise in the percentage of data points for the OPTRAM threshold of 0.45 to 0.5 (0.45 inclusive and 0.5 exclusive) ($\sim 3.23\%$) (Figure 3.4).

When the burned area proxy was set strictly to zero and non-zero, there was no notable trend.

The highest percentage values occurred at 10-day forward shifted OPTRAM thresholds of 0.15 to 0.2 (0.15 inclusive and 0.2 exclusive), 0.25 to 0.3 (0.25 inclusive and 0.3 exclusive), 0.4 to 0.45 (0.4 inclusive and 0.45 exclusive), and 0.45 to 0.5 (0.45 inclusive and 0.5 exclusive) with ~6.12%, ~6.3%, ~5.75%, and ~5.38%, respectively (Figure 3.5).

When including thresholds for burned area proxy in addition to 10-day forward shifted OPTRAM thresholds, there was no apparent trend for data points that had a burned area proxy value of zero across increasing magnitudes of OPTRAM thresholds (Figure 3.6). However, for OPTRAM thresholds of 0.5 to 0.6 (0.5 inclusive and 0.6 exclusive) and ≥ 0.6 , there were no data points within the burned area proxy thresholds of 0.0002 to 0.0003 (0.0002 exclusive and 0.0003 inclusive), 0.0003 to 0.0004 (0.0003 exclusive and 0.0004 inclusive), and > 0.0004 (Figure 3.6).

For 20 day forward-shifted OPTRAM index values where the definition of burned area proxy was ≥ 0.0001 , the percentage of burned area proxy had an increasing trend from an OPTRAM threshold of $0 \leq \text{OPTRAM} < 0.05$ to $0.35 \leq \text{OPTRAM} < 0.4$. Afterwards, there was a percentage drop at $0.4 \leq \text{OPTRAM} < 0.45$ before another generally increasing trend to $\text{OPTRAM} \geq 0.6$ (Figure 3.S3). When peat burned area was defined as $\neq 0$, the trend was similar, but the dramatic drop in peat burned area percentage occurred later at a threshold of $0.45 \leq \text{OPTRAM} < 0.5$ (Figure 3.S4). No trend was observed when also adding in multiple thresholds for peat burned area (Figure 3.S7).

For 30 day forward-shifted OPTRAM indices, generally a larger burned area proxy percentage occurred at higher OPTRAM values. When burned area proxy was defined as ≥ 0.0001 , the largest percentages occurred at OPTRAM thresholds of $0.45 \leq \text{OPTRAM} < 0.5$, $0.55 \leq \text{OPTRAM} < 0.6$, and $\text{OPTRAM} \geq 0.6$ (Figure 3.S5). On the other hand, when burned area proxy was defined as $\neq 0$, the greatest peat burned area percentages were within the OPTRAM thresholds of $0.4 \leq \text{OPTRAM} < 0.45$, $0.45 \leq \text{OPTRAM} < 0.5$, and $\text{OPTRAM} \geq 0.6$ (Figure 3.S6). When adding in thresholds for burned area proxy, no trend was found (Figure 3.S8).

3.3.4.2 Peat Burned Area Dependence on Continuously Low OPTRAM Indices in the Congo Basin

Regardless of the OPTRAM threshold magnitude, burned area proxy was non-zero a day after when OPTRAM was lower than the specific threshold for 2-4 consecutive days (Figure 3.S11). No apparent trend was found between non-zero burned area proxy and the number of consecutive days that OPTRAM index was below a certain threshold. When OPTRAM index was below 0.2, 0.3, 0.35, and 0.45, the percentage of instances for when non-zero burned area proxy occurred were almost identical between the number of consecutive days (Figure 3.S11). For OPTRAM index thresholds that had multiple consecutive days, there was always no instance of non-zero burned area proxy for the highest number of consecutive days.

3.4 Discussion

In this study, we showed that OPTRAM is somewhat capable of predicting burned area in tropical peatlands. The degree of performance varies on a site-to-site basis. This work opens the possibility of using remote sensing methods to detect the probability of future fire occurrences in

tropical peatlands. As a result, it may provide an easier way for assessing peatland fire risk and may also be used as a means for detecting, mitigating, and even eliminating fire-related phenomena such as haze events, before they occur.

3.4.1 OPTRAM's Capability for Predicting Tropical Peatland Burned Area

Our results show OPTRAM to have varying degrees of efficacy when attempting to predict the probability of burned area occurrence. There was high variability based on where OPTRAM was applied. At the Indonesia sites, a strong relationship was found between burned area proxy value and 10, 20, and 30-day forward-shifted OPTRAM thresholds. This shows that OPTRAM plays a major factor in determining the magnitude of the burned area proxy within those sites. One of the reasons for its effectiveness may be the majority of NDVI values that were below 0.7 throughout the defined dry seasons for the years 2003 through 2016. For all the Indonesian sites, the percentages of NDVI below 0.7 ranged from ~73% to ~98% (Table 3.1). This showcases the importance of vegetation cover when attempting to find a suitable location for OPTRAM application. Additionally, due to the high hydraulic conductivity of the upper peat layer, OPTRAM applied at a single site may provide details regarding the temporal water table dynamics of the greater peatland landscape, even if the site has degraded or been drained (Hirano et al., 2012; Hergoualc'h et al., 2020; Burdun et al., 2020b; Koupaei-Abyazani et al., 2024). This means that burned area probabilities may potentially be detected within the peatland landscape even if OPTRAM is not applied in the exact location of interest. This is advantageous since, even if the location of interest has high vegetation density, another location within proximity and with low vegetation density may be chosen to obtain the desired information.

The sites in Malaysia did not show a clear relationship between 10-day and 20-day forward shifted OPTRAM values and burned area proxy relative to the sites in Indonesia. This may be due to the relatively small number of NDVI values below 0.75 (between ~50% and ~70% of the data points) during the defined dry seasons of 2003 through 2016 (Table 3.1). As a result, surface moisture may not have been well represented by OPTRAM indices, resulting in a reduction of the OPTRAM and burned area proxy relationship. For 10-day forward shifted OPTRAM values, there were different results between burned area proxies of zero or non-zero and ≥ 0.0001 or < 0.0001 . There were more instances of non-zero burned area proxy data points within large OPTRAM values relative to low OPTRAM values (Figure 3.5). Conversely, more instances of burned area data points ≥ 0.0001 were found when OPTRAM values were relatively low (Figure 3.4). This may show how sensitive OPTRAM is when defining thresholds for when burned area occurred and did not occur.

The sites in Peru and the Congo Basin showed a differing relationship between 10-day forward shifted OPTRAM index and burned area proxy. Generally, however, a majority of data points with non-zero and ≥ 0.0001 burned area proxy values occurred at small OPTRAM values at both sites (Figure 3.4; Figure 3.5). This may be due to the high percentage of data points that had an NDVI less than 0.7 at each site (~51% to ~84% for Peru and ~65% to ~95% for the Congo Basin), therefore leading to more reliable OPTRAM values. For 20 and 30-day forward shifted OPTRAM values, the relationship at the Peruvian and Congo Basin sites also differed. The greater percentage of burned area proxy occurrences for intermediate OPTRAM values (between 0.25 and 0.45) at the Congo Basin sites relative to the Peruvian sites may indicate that mechanisms other than moisture content are responsible for peat burned area at each site. Future

work may use these results as a starting point for investigating why moisture availability 20 and 30-days beforehand results in such a discrepancy between the two site locations. One explanation may be that Congo Basin peatlands have been subject to less disturbance relative to their Peruvian counterparts ([Dargie et al, 2019](#); [Horn et al., 2018](#)), and therefore this may change the relationship between surface moisture content and burned area proxy for each site.

OPTRAM also has potential for predicting burned area probabilities when the OPTRAM index is below a certain value for a number of consecutive days. This indicates that stakeholders may use this methodology to evaluate tropical peat fire risk and potentially mitigate fires before their occurrence. Fire mitigation measures may include raising the water table, restoring native vegetation, and utilizing fire-free land preparation techniques ([Dohong et al., 2018](#)).

3.4.2 Comparison with Other Studies

To our knowledge, this is the first study that tests OPTRAM's capability for burned area prediction in peatlands. While there are no studies for exact comparison, there are some similar studies. For example, previous work has found a relationship between burned area and soil moisture received from the Soil Moisture Active Passive (SMAP) ([Dadap et al., 2019](#)). This study covered Sumatra, Borneo, and Peninsular Malaysia and focused on the El Niño period of 2015-2016 ([Dadap et al., 2019](#)). It was found that dry soil 30 days prior to fire has a correlation with larger burned area ([Dadap et al., 2019](#)).

Another study used hydrogeological modeling to determine areas with good restoration potential ([Wösten et al., 2008](#)). Furthermore, it was stated that groundwater level prediction

maps may be used to extrapolate groundwater level dynamics to larger areas ([Wösten et al., 2008](#)). This, in turn, may act as a fire hazard warning system for Southeast Asian peatlands ([Wösten et al., 2008](#)).

3.4.3 Study Limitations

Due to the large presence of clouds and cloud shadows in the tropical region, many OPTRAM values were deemed not reliable and therefore omitted from further analysis. This limitation in the number of data points may have impacted the strength of the relationship between burned area proxy and 10, 20, and 30-day forward-shifted OPTRAM values. Additionally, since OPTRAM performance is highly reliant on vegetation density ([Burdun et al., 2020b](#); [Burdun et al., 2023](#); [Koupaei-Abyazani et al., 2024](#)), only site locations with relatively low vegetation cover may be used. Furthermore, site locations near managed systems such as palm plantations may not provide accurate results for landscape-level WTL. This is due to drainage ditches causing a loss of WTL synchronization with the rest of the peatland landscape.

It is important to note that not all NDVI values were less than 0.7 (or less than 0.75 for the Malaysian sites). Therefore, for the timestamps where NDVI was greater than or equal to these values, the OPTRAM values may not have been a reliable estimation of surface moisture content. However, finding sites where daily NDVI values are all below a certain value during the defined dry seasons of 2003 through 2016 is not likely, which is why we used the approach described in section 2.4 for this study.

Another limitation is in our decision to use the MODIS MOD09GA product (version 6.1) which is not BRDF-corrected. The surface reflectance data may therefore be influenced by solar and sensor viewing geometry, causing BRDF-related variability rather than actual surface change. Additionally, the MODIS MOD09GA product (version 6.1) has a 500-meter spatial resolution, which may limit its ability to detect finer-scale surface dynamics. Even though OPTRAM has been shown to perform more optimally using products with finer spatial resolutions ([Burdun et al., 2020b](#)), we prioritized using a product that has a daily temporal resolution to facilitate comparisons with GFED data. The MODIS MOD09GA (version 6.1) product also has a long temporal extent (from 2000 to present), making it a favorable product for use in this study.

3.4.4 Implications of Using OPTRAM for Burned Area Prediction

This work not only has implications for the environment, but also spans the domains of health and economy as well ([Page et al., 2002](#); [Khakim et al., 2020](#)). The ability to predict burned area occurrence can provide stakeholders with an idea of areas in need for restoration. This can then potentially lower the probability of peat fire and decrease the chance of fire-related phenomena such as haze.

Large haze events, for example, are an occurrence in Southeast Asia during the presence of peat fires, especially during El Niño events ([Kunii et al., 2002](#)). OPTRAM may help pinpoint areas most vulnerable to fires many days beforehand, and therefore appropriate action may be taken to reduce the chance of fire before its occurrence. As a result, the associated health impacts ([Afroz et al., 2003](#); [Jayachandran, 2009](#); [Koplitiz et al., 2016](#); [Sahani et al., 2014](#); [Kunii et al., 2002](#)), visibility issues ([Sumaryati et al., 2022](#)), economical losses ([Rosenfeld 1999](#); [Heil and](#)

Goldammer, 2001; Page et al. 2002; Barber & Schweithelm, 2000), and decreases in photosynthetic rates (Fan et al., 1990) may be mitigated.

But perhaps one of the most devastating environmental impacts of fire is the loss of carbon from the peatland to the atmosphere. Due to peat's high carbon content, peat fires can release immense amounts of greenhouse gases (GHGs), including carbon-dioxide and methane, which contributes to global warming and ongoing climate change (Page et al., 2002; Hooijer et al., 2010; Ballhorn et al., 2009; Hergoualc'h & Verhot, 2011; van der Werf et al., 2008). In insular Southeast Asia, the fire situation is unique in that the extent, frequency, and severity of fire is on the rise (Page and Hooijer, 2016). This has been attributed to a drastic conversion of land from pristine peat swamp forest to plantations (Miettinen et al., 2011; Miettinen et al., 2012a; Miettinen et al., 2012b). This study may aid in reducing fire-related carbon emissions by providing stakeholders the necessary information to take action on fire-prone environments. This may be anything from initiating rewetting activities (Ojanen and Minkkinen, 2020; Novita et al., 2024) to restoring the natural water regulation through reforestation (Lampela et al., 2017).

3.5 Conclusion

We demonstrated that OPTRAM has the potential for predicting the probability of burned area occurrence 10, 20, and 30 days ahead of time, albeit with varying degrees of accuracy, at multiple tropical peatland sites spanning Indonesia, Malaysia, Peru, and the Congo Basin. To obtain reliable retrievals of surface moisture content, OPTRAM must be applied in areas with low NDVI. The Indonesia site showed the strongest relationship between 10, 20, and 30-day forward shifted OPTRAM values and burned area proxy, with lower and higher OPTRAM

values corresponding to higher and lower burned area proxy values, respectively. We believe this to be partly due to the high percentage of data points with low NDVI values at the Indonesian sites relative to other sites.

The ability to predict the burned area probability 10, 20, and 30 days ahead of time in tropical peatlands is very beneficial since stakeholders may take informed action before fires occur and therefore lessen its negative impact on health and the environment. For example, fire prevention means that potential haze events may be mitigated, as well as its associated health impacts.

OPTRAM's inherent remote sensing approach allows for a vast application in many tropical peatlands around the globe. As a result, tropical peatlands with low surface moisture content may be identified and restored such that the probability of future fire substantially decreases. Peat fire prevention also leads to a decrease of GHGs to the atmosphere and thereby aids in mitigating the effects of ongoing climate change.

3.6 Supplemental Figures

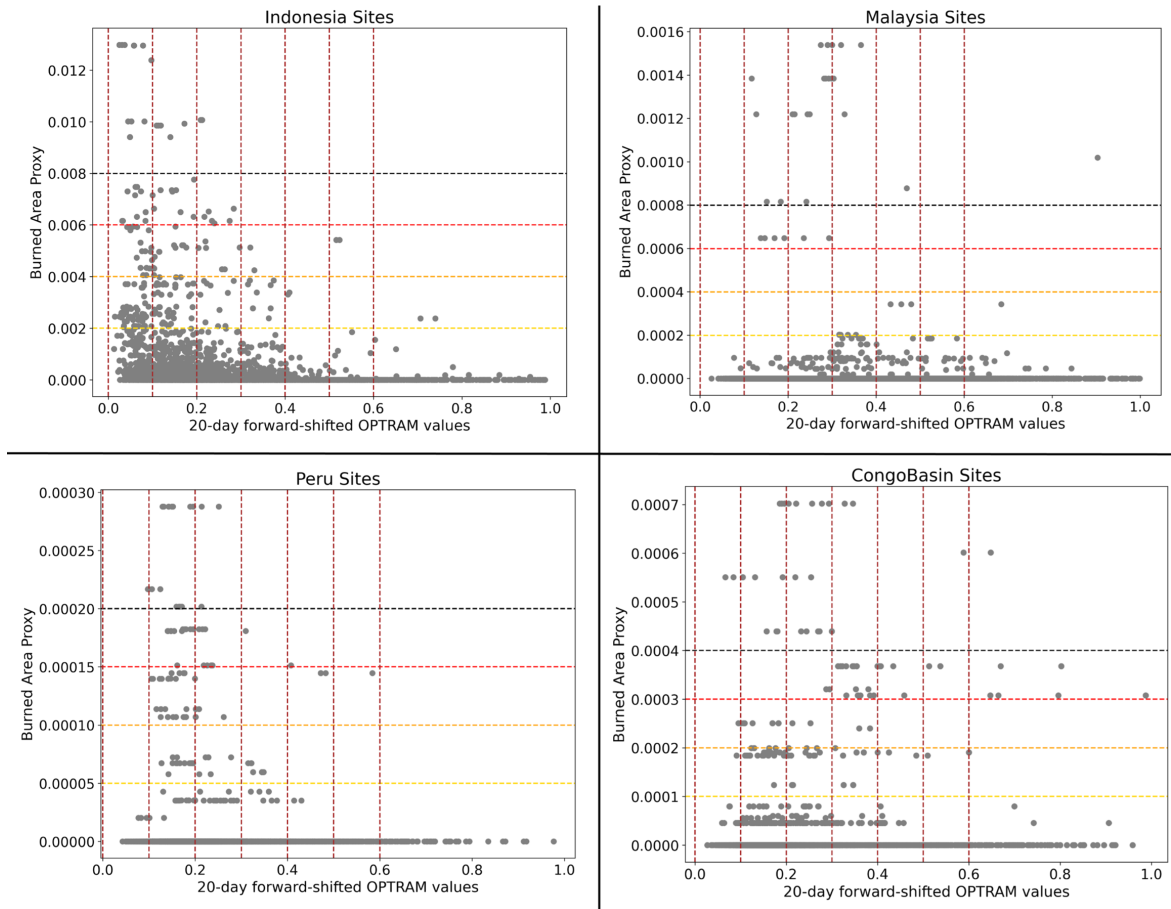


Figure 3.S1: Scatterplot showing the relationship between burned area proxy (unitless) and 20-day forward-shifted OPTRAM values (unitless) at each of the sites. Vertical brown dotted lines indicated constant OPTRAM values of 0, 0.1, 0.2, 0.3, 0.4, 0.5, and 0.6. The yellow, orange, red, and black horizontal dotted lines show constant burned area proxy values for each site. The dotted lines were added to facilitate data visualization.

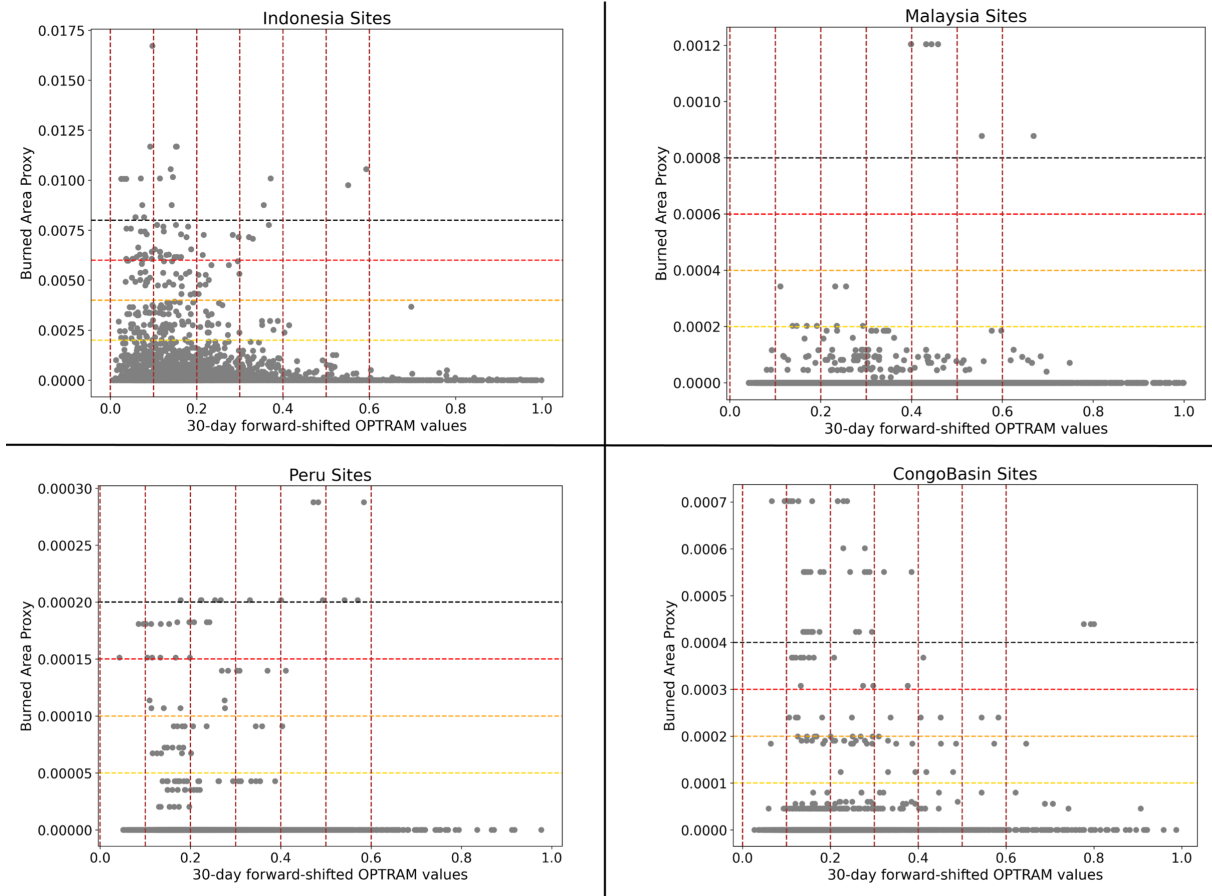


Figure 3.S2: Scatterplot showing the relationship between burned area proxy (unitless) and 30-day forward-shifted OPTRAM values (unitless) at each of the sites. Vertical brown dotted lines indicated constant OPTRAM values of 0, 0.1, 0.2, 0.3, 0.4, 0.5, and 0.6. The yellow, orange, red, and black horizontal dotted lines show constant burned area proxy values for each site. The dotted lines were added to facilitate data visualization.

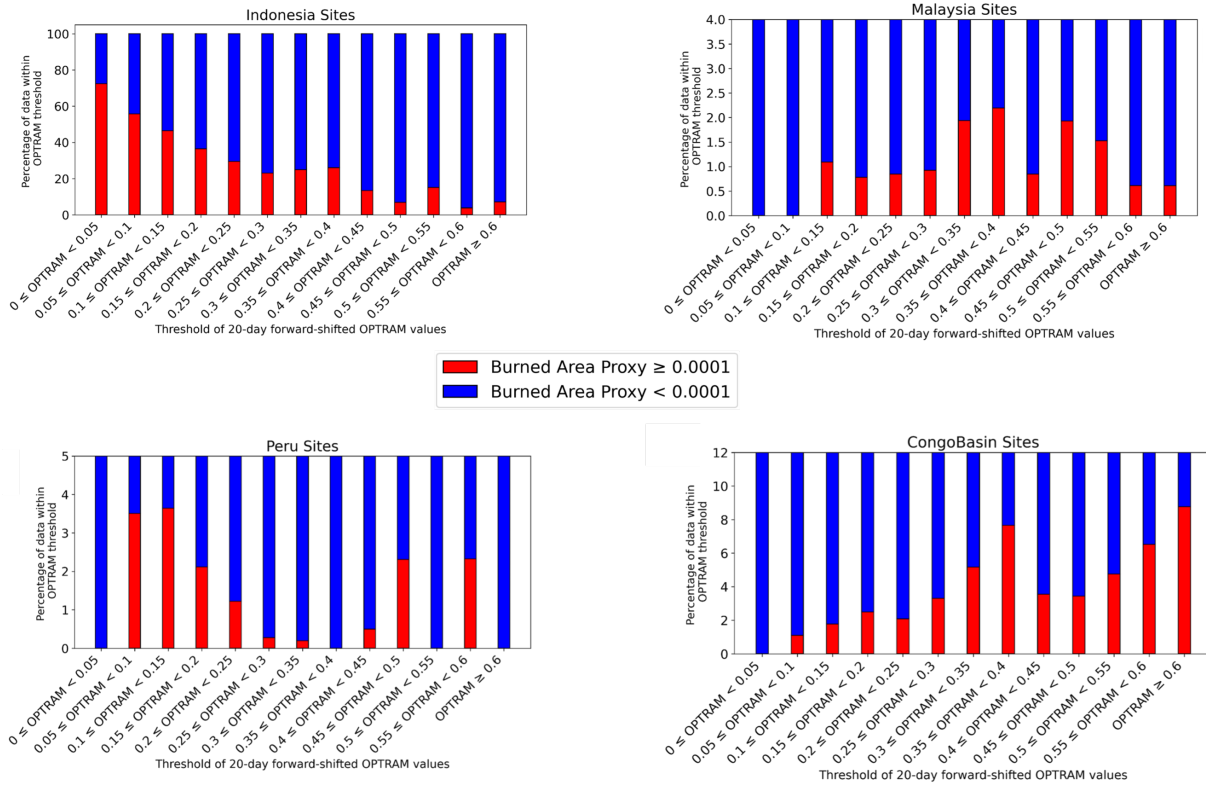


Figure 3.S3: A histogram showcasing the relationship between the percentage of data with burned area proxy ≥ 0.0001 or < 0.0001 that are within each 20-day forward shifted OPTRAM threshold for each site. Red and blue indicate burned area proxy values ≥ 0.0001 and < 0.0001 , respectively. Note that the scale of the y-axis is different for each site.

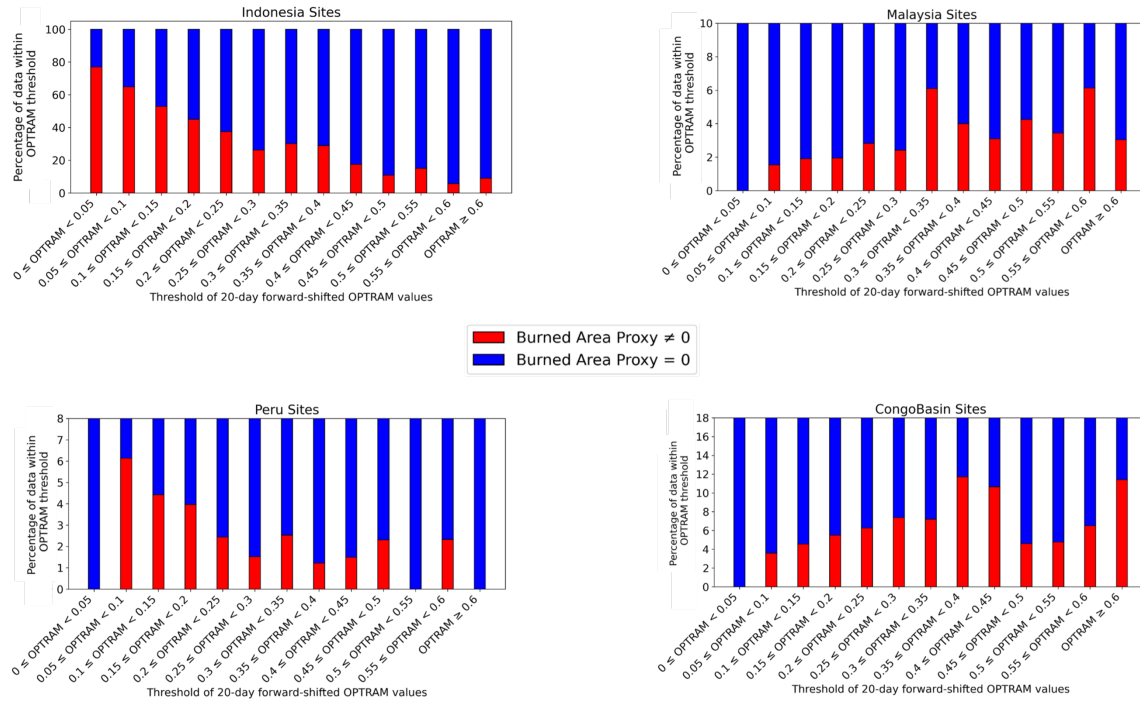


Figure 3.S4: A histogram showcasing the relationship between the percentage of data with burned area proxy equal to zero or not equal to zero that are within each 20-day forward shifted OPTRAM threshold for each site. Red and blue indicate burned area proxy values not equal to zero and equal to zero, respectively. Note that the scale of the y-axis is different for each site.

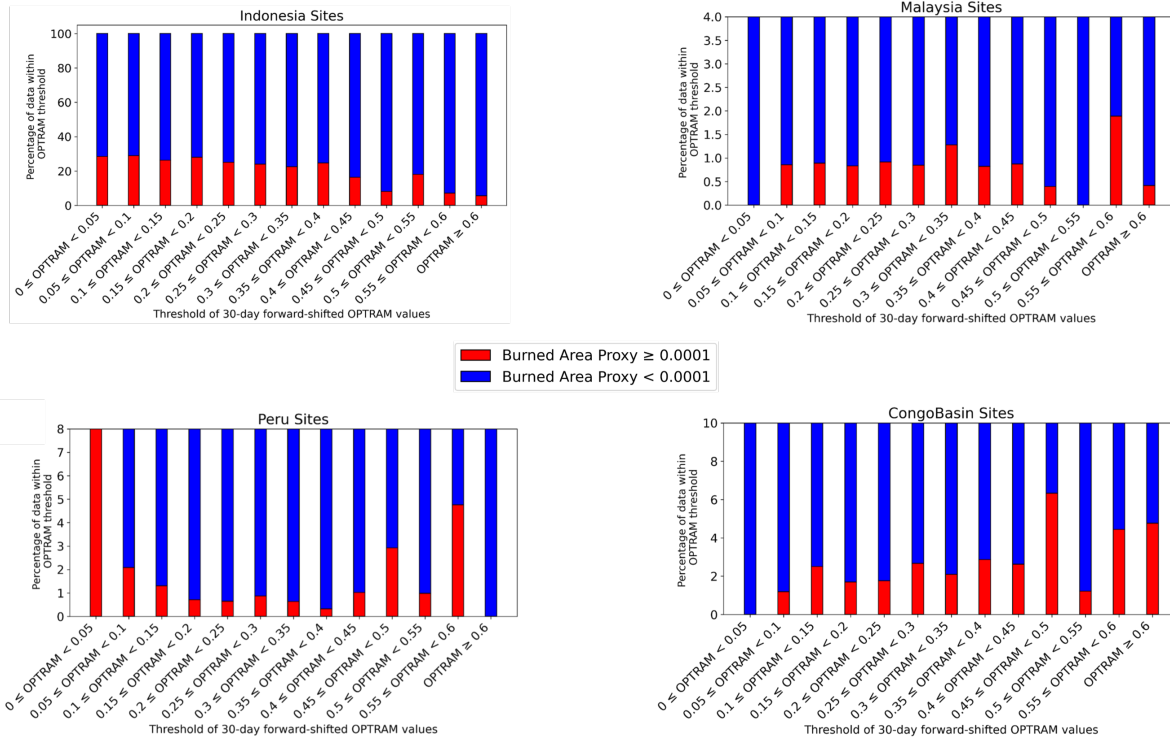


Figure 3.S5: A histogram showcasing the relationship between the percentage of data with burned area proxy ≥ 0.0001 or < 0.0001 that are within each 30-day forward shifted OPTRAM threshold for each site. Red and blue indicate burned area proxy values ≥ 0.0001 and < 0.0001 , respectively. Note that the scale of the y-axis is different for each site.

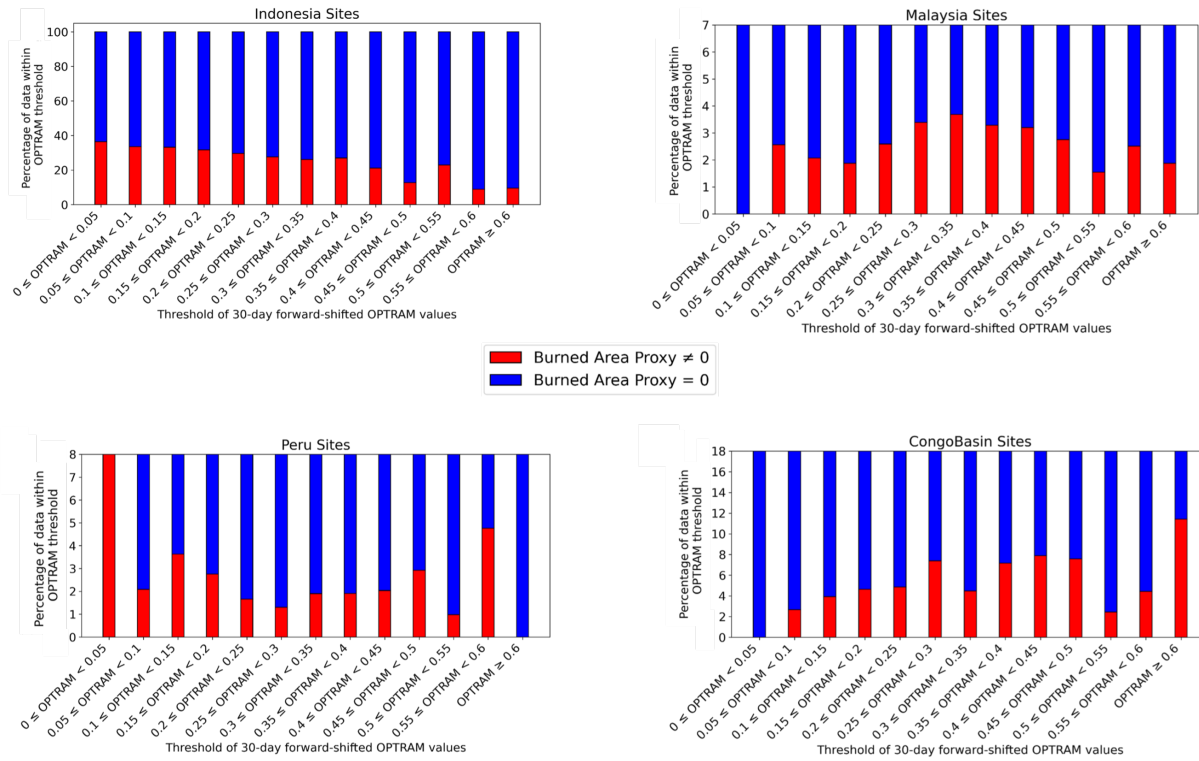


Figure 3.S6: A histogram showcasing the relationship between the percentage of data with burned area proxy equal to zero or not equal to zero that are within each 30-day forward shifted OPTRAM threshold for each site. Red and blue indicate burned area proxy values not equal to zero and equal to zero, respectively. Note that the scale of the y-axis is different for each site.

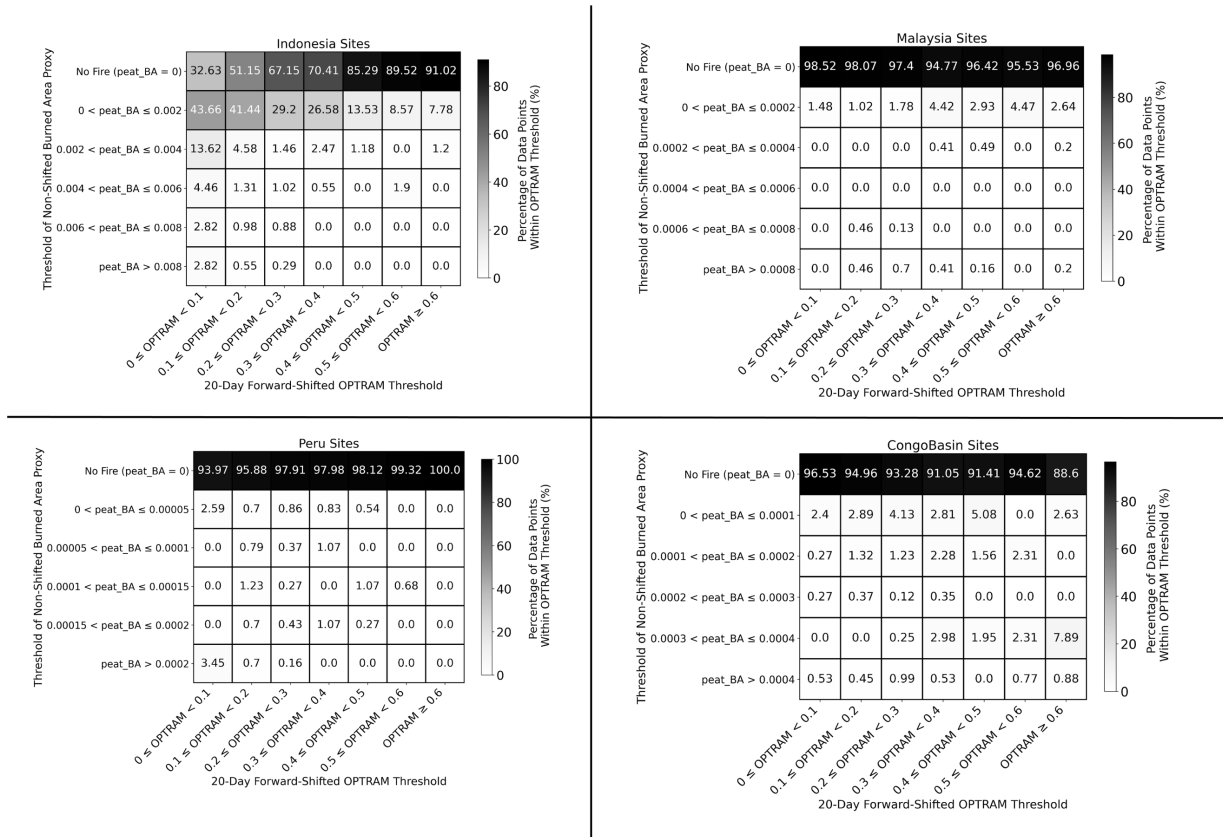


Figure 3.S7: A two-dimensional histogram showing the percentage of data points that fall within a specific 20-day forward shifted OPTRAM threshold *and* peat_BA (burned area proxy) threshold at each site. Percentage values are indicated within each square with white, gray, and black colors representing low, intermediate, and high percentage values. Note that the burned area proxy thresholds vary for each site.

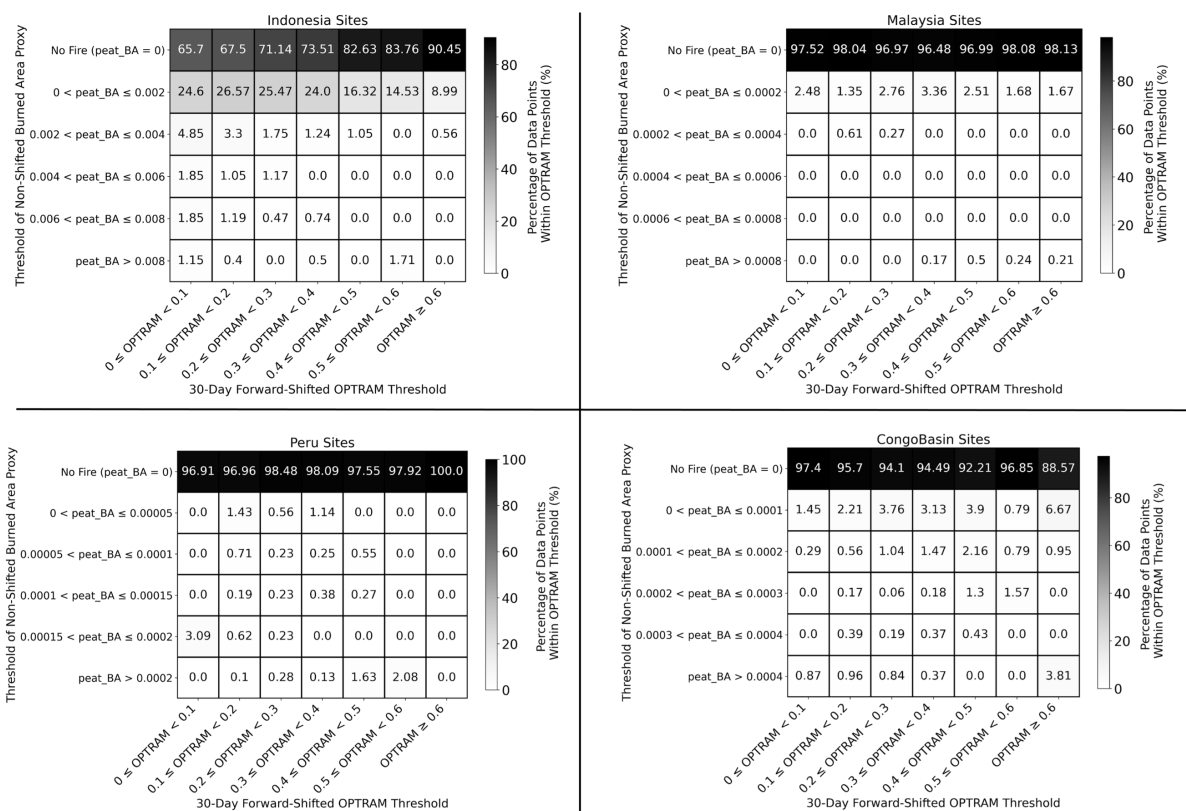


Figure 3.S8: A two-dimensional histogram showing the percentage of data points that fall within a specific 30-day forward shifted OPTRAM threshold *and* peat_BA (burned area proxy) threshold at each site. Percentage values are indicated within each square with white, gray, and black colors representing low, intermediate, and high percentage values. Note that the burned area proxy thresholds vary for each site.

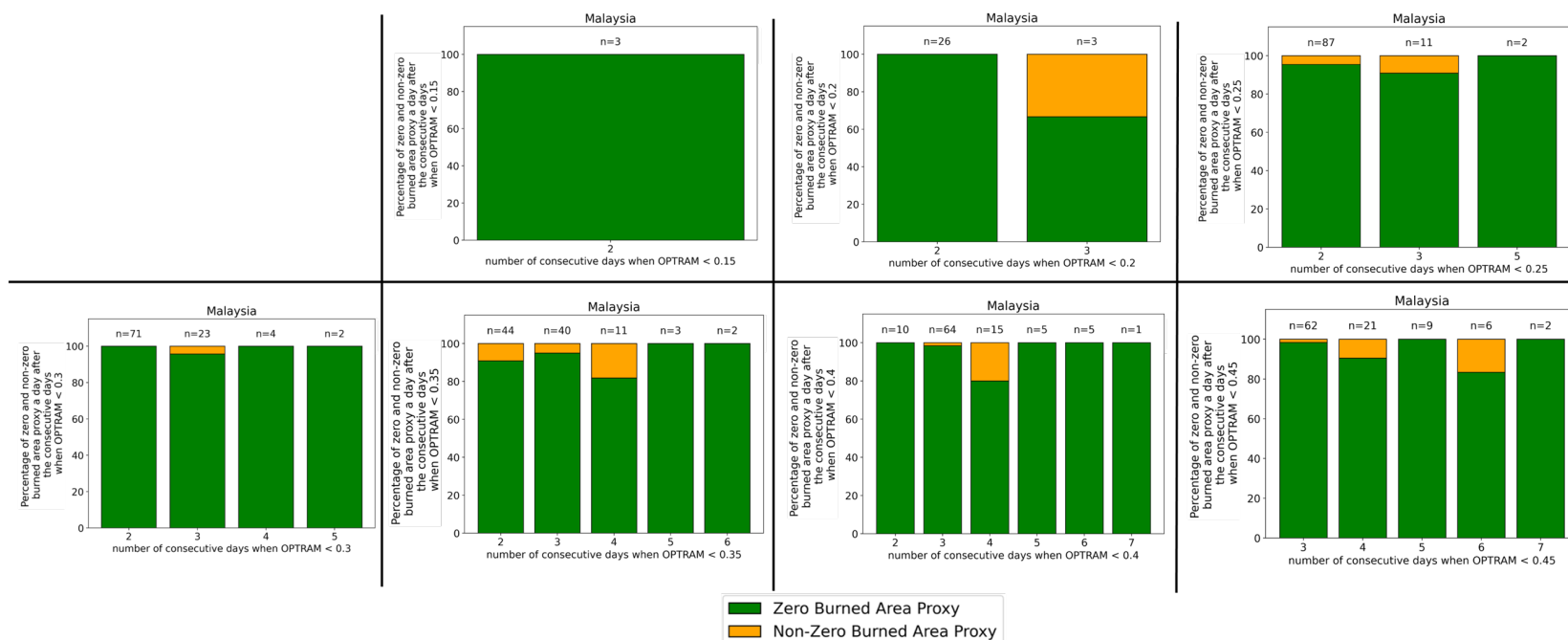


Figure 3.S9: Percentage of zero and non-zero burned area proxy a day after consecutive days when OPTRAM was below a certain threshold at the Malaysian sites. X-axis shows the number of consecutive days that OPTRAM was below a certain threshold. The "n" value shows the number of instances of burned area proxy values for each number of consecutive days. Green and yellow represent zero and non-zero burned area proxy values respectively.

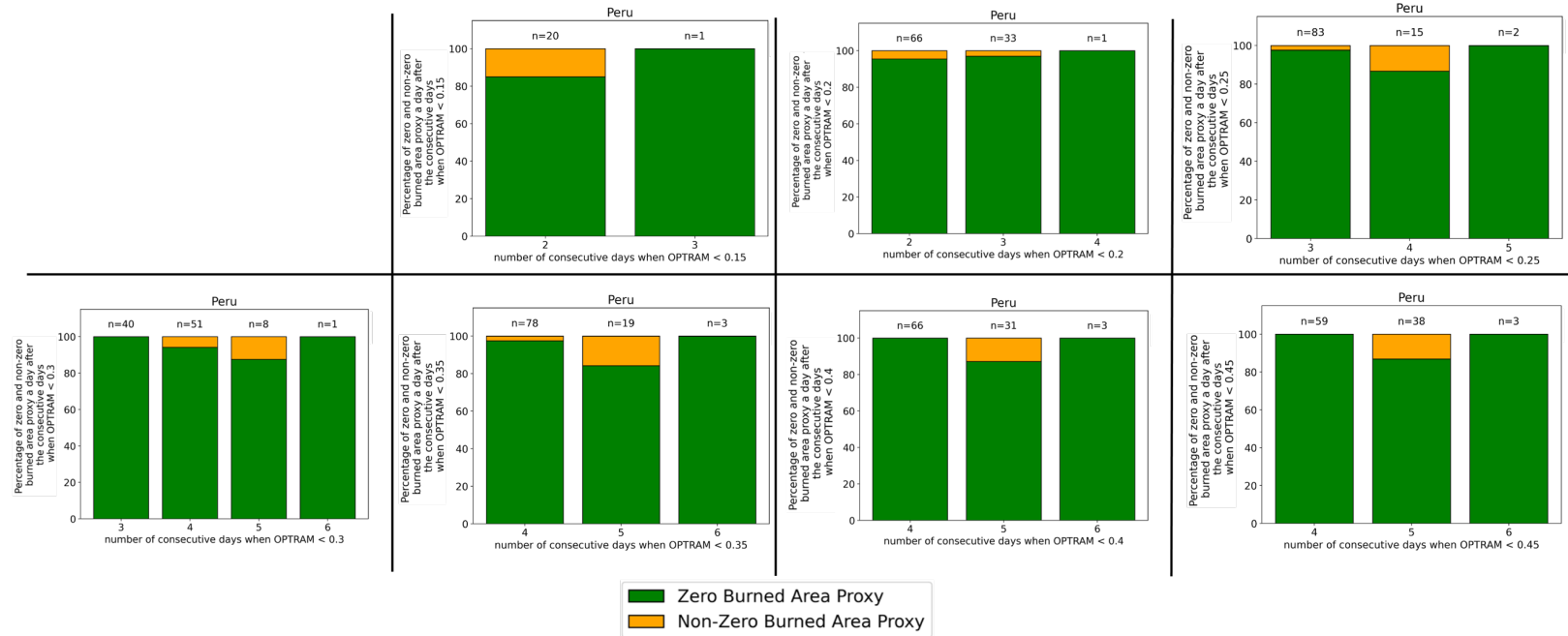


Figure 3.S10: Percentage of zero and non-zero burned area proxy a day after consecutive days when OPTRAM was below a certain threshold at the Peruvian sites. X-axis shows the number of consecutive days that OPTRAM was below a certain threshold. The “n” value shows the number of instances of burned area proxy values for each number of consecutive days. Green and yellow represent zero and non-zero burned area proxy values respectively.

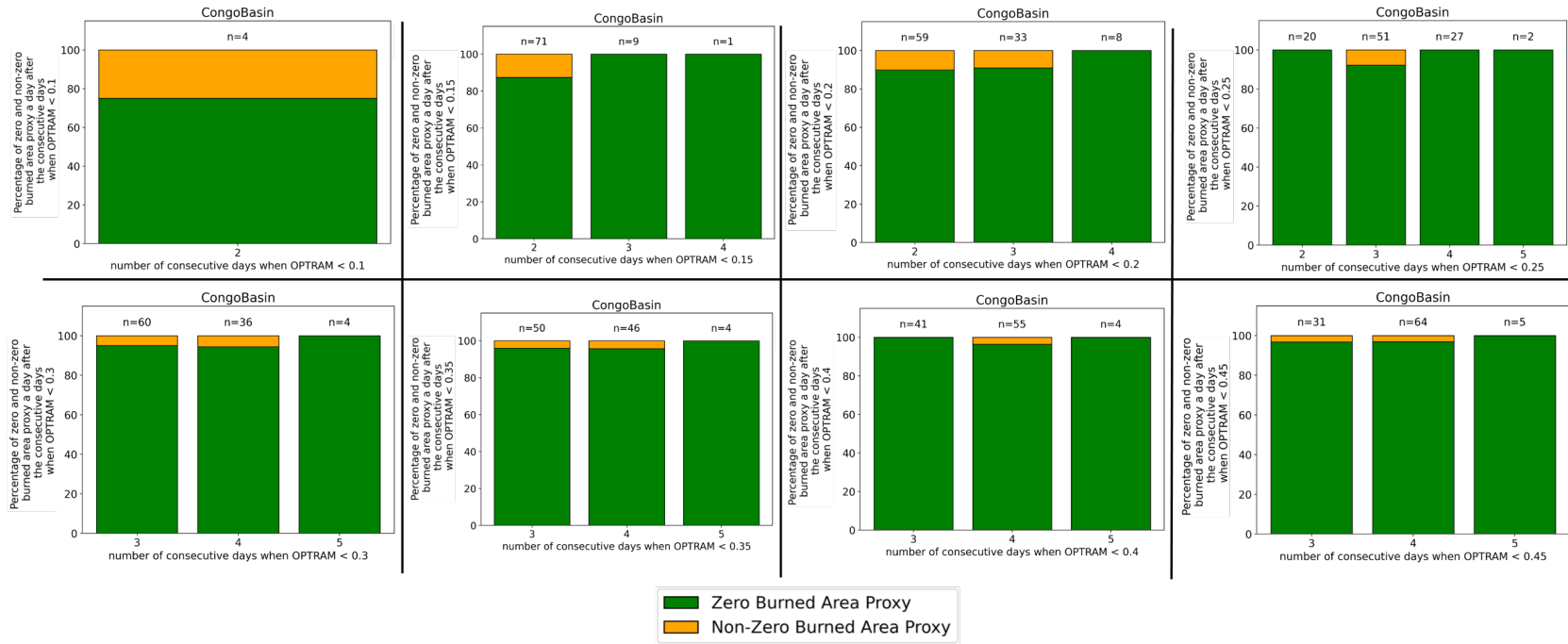


Figure 3.S11: Percentage of zero and non-zero burned area proxy a day after consecutive days when OPTRAM was below a certain threshold at the Congo Basin sites. X-axis shows the number of consecutive days that OPTRAM was below a certain threshold. The “n” value shows the number of instances of burned area proxy values for each number of consecutive days. Green and yellow represent zero and non-zero burned area proxy values respectively.

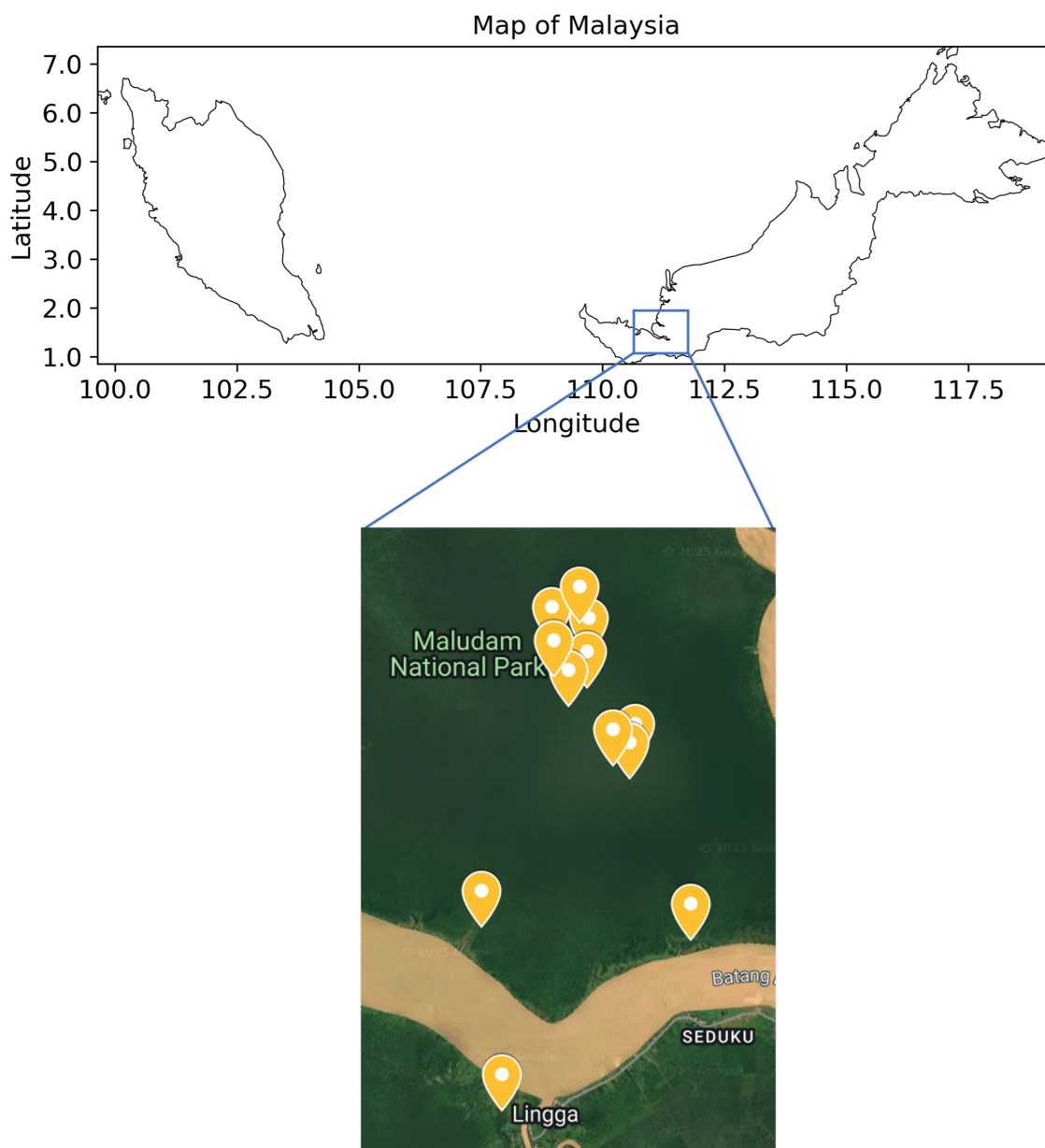


Figure 3.S12: The twelve Malaysian site locations used in this study. Satellite image from Google Maps.

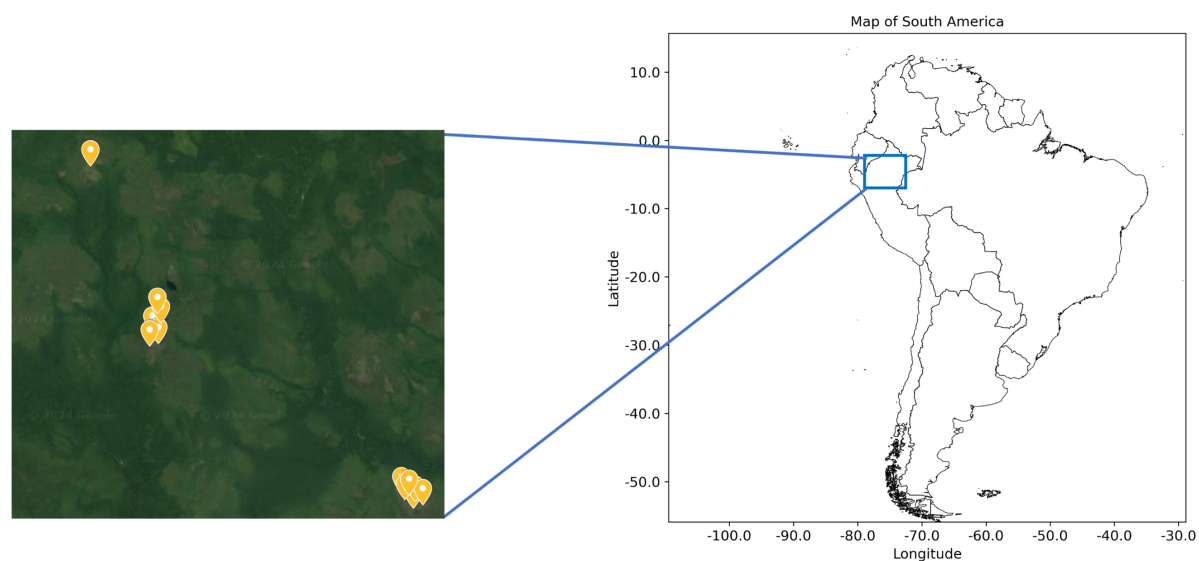


Figure 3.S13: The twelve Peruvian site locations used in this study. Satellite image from Google Maps.

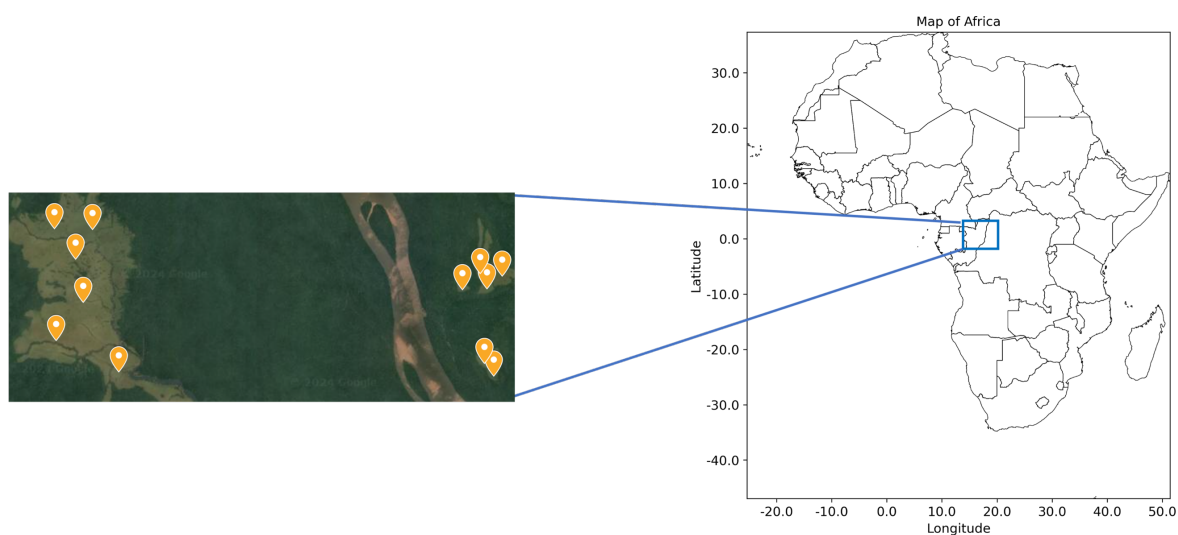


Figure 3.S14: The twelve site locations in the Congo Basin that were used in this study. Satellite image from Google Maps.

3.7 References

- Afroz, Rafia, Mohd Nasir Hassan, and Noor Akma Ibrahim. "Review of Air Pollution and Health Impacts in Malaysia." *Environmental Research* 92, no. 2 (June 2003): 71–77. [https://doi.org/10.1016/S0013-9351\(02\)00059-2](https://doi.org/10.1016/S0013-9351(02)00059-2).
- Ballhorn, Uwe, Florian Siegert, Mike Mason, and Suwido Limin. "Derivation of Burn Scar Depths and Estimation of Carbon Emissions with LIDAR in Indonesian Peatlands." *Proceedings of the National Academy of Sciences* 106, no. 50 (December 15, 2009): 21213–18. <https://doi.org/10.1073/pnas.0906457106>.
- Barber, Charles Victor, and James Schweithelm. "Trial by fire." World Resources Institute, Washington, DC (2000).
- Burdun, Iuliia, Michel Bechtold, Mika Aurela, Gabrielle De Lannoy, Ankur R. Desai, Elyn Humphreys, Santtu Kareksela, et al. "Hidden Becomes Clear: Optical Remote Sensing of Vegetation Reveals Water Table Dynamics in Northern Peatlands." *Remote Sensing of Environment* 296 (October 2023): 113736. <https://doi.org/10.1016/j.rse.2023.113736>.
- Burdun, Iuliia, Michel Bechtold, Valentina Sagris, Viacheslav Komisarenko, Gabrielle De Lannoy, and Ülo Mander. "A Comparison of Three Trapezoid Models Using Optical and Thermal Satellite Imagery for Water Table Depth Monitoring in Estonian Bogs." *Remote Sensing* 12, no. 12 (June 19, 2020) (2020a): 1980. <https://doi.org/10.3390/rs12121980>.
- Burdun, Iuliia, Michel Bechtold, Valentina Sagris, Annalea Lohila, Elyn Humphreys, Ankur R. Desai, Mats B. Nilsson, Gabrielle De Lannoy, and Ülo Mander. "Satellite Determination of Peatland Water Table Temporal Dynamics by Localizing Representative Pixels of A SWIR-Based Moisture Index." *Remote Sensing* 12, no. 18 (September 10, 2020) (2020b): 2936. <https://doi.org/10.3390/rs12182936>.
- Chen, Mingxing, Yuhu Zhang, Yunjun Yao, Jing Lu, Xiao Pu, Tao Hu, and Peng Wang. "Evaluation of the OPTRAM Model to Retrieve Soil Moisture in the Sanjiang Plain of Northeast China." *Earth and Space Science* 7, no. 6 (June 2020). <https://doi.org/10.1029/2020EA001108>.
- Cooper, Hannah V., Stephanie Evers, Paul Aplin, Neil Crout, Mohd Puat Bin Dahalan, and Sofie Sjögersten. "Greenhouse Gas Emissions Resulting from Conversion of Peat Swamp Forest to Oil Palm Plantation." *Nature Communications* 11, no. 1 (January 21, 2020): 407. <https://doi.org/10.1038/s41467-020-14298-w>.
- Dadap, Nathan C, Alexander R Cobb, Alison M Hoyt, Charles F Harvey, and Alexandra G Konings. "Satellite Soil Moisture Observations Predict Burned Area in Southeast Asian Peatlands." *Environmental Research Letters* 14, no. 9 (September 1, 2019): 094014. <https://doi.org/10.1088/1748-9326/ab3891>.

- Dargie, Greta C., Ian T. Lawson, Tim J. Rayden, Lera Miles, Edward T. A. Mitchard, Susan E. Page, Yannick E. Bocko, Suspense A. Ifo, and Simon L. Lewis. "Congo Basin Peatlands: Threats and Conservation Priorities." *Mitigation and Adaptation Strategies for Global Change* 24, no. 4 (April 2019): 669–86. <https://doi.org/10.1007/s11027-017-9774-8>.
- Davies, Stuart J. "Smoke-Haze from the 1997 Indonesian Forest Fires: Effects on Pollution Levels, Local Climate, Atmospheric CO₂ Concentrations, and Tree Photosynthesis." *Forest Ecology and Management*, 1999, 8.
- Dohong, Alue, Ammar Abdul Aziz, and Paul Dargusch. "A Review of the Drivers of Tropical Peatland Degradation in South-East Asia." *Land Use Policy* 69 (December 2017): 349–60. <https://doi.org/10.1016/j.landusepol.2017.09.035>.
- Dohong, Alue, Ammar Abdul Aziz, and Paul Dargusch. "A Review of Techniques for Effective Tropical Peatland Restoration." *Wetlands* 38, no. 2 (April 2018): 275–92. <https://doi.org/10.1007/s13157-018-1017-6>.
- Evers, Stephanie, Catherine M. Yule, Rory Padfield, Patrick O'Reilly, and Helena Varkkey. "Keep Wetlands Wet: The Myth of Sustainable Development of Tropical Peatlands - Implications for Policies and Management." *Global Change Biology* 23, no. 2 (February 2017): 534–49. <https://doi.org/10.1111/gcb.13422>.
- Fan, Song-Miao, Steven C. Wofsy, Peter S. Bakwin, Daniel J. Jacob, and David R. Fitzjarrald. "Atmosphere-Biosphere Exchange of CO₂ and O₃ in the Central Amazon Forest." *Journal of Geophysical Research* 95, no. D10 (1990): 16851. <https://doi.org/10.1029/JD095iD10p16851>.
- Fatoyinbo, Lola. "Vast Peatlands Found in the Congo Basin." *Nature* 542, no. 7639 (February 2017): 38–39. <https://doi.org/10.1038/542038b>.
- Gerin, Stephanie, Henriikka Vekuri, Maarit Liimatainen, Juha-Pekka Tuovinen, Jarkko Kekkonen, Liisa Kulmala, Tuomas Laurila, et al. "Two Contrasting Years of Continuous N₂O and CO₂ Fluxes on a Shallow-Peated Drained Agricultural Boreal Peatland." *Agricultural and Forest Meteorology* 341 (October 2023): 109630. <https://doi.org/10.1016/j.agrformet.2023.109630>.
- Giglio, Louis, James T. Randerson, and Guido R. van der Werf. "Analysis of Daily, Monthly, and Annual Burned Area Using the Fourth-Generation Global Fire Emissions Database (GFED4): ANALYSIS OF BURNED AREA." *Journal of Geophysical Research: Biogeosciences* 118, no. 1 (March 2013): 317–28. <https://doi.org/10.1002/jgrg.20042>.
- Hapsari, Kartika Anggi, Siria Biagioni, Tim C. Jennerjahn, Peter Meyer Reimer, Asmadi Saad, Yudhi Achnopa, Supiandi Sabiham, and Hermann Behling. "Environmental Dynamics and Carbon Accumulation Rate of a Tropical Peatland in Central Sumatra, Indonesia." *Quaternary Science Reviews* 169 (August 2017): 173–87. <https://doi.org/10.1016/j.quascirev.2017.05.026>.

- Heil, A., and J. G. Goldammer. "Smoke-Haze Pollution: A Review of the 1997 Episode in Southeast Asia." *Regional Environmental Change* 2, no. 1 (August 1, 2001): 24–37. <https://doi.org/10.1007/s101130100021>.
- Hergoualc'h, Kristell, Nelda Dezzio, Louis V. Verchot, Christopher Martius, Jeffrey Van Lent, Jhon Del Aguila-Pasquel, and Mariela López Gonzales. "Spatial and Temporal Variability of Soil N₂O and CH₄ Fluxes along a Degradation Gradient in a Palm Swamp Peat Forest in the Peruvian Amazon." *Global Change Biology* 26, no. 12 (December 2020): 7198–7216. <https://doi.org/10.1111/gcb.15354>.
- Hergoualc'h, Kristell, and Louis V. Verchot. "Stocks and Fluxes of Carbon Associated with Land Use Change in Southeast Asian Tropical Peatlands: A Review: PEATLAND CARBON DYNAMICS AND LAND USE CHANGE IN SOUTHEAST ASIA." *Global Biogeochemical Cycles* 25, no. 2 (June 2011): n/a-n/a. <https://doi.org/10.1029/2009GB003718>.
- Hirano, Takashi, Hendrik Segah, Kitso Kusin, Suwido Limin, Hidenori Takahashi, and Mitsuru Osaki. "Effects of Disturbances on the Carbon Balance of Tropical Peat Swamp Forests." *Global Change Biology* 18, no. 11 (November 2012): 3410–22. <https://doi.org/10.1111/j.1365-2486.2012.02793.x>.
- Hooijer, A., S. Page, J. G. Canadell, M. Silvius, J. Kwadijk, H. Wösten, and J. Jauhiainen. "Current and Future CO₂ Emissions from Drained Peatlands in Southeast Asia." *Biogeosciences* 7, no. 5 (May 12, 2010): 1505–14. <https://doi.org/10.5194/bg-7-1505-2010>.
- Hooijer, A., S. Page, J. Jauhiainen, W. A. Lee, X. X. Lu, A. Idris, and G. Anshari. "Subsidence and Carbon Loss in Drained Tropical Peatlands." *Biogeosciences* 9, no. 3 (March 20, 2012): 1053–71. <https://doi.org/10.5194/bg-9-1053-2012>.
- Horn, Christa M., Victor H. Vargas Paredes, Michael P. Gilmore, and Bryan A. Endress. "Spatio-Temporal Patterns of *Mauritia Flexuosa* Fruit Extraction in the Peruvian Amazon: Implications for Conservation and Sustainability." *Applied Geography* 97 (August 2018): 98–108. <https://doi.org/10.1016/j.apgeog.2018.05.004>.
- Huijnen, V., M. J. Wooster, J. W. Kaiser, D. L. A. Gaveau, J. Flemming, M. Parrington, A. Inness, D. Murdiyarto, B. Main, and M. Van Weele. "Fire Carbon Emissions over Maritime Southeast Asia in 2015 Largest since 1997." *Scientific Reports* 6, no. 1 (May 31, 2016): 26886. <https://doi.org/10.1038/srep26886>.
- Jaenicke, Julia, Henk Wösten, Arif Budiman, and Florian Siegert. "Planning Hydrological Restoration of Peatlands in Indonesia to Mitigate Carbon Dioxide Emissions." *Mitigation*

- and Adaptation Strategies for Global Change* 15, no. 3 (March 2010): 223–39.
<https://doi.org/10.1007/s11027-010-9214-5>.
- Jayachandran, Seema. "Air Quality And Early-Life Mortality: Evidence From Indonesia's Wildfires". *Journal Of Human Resources*, vol 44, no. 4, 2009, pp. 916-954. University Of Wisconsin Press, <https://doi.org/10.1353/jhr.2009.0001>.
- Joosten, Hans. "The Global Peatland CO₂ Picture: peatland status and drainage related emissions in all countries of the world." *The Global Peatland CO₂ Picture: peatland status and drainage related emissions in all countries of the world*. (2010).
- Khakim, Mokhammad Yusup Nur, Akhmad Aminuddin Bama, Indra Yustian, Pradanto Poerwono, Takeshi Tsuji, and Toshifumi Matsuoka. "Peatland Subsidence and Vegetation Cover Degradation as Impacts of the 2015 El Niño Event Revealed by Sentinel-1A SAR Data." *International Journal of Applied Earth Observation and Geoinformation* 84 (February 2020): 101953. <https://doi.org/10.1016/j.jag.2019.101953>.
- Knox, Sara Helen, Cove Sturtevant, Jaclyn Hatala Matthes, Laurie Koteen, Joseph Verfaillie, and Dennis Baldocchi. "Agricultural Peatland Restoration: Effects of Land-use Change on Greenhouse Gas (CO₂ and CH₄) Fluxes in the Sacramento-San Joaquin Delta." *Global Change Biology* 21, no. 2 (February 2015): 750–65. <https://doi.org/10.1111/gcb.12745>.
- Kopplitz, Shannon N, Loretta J Mickley, Miriam E Marlier, Jonathan J Buonocore, Patrick S Kim, Tianjia Liu, Melissa P Sulprizio, et al. "Public Health Impacts of the Severe Haze in Equatorial Asia in September–October 2015: Demonstration of a New Framework for Informing Fire Management Strategies to Reduce Downwind Smoke Exposure." *Environmental Research Letters* 11, no. 9 (September 1, 2016): 094023. <https://doi.org/10.1088/1748-9326/11/9/094023>.
- Koupaei-Abyazani, Nikaan, Iuliia Burdun, Ankur R. Desai, Kristell Hergoualc'h, Takashi Hirano, Lulie Melling, Erin Swails, Angela Che Ing Tang, and Guan Xhuan Wong. "Tropical Peatland Water Table Estimations From Space." *Journal of Geophysical Research: Biogeosciences* 129, no. 6 (June 2024): e2024JG008116. <https://doi.org/10.1029/2024JG008116>.
- Kunii, Osamu, Shuzo Kanagawa, Iwao Yajima, Yoshiharu Hisamatsu, Sombo Yamamura, Takashi Amagai, and Ir T. Sachrul Ismail. "The 1997 Haze Disaster in Indonesia: Its Air Quality and Health Effects." *Archives of Environmental Health: An International Journal* 57, no. 1 (January 2002): 16–22. <https://doi.org/10.1080/00039890209602912>.
- Lampela, Maija, Jyrki Jauhiainen, Sakari Sarkkola, and Harri Vasander. "Promising Native Tree Species for Reforestation of Degraded Tropical Peatlands." *Forest Ecology and Management* 394 (June 2017): 52–63. <https://doi.org/10.1016/j.foreco.2016.12.004>.
- Leifeld, J., and L. Menichetti. "The Underappreciated Potential of Peatlands in Global Climate Change Mitigation Strategies." *Nature Communications* 9, no. 1 (December 2018): 1071. <https://doi.org/10.1038/s41467-018-03406-6>.

- Melton, Joe R., Ed Chan, Koreen Millard, Matthew Fortier, R. Scott Winton, Javier M. Martín-López, Hinsby Cadillo-Quiroz, Darren Kidd, and Louis V. Verchot. “A Map of Global Peatland Extent Created Using Machine Learning (Peat-ML).” Preprint. Biogeosciences, February 14, 2022. <https://doi.org/10.5194/gmd-2021-426>.
- Miettinen, Jukka, Aljosja Hooijer, Chenghua Shi, Daniel Tollenaar, Ronald Vernimmen, Soo Chin Liew, Chris Malins, and Susan E. Page. “Extent of Industrial Plantations on Southeast Asian Peatlands in 2010 with Analysis of Historical Expansion and Future Projections.” *GCB Bioenergy* 4, no. 6 (November 2012) (2012a): 908–18. <https://doi.org/10.1111/j.1757-1707.2012.01172.x>.
- Miettinen, Jukka, Aljosja Hooijer, Jianjun Wang, Chenghua Shi, and Soo Chin Liew. “Peatland Degradation and Conversion Sequences and Interrelations in Sumatra.” *Regional Environmental Change* 12, no. 4 (December 2012): 729–37 (2012b). <https://doi.org/10.1007/s10113-012-0290-9>.
- Miettinen, Jukka, Chenghua Shi, and Soo Chin Liew. “Deforestation Rates in Insular Southeast Asia between 2000 and 2010: DEFORESTATION IN INSULAR SOUTHEAST ASIA 2000-2010.” *Global Change Biology* 17, no. 7 (July 2011): 2261–70. <https://doi.org/10.1111/j.1365-2486.2011.02398.x>.
- Novita, Nisa, Adibtya Asyhari, Rasis P. Ritonga, Adi Gangga, Gusti Z. Anshari, Joni Jupesta, Jennifer C. Bowen, et al. “Strong Climate Mitigation Potential of Rewetting Oil Palm Plantations on Tropical Peatlands.” *Science of The Total Environment*, August 2024, 175829. <https://doi.org/10.1016/j.scitotenv.2024.175829>.
- Ojanen, Paavo, and Kari Minkkinen. “Rewetting Offers Rapid Climate Benefits for Tropical and Agricultural Peatlands But Not for Forestry-Drained Peatlands.” *Global Biogeochemical Cycles* 34, no. 7 (July 2020): e2019GB006503. <https://doi.org/10.1029/2019GB006503>.
- Page, S. E., and A. Hooijer. “In the Line of Fire: The Peatlands of Southeast Asia.” *Philosophical Transactions of the Royal Society B: Biological Sciences* 371, no. 1696 (June 5, 2016): 20150176. <https://doi.org/10.1098/rstb.2015.0176>.
- Page, Susan E., John O. Rieley, and Christopher J. Banks. “Global and Regional Importance of the Tropical Peatland Carbon Pool: TROPICAL PEATLAND CARBON POOL.” *Global Change Biology* 17, no. 2 (February 2011): 798–818. <https://doi.org/10.1111/j.1365-2486.2010.02279.x>.
- Page, Susan E., Florian Siegert, John O. Rieley, Hans-Dieter V. Boehm, Adi Jaya, and Suwido Limin. “The Amount of Carbon Released from Peat and Forest Fires in Indonesia during 1997.” *Nature* 420, no. 6911 (November 2002): 61–65. <https://doi.org/10.1038/nature01131>.
- Page, Susan, Agata Hosińska, Henk Wösten, Jyrki Jauhiainen, Marcel Silvius, Jack Rieley, Henk Ritzema, et al. “Restoration Ecology of Lowland Tropical Peatlands in Southeast Asia:

- Current Knowledge and Future Research Directions.” *Ecosystems* 12, no. 6 (September 2009): 888–905. <https://doi.org/10.1007/s10021-008-9216-2>.
- Parker, Robert J., Hartmut Boesch, Martin J. Wooster, David P. Moore, Alex J. Webb, David Gaveau, and Daniel Murdiyarso. “Atmospheric CH₄ and CO₂ Enhancements and Biomass Burning Emission Ratios Derived from Satellite Observations of the 2015 Indonesian Fire Plumes.” *Atmospheric Chemistry and Physics* 16, no. 15 (August 11, 2016): 10111–31. <https://doi.org/10.5194/acp-16-10111-2016>.
- Randerson, J.T., G.R. van der Werf, L. Giglio, G.J. Collatz, and P.S. Kasibhatla. 2017. Global Fire Emissions Database, Version 4.1 (GFEDv4). ORNL DAAC, Oak Ridge, Tennessee, USA. <https://doi.org/10.3334/ORNLDAAAC/1293>
- Randerson, J. T., Y. Chen, G. R. Van Der Werf, B. M. Rogers, and D. C. Morton. “Global Burned Area and Biomass Burning Emissions from Small Fires: BURNED AREA FROM SMALL FIRES.” *Journal of Geophysical Research: Biogeosciences* 117, no. G4 (December 2012): n/a-n/a. <https://doi.org/10.1029/2012JG002128>.
- Ribeiro, Kelly, Felipe S. Pacheco, José W. Ferreira, Eráclito R. Sousa-Neto, Adam Hastie, Guenther C. Krieger Filho, Plínio C. Alvalá, Maria C. Forti, and Jean P. Ometto. “Tropical Peatlands and Their Contribution to the Global Carbon Cycle and Climate Change.” *Global Change Biology* 27, no. 3 (February 2021): 489–505. <https://doi.org/10.1111/gcb.15408>.
- Rosenfeld, Daniel. “TRMM Observed First Direct Evidence of Smoke from Forest Fires Inhibiting Rainfall.” *Geophysical Research Letters* 26, no. 20 (October 15, 1999): 3105–8. <https://doi.org/10.1029/1999GL006066>.
- Sadeghi, Morteza, Ebrahim Babaeian, Markus Tuller, and Scott B. Jones. “The Optical Trapezoid Model: A Novel Approach to Remote Sensing of Soil Moisture Applied to Sentinel-2 and Landsat-8 Observations.” *Remote Sensing of Environment* 198 (September 2017): 52–68. <https://doi.org/10.1016/j.rse.2017.05.041>.
- Sahani, Mazrura, Nurul Ashikin Zainon, Wan Rozita Wan Mahiyuddin, Mohd Talib Latif, Rozita Hod, Md Firoz Khan, Norhayati Mohd Tahir, and Chang-Chuan Chan. “A Case-Crossover Analysis of Forest Fire Haze Events and Mortality in Malaysia.” *Atmospheric Environment* 96 (October 2014): 257–65. <https://doi.org/10.1016/j.atmosenv.2014.07.043>.
- Sumaryati, Dita Fatria Andarini, Nani Cholianawati, and Asri Indrawati. “Smoke Propagation During Fire in Kalimantan and Sumatra in 2015 and 2019.” In *Proceedings of the International Conference on Radioscience, Equatorial Atmospheric Science and Environment and Humanosphere Science, 2021*, edited by Erma Yulihastin, Prayitno Abadi, Peberlin Sitompul, and Wendi Harjupa, 275:145–57. Springer Proceedings in Physics.

- Singapore: Springer Nature Singapore, 2022. https://doi.org/10.1007/978-981-19-0308-3_11.
- Turetsky, Merritt. “Current Disturbance and the Diminishing Peatland Carbon Sink.” *Geophysical Research Letters* 29, no. 11 (2002): 1526. <https://doi.org/10.1029/2001GL014000>.
- Turetsky, Merritt R., Brian Benschoter, Susan Page, Guillermo Rein, Guido R. van der Werf, and Adam Watts. “Global Vulnerability of Peatlands to Fire and Carbon Loss.” *Nature Geoscience* 8, no. 1 (January 2015): 11–14. <https://doi.org/10.1038/ngeo2325>.
- Usup, Aswin, Yoshihiro Hashimoto, Hidenori Takahashi, and Hiroshi Hayasaka. “Combustion and Thermal Characteristics of Peat Fire in Tropical Peatland in Central Kalimantan, Indonesia.” *Tropics* 14, no. 1 (2004): 1–19. <https://doi.org/10.3759/tropics.14.1>.
- Van Der Werf, G. R., J. Dempewolf, S. N. Trigg, J. T. Randerson, P. S. Kasibhatla, L. Giglio, D. Murdiyarso, et al. “Climate Regulation of Fire Emissions and Deforestation in Equatorial Asia.” *Proceedings of the National Academy of Sciences* 105, no. 51 (December 23, 2008): 20350–55. <https://doi.org/10.1073/pnas.0803375105>.
- Varkkey, Helena. “Patronage Politics, Plantation Fires and Transboundary Haze.” *Environmental Hazards* 12, no. 3–4 (December 2013): 200–217. <https://doi.org/10.1080/17477891.2012.759524>.
- Wösten, J.H.M., E. Clymans, S.E. Page, J.O. Rieley, and S.H. Limin. “Peat–Water Interrelationships in a Tropical Peatland Ecosystem in Southeast Asia.” *CATENA* 73, no. 2 (April 2008): 212–24. <https://doi.org/10.1016/j.catena.2007.07.010>.
- Xu, Jiren, Paul J. Morris, Junguo Liu, and Joseph Holden. “PEATMAP: Refining Estimates of Global Peatland Distribution Based on a Meta-Analysis.” *CATENA* 160 (January 2018): 134–40. <https://doi.org/10.1016/j.catena.2017.09.010>.

Chapter 4: Impacts of Anthropogenic Disturbance on Soil Greenhouse Gas Fluxes in Malaysian Peatlands

4.1 Introduction

Tropical peatlands contain high soil carbon (C) stocks and make significant contributions to the global carbon cycle (Yu et al., 2010; Huang et al., 2021; Ribeiro et al., 2021). These systems also provide a variety of services such as hydrological regulation (Harenda et al., 2018; Holden, 2005; Wösten et al., 2008; Posa et al., 2011; Evers et al., 2017) and C sequestration (Ribeiro et al., 2021; Warren et al., 2017; Dommain et al., 2011; Dommain et al., 2014; Kurnianto et al., 2015) while also hosting an immense amount of biodiversity (Posa et al., 2011; Phillips, 1998; Bezuijen et al., 2001; Wibisono & Pusparini, 2010; Evers et al., 2017). In the past several years, tropical peatlands have been subject to high amounts of anthropogenic activity. This includes drainage (lowering the water table), deforestation, and burning (Dohong et al., 2017; Hooijer et al., 2012; Jaenicke et al., 2010). These practices are mainly carried out for the purpose of preparing the land for agriculture. In Southeast Asia, this typically takes the form of an oil palm plantation (Hooijer et al., 2010; Koh et al., 2011; Miettinen et al., 2012).

The disturbances during land conversion not only eliminate tropical peatland ecosystem services but also contribute to ongoing climate change through immense amounts of C emission. A significant amount of tropical peatland C emissions are through human-induced drainage (Dohong et al., 2017; Leng et al., 2019). This can then result in peat oxidation, subsidence, and an increase in fire risk (Hooijer et al., 2012; Usup et al., 2004; Page et al., 2009). A landscape may also be deliberately set on fire using the slash-and-burn tactic, where oil palms from a

previous generation are burned away to open space for the next set of crops ([Dhandapani and Evers, 2020](#); [Myllyntaus et al., 2002](#)). During slash-and-burn, the highly fire prone surface peat layer may catch fire, which may then continuously burn through smoldering for as long as multiple months ([Rein, 2013](#); [Turetsky et al., 2015](#)). The persistency of the fires not only reduces the organic matter content of the peat soil, but also leads to further drying and an increase in susceptibility to more C loss ([Sazawa et al., 2018](#); [Wiggins et al., 2018](#)).

The drastic changes in biogeochemical and hydrological dynamics imposed by land cover change in tropical peatlands is an ongoing area of study. However, given the challenges of site and lab access, and the long history of greater attention paid to mid and high latitude peatlands, studies on tropical peatlands have not been as well-represented in the literature relative to those in temperate and boreal regions. Therefore, more studies must be carried out on natural and disturbed tropical peatlands to better elucidate the change in ecological dynamics and to also inform plantation owners and stakeholders of sustainable alternatives for maintaining the land.

Many studies have used in-situ methods to quantify the greenhouse gas (GHG) fluxes and environmental variables in tropical peatlands. This includes peatlands in Malaysia ([Melling et al., 2005a](#); [Tang et al., 2020](#); [Tang et al., 2018](#); [Ishikura et al., 2019](#); [Kiew et al., 2018](#); [Wong et al., 2018](#)), Indonesia ([Deshmukh et al., 2020](#); [Deshmukh et al., 2021](#); [Hirano et al., 2014](#); [Hirano et al., 2009](#); [Hirano et al., 2007](#); [Hirano et al., 2012](#)), Peru ([Hergoualc'h et al., 2020](#); [Hergoualc'h et al., 2023](#)), and the Congo Basin ([Dargie et al., 2017](#)). Studies have found that disturbed tropical peatland ecosystems are a net C source to the atmosphere ([Hergoualc'h et al., 2020](#); [Hergoualc'h et al., 2023](#); [Hirano et al., 2012](#); [Deshmukh et al., 2023](#)). These findings are

significant since tropical peatlands have typically been found to be a net C sink for thousands of years. (Dommain et al., 2014). Furthermore, some are recently losing annual C at rates exceeding pre-disturbance C uptake, leading these systems to become a substantial net C source (Dommain et al., 2014).

Here, we have a unique opportunity to study the soil GHG fluxes of three tropical peatlands with varying disturbance regimes in Sarawak, Malaysia. The period of the study is from May 2024 through January 2025 and therefore encompasses both the wet and dry seasons in the region. The sites include an undrained peat swamp forest, a young oil palm plantation, and a mature oil palm plantation. Prior studies have found that increased water table levels result in decreased carbon-dioxide (CO₂) emissions and enhanced methane (CH₄) emissions, with data on nitrous oxide (N₂O) generally being limited (Deshmukh et al., 2023; Hirano et al., 2012; Hergoualc'h et al., 2020; Hergoualc'h et al., 2023; Jauhiainen et al., 2012a; Jauhiainen et al., 2012b; Hooijer et al., 2012). Furthermore, environmental controls such as air temperature, soil temperature, vapor pressure deficit (VPD), and precipitation have been found to modulate tropical peatland GHG fluxes (Hergoualc'h et al., 2020; Hirano et al., 2009). For example, soil CH₄ emissions have been found to increase linearly with increasing air temperature and increase exponentially with increased annual precipitation (Hergoualc'h et al., 2020), while increases in soil respiration were observed with increasing soil temperature (Hirano et al., 2009). Increased VPD has also been documented to decrease gross primary production due to stomatal closure (Hirano et al., 2009), leading to a potential reduction in soil C inputs. Therefore, through this dataset, we intend to answer the following questions:

- Do the relationships between soil GHG fluxes and water table level hold across tropical peatlands with differing disturbance regimes? If so, what are the implications for the water table management of these systems to limit soil GHG emissions?
- Does soil GHG flux sensitivity to environmental controls such as air temperature, soil temperature, VPD, and precipitation hold across differing tropical peatland disturbance regimes?

Taking soil gas flux and micrometeorological observations from a relatively undisturbed, recently disturbed, and long-term disturbed tropical peatland provides a path for elucidating the exact impact of land cover change on these systems. With this knowledge, new policies may be proposed to limit or prohibit practices that are contributing to high C emissions.

4.2 Methods

4.2.1 Site Description

The sites in this study are located in Maludam National Park (hereon “Undrained”; 1°27.211'N, 111°8.967'E), Betong (hereon “Young Plantation”; 1°23.988'N, 111°24.111'E), and Sibu (hereon “Mature Plantation”; 2°11.163'N, 111°50.738'E) (Figure 4.1). All three sites in this study are located in Sarawak, Malaysia and are within a 58 km radius. The distance from Undrained to Young Plantation, Undrained to Mature Plantation, and Young Plantation to Mature Plantation is ~29 km, ~113 km, and ~100 km, respectively.

“Undrained” is an undrained peat swamp forest located ~45 km northwest of the Betong division of Sarawak, Malaysia (Wong et al., 2018). It was officially declared a park in 2000 with an area

of ~43200 ha, with further protections in 2015 increasing the area to ~53600 ha (Tang et al., 2020). The peat profile resembles a dome shape and therefore water naturally flows away from the dome center into the surrounding bodies of water when the peat is saturated (Tang et al., 2020). Due to precipitation being the main source of its nutrients, Undrained is classified as ombrotrophic and nutrient poor (oligotrophic). Throughout the year, the water table is typically near or above the peat surface and varies with the amount and duration of precipitation (Tang et al., 2020). The average tree height within the sampling area is ~35 meters and dominated by the *Shorea albida* species (Tang et al., 2020).

“Young Plantation” is a young oil palm plantation near the Betong division in Sarawak, Malaysia (Wong et al., 2025). In the region, the average annual precipitation from 1990 to 2020 was ~3154 mm (Wong et al., 2025). The land was occupied by a secondary peat swamp forest before being converted in March 2017 (Wong et al., 2025). Land conversion took place from March 2017 to April 2018 where the land was drained to lower the water table level (Wong et al., 2025). In May 2018, the seedlings of *Elaeis guineensis* were planted and fertilizer was added two times every year to facilitate oil palm growth (Wong et al., 2025).

“Mature Plantation” is a mature oil palm plantation located southwest of Sibu in Sarawak, Malaysia (Nishina et al., 2023). The average annual air temperature in the area between 2004 and 2016 was 26.5 °C and mean annual precipitation was ~2915 mm (Ishikura et al., 2018). The previous ecosystem on the land was a mixed ombrotrophic peat swamp forest and the initial deforesting and transplanting of oil palm began in 2004 (Nishina et al., 2023). The water table level from April 2018 through June 2019 fluctuated between 16 to 101 cm below the soil surface

and was mostly lower during the dry season relative to the wet season ([Nishina et al., 2023](#)). It is important to note that the specific study sites for Mature Plantation were located in a region where the second rotation of planting was taking place. Therefore, the oil palm trees were not fully grown at the time of sampling.

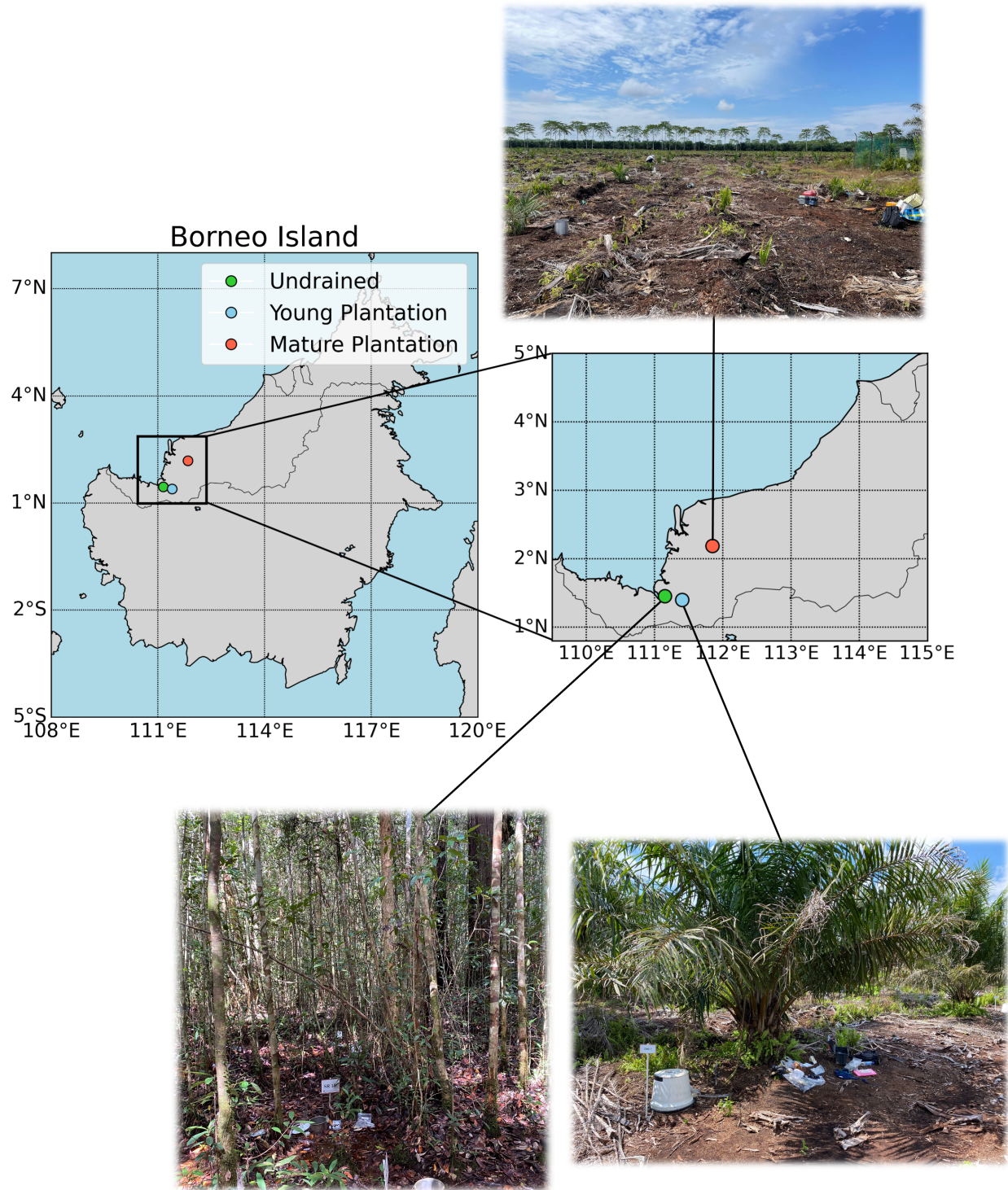


Figure 4.1: A map of Borneo Island showing the three study site locations along with pictures. Undrained, Young Plantation, and Mature Plantation are represented by green, blue, and red, respectively.

4.2.2 Soil and Soil Gas Samples

Soil gas samples were taken using the closed chamber method. A total of 8 stainless steel chambers were placed on the surface of the soil at each site. The chambers were ~20 cm in diameter and ~25 cm in height. A cover was placed on the chamber and clipped with 6 binder clips so that gas may accumulate within the chamber. 20 mL of gas samples were taken via a 25 mL polypropylene syringe and then transferred to a previously vacuumed vial. At each site, gas samples were taken between approximately 9am and 1pm local time and were taken four times: at minute 0, 10, 20, and 40.

CO₂, CH₄, and N₂O concentrations were evaluated after approximately two weeks from the sample date using gas chromatography (Agilent Technologies 7890A). For CO₂, we specifically studied the soil efflux (soil-to-atmosphere exchange). Fluxes for CO₂, CH₄, and N₂O were calculated using the following equation:

$$Gas\ Flux = (p)(h) \left(\frac{\Delta c}{\Delta t} \right) \left(\frac{273}{273+T} \right) (\alpha) \quad (4.1)$$

where p is the density of the gas in question, h is the average chamber height, $\frac{\Delta c}{\Delta t}$ is the change in gas concentration over time, T is the average air temperature, and α is the molecular weight ratio of either C to CO₂ or CH₄ or nitrogen to N₂O. For data quality control, we fit the concentration measurements to a simple linear regression model to determine the coefficient of determination (R^2). We then set predetermined R^2 thresholds for CO₂, CH₄, and N₂O. If any flux value had an associated R^2 value that was less than the threshold, that flux value was omitted from our

analysis. The number of data points remaining for CO₂, CH₄, and N₂O after applying the threshold was 193, 126, and 148 data points, respectively.

Soil samples were taken at each chamber location at each site using a soil auger. Samples were taken from 0-25 cm and 25-50 cm of the soil profile. In the laboratory, all soil samples were weighed using an analytical balance. To determine bulk density, the peat was dried before weighing. The volume for bulk density was calculated using a digital actual volumeter. The electroconductivity and cation exchange capacity of the peat was evaluated using MS 2458:2012 and ammonium acetate (pH 7), respectively.

4.2.3 Other Measured Variables

At each site, VPD (Campbell Scientific HygroVUE10) and precipitation (Texas Electronics TR-525-M10) were measured. We only utilized daytime VPD (9am-3pm) values in our analysis. For each month, we recorded a single averaged VPD value and single summed precipitation value at each site. At the location of each chamber, the air temperature and soil temperature at 5 cm and 10 cm depth (copper & alloy thermocouple) was also recorded.

Perforated polyvinyl chloride tubes were used to measure the water table level relatively near the chambers at each site. Each month, the water table was measured manually using a tape measure and also recorded automatically every 30 minutes (HOBO U20-001-04 Water Level Logger) at each site.

4.2.4 Data Analysis

We used the Python programming language for all data analysis. We used the “linregress” command within the “SciPy” Python package to calculate the Pearson correlation coefficient, p-value, and slope and intercept for the line of best fit. Additionally, we utilized the standard error of the slope of each GHG concentration (CO_2 , CH_4 , and N_2O) over time to calculate flux uncertainty for each chamber.

4.3 Results

4.3.1 Impact of Peatland Conversion to Oil Palm on Soil Greenhouse Gas Fluxes

The GHG flux timeseries had notable variation from site to site. Additionally, some sites experienced large flux variation between the subsites, indicating peat GHG flux heterogeneity even across small distances. At Young Plantation and Mature Plantation, CO_2 flux magnitudes were comparable. On the other hand, CO_2 flux magnitudes at Undrained were notably smaller. The opposite was found for CH_4 , as Young Plantation and Mature Plantation maintained lower CH_4 flux magnitudes over the study period relative to Undrained. N_2O flux magnitudes at Undrained were miniscule when compared to those at Young Plantation and Mature Plantation. While CO_2 and CH_4 flux magnitudes exhibited large month-to-month variability across sites and most subsites, N_2O flux magnitudes were fairly constant, with generally synchronized spikes sometimes occurring across subsites during certain months.

4.3.2 Carbon Dioxide Flux

At the first subsite (Undrained-1A, Undrained-1B, Undrained-1C, Undrained-1D), the largest efflux occurred during July, August, October, and December at Undrained-1D, Undrained-1B, Undrained-1C, Undrained-1A, respectively (Figure 4.2). The flux range (difference between

maximum and minimum flux) for each chamber also varied substantially. Undrained-1A, Undrained-1B, Undrained-1C, and Undrained-1D had CO₂ flux ranges of approximately 1.99, 1.54, 1.28, 1.81 $\mu\text{mol CO}_2 \text{ m}^{-2} \text{ s}^{-1}$, respectively (Figure 4.2). For the second subsite (Undrained-2A, Undrained-2B, Undrained-2C, Undrained-2D), the CO₂ flux patterns were similar among Undrained-2A, Undrained-2B, and Undrained-2C. These chambers exhibited a generally increasing flux from May 2024 to August 2024, and then showed decreasing flux from August 2024 to January 2025 (Figure 4.2). Undrained-2D showed a considerably different pattern, with large fluxes in July and December and the low fluxes in June and September (Figure 4.2).

The chambers at Young Plantation were similar within each subsite, albeit with minor exceptions. The first subsite exhibited increasing fluxes from approximately the May to July months, and then decreased from around August to October (although not the case for Young Plantation-1A and Young Plantation-1D), followed by another increase from October to December (Figure 4.2). At the second subsite, fluxes varied between months, with one high flux occurring in May/June, a low flux in July, and then another high flux in August/September (Figure 4.2). The ranges of CO₂ fluxes were approximately 6.07, 8.51, 5.78, and 12.09 $\mu\text{mol CO}_2 \text{ m}^{-2} \text{ s}^{-1}$ for Young Plantation-2A, Young Plantation-2B, Young Plantation-2C, and Young Plantation-2D, respectively (Figure 4.2).

The CO₂ fluxes at Mature Plantation were relatively more stable than at Undrained and Young Plantation. All chambers at the first subsite showed minimal deviations from a flux value between 0 and 3.16 $\mu\text{mol CO}_2 \text{ m}^{-2} \text{ s}^{-1}$ (Figure 4.2). This was generally true for all chambers at the first subsite from May through October. The flux range for Young Plantation-1A, Young Plantation-1B, Young Plantation-1C, and Young Plantation-1D was 5.53, 5.38, 4.99, 4.15 μmol

$\text{CO}_2 \text{ m}^{-2} \text{ s}^{-1}$, respectively (Figure 4.2). Similar stability was observed at the second subsite. With the exception of Young Plantation-2D, the most stable period occurred from July through November, where the CO_2 efflux remained between 0 and $6.31 \mu\text{mol CO}_2 \text{ m}^{-2} \text{ s}^{-1}$ (Figure 4.2). Young Plantation-2C was the only chamber that exhibited continued flux stability through January 2025 (Figure 4.2). Flux ranges at the second subsite were 9.78, 9.16, 13.02, $9.67 \mu\text{mol CO}_2 \text{ m}^{-2} \text{ s}^{-1}$ for Young Plantation-2A, Young Plantation-2B, Young Plantation-2C, and Young Plantation-2D, respectively (Figure 4.2).

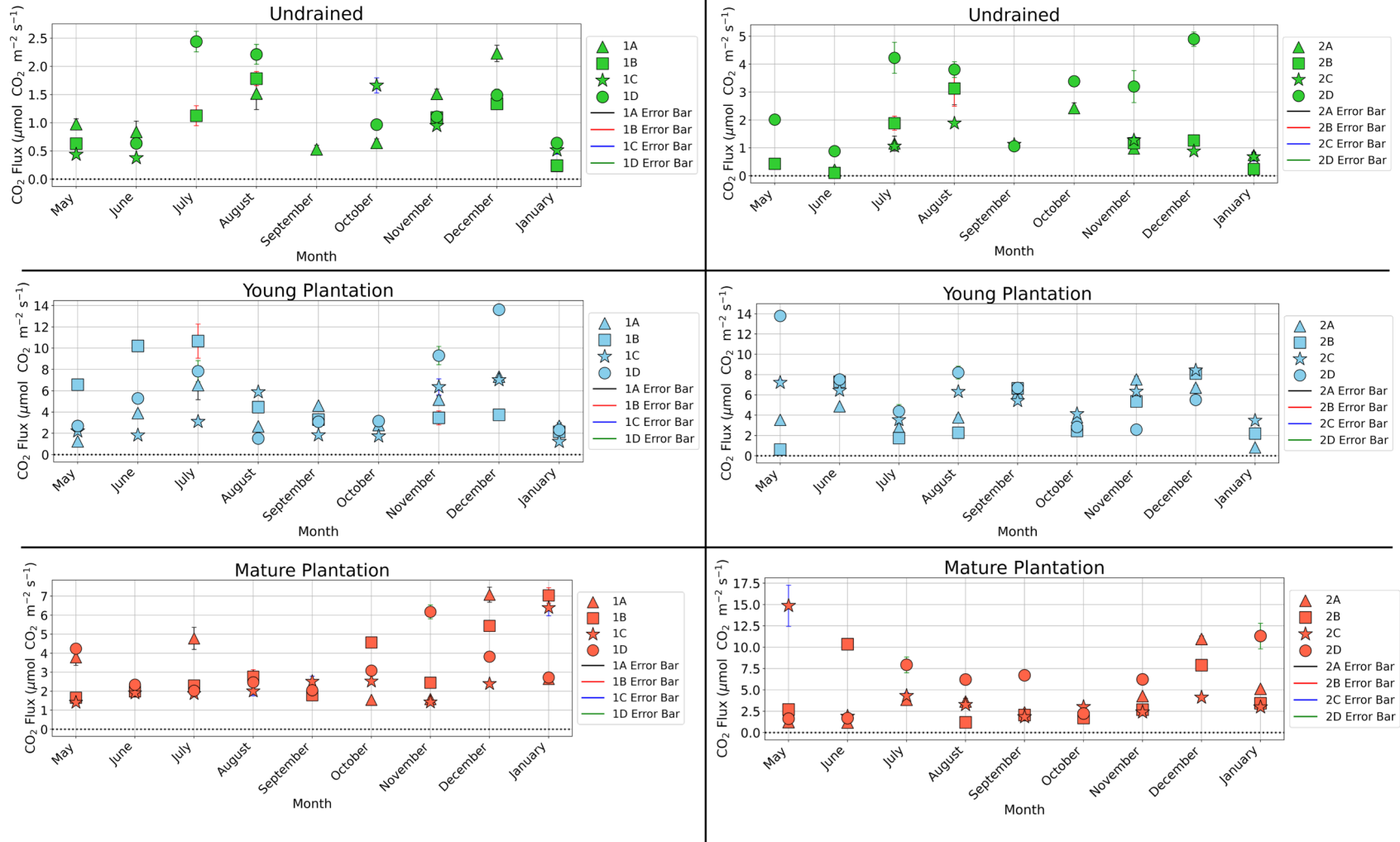


Figure 4.2: CO₂ flux over time at each chamber across all sites and subsites. CO₂ flux error bars are also shown. Positive values indicate CO₂ source. The horizontal black dotted line indicates zero flux.

4.3.3 Methane Flux

Overall, CH₄ flux data was limited at Undrained. However, Undrained-1D and Undrained-2A had the longest continuous records for CH₄ flux data. At the first subsite, all individual chambers showed large variability among themselves, and no particular pattern was present. The continuous record at Undrained-1D showed that CH₄ fluxes were relatively stable from May through July and August through October (Figure 4.3). The largest fluxes were observed in May and November (Figure 4.3). The second subsite also exhibited large flux variations between chambers. For example, Undrained-2B showed some CH₄ flux magnitudes to be between 0.17 to 0.66 $\mu\text{mol CH}_4 \text{ m}^{-2} \text{ s}^{-1}$ while Undrained-2D was between 0.002 and 0.01 $\mu\text{mol CH}_4 \text{ m}^{-2} \text{ s}^{-1}$ (Figure 4.3). The chamber with the most continuous flux data, Undrained-2A showed a peak CH₄ efflux in August and a stable flux from November through January (Figure 4.3). At the Young Plantation site, there was more agreement among the chambers in terms of CH₄ flux patterns. At the first subsite, all chambers exhibited a maximum CH₄ efflux in November (Figure 4.3). Before and after November, the CH₄ flux was relatively stable (Figure 4.3). This same flux pattern was observed at the second subsite (Figure 4.3). It is also worth noting that during some months the chambers reported a CH₄ sink, such as in August for Young Plantation-1D and in January for Young Plantation-2A (Figure 4.3). Data at Mature Plantation was also limited, and therefore most flux data was discontinuous between consecutive months. However, it can be clearly observed that, at both first and second subsites, there are many instances the chamber locations acting as CH₄ sinks (Figure 4.3).

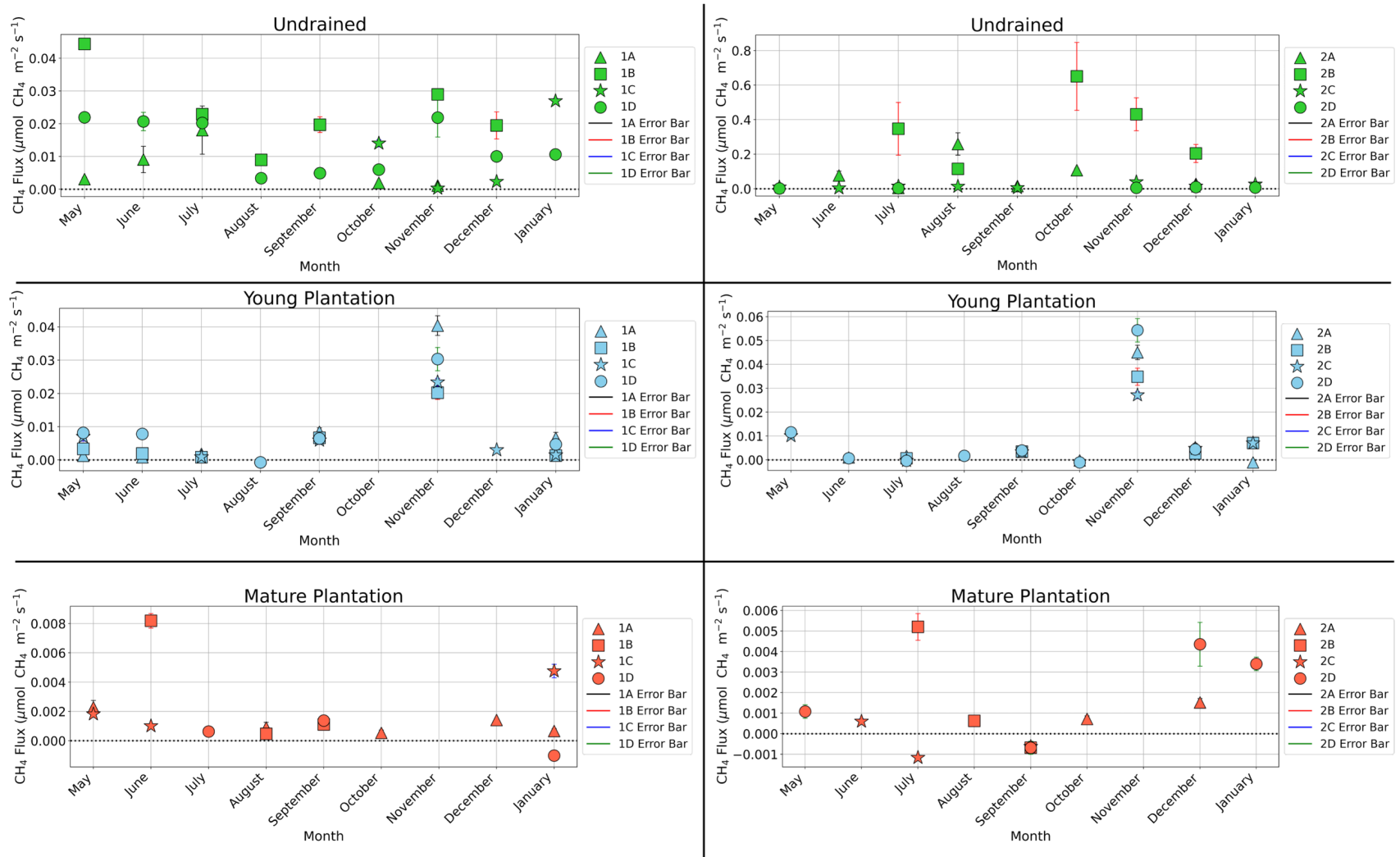


Figure 4.3: CH₄ flux over time at each chamber across all sites and subsites. CH₄ flux error bars are also shown. Positive and negative values indicate CH₄ source and sink, respectively. The horizontal black dotted line indicates zero flux.

4.3.4 Nitrous Oxide Flux

For Young Plantation, the N₂O flux had similar temporal variability at the first subsite (Young Plantation-1A, Young Plantation-1B, Young Plantation-1C, Young Plantation-1D). Within the nine-month period, all chambers at the first subsite showed a maximum land-to-atmosphere N₂O flux in June. This was then followed by a general decline from July through January (Figure 4.4). At the second subsite for Young Plantation (Young Plantation-2A, Young Plantation-2B, Young Plantation-2C, Young Plantation-2D), more variability was observed between chambers. For the data points we recorded, the maximum N₂O flux from the ecosystem to atmosphere over the nine month period occurred during June at Young Plantation-2A and Young Plantation-2B, July at Young Plantation-2C, and May at Young Plantation-2D (Figure 4.4). While at Young Plantation-2B and Young Plantation-2C the N₂O flux declined after the maximum and remained small, Young Plantation-2A and Young Plantation-2D saw an increase from August to November and from November to December, respectively (Figure 4.4). Mature Plantation exhibited the most variable N₂O fluxes out of all sites. It also experienced substantial variability between chambers within a single subsite. At the first subsite (Mature Plantation-1A, Mature Plantation-1B, Mature Plantation-1C, Mature Plantation-1D), the peak land-to-atmosphere N₂O flux occurred in October for Mature Plantation-1B and Mature Plantation-1C. On the other hand, the peak N₂O flux at Mature Plantation-1A and Mature Plantation-1D occurred during December and May, respectively (Figure 4.4). Generally, there was large variability during the nine month period and the N₂O flux did not exhibit any noteworthy pattern (Figure 4.4). The second subsite (Mature Plantation-2A, Mature Plantation-2B, Mature Plantation-2C, Mature Plantation-2D) also showed large temporal variability. The N₂O flux was at its peak during October, December, May, and

January for Mature Plantation-2A, Mature Plantation-2B, Mature Plantation-2C, and Mature Plantation-2D, respectively (Figure 4.4). With the exception of Mature Plantation-2B which exhibited a generally increasing N₂O flux pattern from May 2024 through December 2024, the second subsite did not show a notable pattern throughout the study period (Figure 4.4).

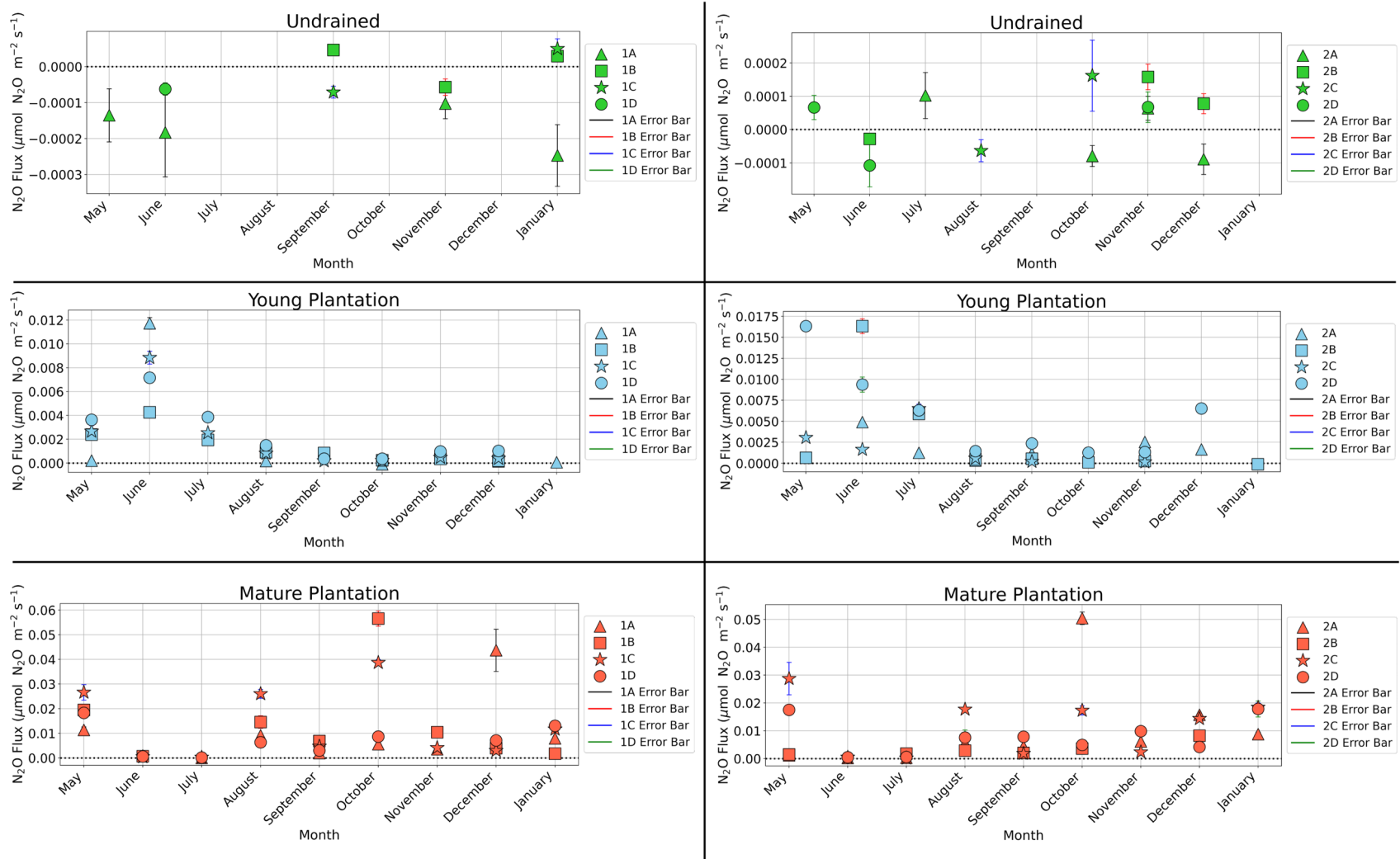


Figure 4.4: N₂O flux over time at each chamber across all sites and subsites. N₂O flux error bars are also shown. Positive and negative values indicate N₂O source and sink, respectively. The horizontal black dotted line indicates zero flux.

4.3.5 Role of Environmental Drivers on Soil Greenhouse Gas Fluxes in Undrained and Drained Tropical Peatlands

4.3.5.1 Water Table Level

The relationship between water table level and CO₂ flux varied between the undrained peat swamp forest and the two oil palm plantations. While a significant inverse relationship was observed between the two variables at Undrained ($R = -0.35$; $p < 0.01$) (Figure 4.5), no correlation was found at Young Plantation ($R = 0.02$; $p > 0.05$) and Mature Plantation ($R = 0.11$; $p > 0.05$) (Figure 4.5). Water table level and CH₄ did not show any relationship among the three sites (Figure 4.5). At Young Plantation and Mature Plantation, N₂O and water table level exhibited a statistically significant positive relationship, while at Undrained, there was a weak negative relationship ($R = -0.24$; $p > 0.05$ at Undrained, $R = 0.32$; $p < 0.05$ at Young Plantation, $R = 0.29$; $p < 0.05$ at Mature Plantation) (Figure 4.5).

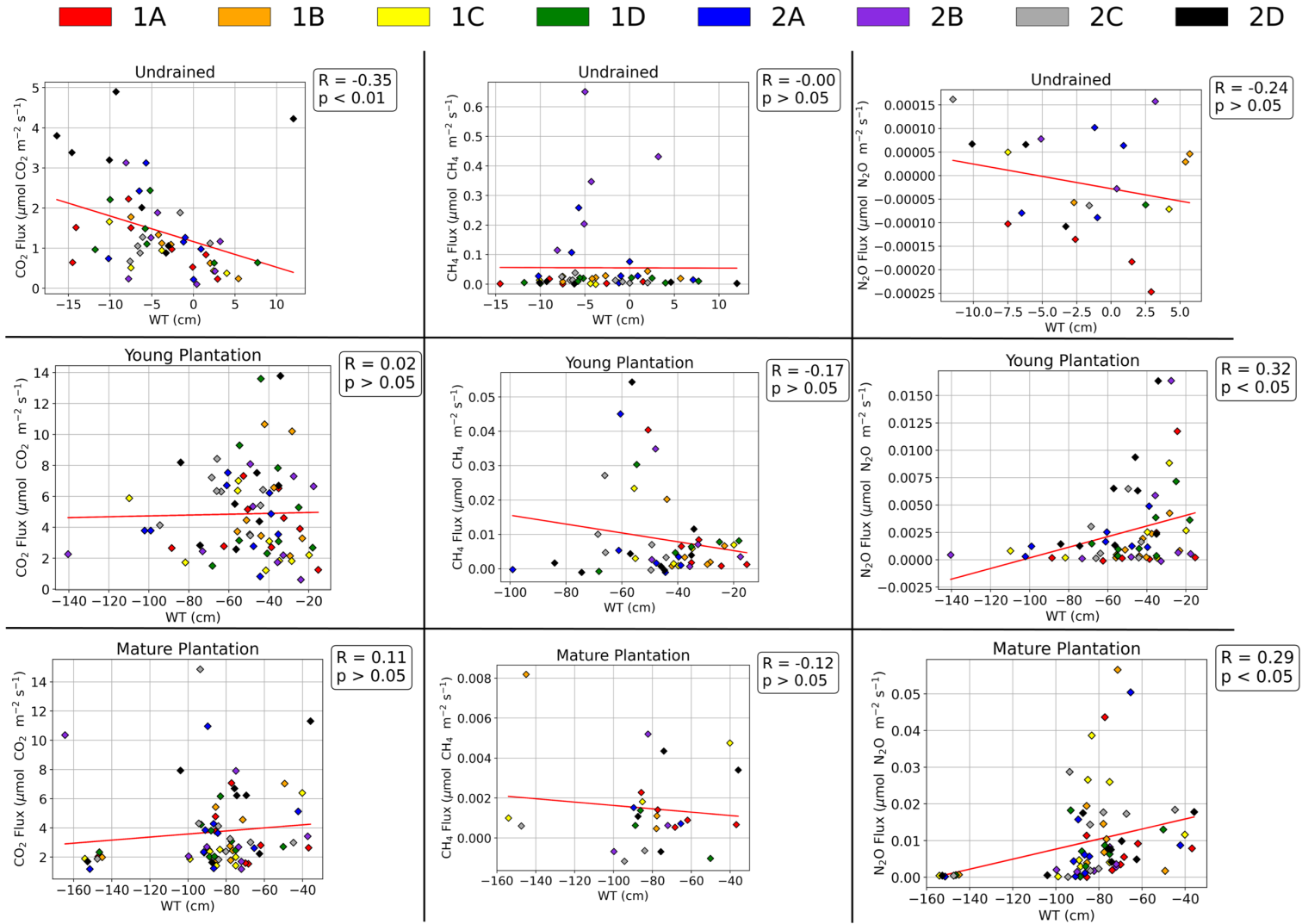


Figure 4.5: CO₂, CH₄, and N₂O flux versus water table level at each of the sites along with the Pearson correlation coefficient (R) and p-value (stated as whether the value is greater or less than 0.05). Each color represents an individual chamber.

4.3.5.2 Average Air Temperature

CO₂ flux showed a weak positive relationship with average air temperature at Undrained, but no relationship at Mature Plantation ($R = 0.2$; $p > 0.05$ at Undrained, $R = -0.09$; $p > 0.05$ at Mature Plantation). At Young Plantation, a moderate and statistically significant positive correlation was found ($R = 0.33$; $p < 0.01$) (Figure 4.6). There was no strong relationship between CH₄ flux and average air temperature at each of the sites ($R = 0$; $p > 0.05$ at Undrained, $R = 0.23$; $p > 0.05$ at Young Plantation, $R = -0.08$; $p > 0.05$ at Mature Plantation) (Figure 4.6). N₂O flux showed a very weak and insignificant positive relationship with average air temperature at Undrained ($R = 0.22$; $p > 0.05$). At Young Plantation and Mature Plantation, there was little to no correlation ($R = 0.18$; $p > 0.05$ at Young Plantation, $R = -0.18$; $p > 0.05$ at Mature Plantation) (Figure 4.6).

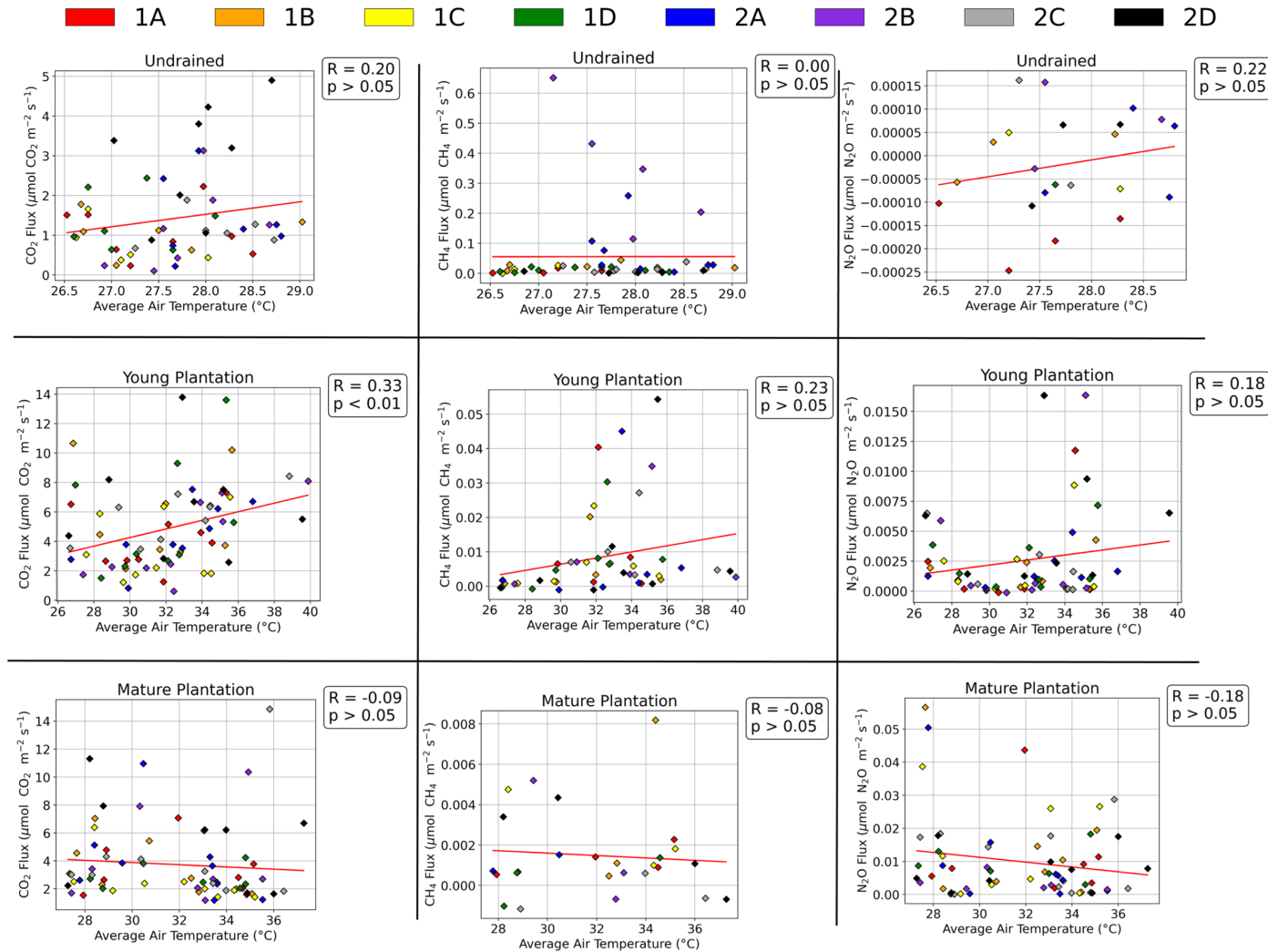


Figure 4.6: CO₂, CH₄, and N₂O flux versus average air temperature at each of the sites along with the Pearson correlation coefficient (R) and p-value (stated as whether the value is greater or less than 0.05). Each color represents an individual chamber.

4.3.5.3 Soil Temperature at 5 cm and 10 cm Depth

Soil temperature at 5 cm depth had opposite effects on CO₂ flux at Undrained and Young Plantation. As soil temperature at 5 cm depth increased, Undrained and Young Plantation experienced a decrease and increase in CO₂ flux, respectively ($R = -0.32$; $p < 0.05$ at Undrained, $R = 0.37$; $p < 0.01$ at Young Plantation) (Figure 4.7). At Mature Plantation, no relationship was found between soil temperature at 5 cm depth and CO₂ flux ($R = 0.01$; $p > 0.05$) (Figure 4.7). At all three sites, soil temperature at 5 cm depth did not have an effect on CH₄ flux ($R = -0.09$; $p > 0.05$ at Undrained, $R = 0.19$; $p > 0.05$ at Young Plantation, $R = -0.04$; $p > 0.05$ at Mature Plantation) (Figure 4.7). There was also no relationship found between soil temperature at 5 cm and N₂O flux at Young Plantation and Mature Plantation ($R = -0.02$; $p > 0.05$ at Young Plantation, $R = -0.01$; $p > 0.05$ at Mature Plantation) (Figure 4.7). At Undrained, the correlation between soil temperature at 5 cm and N₂O flux was negative and statistically insignificant ($R = -0.29$; $p > 0.05$ at Undrained) (Figure 4.7).

For soil temperature at 10 cm depth, Undrained and Mature Plantation exhibited no relationship with CO₂ flux ($R = 0.09$; $p > 0.05$ at Undrained, $R = 0.04$; $p > 0.05$ at Mature Plantation) while Young Plantation showed a weak positive relationship ($R = 0.22$; $p > 0.05$) (Figure 4.8). The correlation between soil temperature at 10 cm depth and CH₄ flux was non-existent at Young Plantation and Mature Plantation ($R = 0.07$; $p > 0.05$ at Young Plantation, $R = 0$; $p > 0.05$ at Mature Plantation) (Figure 4.8). However, there was a weak negative relationship at Undrained ($R = -0.24$; $p > 0.05$) (Figure 4.8). When observing the dependency of N₂O flux on soil temperature at 10 cm depth, Undrained was found to have a weak negative correlation ($R = -$

0.21; $p > 0.05$) while Young Plantation and Mature Plantation did not show any relationship ($R = -0.04$; $p > 0.05$ at Young Plantation, $R = 0.02$; $p > 0.05$ at Mature Plantation) (Figure 4.8).

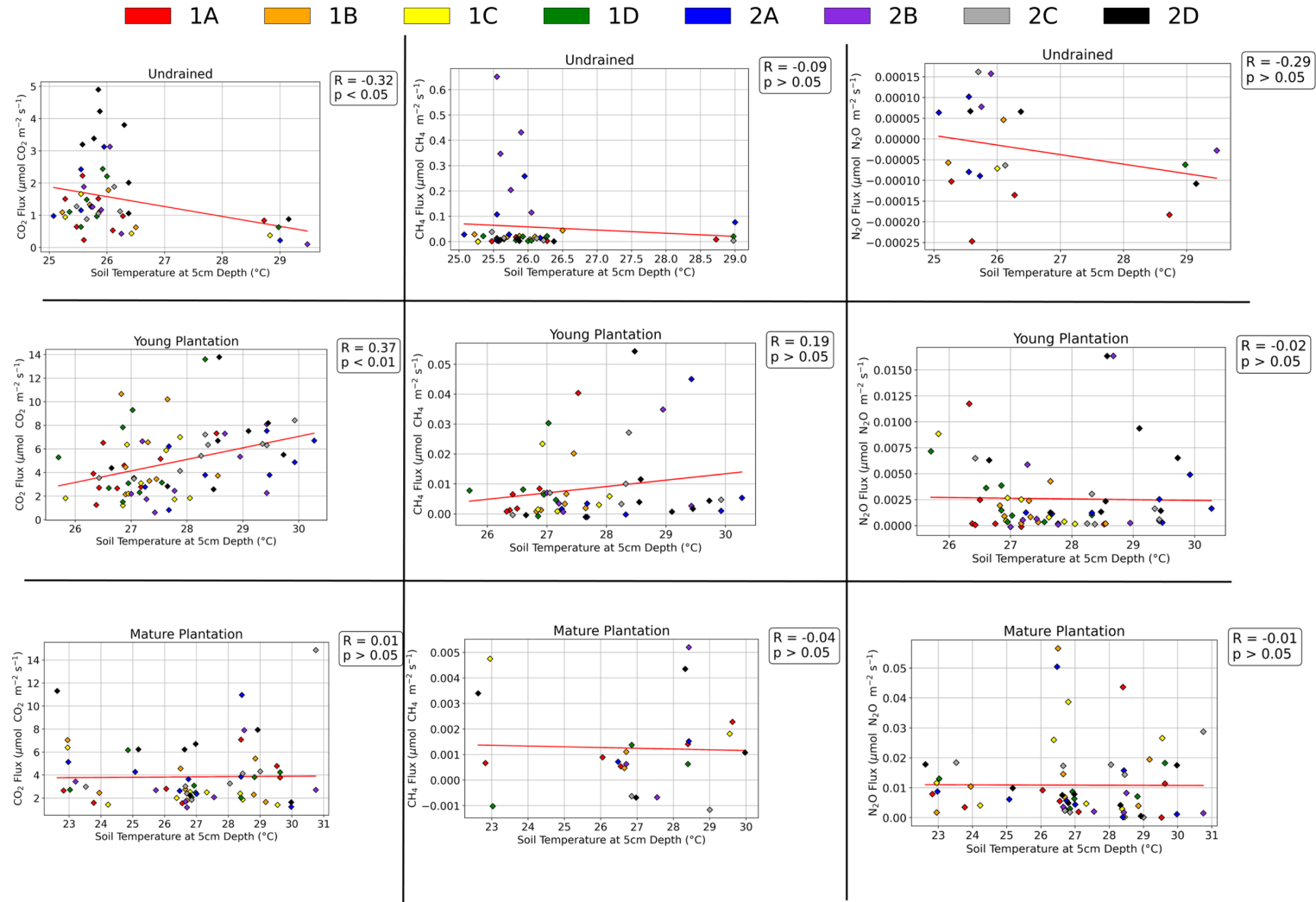


Figure 4.7: CO₂, CH₄, and N₂O flux versus soil temperature at 5 cm depth at each of the sites along with the Pearson correlation coefficient (R) and p-value (stated as whether the value is greater or less than 0.05). Each color represents an individual chamber.

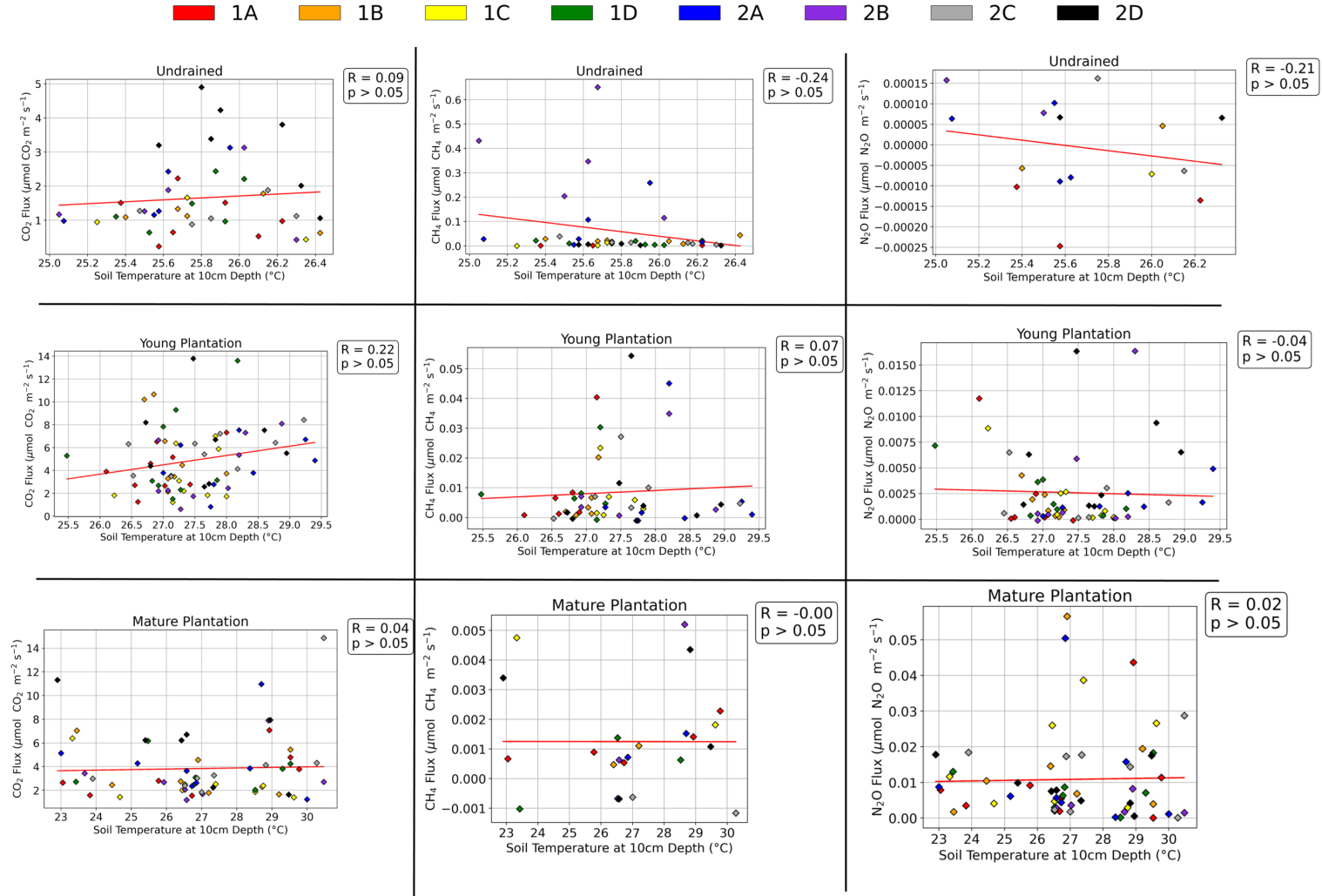


Figure 4.8: CO₂, CH₄, and N₂O flux versus soil temperature at 10 cm depth at each of the sites along with the Pearson correlation coefficient (R) and p-value (stated as whether the value is greater or less than 0.05). Each color represents an individual chamber.

4.3.5.4 Precipitation

Overall, CO₂ efflux showed large chamber-to-chamber variability with increasing precipitation at Undrained. For example, while at Undrained-2D there was a large CO₂ efflux ($\sim 4.9 \mu\text{mol CO}_2 \text{ m}^{-2} \text{ s}^{-1}$) at a monthly precipitation of 396.8 mm, there was a notably smaller CO₂ efflux for Undrained-2C ($\sim 0.88 \mu\text{mol CO}_2 \text{ m}^{-2} \text{ s}^{-1}$) (Figure 4.9) for the same precipitation value. There was, however, a generally increasing flux pattern when considering all chambers up until a precipitation value of 611.1 mm. At a monthly precipitation of 611.1 mm, all recorded CO₂ effluxes substantially decreased. At Young Plantation, chamber-to-chamber variability was also high, and low CO₂ effluxes were also observed at the highest monthly precipitation value (Figure 4.9). For Mature Plantation, some chambers experience a sudden spike in CO₂ efflux at intermediate monthly precipitation values, before decreasing and then increasing again at the highest monthly precipitation value (Figure 4.9). Due to the limited amount of CH₄ flux data, it was difficult to observe any relationships between CH₄ flux and precipitation. However, at Young Plantation there were relatively large CH₄ effluxes at all the chambers when monthly precipitation was at an intermediate value of 284.5 mm (Figure 4.9). The N₂O flux and precipitation relationship was not able to be determined at Undrained due to lack of data. Although, at Young Plantation and Mature Plantation, there were relatively large N₂O fluxes at some chambers when monthly precipitation was at lower-intermediate values (191.8 mm and 238.3 mm, respectively) (Figure 4.9).

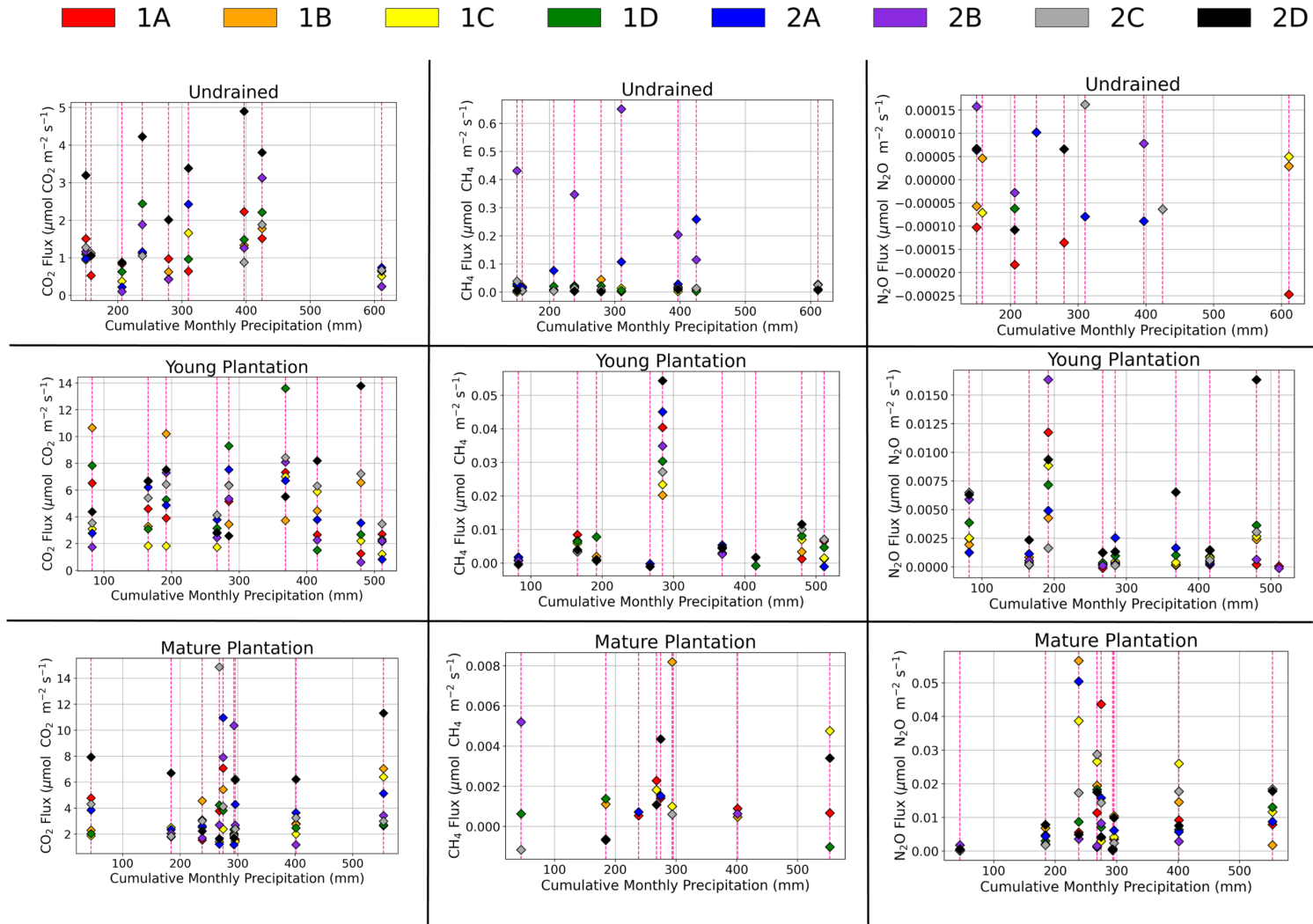


Figure 4.9: A bar plot showing CO₂, CH₄, and N₂O flux of individual chambers for a single monthly precipitation value. Precipitation values were summed for each month.

4.3.5.5 Vapor Pressure Deficit

The CO₂ flux at each site showed substantial variability with increasing VPD (Figure 4.10). At Undrained, there were notably smaller CO₂ fluxes at VPD values of ~0.49 and ~0.79 kPa (Figure 4.10). Relatively higher CO₂ fluxes were recorded at a VPD of ~0.69, ~0.7, and ~0.75 kPa (Figure 4.10). At Young Plantation, some chambers experienced CO₂ fluxes that were large at low VPD values (with the exception of when VPD was ~0.5) (Figure 4.10). No relationship was observed between CO₂ fluxes and VPD at Mature Plantation (Figure 4.10). Unfortunately, due to the lack of CH₄ flux data at Undrained and Mature Plantation, we could not resolve any relationship between CH₄ flux and VPD at those sites (Figure 4.10). However, Young Plantation did show higher CH₄ fluxes across all recorded chambers at a VPD of ~0.745 kPa (Figure 4.10). For N₂O flux, lack of data prevented us from determining its relationship with VPD at Undrained (Figure 4.10). At Young Plantation, the highest N₂O fluxes at many of the chambers occurred at a VPD of ~0.77 and ~0.89 kPa (Figure 4.10). However, no general pattern was found between VPD and N₂O flux at the site. N₂O flux increased at some chambers and decreased at others at Mature Plantation. For example, from a VPD of 0.72 to 0.83 kPa, the N₂O flux generally increased at Mature Plantation-1D and Mature Plantation-2A (Figure 4.10). On the other hand, Mature Plantation-2D showed a decreasing pattern in N₂O flux from ~0.74 to ~0.92 kPa (Figure 4.10).

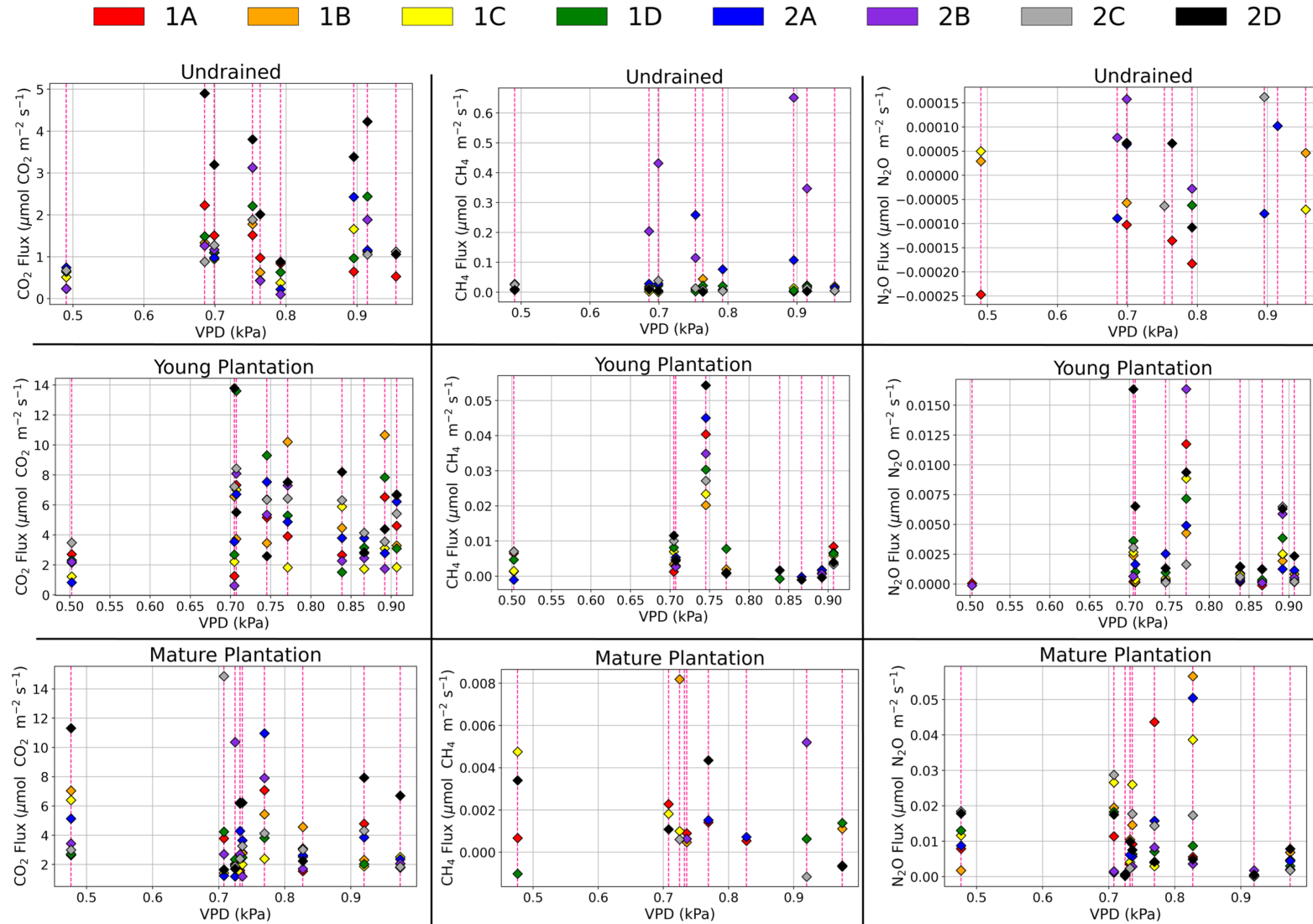


Figure 4.10: A bar plot showing CO₂, CH₄, and N₂O flux of individual chambers for a single monthly VPD value. VPD values were averaged for the times of 9am to 3pm only.

4.4 Discussion

The differences in soil GHG flux at each site shows that agriculture-related disturbance can have an immense impact on peat's ability to maintain carbon and nitrogen (Figure 4.11). These impacts are mainly observed through drainage, which lowers the water table, promotes peat oxidation, and releases CO₂ to the atmosphere ([Carlson et al., 2015](#); [Hooijer et al., 2012](#); [Evans et al., 2019](#)). Peatland drainage also tends to decrease CH₄ emissions due to the presence of oxygen reducing methanogenic processes ([Murdiyarso et al., 2010](#); [Somers et al., 2023](#); [Deshmukh et al., 2020](#); [Hirano et al., 2009](#); [Melling et al., 2005b](#)). N₂O emissions are minimal in undisturbed tropical peatlands due to the limitation of nitrogen within the system ([Jauhiainen et al., 2012b](#); [Teh et al., 2017](#)). On the other hand, nitrogen is abundant in agricultural settings due to anthropogenic input of nitrogen fertilizer ([Nishina et al., 2023](#); [Hayashi et al., 2020](#)). Our study observed a similar pattern in magnitude of flux differences between the undrained and both oil palm plantations, suggesting that peatland drainage and oil palm cultivation has a broadly consistent set of impacts across tropical peatland systems.




	Undrained 	Young Plantation 	Mature Plantation 
CO_2 ($\mu\text{mol CO}_2 \text{ m}^{-2} \text{ s}^{-1}$)	1.42 [0.1-4.9]	4.87 [0.62-13.79]	3.74 [1.19-14.86]
CH_4 ($\mu\text{mol CH}_4 \text{ m}^{-2} \text{ s}^{-1}$)	0.06 [0-0.65]	0.01 [-0.001-0.05]	0.001 [-0.001-0.008]
N_2O ($\mu\text{mol N}_2\text{O m}^{-2} \text{ s}^{-1}$)	0 [-0.0002-0.0002]	0.003 [0-0.02]	0.01 [0-0.06]
$\text{CO}_2\text{-eq (CH}_4\text{)}$ ($\mu\text{mol CO}_2\text{-eq m}^{-2} \text{ s}^{-1}$)	0.83 [0-9]	0.14 [-0.01-0.69]	0.01 [-0.01-0.11]
$\text{CO}_2\text{-eq (N}_2\text{O)}$ ($\mu\text{mol CO}_2\text{-eq m}^{-2} \text{ s}^{-1}$)	0 [-0.05-0.05]	0.82 [0-5.46]	2.73 [0-16.38]

Figure 4.11: Approximate mean [minimum-maximum] soil greenhouse gas fluxes across all months for all sites. Negative and positive values indicate sink and source, respectively. CO_2 -equivalent ($\text{CO}_2\text{-eq}$) fluxes were calculated using 100-year time horizon global warming potential values of 38 (Neubauer, 2014) and 273 (IPCC, 2023) for CH_4 and N_2O , respectively (Frolking et al., 2006).

4.4.1 Drainage and Oil Palm Cultivation on Tropical Peat Decreases Methane Emissions and Promotes Carbon Dioxide and Nitrous Oxide Emissions

Elevated N_2O fluxes at Young Plantation and Mature Plantation suggest increased nitrogen inputs compared to Undrained. Most fertilizers used in oil palm plantations contain nitrogen in the form of ammonium and therefore provide ample substrate for ammonia-oxidizing bacteria to undergo nitrification. This results in a high abundance of nitrate in the soil which, combined with anaerobic conditions, can result in denitrification and consequently an increase in N_2O flux from the soil to the atmosphere. Due to the drained nature of the oil palm plantation sites, the water table is low, creating aerobic conditions that are unfavorable for denitrification on a bulk soil scale. However, small pockets of oxygen-limited areas may exist within the peat structure and therefore act as local hot spots for N_2O emission. On a larger scale, precipitation events can temporarily increase water saturation in the soil and may thereby expand anaerobic conditions and consequently increase N_2O emissions over a larger area. At undrained sites (such as Undrained in this study), saturated soils promote anaerobic conditions that are prevalent across much of the landscape. Although these conditions favor denitrification, low nitrate availability—resulting from decreased nitrification—limits N_2O emissions. In general, our study agrees with similar previous studies ([Jauhiainen et al., 2012b](#); [Teh et al., 2017](#)). We attributed the large spikes in N_2O emissions at Young Plantation and Mature Plantation to the fertilizer applied many days before.

CO_2 emissions are highly dependent on oxygen availability since microbes mainly use oxygen to break down organic C and emit CO_2 . One of the common ways to achieve an oxygen-limited environment is through water-logged conditions. In these conditions, pore spaces are filled

entirely with water which blocks air from entering. Furthermore, due to its significantly lower diffusivity in water than in air, oxygen is poorly distributed in saturated soils. As a result, CO₂ emissions are decreased in tropical peatlands under these conditions ([Lam et al., 2022](#); [Hirano et al., 2012](#)). This was clearly displayed in our study at Undrained, where soil CO₂ fluxes were markedly lower at various points during the study period than at Young Plantation and Mature Plantation. Low water tables at Young Plantation and Mature Plantation allowed for more soil aeration and therefore more oxygen availability, leading to an increase in peat oxidation and CO₂ emissions. In addition, intensified microbial activity indicates ongoing loss of organic matter within the peat profile which, when combined with compaction and shrinkage, contributes to peat subsidence and an increase in overall peat bulk density ([Hooijer et al., 2012](#)). As pore space within the peat profile decreases, the soil's capacity to retain and regulate water declines, increasing the risk of flooding ([Hein et al., 2022](#); [Uda et al., 2017](#)). Furthermore, lowered moisture content increases fire risk due to dry peat being more susceptible to ignition and combustion ([Turetsky et al., 2015](#)), especially if there is high oxygen availability.

At many points throughout the study period, the chambers at Undrained showed much larger CH₄ emissions than at Young Plantation and Mature Plantation. Since Undrained is undrained, the landscape is waterlogged and oxygen-limited, favoring anaerobic decomposition ([Hergoualc'h et al., 2020](#)). Specifically, methanogenic archaea produce CH₄ as a byproduct of their metabolic process, and this CH₄ is then emitted from the soil to the atmosphere. In aerobic environments such as those at Young Plantation and Mature Plantation, CH₄ emissions are inhibited due to the presence of oxygen. Methanogenic activity is greatly reduced in these

environments due to the oxygen sensitivity of both methanogenic enzymes and the archaea themselves.

We found some differences when comparing our flux values to other studies that also took place in Sarawak, Malaysia ([Melling et al., 2005a](#); [Melling et al., 2005b](#); [Melling et al., 2007](#)). Soil CO₂ flux in [Melling et al., 2005b](#) ranged from ~2.31 to ~12.33 $\mu\text{mol CO}_2 \text{ m}^{-2} \text{ s}^{-1}$, ~1.46 to ~5.67 $\mu\text{mol CO}_2 \text{ m}^{-2} \text{ s}^{-1}$ and ~1.06 to ~7.75 $\mu\text{mol CO}_2 \text{ m}^{-2} \text{ s}^{-1}$ at a peatland forest, sago plantation, and oil palm plantation site, respectively. This is in slight contrast with the soil CO₂ flux ranges we reported in Figure 4.11. In [Melling et al., 2005a](#), the soil CH₄ flux ranges were substantially lower than what we reported, especially between the respective peat swamp forest sites in each study. The range of soil N₂O fluxes reported at the peat swamp forest in [Melling et al., 2007](#) was comparable to that of Undrained. However, the two plantation sites in [Melling et al., 2007](#) had substantially lower soil N₂O flux ranges when compared to the Young Plantation and Mature Plantation sites in our study. Differences in CO₂ and CH₄ fluxes are likely due to peat C exhibiting a high degree of spatial heterogeneity due to differing plant material, management practices, and peat depth even within the same region ([Girkin et al., 2019](#); [Girkin et al., 2022](#)). On the other hand, N₂O flux differences may be attributed to variations in anthropogenic nitrogen input. In [Melling et al., 2007](#), no fertilizer was applied at the sago plantation, which may be one explanation for the lower N₂O fluxes relative to those at the plantations in our study.

It is also important to note that the relatively large distances between sites may yield observed soil GHG flux differences that are not solely due to land-use change. Regional differences in climate and each site's ecological history may have confounding effects which contribute to site-to-site soil GHG flux variability.

4.4.2 Drivers of Soil Greenhouse Gas Fluxes

At Undrained, the CO₂ flux decreased as the water table level increased, showcasing the role of oxygen in facilitating aerobic decomposition. As previously mentioned, CO₂ fluxes occur when oxygen availability is high. Therefore, the water table typically needs to be below the peat surface so that oxygen can fill pores within the peat profile. We observed this phenomenon at Undrained—when water table values turned negative (below peat surface), the soil CO₂ efflux increased. This has also been observed in various other studies covering tropical peatland CO₂ fluxes ([Hirano et al., 2012](#); [Deshmukh et al., 2021](#)). CH₄ fluxes at Undrained exhibited no relationship with water table level which goes against previous literature ([Deshmukh et al., 2021](#); [Hergoualc’h et al., 2020](#)). This may be due to the lack of labile substrates that are essential for methanogenesis. In these forested systems, highly recalcitrant (lignin-rich) material such as tree branches and trunks are omnipresent. Once trees die and their biomass reaches the surface, decomposition slows down due to high lignin content, especially compared to more labile materials like fresh leaves ([Gandois et al., 2012](#); [Gandois et al., 2014](#)). This, in turn, may slow methanogenic activity, leading to reduced and potentially delayed CH₄ emissions.

Microtopographic variability can also play a role through the widespread distribution of hummocks and hollows ([Wösten et al., 2006](#); [Page et al., 1999](#)). Hummocks often remain aerated even at high water tables, reducing CH₄ emissions, while hollows can stay waterlogged at low water tables, which promotes CH₄ production. With regards to N₂O emissions, a weak negative relationship was found with increasing water table at Undrained. Therefore, it is unlikely that the aerobic and anaerobic conditions caused by the water table modulate N₂O fluxes in this setting. Rather, it may be more about the lack of nitrate availability which limits denitrification and thus

decreases N_2O production. At Young Plantation and Mature Plantation, CO_2 fluxes were less sensitive to water table level fluctuations when compared to Undrained. This is in agreement with [Deshmukh et al., 2021](#), which found net ecosystem CO_2 exchange to be less sensitive to water table levels at a degraded peatland site relative to an intact site in Indonesia. This may be due to peat oxidation decelerating rapidly within the first five years after drainage ([Hirano et al., 2012](#); [Hooijer et al., 2012](#)). CH_4 fluxes also exhibited minimal sensitivity to water table level. We attribute this to high methanotrophic activity in the upper peat layers. While CH_4 production is possible within the deeper peat layers, it will likely be oxidized before it reaches the peat surface. Therefore, methane oxidation is the primary process suppressing CH_4 emissions at low water table levels at the plantation sites ([Horwath, 2007](#); [Strack et al., 2008](#)). N_2O fluxes at the plantation sites showed an exponential increase with increasing water table level. This is likely due to increased nitrogen inputs from fertilizer application in combination with nitrification and denitrification processes. At low water table levels, greater oxygen availability promotes nitrification which leads to increased nitrate production. During periods of relatively higher water tables, anaerobic conditions favor denitrification which reduces nitrate and produces N_2O as an intermediate product ([Jauhiainen et al., 2012b](#); [Schlesinger, 2013](#)). This is likely the reason for elevated N_2O fluxes at higher water table levels at Young Plantation and Mature Plantation.

Air temperature also had some effects on GHG fluxes at each site, with the most prominent being an increase in GHG flux with increases in average air temperature. The general increase in flux may be attributed to increased microbial activity. At higher temperatures, the rate of chemical reactions is accelerated, meaning that microbes undergo their metabolic processes more quickly. Interestingly, this positive relationship was held for N_2O fluxes at Undrained, even

though there was limited nitrogen substrate to undergo nitrification and denitrification. Due to higher temperatures, it is possible that the increased microbial activity can cycle even the smaller pools of nitrogen (Pärn et al., 2018). This is especially the case for nitrate, which is in an ideal condition to be converted to N_2O through denitrification due to anaerobic conditions. At Young Plantation, the CH_4 flux exhibited relatively high values at many chambers between temperatures of 31°C and 36°C , but some of the same chambers showed a decrease in CH_4 flux when temperatures rose above 36°C . This is likely due to higher temperatures promoting soil drying, which shifts redox conditions such that anaerobic microbial processes are decreased. N_2O fluxes at Young Plantation showed that they may be promoted when air temperature surpasses a certain threshold. Between 28°C and 34°C , low N_2O flux values were recorded. However, between 34°C and 36°C , N_2O flux values increased drastically. A possible explanation may be that, in addition to increased microbial activity and nitrogen inputs via fertilizer, the drained nature of the plantation creates aerobic and anaerobic zones that facilitate coupled nitrification–denitrification processes. Nitrification dominates in aerobic zones which supports nitrate production. This nitrate may then diffuse into anaerobic zones and undergo denitrification, causing elevated N_2O emissions. Air temperature’s lack of influence on soil GHG fluxes at Mature Plantation suggest that this may be because this area recently underwent a second rotation of planting. Therefore, the associated soil disturbance may have disrupted microbial activity and subsequently diminished the sensitivity of GHG fluxes to air temperature changes. However, it is important to note that one study found certain methanotrophs to be unaffected in a disturbed Indonesian peatland (Arai et al., 2014). Despite our expectation to observe enhanced soil CH_4 and N_2O fluxes with increased precipitation, no relationship was found at most chambers within all sites. In fact, we found this relationship to be quite variable between sites, subsites, and individual

chambers. A similar observation was made between the VPD and soil GHG fluxes. For CO₂, it is expected for the flux to increase (to a point) with increasing VPD due to higher VPD facilitating aerobic conditions ([Ahmad et al., 2021](#)). Soil CH₄ fluxes, on the other hand, are expected to decrease with increasing VPD since oxygen-rich conditions inhibit methanogenesis. At our study sites, these relationships were quite variable and no clear pattern was observed, reinforcing the complex, multifaceted processes required for these gas emissions to occur in these systems. At all sites, soil N₂O fluxes were highly variable with increasing VPD. This is likely due to the aforementioned nitrification and denitrification coupling that comes with varying oxygen availability, resulting in more sporadic N₂O fluxes.

4.4.3 Recommendations for Tropical Peatland Restoration and Sustainability

Given these findings, numerous recommendations can be made to mitigate GHG emissions from tropical peatland soils. Our work clearly shows that Young Plantation and Mature Plantation, the converted peatlands, have a higher soil CO₂ efflux relative to Undrained, the undrained peatlands. We have attributed this to aerobic conditions caused by low water table levels. Therefore, we recommend raising the water table so that peat oxidation may be slowed down. This can be achieved through the blocking of drainage canals in already-drained tropical peatlands ([Novita et al., 2024](#)). Agricultural land conversion should also avoid extremely deep drainage since this may increase fire risk in addition to CO₂ emissions ([Hirano et al., 2009](#); [Hirano et al., 2012](#); [Inubushi et al., 2003](#); [Roucoux et al., 2017](#)). However, stakeholders should be aware that while rewetting efforts have been documented to decrease CO₂ emissions, the associated anaerobic conditions do promote elevated CH₄ emissions ([Ojanen and Minkkinen,](#)

2020). It is therefore not advisable to raise the water table as much as possible, but rather to maintain it at a certain level to minimize the impact of GHG emissions.

Alternatively, restoring native vegetation may also help in this endeavor. Canopy closure provides shade for the underlying soil surface, which reduces evaporation and allows the peat to retain more moisture. Furthermore, this can promote carbon sequestration through biomass accumulation and may contribute to long-term peat formation through woody detritus and leaf litter.

It is important to note that, because measurements at Mature Plantation were collected during the second rotation of planting, the peat structure, microclimate, and nutrient dynamics may not fully reflect those of a fully stabilized mature stand. Therefore, the reader is cautioned that observations reported for this site may not completely represent mature conditions, and may also affect our recommended restoration measures. These efforts, along with other restoration strategies such as wet agriculture (also known as paludiculture) and fire management practices, can move these systems towards partial regeneration and restore some of their ecosystem services.

4.5 Conclusion

Our study shows that tropical peatland GHG flux dynamics are substantially altered after land conversion. Specifically, the converted sites exhibited larger CO₂ fluxes and diminished CH₄ fluxes relative to the undrained site. N₂O fluxes were generally higher at the converted sites, likely being due to increased nitrogen substrate within the soil through fertilizer application. Air

temperature and water table level were the largest contributors to soil GHG flux variability, while effects of precipitation and VPD were variable and did not show a clear relationship. We recommend rewetting and reforestation initiatives to help restore the native peatland vegetation while also promoting enhanced carbon sequestration and peat formation. These efforts will not only partially restore the many valuable ecosystem services, but will also contribute to mitigating the effects of ongoing climate change.

4.6 References

- Ahmad, S., Liu, H., Alam, S., Günther, A., Jurasinski, G., & Lennartz, B. (2021). Meteorological Controls on Water Table Dynamics in Fen Peatlands Depend on Management Regimes. *Frontiers in Earth Science*, 9, 630469. <https://doi.org/10.3389/feart.2021.630469>
- Arai, H., Hadi, A., Darung, U., Limin, S. H., Hatano, R., & Inubushi, K. (2014). A methanotrophic community in a tropical peatland is unaffected by drainage and forest fires in a tropical peat soil. *Soil Science and Plant Nutrition*, 60(4), 577–585. <https://doi.org/10.1080/00380768.2014.922034>
- Bezuijen, M. R., Webb, G. J. W., Hartoyo, P., & Samedi. (2001). Peat swamp forest and the false gharial *Tomistoma schlegelii* (Crocodylia, Reptilia) in the Merang River, eastern Sumatra, Indonesia. *Oryx*, 35(4), 301–307. <https://doi.org/10.1046/j.1365-3008.2001.00195.x>
- Carlson, K. M., Goodman, L. K., & May-Tobin, C. C. (2015). Modeling relationships between water table depth and peat soil carbon loss in Southeast Asian plantations. *Environmental Research Letters*, 10(7), 074006. <https://doi.org/10.1088/1748-9326/10/7/074006>
- Dargie, G. C., Lewis, S. L., Lawson, I. T., Mitchard, E. T. A., Page, S. E., Bocko, Y. E., & Ifo, S. A. (2017). Age, extent and carbon storage of the central Congo Basin peatland complex. *Nature*, 542(7639), 86–90. <https://doi.org/10.1038/nature21048>
- Deshmukh, C. S., Julius, D., Desai, A. R., Asyhari, A., Page, S. E., Nardi, N., Susanto, A. P., Nurholis, N., Hendrizal, M., Kurnianto, S., Suardiwerianto, Y., Salam, Y. W., Agus, F., Astiani, D., Sabiham, S., Gauci, V., & Evans, C. D. (2021). Conservation slows down emission increase from a tropical peatland in Indonesia. *Nature Geoscience*, 14(7), 484–490. <https://doi.org/10.1038/s41561-021-00785-2>

- Deshmukh, C. S., Julius, D., Evans, C. D., Nardi, Susanto, A. P., Page, S. E., Gauci, V., Laurén, A., Sabiham, S., Agus, F., Asyhari, A., Kurnianto, S., Suardiwerianto, Y., & Desai, A. R. (2020). Impact of forest plantation on methane emissions from tropical peatland. *Global Change Biology*, 26(4), 2477–2495. <https://doi.org/10.1111/gcb.15019>
- Deshmukh, C. S., Susanto, A. P., Nardi, N., Nurholis, N., Kurnianto, S., Suardiwerianto, Y., Hendrizal, M., Rhinaldy, A., Mahfiz, R. E., Desai, A. R., Page, S. E., Cobb, A. R., Hirano, T., Guérin, F., Serça, D., Prairie, Y. T., Agus, F., Astiani, D., Sabiham, S., & Evans, C. D. (2023). Net greenhouse gas balance of fibre wood plantation on peat in Indonesia. *Nature*, 616(7958), 740–746. <https://doi.org/10.1038/s41586-023-05860-9>
- Dhandapani, S., & Evers, S. (2020). Oil palm ‘slash-and-burn’ practice increases post-fire greenhouse gas emissions and nutrient concentrations in burnt regions of an agricultural tropical peatland. *Science of The Total Environment*, 742, 140648. <https://doi.org/10.1016/j.scitotenv.2020.140648>
- Dohong, A., Aziz, A. A., & Dargusch, P. (2017). A review of the drivers of tropical peatland degradation in South-East Asia. *Land Use Policy*, 69, 349–360. <https://doi.org/10.1016/j.landusepol.2017.09.035>
- Dommain, R., Couwenberg, J., Glaser, P. H., Joosten, H., & Suryadiputra, I. N. N. (2014). Carbon storage and release in Indonesian peatlands since the last deglaciation. *Quaternary Science Reviews*, 97, 1–32. <https://doi.org/10.1016/j.quascirev.2014.05.002>
- Dommain, R., Couwenberg, J., & Joosten, H. (2011). Development and carbon sequestration of tropical peat domes in south-east Asia: Links to post-glacial sea-level changes and Holocene climate variability. *Quaternary Science Reviews*, 30(7–8), 999–1010. <https://doi.org/10.1016/j.quascirev.2011.01.018>
- Evans, C. D., Williamson, J. M., Kacaribu, F., Irawan, D., Suardiwerianto, Y., Hidayat, M. F., Laurén, A., & Page, S. E. (2019). Rates and spatial variability of peat subsidence in Acacia plantation and forest landscapes in Sumatra, Indonesia. *Geoderma*, 338, 410–421. <https://doi.org/10.1016/j.geoderma.2018.12.028>
- Evers, S., Yule, C. M., Padfield, R., O’Reilly, P., & Varkkey, H. (2017). Keep wetlands wet: The myth of sustainable development of tropical peatlands - implications for policies and management. *Global Change Biology*, 23(2), 534–549. <https://doi.org/10.1111/gcb.13422>
- Frolking, S., Roulet, N., & Fuglestedt, J. (2006). How northern peatlands influence the Earth’s radiative budget: Sustained methane emission versus sustained carbon sequestration. *Journal of Geophysical Research: Biogeosciences*, 111(G1), 2005JG000091. <https://doi.org/10.1029/2005JG000091>

- Gandois, L., Cobb, A. R., Hei, I. C., Lim, L. B. L., Salim, K. A., & Harvey, C. F. (2012). Impact of deforestation on solid and dissolved organic matter characteristics of tropical peat forests: Implications for carbon release. *Biogeochemistry*, 114(1–3), 183–199. <https://doi.org/10.1007/s10533-012-9799-8>
- Gandois, L., Teisserenc, R., Cobb, A. R., Chieng, H. I., Lim, L. B. L., Kamariah, A. S., Hoyt, A., & Harvey, C. F. (2014). Origin, composition, and transformation of dissolved organic matter in tropical peatlands. *Geochimica et Cosmochimica Acta*, 137, 35–47. <https://doi.org/10.1016/j.gca.2014.03.012>
- Girkin, N. T., Cooper, H. V., Ledger, M. J., O'Reilly, P., Thornton, S. A., Åkesson, C. M., Cole, L. E. S., Hapsari, K. A., Hawthorne, D., & Roucoux, K. H. (2022). Tropical peatlands in the Anthropocene: The present and the future. *Anthropocene*, 40, 100354. <https://doi.org/10.1016/j.ancene.2022.100354>
- Girkin, N. T., Vane, C. H., Cooper, H. V., Moss-Hayes, V., Craigon, J., Turner, B. L., Ostle, N., & Sjögersten, S. (2019). Spatial variability of organic matter properties determines methane fluxes in a tropical forested peatland. *Biogeochemistry*, 142(2), 231–245. <https://doi.org/10.1007/s10533-018-0531-1>
- Harenda, K. M., Lamentowicz, M., Samson, M., & Chojnicki, B. H. (2018). The Role of Peatlands and Their Carbon Storage Function in the Context of Climate Change. In T. Zielinski, I. Sagan, & W. Surosz (Eds.), *Interdisciplinary Approaches for Sustainable Development Goals* (pp. 169–187). Springer International Publishing. https://doi.org/10.1007/978-3-319-71788-3_12
- Hayashi, K., Oita, A., & Nishina, K. (2020). Concealed nitrogen footprint in protein-free foods: An empirical example using oil palm products. *Environmental Research Letters*, 15(3), 035006. <https://doi.org/10.1088/1748-9326/ab68ea>
- Hein, L., Sumarga, E., Quiñones, M., & Suwarno, A. (2022). Effects of soil subsidence on plantation agriculture in Indonesian peatlands. *Regional Environmental Change*, 22(4), 121. <https://doi.org/10.1007/s10113-022-01979-z>
- Hergoualc'h, K., Dezzeo, N., Verchot, L. V., Martius, C., Van Lent, J., Del Aguila-Pasquel, J., & López Gonzales, M. (2020). Spatial and temporal variability of soil N₂O and CH₄ fluxes along a degradation gradient in a palm swamp peat forest in the Peruvian Amazon. *Global Change Biology*, 26(12), 7198–7216. <https://doi.org/10.1111/gcb.15354>
- Hergoualc'h, K., Van Lent, J., Dezzeo, N., Verchot, L. V., Van Groenigen, J. W., López Gonzales, M., & Grandez-Rios, J. (2023). Major carbon losses from degradation of *Mauritia flexuosa* peat swamp forests in western Amazonia. *Biogeochemistry*. <https://doi.org/10.1007/s10533-023-01057-4>
- Hirano, T., Jauhiainen, J., Inoue, T., & Takahashi, H. (2009). Controls on the Carbon Balance of Tropical Peatlands. *Ecosystems*, 12(6), 873–887. <https://doi.org/10.1007/s10021-008-9209-1>

- Hirano, T., Kusin, K., Limin, S., & Osaki, M. (2014). Carbon dioxide emissions through oxidative peat decomposition on a burnt tropical peatland. *Global Change Biology*, 20(2), 555–565. <https://doi.org/10.1111/gcb.12296>
- Hirano, T., Segah, H., Harada, T., Limin, S., June, T., Hirata, R., & Osaki, M. (2007). Carbon dioxide balance of a tropical peat swamp forest in Kalimantan, Indonesia. *Global Change Biology*, 13(2), 412–425. <https://doi.org/10.1111/j.1365-2486.2006.01301.x>
- Hirano, T., Segah, H., Kusin, K., Limin, S., Takahashi, H., & Osaki, M. (2012). Effects of disturbances on the carbon balance of tropical peat swamp forests. *Global Change Biology*, 18(11), 3410–3422. <https://doi.org/10.1111/j.1365-2486.2012.02793.x>
- Hooijer, A., Page, S., Canadell, J. G., Silvius, M., Kwadijk, J., Wösten, H., & Jauhiainen, J. (2010). Current and future CO₂ and CH₄ emissions from drained peatlands in Southeast Asia. *Biogeosciences*, 7(5), 1505–1514. <https://doi.org/10.5194/bg-7-1505-2010>
- Hooijer, A., Page, S., Jauhiainen, J., Lee, W. A., Lu, X. X., Idris, A., & Anshari, G. (2012). Subsidence and carbon loss in drained tropical peatlands. *Biogeosciences*, 9(3), 1053–1071. <https://doi.org/10.5194/bg-9-1053-2012>
- Horwath, W. (2007). Carbon cycling and formation of soil organic matter. In E. A. Paul (Ed.), *Soil microbiology, ecology and biogeochemistry* (pp. 303–339). Elsevier.
- Huang, Y., Ciais, P., Luo, Y., Zhu, D., Wang, Y., Qiu, C., Goll, D. S., Guenet, B., Makowski, D., De Graaf, I., Leifeld, J., Kwon, M. J., Hu, J., & Qu, L. (2021). Tradeoff of CO₂ and CH₄ emissions from global peatlands under water-table drawdown. *Nature Climate Change*, 11(7), 618–622. <https://doi.org/10.1038/s41558-021-01059-w>
- Inubushi, K., Furukawa, Y., Hadi, A., Purnomo, E., & Tsuruta, H. (2003). Seasonal changes of CO₂, CH₄ and N₂O fluxes in relation to land-use change in tropical peatlands located in coastal area of South Kalimantan. *Chemosphere*, 52(3), 603–608. [https://doi.org/10.1016/S0045-6535\(03\)00242-X](https://doi.org/10.1016/S0045-6535(03)00242-X)
- IPCC, 2023: *Climate Change 2023: Synthesis Report*. Contribution of Working Groups I, II and III to the Sixth Assessment Report of the Intergovernmental Panel on Climate Change [Core Writing Team, H. Lee and J. Romero (eds.)]. IPCC, Geneva, Switzerland, pp. 35–115, doi: [10.59327/IPCC/AR6-9789291691647](https://doi.org/10.59327/IPCC/AR6-9789291691647).
- Ishikura, K., Hirano, T., Okimoto, Y., Hirata, R., Kiew, F., Melling, L., Aeries, E. B., Lo, K. S., Musin, K. K., Waili, J. W., Wong, G. X., & Ishii, Y. (2018). Soil carbon dioxide emissions due to oxidative peat decomposition in an oil palm plantation on tropical peat. *Agriculture, Ecosystems & Environment*, 254, 202–212. <https://doi.org/10.1016/j.agee.2017.11.025>

- Ishikura, K., Hirata, R., Hirano, T., Okimoto, Y., Wong, G. X., Melling, L., Aeries, E. B., Kiew, F., Lo, K. S., Musin, K. K., Waili, J. W., & Ishii, Y. (2019). Carbon Dioxide and Methane Emissions from Peat Soil in an Undrained Tropical Peat Swamp Forest. *Ecosystems*, 22(8), 1852–1868. <https://doi.org/10.1007/s10021-019-00376-8>
- Jaenicke, J., Wösten, H., Budiman, A., & Siegert, F. (2010). Planning hydrological restoration of peatlands in Indonesia to mitigate carbon dioxide emissions. *Mitigation and Adaptation Strategies for Global Change*, 15(3), 223–239. <https://doi.org/10.1007/s11027-010-9214-5>
- Jauhiainen, J., Hooijer, A., & Page, S. E. (2012a). Carbon dioxide emissions from an *Acacia* plantation on peatland in Sumatra, Indonesia. *Biogeosciences*, 9(2), 617–630. <https://doi.org/10.5194/bg-9-617-2012>
- Jauhiainen, J., Silvennoinen, H., Hämäläinen, R., Kusin, K., Limin, S., Raison, R. J., & Vasander, H. (2012b). Nitrous oxide fluxes from tropical peat with different disturbance history and management. *Biogeosciences*, 9(4), 1337–1350. <https://doi.org/10.5194/bg-9-1337-2012>
- Kiew, F., Hirata, R., Hirano, T., Wong, G. X., Aeries, E. B., Musin, K. K., Waili, J. W., Lo, K. S., Shimizu, M., & Melling, L. (2018). CO₂ balance of a secondary tropical peat swamp forest in Sarawak, Malaysia. *Agricultural and Forest Meteorology*, 248, 494–501. <https://doi.org/10.1016/j.agrformet.2017.10.022>
- Koh, L. P., Miettinen, J., Liew, S. C., & Ghazoul, J. (2011). Remotely sensed evidence of tropical peatland conversion to oil palm. *Proceedings of the National Academy of Sciences*, 108(12), 5127–5132. <https://doi.org/10.1073/pnas.1018776108>
- Kurnianto, S., Warren, M., Talbot, J., Kauffman, B., Murdiyarso, D., & Frolking, S. (2015). Carbon accumulation of tropical peatlands over millennia: A modeling approach. *Global Change Biology*, 21(1), 431–444. <https://doi.org/10.1111/gcb.12672>
- Lam, S. K., Goodrich, J. P., Liang, X., Zhang, Y., Pan, B., Schipper, L. A., Sulaeman, Y., Nelson, L., & Chen, D. (2022). Mitigating soil greenhouse-gas emissions from land-use change in tropical peatlands. *Frontiers in Ecology and the Environment*, 20(6), 352–360. <https://doi.org/10.1002/fee.2497>
- Leng, L. Y., Ahmed, O. H., & Jalloh, M. B. (2019). Brief review on climate change and tropical peatlands. *Geoscience Frontiers*, 10(2), 373–380. <https://doi.org/10.1016/j.gsf.2017.12.018>
- Melling, L., Hatano, R., & Goh, K. J. (2005a). Methane fluxes from three ecosystems in tropical peatland of Sarawak, Malaysia. *Soil Biology and Biochemistry*, 37(8), 1445–1453. <https://doi.org/10.1016/j.soilbio.2005.01.001>

- Melling, L., Hatano, R., & Goh, K. J. (2007). Nitrous oxide emissions from three ecosystems in tropical peatland of Sarawak, Malaysia. *Soil Science and Plant Nutrition*, 53(6), 792–805. <https://doi.org/10.1111/j.1747-0765.2007.00196.x>
- Melling, L., Hatano, R., & Goh, K. J. (2005b). Soil CO₂ flux from three ecosystems in tropical peatland of Sarawak, Malaysia. *Tellus B: Chemical and Physical Meteorology*, 57(1), 1–11. <https://doi.org/10.3402/tellusb.v57i1.16772>
- Miettinen, J., Shi, C., & Liew, S. C. (2012). Two decades of destruction in Southeast Asia's peat swamp forests. *Frontiers in Ecology and the Environment*, 10(3), 124–128. <https://doi.org/10.1890/100236>
- Murdiyarso, D., Hergoualc'h, K., & Verchot, L. V. (2010). Opportunities for reducing greenhouse gas emissions in tropical peatlands. *Proceedings of the National Academy of Sciences*, 107(46), 19655–19660. <https://doi.org/10.1073/pnas.0911966107>
- Myllyntaus, T., Hares, M., & Kunnas, J. (2002). Sustainability in Danger? Slash-and-Burn Cultivation in Nineteenth-Century Finland and Twentieth-Century Southeast Asia. *Environmental History*, 7(2), 267–302. <https://doi.org/10.2307/3985685>
- Neubauer, S. C. (2014). On the challenges of modeling the net radiative forcing of wetlands: Reconsidering Mitsch et al. 2013. *Landscape Ecology*, 29(4), 571–577. <https://doi.org/10.1007/s10980-014-9986-1>
- Nishina, K., Melling, L., Toyoda, S., Itoh, M., Terajima, K., Waili, J. W. B., Wong, G. X., Kiew, F., Aeries, E. B., Hirata, R., Takahashi, Y., & Onodera, T. (2023). Dissolved N₂O concentrations in oil palm plantation drainage in a peat swamp of Malaysia. *Science of The Total Environment*, 872, 162062. <https://doi.org/10.1016/j.scitotenv.2023.162062>
- Novita, N., Asyhari, A., Ritonga, R. P., Gangga, A., Anshari, G. Z., Jupesta, J., Bowen, J. C., Lestari, N. S., Kauffman, J. B., Hoyt, A. M., Perryman, C. R., Albar, I., Putra, C. A. S., Adinugroho, W. C., Winarno, B., Castro, M., Yeo, S., Budiarna, T., Yuono, E., & Sianipar, V. C. (2024). Strong climate mitigation potential of rewetting oil palm plantations on tropical peatlands. *Science of The Total Environment*, 952, 175829. <https://doi.org/10.1016/j.scitotenv.2024.175829>
- Ojanen, P., & Minkinen, K. (2020). Rewetting Offers Rapid Climate Benefits for Tropical and Agricultural Peatlands But Not for Forestry-Drained Peatlands. *Global Biogeochemical Cycles*, 34(7), e2019GB006503. <https://doi.org/10.1029/2019GB006503>
- Page, S. E., Rieley, J. O., Shotyk, W., & Weiss, D. (1999). *Interdependence of peat and vegetation in a tropical peat swamp forest*. 14.
- Page, Susan, Hossain, A., Wösten, H., Jauhiainen, J., Silvius, M., Rieley, J., Ritzema, H., Tansey, K., Graham, L., Vasander, H., & Limin, S. (2009). Restoration Ecology of Lowland

Tropical Peatlands in Southeast Asia: Current Knowledge and Future Research Directions. *Ecosystems*, 12(6), 888–905. <https://doi.org/10.1007/s10021-008-9216-2>

- Pärn, J., Verhoeven, J. T. A., Butterbach-Bahl, K., Dise, N. B., Ullah, S., Aasa, A., Egorov, S., Espenberg, M., Järveoja, J., Jauhiainen, J., Kasak, K., Klemedtsson, L., Kull, A., Laggoun-Défarge, F., Lapshina, E. D., Lohila, A., Lõhmus, K., Maddison, M., Mitsch, W. J., ... Mander, Ü. (2018). Nitrogen-rich organic soils under warm well-drained conditions are global nitrous oxide emission hotspots. *Nature Communications*, 9(1), 1135. <https://doi.org/10.1038/s41467-018-03540-1>
- Phillips, V. D. (n.d.). *Peat swamp ecology and sustainable development in Borneo*. 21.
- Posa, M. R. C., Wijedasa, L. S., & Corlett, R. T. (2011). Biodiversity and Conservation of Tropical Peat Swamp Forests. *BioScience*, 61(1), 49–57. <https://doi.org/10.1525/bio.2011.61.1.10>
- Rein, G. (2013). Smouldering Fires and Natural Fuels. In C. M. Belcher (Ed.), *Fire Phenomena and the Earth System* (1st ed., pp. 15–33). Wiley. <https://doi.org/10.1002/9781118529539.ch2>
- Ribeiro, K., Pacheco, F. S., Ferreira, J. W., Sousa-Neto, E. R., Hastie, A., Krieger Filho, G. C., Alvalá, P. C., Forti, M. C., & Ometto, J. P. (2021). Tropical peatlands and their contribution to the global carbon cycle and climate change. *Global Change Biology*, 27(3), 489–505. <https://doi.org/10.1111/gcb.15408>
- Roucoux, K. H., Lawson, I. T., Baker, T. R., Del Castillo Torres, D., Draper, F. C., Lähteenoja, O., Gilmore, M. P., Honorio Coronado, E. N., Kelly, T. J., Mitchard, E. T. A., & Vriesendorp, C. F. (2017). Threats to intact tropical peatlands and opportunities for their conservation: Tropical Peatlands. *Conservation Biology*, 31(6), 1283–1292. <https://doi.org/10.1111/cobi.12925>
- Sazawa, K., Wakimoto, T., Fukushima, M., Yustiawati, Y., Syawal, M. S., Hata, N., Taguchi, S., Tanaka, S., Tanaka, D., & Kuramitz, H. (2018). Impact of Peat Fire on the Soil and Export of Dissolved Organic Carbon in Tropical Peat Soil, Central Kalimantan, Indonesia. *ACS Earth and Space Chemistry*, 2(7), 692–701. <https://doi.org/10.1021/acsearthspacechem.8b00018>
- Schlesinger, W. H. (2013). An estimate of the global sink for nitrous oxide in soils. *Global Change Biology*, 19(10), 2929–2931. <https://doi.org/10.1111/gcb.12239>
- Somers, L. D., Hoyt, A., Cobb, A. R., Isnin, S., Suhip, M. A. A. B. H., Sukri, R. S., Gandois, L., & Harvey, C. (2023). Processes Controlling Methane Emissions From a Tropical Peatland Drainage Canal. *Journal of Geophysical Research: Biogeosciences*, 128(3), e2022JG007194. <https://doi.org/10.1029/2022JG007194>

- Strack, M., Waddington, J. M., Turetsky, M., Roulet, N. T., & Byrne, A. (2008). Northern peatlands, greenhouse gas exchange and climate change. In M. Strack (Ed.), *Peatland and climate change* (pp. 44–69). International Peat Society. Vapaudenkatu.
- Tang, A. C. I., Melling, L., Stoy, P. C., Musin, K. K., Aeries, E. B., Waili, J. W., Shimizu, M., Poulter, B., & Hirata, R. (2020). A Bornean peat swamp forest is a net source of carbon dioxide to the atmosphere. *Global Change Biology*, 26(12), 6931–6944.
<https://doi.org/10.1111/gcb.15332>
- Tang, A. C. I., Stoy, P. C., Hirata, R., Musin, K. K., Aeries, E. B., Wenceslaus, J., & Melling, L. (2018). Eddy Covariance Measurements of Methane Flux at a Tropical Peat Forest in Sarawak, Malaysian Borneo. *Geophysical Research Letters*, 45(9), 4390–4399.
<https://doi.org/10.1029/2017GL076457>
- Teh, Y. A., Murphy, W. A., Berrio, J.-C., Boom, A., & Page, S. E. (2017). Seasonal variability in methane and nitrous oxide fluxes from tropical peatlands in the western Amazon basin. *Biogeosciences*, 14(15), 3669–3683. <https://doi.org/10.5194/bg-14-3669-2017>
- Turetsky, M. R., Benscoter, B., Page, S., Rein, G., van der Werf, G. R., & Watts, A. (2015). Global vulnerability of peatlands to fire and carbon loss. *Nature Geoscience*, 8(1), 11–14.
<https://doi.org/10.1038/ngeo2325>
- Uda, S. K., Hein, L., & Sumarga, E. (2017). Towards sustainable management of Indonesian tropical peatlands. *Wetlands Ecology and Management*, 25(6), 683–701.
<https://doi.org/10.1007/s11273-017-9544-0>
- Usup, A., Hashimoto, Y., Takahashi, H., & Hayasaka, H. (2004). Combustion and thermal characteristics of peat fire in tropical peatland in Central Kalimantan, Indonesia. *Tropics*, 14(1), 1–19. <https://doi.org/10.3759/tropics.14.1>
- Warren, M., Hergoualc'h, K., Kauffman, J. B., Murdiyarso, D., & Kolka, R. (2017). An appraisal of Indonesia's immense peat carbon stock using national peatland maps: Uncertainties and potential losses from conversion. *Carbon Balance and Management*, 12(1), 12.
<https://doi.org/10.1186/s13021-017-0080-2>
- Wibisono, H. T., & Pusparini, W. (2010). Sumatran tiger (*Panthera tigris sumatrae*): A review of conservation status. *Integrative Zoology*, 5(4), 313–323.
<https://doi.org/10.1111/j.1749-4877.2010.00219.x>
- Wiggins, E. B., Czimeczik, C. I., Santos, G. M., Chen, Y., Xu, X., Holden, S. R., Randerson, J. T., Harvey, C. F., Kai, F. M., & Yu, L. E. (2018). Smoke radiocarbon measurements from Indonesian fires provide evidence for burning of millennia-aged peat. *Proceedings of the National Academy of Sciences*, 115(49), 12419–12424.
<https://doi.org/10.1073/pnas.1806003115>

- Wong, G. X., Hirata, R., Hirano, T., Kiew, F., Aeries, E. B., Musin, K. K., Waili, J. W., Lo, K. S., & Melling, L. (2018). Micrometeorological measurement of methane flux above a tropical peat swamp forest. *Agricultural and Forest Meteorology*, 256–257, 353–361. <https://doi.org/10.1016/j.agrformet.2018.03.025>
- Wong, G. X., Hirata, R., Hirano, T., Kiew, F., Waili, J. W., Mander, Ü., Soosaar, K., & Melling, L. (2025). Impact of land conversion on environmental conditions and methane emissions from a tropical peatland. *Science of The Total Environment*, 962, 178466. <https://doi.org/10.1016/j.scitotenv.2025.178466>
- Wösten, J. H. M., Clymans, E., Page, S. E., Rieley, J. O., & Limin, S. H. (2008). Peat–water interrelationships in a tropical peatland ecosystem in Southeast Asia. *CATENA*, 73(2), 212–224. <https://doi.org/10.1016/j.catena.2007.07.010>
- Wösten, J. H. M., Van Den Berg, J., Van Eijk, P., Gevers, G. J. M., Giesen, W. B. J. T., Hooijer, A., Idris, A., Leenman, P. H., Rais, D. S., Siderius, C., Silvius, M. J., Suryadiputra, N., & Wibisono, I. T. (2006). Interrelationships between Hydrology and Ecology in Fire Degraded Tropical Peat Swamp Forests. *International Journal of Water Resources Development*, 22(1), 157–174. <https://doi.org/10.1080/07900620500405973>
- Yu, Z., Loisel, J., Brosseau, D. P., Beilman, D. W., & Hunt, S. J. (2010). Global peatland dynamics since the Last Glacial Maximum: GLOBAL PEATLANDS SINCE THE LGM. *Geophysical Research Letters*, 37(13), n/a-n/a. <https://doi.org/10.1029/2010GL043584>

Chapter 5: Conclusion

5.1 Dissertation Overview

Quantifying the carbon cycle and its hydrological drivers in tropical peatlands is challenging for multiple reasons. My dissertation is among the first to evaluate how space-based approaches to estimating tropical peatland properties relevant to the carbon cycle can resolve that challenge. Specifically, it showcases that remote sensing may give researchers an accurate quantification of temporal water table fluctuations within a tropical peatland landscape and also provide meaningful forecasting of burning area. Together, these two indicators are critical drivers of the carbon cycle. Furthermore, this dissertation has contributed to the traditional approach of tropical peatland study by taking in situ measurements of soil, soil gas, water table, and other environmental variables to provide challenging, rarely measured observations of greenhouse gas emissions together with drivers. This on-the-ground work aimed to compare the soil greenhouse gas fluxes within three peatland sites of varying disturbance. It also analyzed how the relationship between soil gas flux and environmental variables differed between the three sites. The combined work of these chapters provides a pathway to future greenhouse gas information systems for tropical peatlands, essential for improving reporting of peatland-related carbon emission changes and the revising of emission factors used in international emission reduction policies.

Chapter 2 used a surface reflectance-based remote sensing model, the Optical Trapezoid Model (OPTRAM), to estimate tropical peatland water table level. It was found that OPTRAM performs optimally in areas with sparse vegetation and performs poorly in areas with high

vegetation. This indicates that, even within the densely vegetated tropical peat swamp forests, the landscape-level temporal fluctuations in water table level may be monitored. This is due to the high horizontal hydraulic conductivity of the upper peat layer which synchronizes the rising and falling of water table across the peatland landscape (Hirano et al., 2012; Burdun et al., 2020; Burdun et al., 2023). This suggests that if a single location with sparse vegetation is found within a tropical peat swamp forest, OPTRAM may be successfully applied to retrieve temporal fluctuations in water table level at the landscape scale. It is important to note, however, that this is only possible in undrained tropical peatland systems where horizontal hydraulic conductivity is high. In drained and converted tropical peatland systems, where the horizontal hydraulic conductivity is low, OPTRAM-based retrieval of landscape-level water table level may not be possible. Furthermore, OPTRAM indicates the vegetation moisture status and uses the water table-vegetation moisture connection to make water table estimations. In drained and converted tropical peat systems, this connection is low due to an excessively low water table, and therefore OPTRAM may not be able to reliably retrieve water table regardless of vegetation density. Despite this, this work has large implications for tropical peatland management and may provide stakeholders and practitioners with an idea of water table fluctuations in peat ecosystems that are inaccessible for in situ measurements.

Chapter 3 uses the findings of chapter 2 to elevate OPTRAM's application in tropical peatlands. Specifically, it shows that it is possible to use OPTRAM to forecast burned area 10, 20, and 30 days ahead of time in the peatlands of Indonesia, Malaysia, Peru, and the Congo Basin. For some sites, when 10, 20, and 30-day forward shifted OPTRAM values were low, the proxy value for the burned area was high, indicating that low OPTRAM values in the past may be indicators of

non-zero burned area in the present. Like in chapter 2, OPTRAM must be applied in areas with low vegetation density to obtain accurate retrievals of surface moisture content. This work may provide a way to detect peat fire before they occur, allowing stakeholders and practitioners to prepare for or even prevent upcoming fire events.

Chapter 4 quantified soil greenhouse gas fluxes using the closed chamber method at an undrained peat swamp forest, a young oil palm plantation, and mature oil palm plantation (in a region where the second rotation of planting was taking place) over nine months. This work also gathered environmental data (water table level, air temperature, precipitation, etc.) to determine how soil greenhouse gas fluxes were impacted by these variables. It was discovered that land conversion for the purposes of agriculture drastically changes soil greenhouse gas flux magnitudes. Specifically, it was found that soil carbon-dioxide and nitrous oxide fluxes toward the atmosphere generally increased at the two plantation sites. Meanwhile, soil methane fluxes toward the atmosphere were generally lower at the plantation sites relative to the undrained site. Water table level and average air temperature were found to be major contributors to soil greenhouse gas flux variability, whereas precipitation and vapor pressure deficit had minimal impact.

5.2 Study Limitations

This dissertation was faced with some limitations. For example, the heavy reliance on optical remote sensing in Chapters 2 and 3 made OPTRAM calculations highly affected by clouds. Even though the affected pixels were removed, this still impacted these studies by reducing the overall number of data points used and thereby potentially diminishing the robustness of results. In chapter 3, the MODIS MOD09GA v6.1 surface reflectance product was used rather than Landsat

in favor of its daily temporal resolution. However, this product has a 500m resolution which may miss some tropical peatland properties that may have otherwise been observed with higher resolution. One of the major limitations in chapter 4 was during data collection in the field. For example, the water table was measured using a tape measure, which made it quite challenging to obtain exact values. Moreover, when the water table was extremely low, which was often the case at the plantation sites, the measurement was particularly arduous.

5.3 Implications

Since many tropical peatlands are difficult to access due to being in remote locations, a remote sensing approach for estimating variables has large implications for advancing the field. In terms of this dissertation work, being able to estimate water table fluctuations is essential for many aspects of tropical peatland conservation. For example, if OPTRAM is found to be decreasing in a certain tropical peatland area, then efforts may be made to rewet the area to prevent excessive carbon dioxide emissions. Furthermore, this approach can inform future policy, especially in the Southeast Asia region where peatland conversion to plantation is rampant. Undrained and minimally disturbed tropical peatlands can have their water tables monitored and new policies may be created to sustain high water tables and prevent land conversion. Monitoring water table in tropical peatlands gives stakeholders and practitioners the power to make informed decisions about the land and prevent carbon dioxide emissions. This can be seen as a significant global warming mitigation tool for the tropics which, in past decades, has been known to be a significant carbon source in certain regions.

While there have been efforts in mitigating the carbon release in tropical peatlands, many of these regulations are not strictly enforced and sometimes act as nothing more than symbolic legislation to appease the local and international community. For example, in 2011, Indonesia established a moratorium on the granting of new licenses that allowed primary peatland forest conversion to palm oil plantations and timber concessions ([Government of Indonesia, 2011](#); [Purnomo, 2012](#)). Additional restrictions were later implemented by Indonesia in 2017, followed in 2018 by a 3-year moratorium on new palm oil concessions ([Government of Indonesia, 2011](#); [Purnomo, 2012](#)). However, from 2011-2018, there was found to be substantial forest cover loss despite these conservation efforts, and the most likely explanation was that deforestation was continuing to occur largely unchecked ([Groom et al., 2022](#)).

Moreover, this work may inform fire prevention tactics. Not only does peat fire contribute substantially to carbon emissions and the exacerbation of climate change, but it also has many immediate effects. For instance, some megafires, such as those that took place in Indonesia in 1997 and 2015, can cause massive haze events. This can lower visibility and dramatically decrease air quality, leading to adverse and sometimes lethal health effects ([Davies et al., 1999](#); [Sahani et al., 2014](#); [Koplitz et al., 2016](#); [Kunii et al., 2002](#)). Peat fires are also different from conventional soils, in that, they may experience smoldering combustion that can continue to burn even if flames are not present ([Turetsky et al., 2015](#)). Chapter 3 of this dissertation can make meaningful contributions to existing fire prevention strategies, especially in Southeast Asia. It introduces a method where peat fire vulnerability can be actively monitored, which can inform stakeholders and practitioners as to when they would need to intervene to reduce future peat fire risk. This work may also inform sustainable agricultural practices through the findings of chapter

4. The in situ measurements presented in the chapter provide valuable information regarding the state of a tropical peatland ecosystem across varying disturbance levels. This type of study is not very common in the literature due to the many limitations that come with studying peatlands in the tropics. Based on the results in this study, plantation owners may be advised to transition to more sustainable practices that mitigate carbon dioxide and nitrous oxide emissions from the peat soil.

5.4 Future Directions

Future research should prioritize in leveraging the application of OPTRAM such that it may quantify other moisture-dependent tropical peatland variables. This can include estimations for variables such as peatland carbon dioxide emissions and subsidence. A relationship between water table level and carbon dioxide flux has been empirically found in past studies on tropical peatlands ([Hirano et al., 2007](#); [Hirano et al., 2012](#); [Hirano et al., 2014](#)). This relationship may be combined with OPTRAM to estimate soil carbon dioxide emissions for many of the peatlands in the tropics. OPTRAM's capability of predicting the probability of future burned area may also aid in quantifying fire-related peat carbon emissions. Furthermore, due to OPTRAM's inherent remote sensing approach, soil carbon dioxide emission estimates may be made even in the most remote tropical peatlands. This will give stakeholders an advantage by allowing estimations of peat carbon fluxes in landscapes that are otherwise not accessible for on-the-ground measurements. Existing in situ measurements of tropical peatland carbon flux can even be combined with OPTRAM to improve the accuracy of peat carbon flux estimations (Figure 5.1).

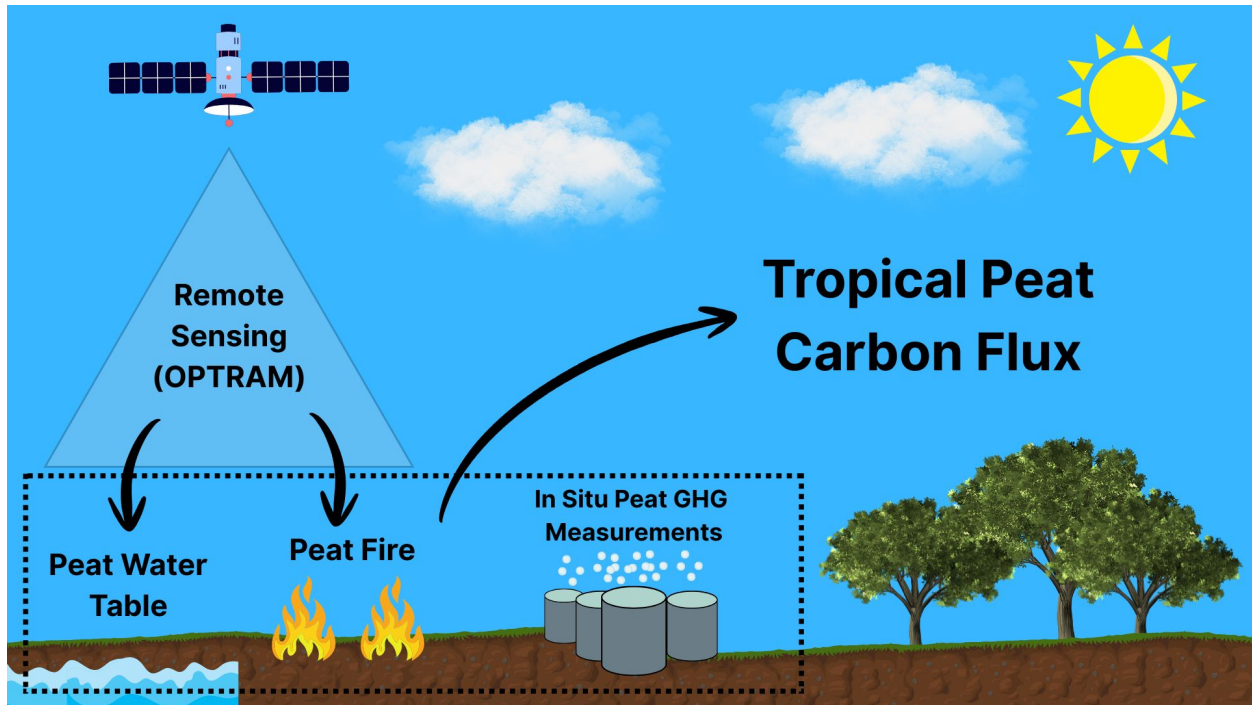


Figure 5.1: Conceptual figure showing how a combination of remote sensing and in situ measurements may offer a more precise assessment of overall tropical peat carbon flux. Figure created in Canva.

OPTRAM-based estimates for peat subsidence may also be possible. In past studies, peat subsidence has been linked to peatland drainage ([Hooijer et al., 2012](#)). I showed that OPTRAM has the potential to track water table over time. Therefore, if the OPTRAM index is persistently decreasing in an area, it may also indicate greater peat subsidence in the area. Of course, future studies must focus on deriving a relationship between OPTRAM and in situ peat subsidence to determine the specific correlation between the two variables in tropical peatlands. Peat subsidence greatly impacts the system's hydrology through increases in peat bulk density and decreases in water storage capacity. With this comes a high risk of severe flooding after heavy rainfall. Therefore, with this knowledge, interventions may take place to lower the risk of

flooding and to potentially re-establish, to an extent, the peat's hydrological self-regulation capabilities.

An effort must also be made to apply OPTRAM to more tropical peatlands to obtain a more robust association between in situ water table and OPTRAM index. Furthermore, OPTRAM should be applied to peatlands in the mountainous regions of the tropics to determine whether a highland system would yield a different relationship relative to the lowland peatlands that were tested in chapter 2.

Future work can also involve integrating OPTRAM into tropical peatland-related models to determine whether model performance is improved. Since in situ tropical peatland water table data is relatively insufficient, OPTRAM may be a worthy proxy to consider as model input. This can potentially allow for more accurate modeling of tropical peatland hydrology and build upon existing work ([Apers et al., 2022](#)).

On the other hand, researchers may also consider using bands that are not affected by clouds. For example, Synthetic Aperture Radar uses microwave radiation which is largely unaffected by clouds. Moreover, the use of remote sensing products with higher spatial resolution is encouraged since this may possibly yield more accurate results.

5.5 Concluding Remarks

Overall, this dissertation has shown that remote sensing may be used to quantify the water table level in tropical peatlands. This finding creates numerous opportunities to build upon this

methodology and invites future work to further explore the capabilities of remote sensing for quantifying tropical peatland dynamics. It can also contribute to decreasing uncertainties in the contributions of tropical ecosystems to the global carbon budget. As a result, this may help in providing more accurate information for future global scientific reports such as for the Intergovernmental Panel on Climate Change.

This dissertation also takes a traditional approach to tropical peatland study and adds to the growing literature of in situ studies. It is important to continue conducting on-the-ground studies in tropical peatlands since this approach provides a more direct a measurement and therefore a relatively reliable quantification of numerous variables. This work aimed to provide a comparison of soil greenhouse gas emissions and its relationship with environmental variables between tropical peatlands at differing disturbance stages. Having this information is crucial if we are to fully understand the impacts of land use and land cover change on tropical peatlands.

This dissertation has shown that a remote sensing approach poses a promising future for tropical peatland study. Through in situ measurements, it has also indicated that large changes occur to the system's dynamics when converted to oil palm plantation. With this understanding, stakeholders and practitioners may not only make more well-informed decisions regarding ongoing tropical peatland sustainability initiatives, but they may also monitor these systems from space to mitigate or even prevent future degradation.

5.6 References

- Apers, S., G. J. M. De Lannoy, A. J. Baird, A. R. Cobb, G. C. Dargie, J. Del Aguila Pasquel, A. Gruber, et al. "Tropical Peatland Hydrology Simulated With a Global Land Surface Model." *Journal of Advances in Modeling Earth Systems* 14, no. 3 (March 2022): e2021MS002784. <https://doi.org/10.1029/2021MS002784>.
- Burdun, Iuliia, Michel Bechtold, Mika Aurela, Gabrielle De Lannoy, Ankur R. Desai, Elyn Humphreys, Santtu Kareksela, et al. "Hidden Becomes Clear: Optical Remote Sensing of Vegetation Reveals Water Table Dynamics in Northern Peatlands." *Remote Sensing of Environment* 296 (October 2023): 113736. <https://doi.org/10.1016/j.rse.2023.113736>.
- Burdun, Iuliia, Michel Bechtold, Valentina Sagris, Annalea Lohila, Elyn Humphreys, Ankur R. Desai, Mats B. Nilsson, Gabrielle De Lannoy, and Ülo Mander. "Satellite Determination of Peatland Water Table Temporal Dynamics by Localizing Representative Pixels of A SWIR-Based Moisture Index." *Remote Sensing* 12, no. 18 (September 10, 2020): 2936. <https://doi.org/10.3390/rs12182936>.
- Davies, Stuart J. "Smoke-Haze from the 1997 Indonesian Forest Fires: Effects on Pollution Levels, Local Climate, Atmospheric CO₂ Concentrations, and Tree Photosynthesis." *Forest Ecology and Management*, 1999, 8.
- Government of Indonesia, "Moratorium on granting of new licenses and improvement of natural primary forest and peatland governance" (Presidential Instruction 10/2011, Republic of Indonesia, 2011).
- Groom, B., Palmer, C., & Sileci, L. (2022). Carbon emissions reductions from Indonesia's moratorium on forest concessions are cost-effective yet contribute little to Paris pledges. *Proceedings of the National Academy of Sciences*, 119(5), e2102613119. <https://doi.org/10.1073/pnas.2102613119>
- Hirano, Takashi, Kitso Kusin, Suwido Limin, and Mitsuru Osaki. "Carbon Dioxide Emissions through Oxidative Peat Decomposition on a Burnt Tropical Peatland." *Global Change Biology* 20, no. 2 (February 2014): 555–65. <https://doi.org/10.1111/gcb.12296>.
- Hirano, Takashi, Hendrik Segah, Tsuyoshi Harada, Suwido Limin, Tania June, Ryuichi Hirata, and Mitsuru Osaki. "Carbon Dioxide Balance of a Tropical Peat Swamp Forest in Kalimantan, Indonesia." *Global Change Biology* 13, no. 2 (February 2007): 412–25. <https://doi.org/10.1111/j.1365-2486.2006.01301.x>.
- Hirano, Takashi, Hendrik Segah, Kitso Kusin, Suwido Limin, Hidenori Takahashi, and Mitsuru Osaki. "Effects of Disturbances on the Carbon Balance of Tropical Peat Swamp Forests." *Global Change Biology* 18, no. 11 (November 2012): 3410–22. <https://doi.org/10.1111/j.1365-2486.2012.02793.x>.

- Hooijer, A., S. Page, J. Jauhiainen, W. A. Lee, X. X. Lu, A. Idris, and G. Anshari. "Subsidence and Carbon Loss in Drained Tropical Peatlands." *Biogeosciences* 9, no. 3 (March 20, 2012): 1053–71. <https://doi.org/10.5194/bg-9-1053-2012>.
- Kopplitz, Shannon N, Loretta J Mickley, Miriam E Marlier, Jonathan J Buonocore, Patrick S Kim, Tianjia Liu, Melissa P Sulprizio, et al. "Public Health Impacts of the Severe Haze in Equatorial Asia in September–October 2015: Demonstration of a New Framework for Informing Fire Management Strategies to Reduce Downwind Smoke Exposure." *Environmental Research Letters* 11, no. 9 (September 1, 2016): 094023. <https://doi.org/10.1088/1748-9326/11/9/094023>.
- Kunii, Osamu, Shuzo Kanagawa, Iwao Yajima, Yoshiharu Hisamatsu, Sombo Yamamura, Takashi Amagai, and Ir T. Sachrul Ismail. "The 1997 Haze Disaster in Indonesia: Its Air Quality and Health Effects." *Archives of Environmental Health: An International Journal* 57, no. 1 (January 2002): 16–22. <https://doi.org/10.1080/00039890209602912>.
- Purnomo, A. "Protecting Our Forests, Pros-Cons of Moratorium on Forests and Peatlands' Policy" (Kepustakaan Populer Gramedia, Jakarta, Indonesia, 2012).
- Sahani, Mazrura, Nurul Ashikin Zainon, Wan Rozita Wan Mahiyuddin, Mohd Talib Latif, Rozita Hod, Md Firoz Khan, Norhayati Mohd Tahir, and Chang-Chuan Chan. "A Case-Crossover Analysis of Forest Fire Haze Events and Mortality in Malaysia." *Atmospheric Environment* 96 (October 2014): 257–65. <https://doi.org/10.1016/j.atmosenv.2014.07.043>.
- Turetsky, Merritt R., Brian Benscoter, Susan Page, Guillermo Rein, Guido R. van der Werf, and Adam Watts. "Global Vulnerability of Peatlands to Fire and Carbon Loss." *Nature Geoscience* 8, no. 1 (January 2015): 11–14. <https://doi.org/10.1038/ngeo2325>.